Technische Universität München

Fakultät für Chemie

Biosystemchemie

Investigations into the (Bio-)Synthesis of Antimicrobial Natural Products Kistamicin A and Myxocoumarin B

Hannah Kalina Kusserow, M.Sc.

Vollständiger Abdruck der von der Fakultät für Chemie der Technischen Universität München zur Erlangung des akademischen Grades eines Doktors der Naturwissenschaften (Dr. rer. nat.) genehmigten Dissertation.

Vorsitzende(r):   Prof. Dr. Franz Hagn

Prüfer der Dissertation:

  1. Prof. Dr. Tobias A.M. Gulder

  2. Prof. Dr. Kathrin Lang

Die Dissertation wurde am 07.08.2019 bei der Technischen Universität München eingereicht und durch die Fakultät für Chemie am 11.09.2019 angenommen.

It is good to have an end to journey toward,
but it is the journey that matters, in the end.

Ursula K. Le Guin, The Left Hand of Darkness

Für meine Familie

Acknowledgements

Parts of this thesis have been published in:

- **Kusserow, K.**; Gulder, T.A.M. Complete Genome Sequence of *Actinomadura Parvosata* Subsp. *Kistnae*, A Rich Source of Novel Natural Product (Bio-)Chemistry. *J. Genomics* **2017**, *5*, 75-76.

- Müller, J. I.*; **Kusserow, K.***; Hertrampf, G.; Pavic, A; Nikodinovic-Runic, J.; Gulder, T.A.M. Synthesis and Initial Biological Evaluation of Myxocoumarin B. *Org. Biomol. Chem.* **2019**, *17*, 1966-1969.
  *equally contributing authors

Contents

Contents

Contents

Chapter 1

Introduction

1.1. Antimicrobial Drugs from Natural Products

For millenia, bioactive compounds produced by plants and microorganisms have been used as drugs in medicinal applications. Pharmaceutical records, created throughout human history, attest to their use in the treatment of various diseases and illnesses.[1,2] The egyptian Ebers Papyrus (1500 B.C.), for example, documents some 700 drugs and remedies, most of them plant-based,[1] while other egyptian sources describe the topical application of mouldy bread to infected wounds.[3] Today, we can isolate and identify these bioactive compounds from plants, bacteria, fungi and even marine animal origins. They belong to a large and diverse family of chemical entities, termed natural products. Natural products are produced by their hosts as secondary metabolites, for example as molecules that are not required for survival, but provide the host some advantage in its native environment. Natural macromolecules (DNA, RNA, proteins), their building blocks and precursors as well as intermediates of primary metabolism are typically excluded from the definition of natural products.[4] With the progress in the natural sciences at the beginning of the 19th century, pure and defined natural products were increasingly explored. An event of epochal importance was A. Flemings discovery of the antibiotic activity of the penicillins produced by fungi of the genus *Penicillium* (1928/29). With the help of antibiotics and vaccines, infectious diseases, which were the main killer until the second half of the 20th century, could finally be treated. Since then, natural products have served as a major source for modern pharmaceutical agents and their investigation has afforded a very large number of new compounds with strong antibiotic, antifungal, antiviral, immunosuppressive, antitumor, and other activities.[2,5,6] Today, most antibacterial drugs

are either natural products or derivatives thereof, usually obtained by semi-synthetic modification.[7] Important classes of antibiotic natural products include aminoglycosides (e.g. streptomycin (**1**)), β-lactams (e.g. penicillin G (**2**)), tetracyclines (e.g. tetracycline (**3**)), polyketides (e.g. rifamycin SV (**4**)), glycopeptides (e.g. teicoplanin A_2-2 (**5**)), lipopeptides (e.g. daptomycin (**6**)) and macrolides (e.g. erythromycin (**7**)).[8] In addition, approximately 49 % of modern chemotherapeutics as well as a large number of antivirals are natural products or natural product derived.[7] A well known example for a natural product derivative is oseltamivir (**8**), which was marketed as Tamiflu®to treat Influenza A, B, and H5N1 virus infections.[9,10] In contrast, most antifungal drugs are totally synthetic,[7] with bacterially produced amphotericin B (**9**) being a noteworthy exception.[11,12]

Despite this success of natural products, new, threatening strains of bacteria, fungi and viruses have emerged during the last decades. For instance, more and more bacterial strains develop (multi-) drug resistances, resulting in difficult or even un-treatable infections. Most notable are Gram-positive methicillin-resistant *Staphylococcus aureus* and vancomycin-resistant enterococci (VRE), Gram-negative multidrug-resistant (MDR) bacteria as well as MDR or extensively drug-resistant (XDR) *Mycobacterium tubercolosis*.[13] Unfortunately, a 40 year innovation gap between the 1960s and 2000s, in which antibiotic research and development was de-emphasized in the pharmaceutical industry, combined with scientific difficulties in the identification of novel scaffolds led to an inadequate number of novel antibiotic drugs.[14–17] In addition to bacteria, fungal strains of *Aspergillus*, *Cryptococcus* and, especially, *Candida* are increasingly responsible for severe, life-threatening infections. Patients with weakened immune systems, caused, for example, by human immunodeficiency virus (HIV), cancer therapy or immunosupressant drugs after organ transplantation, are especially at risk.[18–25] Moreover, virus infections, such as HI, Ebola, and Influenza A have been proven to be difficult to combat using conventional vaccine approaches.[26,27] Indeed, the World Health Organization (WHO) named antimicrobial resistance as one of the major threats against human health in 2018.[28] As a result of this pressing need for new, clinically efficient drugs, a high priority has been placed on the discovery of antimicrobial agents, both naturally occurring and synthetic.[29–31] With only a very small part of the world's biodiversity having been evaluated for potential biologically active compounds,[32–35] many more useful natural products await discovery, with the challenge being how to access this structural diversity.

A true treasure trove for natural product drug discovery lies within the realm of microorganisms, which promises abundant genetic diversity. Unfortunately, rather few
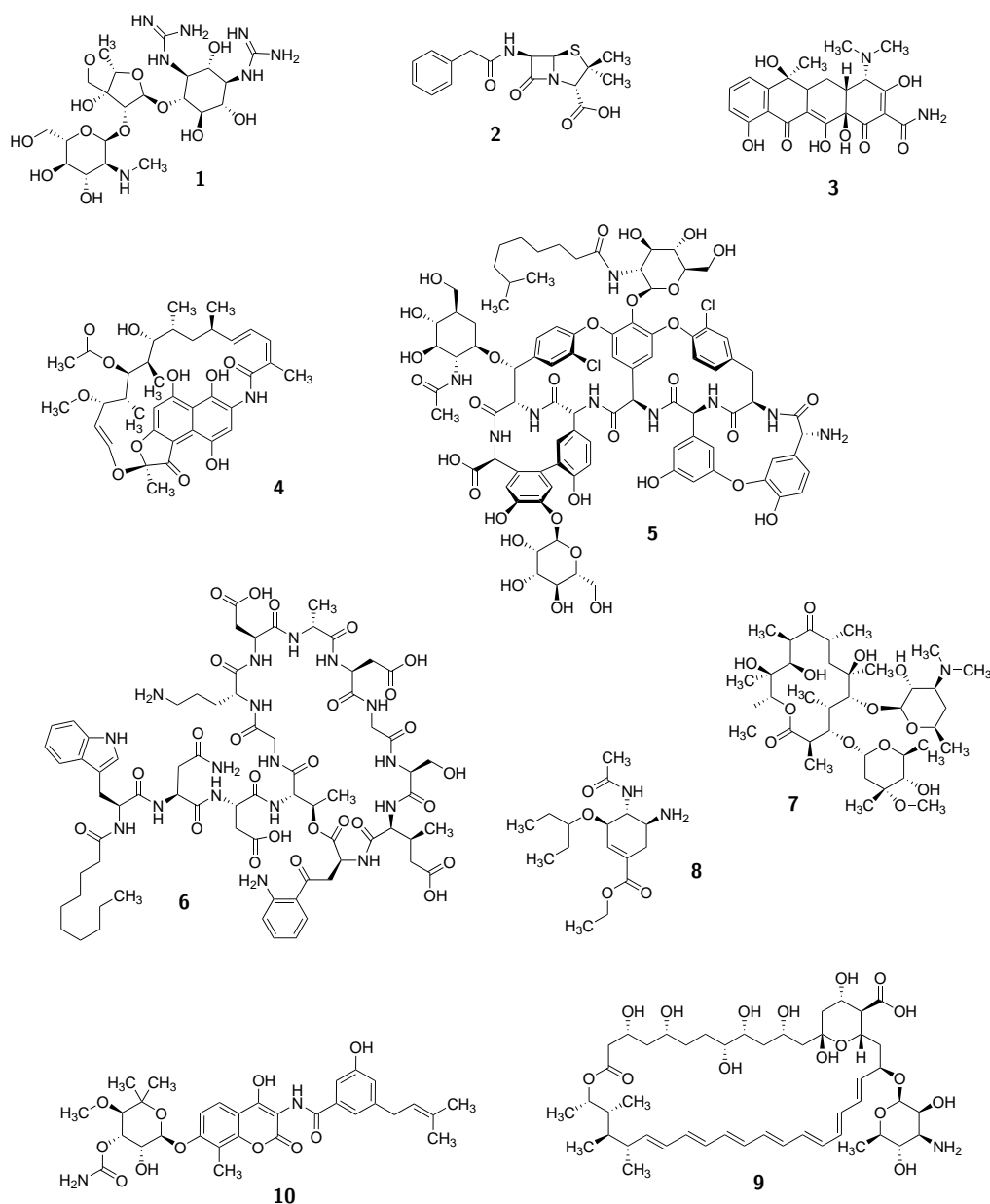
Figure 1. Chemical structures of various natural produtcs employed as antimicrobial drugs: streptomycin (**1**; aminoglycoside antibiotic), penicillin G (**2**; β-lactam antibiotic), tetracycline (**3**; tetracycline antibiotic), rifamycin SV (**4**; polyketide antibiotic), teicoplanin A$_2$-2 (**5**; glycopeptide antibiotic), daptomycin (**6**; lipopeptide antibiotic), erythromycin (**7**; macrolide antibiotic), oseltamivir (**8**; antiviral γ-amino acid), novobiocin (**10**; aminocoumarin antibiotic), amphotericin B (**9**; antifungal macrolide).

microorganisms, which can be cultured and express a large variety of natural products under standard-laboratory conditions, exist.[32,33] The most important ones are actinomyctes, pseudomonas, strains of bacilii and fungi. Therefore, many research groups have tried to identify novel groups of prolific producers, but in 50 years only two new groups of bacteria have been added - cyanobacteria as well as myxobacteria.[36–40] The classic approach to the discovery of novel natural products from microorganisms is the acquisition of unexplored strains, followed by fermentation, product isolation, and testing of fermentation broths or purified compounds in bioactivity assays. Promising isolates subsequently undergo structure elucidation and, in some cases, their molecular target or mode of action may be identified. Modifications of the lead compound in structure-activity relationship (SAR) studies help to identify the pharmacophore and to optimize potency, selectivity, toxicity or pharmcokinetic parameters. If drug candidates are successful in preclinical and clinical trials, they will ultimately be approved as drugs and marketed. During the Golden Age of natural product drug discovery (1940s to 1960s), this approach was used to easily yield large numbers of novel bioactive compounds with high structural diversity and complexity.[4] A prominent example for a clinically important drug isolated from bacterial fermentation broth is the antibiotic vancomycin (**11**). The compound is produced by actinomycete strain *Streptomyces orientalis* (later reclassified as *Amicolatopsis orientalis*), which was grown from a soil sample collected in the jungle of Borneo. After isolating the compound from *S. orientalis*, scientists at *Eli Lilly* found that **11** exhibited potent antibacterial activity against all tested strains of *Staphylococcus* and other Gram-positive bacteria.[41–44] The complex structure - a cyclic peptide decorated with sugar moeities - was deduced only 25 years later by Williams, Harris and co-workers.[45,46] In 1958 vancomycin was the first glycopeptide antibiotic (GPA) approved for the clinic and used to combat highly virulent MRSA. Due to its potency, the lack of cross-resistances with other antibiotics, as well as medicinal side effects, vancomycin was hold in reserve against infections with multiresistant pathogens. Today, vancomycin and its sister antibiotic teicoplanin (**5**) (produced by *Actinoplanes teichomyceticus*) are indispensable - and sometimes the last resort - in the fight against life-threatening infections with multiresistant Gram-positive bacteria.[43,47,48] Indeed, it features on the current World Health Organiszation's List of Essential Medicines.[49] However, after 30 years of clinical use first resistances against vancomycin became known in enterococi (VRE).[50,51]

In the hope to improve biological activity and conquer resistance, resistance mechanisms were investigated and the vancomycin structure readjusted. Glycopeptides function by inhibition of bacterial cell wall biosynthesis. They bind L-Lys-D-Ala-D-Ala residues
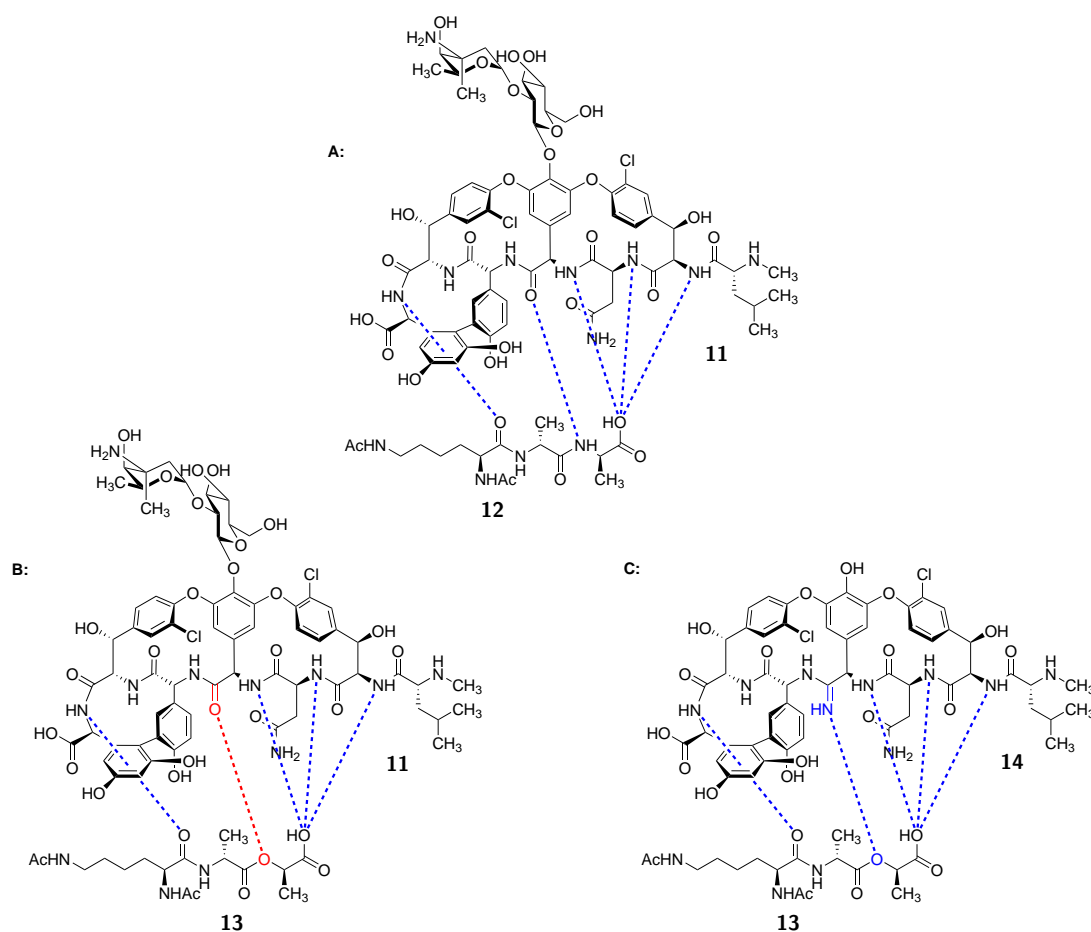
Figure 2. **A:** Vancomycin (**11**) inhibits bacterial cell wall biosynthesis by binding L-Lys-D-Ala-D-Ala (**12**) ends of peptidoglycane strands. **B:** Substitution of **12** by L-Lys-D-Ala-D-Lac (**13**) leads to antibacterial resistance. **C:** Boger and co-workers could overcome resistance by adjusting the chemical structure to vancomycin aglycon analogon **14**. Blue: hydrogen bond; red: repulsion of free electron pairs. [47]

positioned at the end of bacterial peptidoglycan strands, which are integral for cell wall biosynthesis, and thereby withhold necessary precursors. [44,48,52] The most common resistance mechanism is based on substitution of the terminal D-Ala moeity in the peptidoglycan chain by D-Lac as in **13**. [53] This substitution prevents the formation of one hydrogen bond and instead introduces a destabilizing interaction between free electron pairs. The binding affinity between the antibiotic and the ligand is thereby reduced to a thousandth part. [54,55] By replacing the involved amide function in vancomycin (**11**) with an amidine in **14** in a ground-breaking, rationally designed de-novo synthesis [56] Boger and co-workers could prevent the destabilizing interaction with the L-Lys-D-Ala-D-Lac (**13**) ligand. At the same time, a hydrogen acceptor could be maintained for bond formation with the original L-Lys-D-Ala-D-Ala (**12**) ligand. Thereby, the antibiotic activity of **14** was restored against

VRE with equipotency against the unmutated strain.[44,56–59] This example clearly illustrates the importance of SAR studies to improve activity profiles, increase medical potency and overcome resistance. Until today, SAR studies comprise an integral part of drug development, and have also led to the generation of novel, semisynthetic GPAs for the clinic.[60]

Following the Golden Age of natural product drug discovery, less and less natural products, that were eventually approved as drugs, were discovered (1960s to 2000s).[4] Instead, the pursuit of classic approaches frequently resulted in the reisolation of already known compounds.[17,61] At the same time, advances in combinatorial chemistry, where thousands of unique molecules could be synthesized from hundreds of scaffolds, equipped pharmaceutical companies with new promising sources for potential drugs. Robotics and bioassays with facile read-outs enabled companies to search their extensive 'combi-chem' libraries in high-throughput screenings (HTS).[4,62] In contrast, natural products were thought to be incompatible with HTS: The respective collections often consist of extracts as well as partially purified fractions, with low or even immeasurable concentrations of bioactive substances. Moreover, considerable time is required for compound isolation, structural characterization and to determine, whether the isolated molecule is still unknown.[61] Accordingly, pharmaceutical companies backed up from natural product research (1990s and 2000s) and focussed on the screening of synthetic 'combi-chem' libraries. Although more compounds were screened in this period than in the preceding 60 years of drug discovery, only very few promising hits and no marketed drug were discovered.[4] Then, the advent of rapid and cheap DNA sequencing (most notably next-generation sequencing), advances in bioinformatic methods, as well as a better understanding of secondary metabolite biosynthesis opened new avenues to natural product discovery since the 2000s. Sequencing of bacterial genomes, especially from actinomycetes and myxobacteria, has revealed that many more biosynthetic gene clusters (BGCs) are encoded in these genomes than predicted from their expressed secondary metabolomes.[34,63,64] It is estimated that less than 10 % of BGCs are expressed in sufficient quantities to be observed under standard fermentation conditions,[34,35] while the others require special conditions or genetic manipulations to produce their secondary metabolite.[65–68] In addition, less than 1 % of microorganisms on Earth are thought to be readily cultivated.[32,33] DNA extraction from environmental samples and metagenome sequencing could access this inexhaustible source of new microbial genomes.[69,70] Genome analyis with bioinformatic methods, today already allowing prediction of novel biosynthetic pathways as well as (at least) partial structures of novel secondary metabolites,[71–74] bypasses the tedious task of reisolation of

known compounds.[17,64,67] Moreover, improved technology for DNA synthesis, cloning and heterologous expression allows transplantation of BGCs from the sequenced host into well engineered organisms for production of novel natural products.[17,67] These methods can also be used for combinatorial biosynthesis, which attempts to produce novel structures by genetic manipulation and reassembly of biosynthetic pathways.[75,76] In combination with medicinal chemistry combinatorial biosynthesis can further increase the number and diversity of compounds available for drug discovery.[77] All in all, we have only begun to uncover the genetic potential of microorganisms and many novel natural products and thus potent biological activities just await their discovery.

1.2. The Vancomycin Group of Nonribosomal Peptides

For more than half a century glycopeptide antibiotics have been a key weapon in the fight against serious infections with Gram-positive bacteria, including highly virulent MRSA. Several GPAs, including natural products vancomycin (**11**) and teicoplanin (**5**), as well as second-generation semisynthetic derivatives, are currently in use in the clinic.[43,44,48,60]
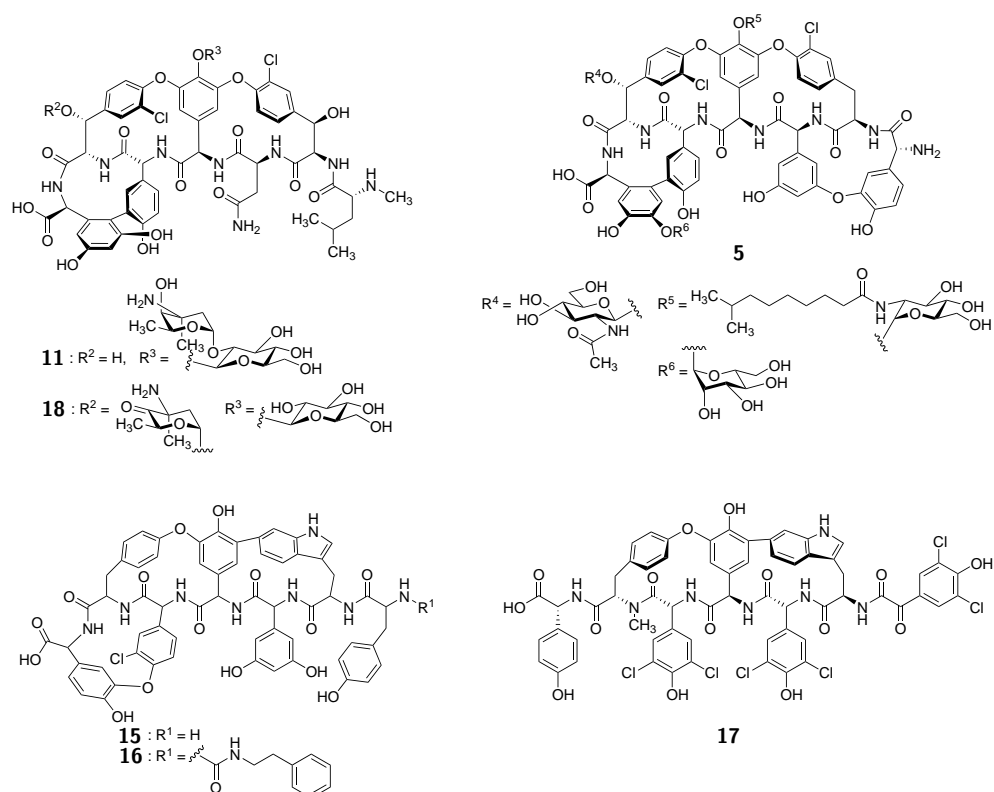
Figure 3. Nonribosomal peptides kistamicin A (**15**) and B (**16**), as well as complestatin (**17**) are closely related to GPAs vancomycin (**11**), balhimycin (**18**), and teicoplanin A$_2$-2 (**5**).

GPA aglycones are comprised of a heptapeptide backbone with a high percentage of non-proteinogenic amino acids. Their aromatic side chains are constricted by biaryl and biarylether bonds, which thereby induce a rigid and well defined 3D structure. This three dimensional shape confers both biological activity – by allowing ideal binding to the molecular target (Figure 2) – and also metabolic stability, for example, against proteases of a target pathogen.[60,78,79] Vancomycin and teicoplanin aglycons are produced by megaenzymes, so called nonribosomal peptide synthetases (NRPS). They are structurally closely related to several other nonribosomal peptides, including balhimycin (**18**), an antibiotic from *Amycolatopsis mediterranei* with an identical aglycon when compared to **11**, complestatin (**17**) and, putatively, kistamicin A (**15**) and B (**16**).[43,44] Complestatin (**17**) is produced by *Streptomyces lavendulae*[80–82] and shows a wide range of biological activities, including antiviral activity against HIV,[83] antibacterial,[84] or neuro-protective[85] effects. The kistamicins **15** and **16**, isolated from *Actinomadura parvosata*, have been found to exhibit potent antiviral activity against Influenza virus type A, and moderate antimicrobial activity against *S. aureus*.[86,87] The kistamicins **15** and **16** as well as complestatin (**17**) thus represent potential new drug candidates. However, the complex structural frameworks of vancomycin-type compounds are a big challenge and current total synthetic routes require an excess of steps, the use of large amounts of metal catalysts resulting in low overall yields.[88] Together, these hurdles do not only render chemical total synthesis economically and environmentally unsustainable for industrial production, but also impede SAR studies to further improve biological activity or overcome resistance. Research into the biosynthetic machinery of vancomycin-type compounds can contribute to facilitate efficient synthetic access to these molecules and their analogues.

1.2.1. Biosynthesis of Vancomycin-Type Nonribosomal Peptides

1.2.1.1. NRPS Assembly Line of Complestatin

Nonribosomal peptides are synthesized on large, multidomain enzymes, the nonribosomal peptide synthetases (NRPS). NRPS multienzymes can be further subdivided into distinct sections, the so-called modules, each of which being responsible for the incorporation of one specific amino acid building block into a linear peptide chain by peptide coupling reactions. The modules consist of a catalytically independent set of domains responsible for substrate recognition, activation, binding, modification, elongation and release.[78,89–91] The mechanism of NRPS-catalyzed peptide formation will be briefly discussed exemplarily for complestatin (**17**). This cyclic heptapeptide is built from proteinogenic amino acids,

tyrosine (Tyr, **19**) and tryptophane (Trp, (**20**)), as well as non-proteinogenic amino acids, 4-hydroxyphenyl glycine (Hpg, (**21**)) and its derivative 4-hydroxyphenyl benzoylformate (Hbf, **22**). Hbf and two out of four Hpg building blocks are chlorinated twice. Moreover, three amino acids are linked by one biarylether (forming ring B-O-D) and one biaryl bond (forming ring D-F), respectively.[81]

The complestatin biosynthetic gene cluster was first sequenced and annotated in 2001.[82] Bioinformatic analysis of the 48.7 kb long DNA section revealed genes encoding for four NRPS proteins, designated ComA, ComB, ComC, and ComD. These proteins harbor seven NRPS modules, M1 to M7 (Scheme 1).[82] Complestatin biosynthesis is initiated by the adenylation domain (A) of the first module M1. It is responsible for the specific recognition and activation of the relevant building block, here **22**. The reactive intermediate is then transferred onto the free thiol group of the phosphopantetheine (ppant) prothetic group of the adjacent peptidyl carrier protein domain (PCP) by utilizing coenzyme A (**23**), establishing a covalent thioester bond between enzyme and substrate. Peptide synthesis proceeds by condensation with a second amino acid, catalyzed by a condensation domain (C), which was recognized, activated, and transferred to the next PCP^2 by the second A^2. At this stage, the peptide attached to PCP^2 can undergo further modifications, such as epimerization or *N*-methylation, by suitable, optional catalytic domains. Indeed, in the biosynthesis of **17** the second amino acid introduced is epimerized from L to D by an epimerization domain (E). Alternative modifications are also feasible: replacing E with, for example, a methylation domain (M) would lead to *N*-methylation of the respective amino acid, as seen for L-Hpg (L-**21**) in module M6. Peptide biosynthesis proceeds along all modules of the complestatin biosynthetic assembly line, thereby attaching all required amino acids to the growing linear peptide precursor. After the last elongation step, the mature peptide reaches the end of the machinery. It can then be cleaved from the synthetase by a thioesterase domain (TE) and be further structurally modified (prior
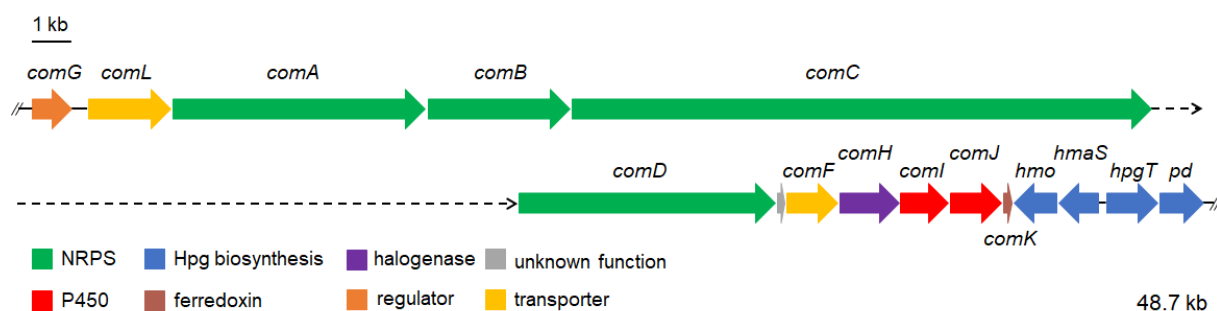
Figure 4. Gene organization of the complestatin biosynthetic gene cluster.[82]
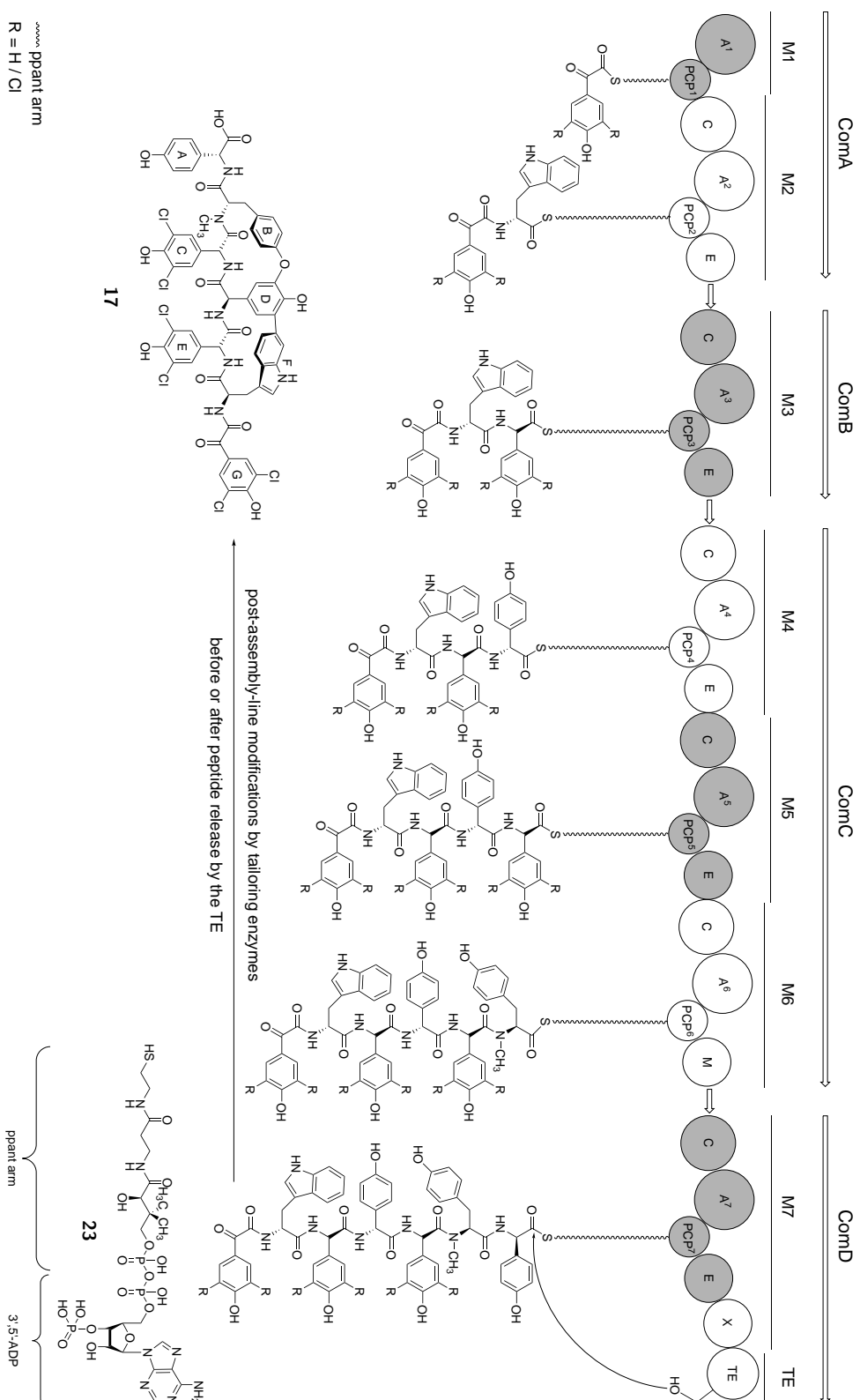
Scheme 1. Biosynthesis of complestatin (**17**) by the NRPS system ComABCD organised into modules M1 to M7. The exact timing of the modification reactions, such as biaryl-bond formation, is unknown. A: adenylation domain; PCP: peptidyl carrier protein domain; C: condensation domain; E: epimerization domain; M: methylation domain; X: X domain; TE: thioesterase domain; ppant: phosphopantetheine moeity of coenzyme A (**23**); 3',5'-ADP: 3',5'-adenosine diphosphate moeity of **23**.

or after the release form the NRPS) by so-called tailoring enzymes. The complestatin BGC harbors a number of genes encoding proteins likely responsible for such post assembly-line modifications.[78,82,90,91] These include a non-heme dependent halogenase (ComH), putatively responsible for chlorination of the respective aromatic residues (two Hpg building blocks as well as Hbf).[82] The exact timing of halogenations remains unclear, although newer studies into teicoplanin and balhimycin systems suggest that halogenation during GPA biosynthesis occurs at the PCP-bound amino acid. In contrast, free amino acids or PCP-bound peptides are not halogenated.[92,93] Other encoded tailoring enzymes are two cytochrome P450 oxidases (ComI and ComJ), which are responsible for biaryl and biarylether bond formation between rings B-O-D and D-F.[82,94,95] One of these oxidases, ComI, presumably requires the assistance of a special NRPS domain to be catalytically active. The X domain is located in the final NRPS module M7, just before the terminal TE domain, and is involved in the recruitment of P450 oxidases to the linear peptide precursor (Chapter 1.2.1.3).[95–97]

1.2.1.2. Biosynthesis of Non-Proteinogenic Amino Acids

NRPS can use all 22 proteinogenic as well as a wide variety of non-proteinogenic amino acids for peptide assembly. Genes required for the biosynthesis of non-proteinogenic amino acids are usually encoded in the respective BGC.[78,90,91] In the case of complestatin (**17**), the genes *hmaS*, *hmo*, *hpgT*, and *pd* are responsible for L-Hpg (L-**21**) formation (Figure 4).[98] The L-Hpg biosynthetic pathway starts with the decarboxylation and hydroxylation of 4-hydroxyphenylpyruvate (**24**) to L-4-hydroxymandelate (**25**) by the enzyme 4-hydroxymandelate synthase (HmaS). The HmaS reaction is coupled with the next enzyme
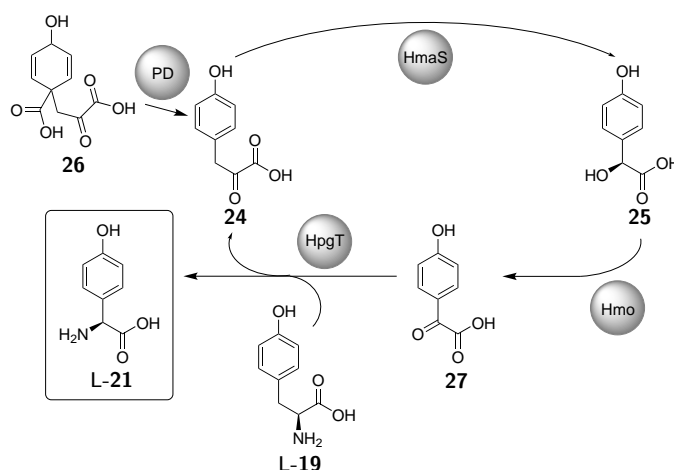
Scheme 2. Catalytic cycle for the biosynthesis of L-Hpg (L-**21**).[98]

of the pathway, L-4-hydroxymandelate oxidase (Hmo), which catalyzes the oxidation of **25** to L-4-hydroxybenzoylformate (**27**). **27** is finally converted to L-Hpg (L-**21**) by Hpg transaminase (HpgT) in a reductive amination reaction, using L-tyrosine (L-**19**) as co-substrate. In the same step, L-**19** is transformed to **24**, which serves again as substrate for HmaS and primes the three enzyme cycle HmaS, Hmo and HpgT for another turn. **24** is also generated by the enzyme prephenate dehydrogenase (PD) from prephenate (**26**), an intermediate in the shikimic acid pathway and a precursor to L-tyrosine (L-**19**).[98,99] Another non-proteinogenic amino acid present in many GPAs, for example, teicoplanin (**5**), vancomycin (**11**), the kistamicins **15** and **16**, as well as balhimycin (**18**) is L-3,5-dihydroxy-phenylglycine (L-Dpg, L-**28**). In these cases, the L-Dpg biosynthesis is, similar to the L-Hpg biosynthesis, directly encoded in the respective BGC by the genes *dpgA*, *dpgB*, *dpgC*, *dpgD*, and *hpgT*.[78,100,101] Enzyme DpgA is a type III polyketide synthase (PKS), which converts four malonyl-coenzyme A (**29**) building blocks to a pentaketide (**30**) and subsequently acts as a Claisen condensation catalyst. In the next step, DpgB and DpgD function as dehydratases on the cyclic DpgA product (**31**), with the following isomerization yielding 3,5-dihydroxyphenylacetyl-CoA (**32**). Importantly, these enzymes greatly accelerate the rate of **31** formation during the DpgA reaction. Enzyme DpgC then converts **32** to 3,5-dihydroxyphenylglyoxylate (**33**) and CoA (**23**).[78,100,101] It has been found, that the oxygenase activity of DpgC is highly unusual since it is independent off an accessory cofactor or metal ion.[100] The exact mode of action remains unclear, although Chen *et al.* have proposed a possible route including a peroxide intermediate.[100] This
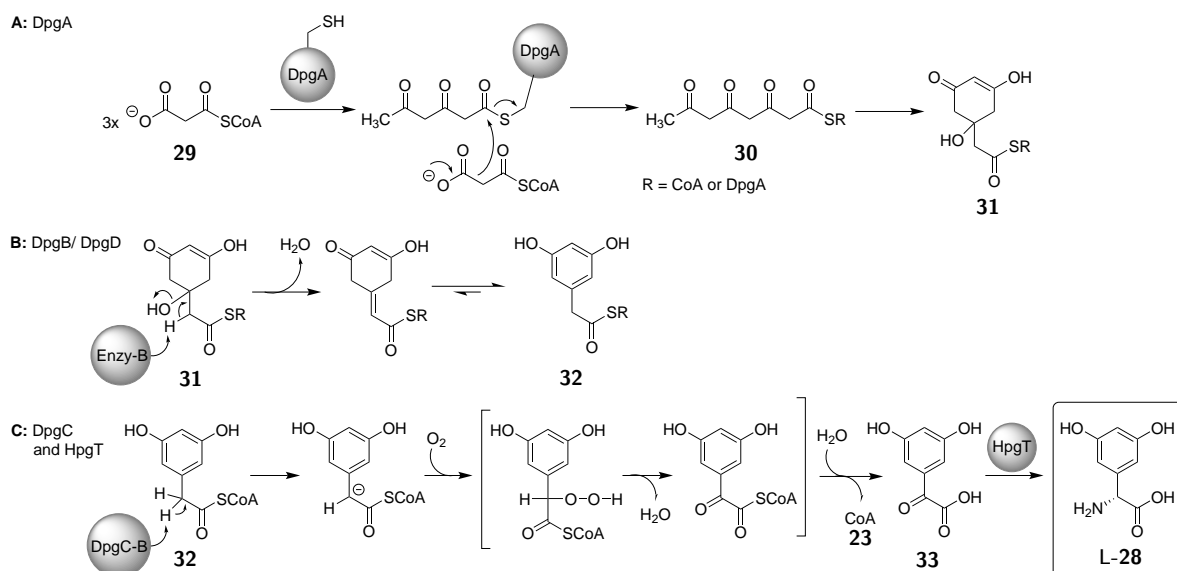
Scheme 3. Catalytic cascade for the biosynthesis of L-Dpg (L-**28**).[100]

mechanism is supported by a study of Widboom *et al.*[102] The final step in L-Dpg biosynthesis consist of the transamination of **33** to L-Dpg (L-**28**), which is mediated by HpgT using tyrosine (**19**) as a co-substrate.[101]

1.2.1.3. Oxidative Phenol Coupling Reactions

Biaryl and biarylether bonds in nonribosomal peptides are formed in oxidative phenol coupling reactions (OPCRs), which are catalyzed by a family of cytochrome P450 enzymes (CYPs).[82,103–106] They have been studied in detail for the biosynthesis of vancomycin-type compounds, in particular using *in vivo* methods. In the case of balhimycin (**18**), the three cross-links are catalyzed by three CYPs, OxyA, OxyB, and OxyC.[103] Gene knockout studies in *Amycolatopsis balhimycina*, the producer of balhimycin (**18**), revealed that OxyA catalyzes formation of ring D-O-E, OxyB formation of ring C-O-D, and OxyC that of ring A-B. The order of ring formation is OxyB - ring one, OxyA - ring two, OxyC - ring three.[107–109] Knockout studies together with *in vitro* experiments on purified, recombinant OxyB strongly indicate that the hexa- or heptapeptide precursors still bound to the NRPS PCP domain are the coupling substrates, rather than the corresponding free acids.[103,110–112] For complestatin biosynthesis, gene knockout studies in heterologous producer *Streptomyces lividans* show that ComI is responsible for biaryl bond formation in ring D-F, and ComJ for biarylether bond formation in ring B-O-D. Here, too, biaryl bond formation seems to be dependent on the already established biarylether bond.[94,95] Until 2015, the mechanism underlying recruitment of CYPs to the GPA peptide precursor was unknown. Then, an *in vitro* study by Cryle and co-workers showed that a conserved domain of unknown function, which is present in all glycopeptide antibiotic NRPS machineries, is
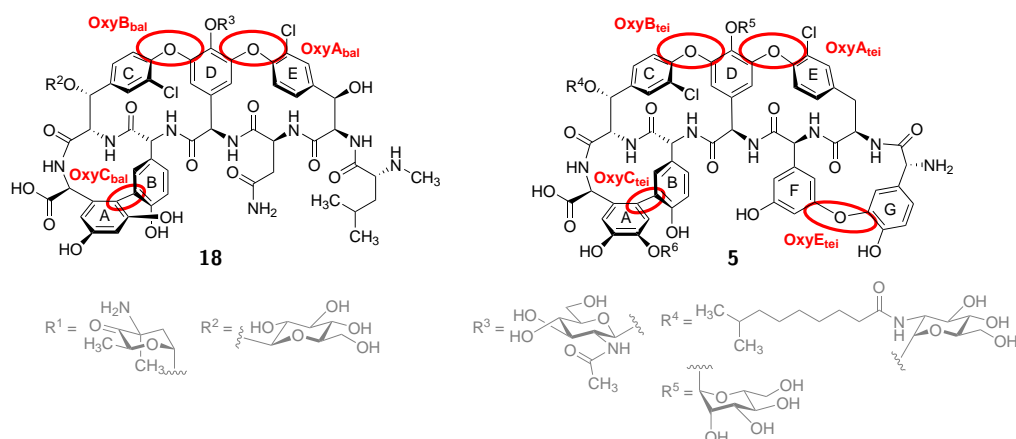
Figure 5. P450 enzymes catalyze biaryl and biarylether bond formation in glycopeptides such as balhimycin (**18**) and teicoplanin (**5**).
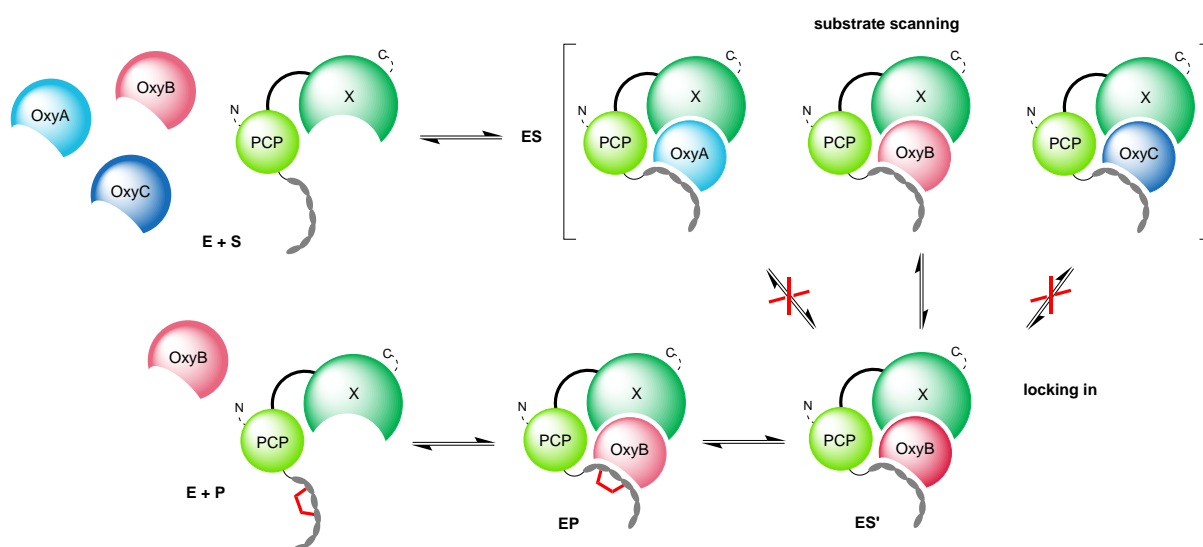
Scheme 4. Recruitment of the correct cytochrome P450 enzyme (E) to the peptide precursor (S) by the X domain and recognition of the peptide cyclization state by the CYP ('substrate scanning'), followed by an induced conformational change of the CYP ('locking in'), catalysis and product (P) release as suggested by Cryle and co-workers.[113]

responsible for the recruitment of CYPs to the NRPS-bound peptide.[96] This domain is encoded in the final NRPS module of glycopeptide antibiotics, just before the terminal TE domain, and is referred to as the 'X' domain. The exact function of the X domain lies in the sequential recruitment of the required CYPs via a shared binding site. Thereby, recruitment seems to function via a process called 'substrate scanning', where different CYPs compete for the respective binding site. Depending on type and number of already installed cross-links, and the enzyme function during GPA biosynthesis, the respective CYP will then catalyze the correct OPCR. Moreover, the same studies demonstrate that certain biaryl/ biarylether bond formations *in vitro* only occur in the presence of an X domain. This indicates that some OPCRs require assistance of the NRPS X domain to ensure the conversion of the PCP-bound peptide into a mature aglycone, and that the PCP alone is not always sufficient to generate a competent substrate.[96,113,114]

In the endeavour to investigate OPCRs during GPA biosynthesis in greater detail, recent studies employ chemo-enzymatic assays.[97,110,112,114–119] For these assays, the linear model peptide precursor of the studied GPA is prepared by solid phase peptide synthesis[120–123] and activated as a thioester. By addition of coenzyme A (**23**), the activated peptide precursor is loaded onto the terminal PCP domain of the respective NRPS via a ppant arm.[97,114,115,117,123] Initially, only isolated PCP domains were used for peptide loading.[110,112] However, since the involvement of X domains in GPA biosynthesis became

known, an X domain supplements the system.[97,114,117–119] For the peptide-enzyme transfer surfactin-phosphapantetheinyltransferase (Sfp), e.g., from *Bacillus subtilis*, can be employed.[97,115,124,125] Subsequently, the PCP-bound peptide precursor is subjected to the actual chemo-enzymatic assay, which includes the relevant CYPs as well as an electron shuttle system. The electron shuttle system provides the CYPs with the required electrons and consists of a reductase (Red), ferredoxin (Fd) as well as glucose dehydrogenase (Gdh). Red transfers electrons from cofactor NADPH to oxidized ferredoxin (Fd_{ox}), while the thus formed reduced ferredoxin (Fd_{red}) serves as an electron donor to CYPs. In turn, CYPs catalyze the OPCRs between aromatic side chains of the peptide precursor while reducing oxygen to water. The product of the chemo-enzymatic assay is the PCP-bound cyclic peptide, which can be cleaved off the enzyme by addition of, for example, methylhydrazine (**34**).[97,110,112,114–119] Regeneration of the actual electron donor, NADPH, can be achieved by oxidation of D-glucose to D-glucono-1,5-lactone by Gdh (derived, e.g., from *Bacillus*

Scheme 5. Chemo-enzymatic synthesis of a simplified teicoplanin model (**37**) by Cryle and co-workers. **A:** The synthesized, linear model peptide precursor of teicoplanin (**r-35**) was cleaved off the SPPS resin and activated as a thioester (**36**) for subsequent use in a chemo-enzymatic assay.[123] **B:** Chemo-enzymatic assay for the (sequential) installation of biaryl and biarylether bonds in **36** with cytochrome P450 enzymes OxyA, OxyB, and OxyE.[116,117]

megaterium).[126] Some GPA biosynthetic gene clusters contain genes for ferredoxin and a corresponding NAD(P)H-dependent ferredoxin oxidoreductase, while in other cases enzymes derived from other parts of the genome are utilized.[82,127] For example, in the complestatin gene cluster *comK* encodes for ferredoxin, whereas the absence of a dedicated oxidoreductase gene suggests that ComK pairs with an endogenous ferredoxin oxidoreductase.[82] Therefore, ComK could be used for the *in vitro* electron shuttle system, while the corresponding reductase has to be adapted from other sources.[97,117] Several studies have already shown that such systems can be used for the *in vitro* construction of biaryl and biarylether bond elements in GPAs. In case of teicoplanin (**5**), for example, all three biarylether bonds have been installed between the aromatic side chains of a simplified peptide precursor in chemo-enzymatic assays. Here, OxyB[116,117] catalyzes formation of ring C-O-D, OxyE[117] formation of ring F-O-D and OxyA[117] that of ring D-O-E (Scheme 5). The formation of the last cross-link, the biaryl bond of ring A-B, has not yet been reported. In a similar study, the construction of one biarylether bond in a simplified complestatin precursor using ComJ as a catalyst has been achieved.[95] Moreover, the actual complestatin peptide precursor has been synthesized in the To. Gulder laboratory by H. Aldemir,[115] and the complestatin biosynthetic machinery as well as the total synthesis of complestatin using chemo-enzymatic assays is currently under investigation.[97,115]

Regrettably, challenges in the synthesis of linear peptide precursors have so far hampered the study of OPCRs in biomedically interesting nonribosomal peptides. The synthetic challenge predominantly is due to the presence of Dpg or Hpg units within the peptide chains, which are very sensitive to epimerization under conditions employed in classic solid phase peptide synthesis (SPPS).[120,128,129] Instead, they require the development of special synthetic protocols. So far, only two methods for the synthesis of vancomycin- and teicoplanin-type precursors, based on Alloc protective groups[120,121] (requiring expensive and difficult palladium-mediated deprotection) or very mild Fmoc deprotection, have been developed, yet only used with the less-problematic non-halogenated analogs of Hpg/Dpg.[122] Moreover, sterically hindering moeities, such as *N*-methyl groups, can hamper SPPS: In case of the complestatin linear peptide precursor (**38**) one *N*-methyl group made SPPS unfeasible. Instead, a complex, highly convergent liquid phase peptide synthesis (LPPS) had to be developed, which is based on the assembly of **38** from two halves.[115]

1.2.2. Isolation, Biological Activity and Chemical Structure of the Kistamicins
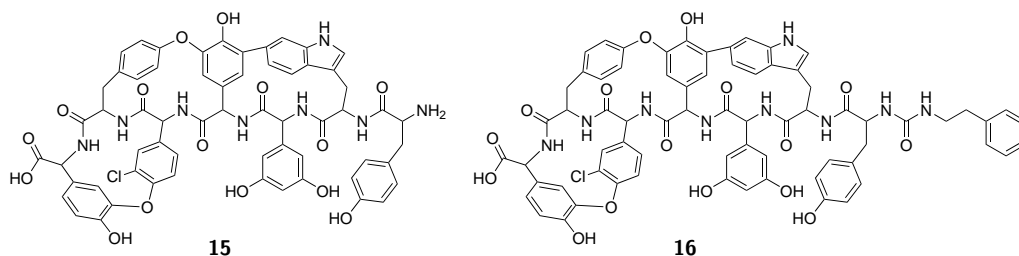
Figure 6. Chemical structure of kistamicin A (**15**) and B (**16**). The absolute stereoconformation of the amino acid building blocks is unknown.[87]

In 1993 Naruse *et al.* reported the isolation of two novel representatives of biaryl-containing nonribosomal peptides, the kistamicins A (**15**) and B (**16**).[86,87] The research group had explored the metabolic potential of actinomycete strain *Actinomadura parvosata* subsp. *kistnae* and isolated **15** and **16** from liquid culture. In *in vitro* assays those compounds exhibited potent antiviral activity against Influenza virus type A as well as moderate antimicrobial activity against Gram-positive bacteria.[86] Structure elucidation by Naruse *et al.* revealed that both molecules consist of a linear heptapeptide chain featuring one Dpg (**28**), two Hpg (**21**), one monochlorinated Hpg (**39**), two tyrosin (**19**) as well as one tryptophan (**20**) units. Kistamicin B (**16**) additionally features an unusal *N*-terminal ureido linkage to a phenylethyl moeity. The absolute stereoconformation of the amino acid building blocks was not established in the study. Moreover, the described peptide chain is constrained in its biologically active conformation by one biaryl and two biarylether bonds.[87] Since the publication of the study by Naruse *et al.*, the kistamicins have attracted little attention. Initial trials at a total chemical synthesis by Beugelmans *et al.* (1997 to 1999)[130,131] featured separation of the cyclic peptide into two halves, **40** and **41**, and
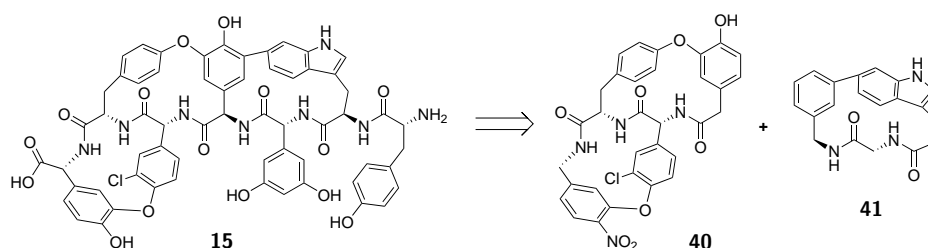
Scheme 6. Retrosynthetic separation of kistamicin A (**15**) as planned by Beugelmans *et al.* The indicated absolute stereoconformation of the amino acids units was assumed by the authors.[130,131]

17

construction of biaryl and biarylether bond elements by cross coupling reactions. Owing to the lack of information on the conformation of stereocenters Beugelmans *et al.* estimated that the amino acids in the kistamicin peptide chain showed the same configuration as the amino acids in the complestatin peptide chain.[130,131] This assumption might be incorrect and an assembly of the whole molecule was never published. However, the potentially incorrectly postulated stereoconformation of the kistamicin backbone disseminates the literature.[43,123,132,133] In a new investigation of the kistamicins **15** and **16** the elucidation of their stereostructure will thus be of paramount importance. Due to their biological activity as well as close structural similarity to clinically important antibiotics vancomycin (**11**) and teicoplanin (**5**) the kistamicins **15** and **16** are interesting as antibacterial and antiviral lead structures as well as from a (bio-)synthetic point of view. Their (bio-)synthetic investigation was therefore chosen as one of two main topics of this work.

1.3. Novel Antimicrobial Coumarins from Myxobacteria

Myxobacteria have attracted considerable attention as prolific producers of natural products. Like actinomycetes, they frequently produce metabolites from multiple structural classes and thus belong to the multi-producers. It is particularly remarkable that many of these compounds exhibit unique structural features relative to compounds known from other microorganisms as well as rare or wholly novel modes-of-action.[38,39] Until today, myxobacterial strains have already yielded at least 100 distinct core structures,[134,135] and some 500 derivatives.[134,135] The majority of these compounds are polyketides, nonribosomal peptides or polyketide-peptide-hybrids, but steroids, terpenoids, alkaloids, and other classes have also been identified. In particular, many bioactive compounds from myxobacteria feature unique structural elements as well as rare or wholly novel modes-of-action. Furthermore, genome sequencing data of myxobacterial strains indicate that their biosynthetic potential is by far greater than previously assumed.[38,39] Thus, myxobacteria represent a promising source for novel bioactive secondary metabolites.

1.3.1. Isolation, Biological Activity and Chemical Structure of the Myxocoumarins

In search of new bioactive natural products the working group To. Gulder and *Syngenta Crop Protection AG* investigated a collection of myxobacterial isolates in high-throughput screens (HTS). During screening the strain *Stigmatella aurantiaca* MYX-030 emerged as a promising source for novel antifungal lead structures. Therefore, the raw culture extract of the *S. aurantiaca* MYX-030 isolate was further separated by chromatography and isolated fractions submitted to bioassyas. Besides already known fungicides, myxothiazole A[136] as well as aurachin A and C,[137] two novel secondary metabolites exhibiting strong antifungal activity were found.[138] Structure elucidation by UV-, 1D- and 2D-NMR-spectroscopy as well as mass spectrometry showed that both compounds, **42** and **43**, consist of a coumarin core structure with a 5-hydroxy-7-nitro substitution pattern, and a long, saturated alkyl chain at C-4. Moreover, a stereocenter was found at C-4 of compound **42**, but its absolute configuration remains unknown.[138] There are only few nitrogen containing coumarins found in nature, with bacterial aminocoumarins such as novobiocin (**10**, Figure 1) being the most well known examples.[139] The nitrogen substitution pattern together with the unusually long alkyl chain constitutes an unique structure and the newly discovered compounds **42** and **43** thus represent a novel class of secondary metabolites. Due to their origin and core structure they were named myxocoumarins A (**42**) and B (**43**).[138] The isolated amount
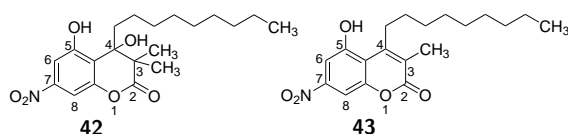
Figure 7. Chemical structures of myxocoumarin A (**42**) and B (**43**).[138]

of myxocoumarin B (**43**) was not sufficient to verify the initially detected antifungal activity. However, in assays against a series of agrochemically important pathogenic fungi myxocoumarin A (**42**) showed a strong and broad range activity comparable to commercial standard fungicides, albeit at a somewhat lower activity level. The growth of pathogens such as *Botrytis cinerea*, *Fusarium culmorum*, and *Phaeosphaeria nodorum* was completely inhibited (MIC_{100}: Minimum Inhibitory Concentration) at $2\,mg\,mL^{-1}$, and *Magnaporthe grisea* as low as at $0.7\,mg\,mL^{-1}$ in liquid culture assays. Neither insecticidal nor herbicidal bioactivity was observed.[138]

1.3.2. (Bio-)Synthesis of the Myxocoumarins

The research group To. Gulder and *Syngenta Crop Protection AG* postulated that the biosynthesis of myxocoumarin A (**42**) and B (**43**) proceeds via precursor molecule 5-nitroresorcinol (**44**),[138] which has already been found to be produced by myxobacterial strains *S. aurantiaca* and *S. erecta*. These myxobacteria strains synthesize **44** from erythrose-4-phosphate (**45**) and phosphoenol-pyruvate (**46**) via phloroglucinol (**47**).[140,141] Putative *O*-acetylation of **44** with β-keto acid **48**, which may originate from fatty acid biosynthesis, would result in an intermediate ester **49**. Intermediate **49** could undergo C,C-bond formation by nucleophilic attack of the aromatic system to the side chain keto
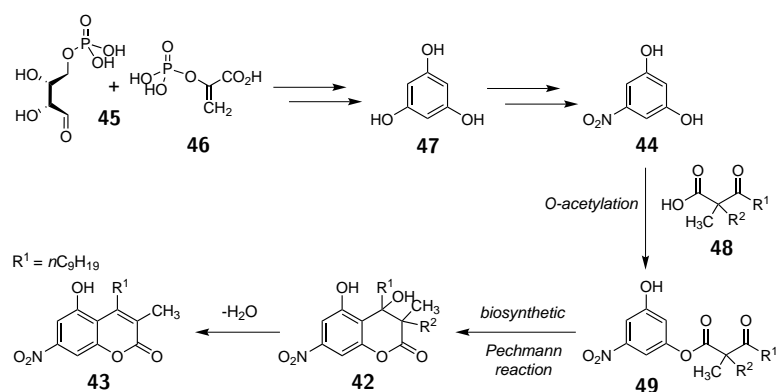
Scheme 7. Postulated biosynthetic pathway to myxocoumarins A (**42**) and B (**43**) (with $R^2 =$ CH_3 for **42** and $R^2 =$ H for **43**).
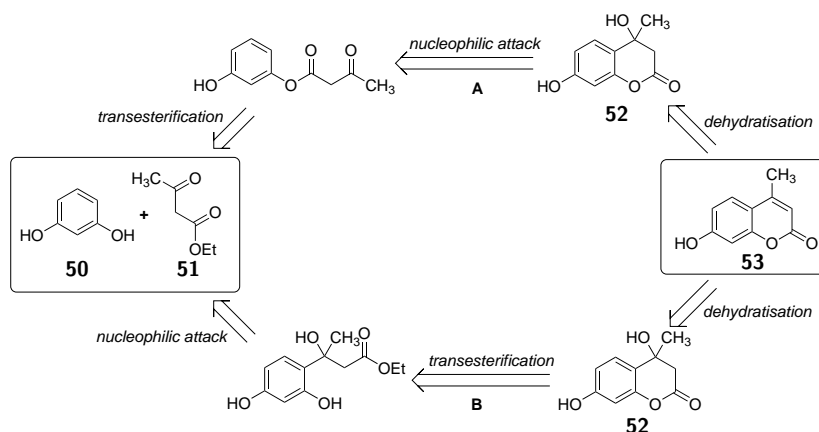
Scheme 8. Formation of a 4-substituted coumarin (**53**) by Pechmann condensation reaction of a phenol (**50**) and a β-keto ester (**51**). The reaction proceeds in the presence of a catalyst, such as a Brønsted or Lewis acid.

function, similar to a Pechmann reaction. The direct product would be myxocoumarin A (**42**), with myxocoumarin B (**43**) formation after condensation (Scheme 7).[138] The Pechman condensation reaction is widely used in synthetic chemistry to synthesize 4-substituted coumarins. Here, a phenol **50** reacts with a β-keto ester **51** or α, β-unsaturated carboxylic acid in the presence of a catalyst (e.g. Brønsted or Lewis acids) to intermediate **52**.[142–152] Despite various studies, it has not definitively been established whether the formation of **52** proceeds via transesterification followed by nucleophilic attack (Scheme 8, route A) or the other way around (Scheme 8, route B).[144,153–157] In any case, formation of **52** is succeeded by dehydratisation to final coumarine **53**.

Since the Pechmann reaction utilizes cheap, easily available starting materials and a wide range of phenols and β-keto esters have already been employed,[144,146–152,158–160] it represents a straightforward approach to the biomimetic total synthesis of myxocoumarins A (**42**) and B (**43**). Moreover, variation of reactants would allow the generation of diverse myxocoumarin derivatives in a single step. Efficient access to the myxocoumarins **42** and **43** and derivatives would, in turn, facilitate close examination of their activity profiles, including possible antifungal activities against clinically relevant pathogens, such as *Candida albicans* and *C. krusei*. Therefore, the chemical synthesis of myxocoumarin B (**43**) and various derivatives for structure-activity relationship studies was chosen as the second goal of this thesis.

Chapter 2

Aims

Natural products represent a main source for leads and drugs in medicinal applications.[2,5,6] Due to the continued emergence of new, untreatable diseases and pathogens developing resistance against existing pharmaceuticals, research and development into new scaffolds with potent biological activities is of fundamental importance.[13,24,26,28] The putative nonribosomal peptides kistamicin A (**15**) and B (**16**),[86,87] as well as the coumarins myxocoumarin A (**42**) and B (**43**)[138] not only feature desirable antimicrobial activity profiles, but also intriguing molecular architectures. Thus, this interdisciplinary thesis aimed at the investigation of the (bio-)synthesis of kistamicin A (**15**) and myxocoumarin B (**43**). It can thereby provide innovative new approaches for the efficient preparation of **15** and **43** for structure-activity relationship studies and drug development.
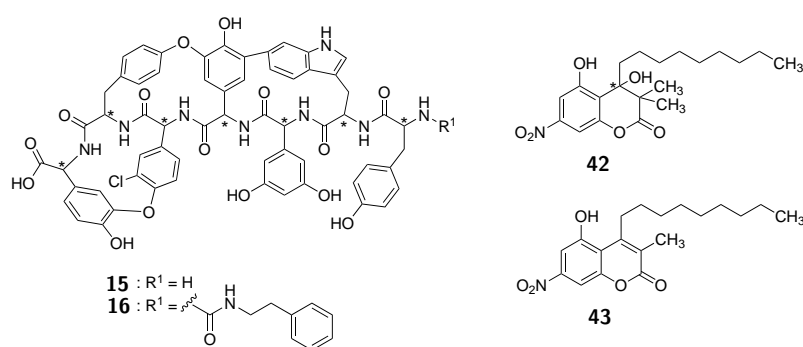
Figure 8. Chemical structures of the putative nonribosomal peptides kistamicin A (**15**) and B (**16**) as well as of the coumarins myxocoumarin A (**42**) and B (**43**). Unknown stereocenters are indicated with *.

2. Aims

The kistamicins A (**15**) and B (**16**) are cyclic peptides, consisting of a linear, monochlorinated heptapeptide chain featuring several non-proteinogenic amino acid building blocks. One biaryl and two biarylether bonds between the aromatic side chains constrict the peptides in their rigid three dimensional structures and confer biological activity. Previous studies[87] did not determine the absolute configuration of the amino acid building blocks. **16** additionally features an unusual *N*-terminal ureido linkage to a phenylethyl moeity.[87] The kistamicins **15** and **16** show close structural similarity to nonribosomal peptides, such as the clinically important gylcopeptide antibiotic vancomycin (**11**) and especially to the highly bioactive peptide complestatin (**17**).[43,44,48,60] Due to their promising biological activity, as well as their close ties to vancomycin-type compounds the kistamicins **15** and **16** are interesting from a (bio-)synthetic point of view and represent new pharmaceutical lead structures. However, as for all vancomycin-type compounds their complex structural framework poses a big challenge: previous total synthetic routes for this class of nonribosomal peptides require an excess of steps, the use of large amounts of metal catalysts and result in low overall yields.[88] Together, these hurdles impede structure-activity relationship studies to further improve biological activity or overcome resistance, thus generating new drug candidates. Research into the biosynthetic machinery of vancomycin-type compounds can contribute to facilitate efficient access to these molecules and their analogues.

Analysis of the respective biosynthetic gene clusters (BGC) reveals the presence of mega-enzymes, so called nonribosomal peptide synthetases (NRPS), which produce the linear peptide backbones. Further modifications, like halogen atoms or biaryl and biarylether bonds, are introduced by tailoring enzymes, such as halogenases or cytochrome P450 enzymes.[78,89–91] An innovative, straightforward approach to an efficient synthesis of vancomycin-type compounds is the combination of solid phase peptide synthesis (SPPS) of the linear peptide precursors with the use of cytochrome P450 enzymes as biocatalysts to perform the regio- and stereoselective phenol oxidative coupling reactions (OPCRs) for biaryl and biarylether bond formation. In one of two main projects, the present thesis aimed to identify the yet unknown biosynthetic machinery encoding the kistamicins **15** and **16**, to determine their absolute stereostructure, and to develop an SPPS strategy for the synthesis of the kistamicin A linear peptide precursor (**54**). In addition, enzymes required for OPCRs were to be cloned from the kistamicin biosynthetic gene cluster and heterologously expressed in *E. coli*. This thesis thereby aimed to provide the foundation for the chemo-enzymatic total synthesis of **15** and further its investigation as a promising antiviral and antibiotic drug lead.
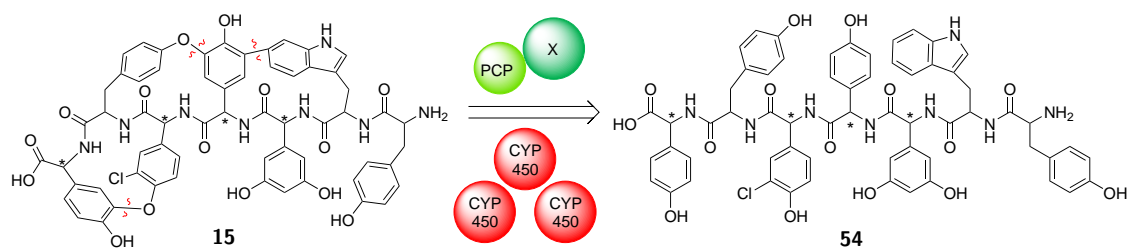
Scheme 9. Chemo-enzymatic synthesis of kistamicin A (**15**) from its linear peptide precursor (**54**). This thesis aims at the chemical synthesis of **54**. (Stereocenters prone to epimerization are indicated with *.) Another goal is the identification of cytochrome P450 enzymes, the terminal PCP and X domain putatively encoded in the kistamicin biosynthetic gene cluster. These enzymes are to be cloned and heterologously expressed for later use in chemo-enzymatic assays.

As a first step in this direction, the genomic DNA of kistamicin producer *A. parvosata* was to be isolated in this thesis and sent to a commercial provider for genome sequencing and assembly. This work should then bioinformatically analyze the *A. parvosata* genome and strive to identify and examine the kistamicin BGC. Based on the close structural similarity between kistamicin A (**15**) and complestatin (**17**), it could be assumed that the kistamicin BGC is highly related to that of **17**. The identified genes encoding cytochrome P450 enzymes as well as the terminal peptidyl carrier protein (PCP), and X domain, which will later be required for the enzymatic catalysis of OPCRs, should be cloned and heterologously expressed in *Escherichia coli*. Moreover, as exemplified for **17** (Chapter 1.2.1.1), the structure of nonribosomal peptides can often directly be used to predict the encoding biosynthetic assembly line and *vice versa*.[89] This principle of co-linearity was to be utilized in the course of this work to tentatively elucidate the expected absolute stereostructure of **15** based on NRPS domain architecture, thereby providing crucial information for the synthetic work. Subsequently, this thesis aimed at the synthesis of the respective linear peptide precursor **54** via SPPS. A known major challenge here was the sensitivity of non-proteinogenic amino acids 3,5-dihydroxyphenylglycine (Dpg, (**28**)) and 4-hydroxyphenyl glycine (Hpg, (**21**)) to epimerization under traditional SPPS conditions. Previously, Alloc chemistry[120,121] has been used to address this issue, which required tedious synthesis of all protected building blocks as well as expensive palladium-mediated cleavage. However, the kistamicin heptapeptide chain (**54**) contains no less than one Dpg (**28**) and three Hpg (**21**) or Hpg-derived (**39**) building blocks, thus making cheaper Fmoc chemistry with its easy access to protected amino acids - commercially available in a large range or simple to synthesize - highly desirable. For this purpose, application of a mild Fmoc protection strategy[122] in combination with the use of an SPPS resin featuring a sterically hindered linker appeared to be promising. All in all, those efforts endeavored to

contribute to the development of a chemo-enzymatic strategy to achieve the first total synthesis of kistamicin A (**15**) and facilitate structure-activity relationship studies.

In the second main project, this thesis focussed on the yet barely investigated myxocoumarin B (**43**), which unlike kistamicin A (**15**) belongs to a novel class of secondary metabolites. Myxocoumarin B (**43**) is comprised of an unusual 5-hydroxy-7-nitro substitution pattern as well as a long, saturated alkyl chain, and was suspected to exhibit potent antifungal activities.[138] It was deemed to be particularly interesting to examine its activity profiles, including possible antifungal activities against clinically relevant pathogens such as *Candida albicans* and *C. krusei*. Therefore, this thesis endeavored to gain synthetic access to **43**. The Pechmann reaction was expected to be the most straightforward approach and utilizes cheap, easily available starting materials, as well as a wide range of phenols and β-keto esters.[142–152] Variation of reactants should allow the generation of diverse myxocoumarin B derivatives in a single step and thus facilitate structure-activity relationship studies. For the investigation of activity profiles and structure-activity relationship studies all myxocoumarins synthesized in this work were to be sent to cooperation partners.
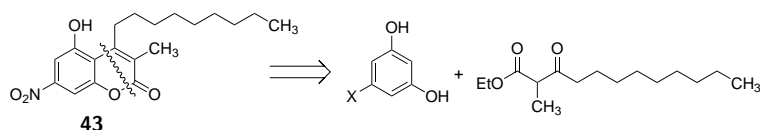
Scheme 10. Chemical synthesis of myxocoumarin B (**43**) via Pechmann reaction. Variation of phenols and β-keto esters would allow generation of diverse derivatives in a single step.

Chapter 3

Results and Discussion

3.1. Myxocoumarin B and Derivatives

3.1.1. Synthesis and Initial Biological Evaluation of Myxocoumarin B

In 2013 the research group To. Gulder reported the isolation of a novel class of secondary metabolites from myxobacteria, the myxocoumarins A (**42**) and B (**43**) (Figure 9).[138] This thesis contributed to the developedment of a short, efficient chemical total synthesis of myxocoumarin B (**43**). The obtained compound was sent for a first assessment of its biological potential to the research group Nikodinovic-Runic in Belgrade. The results of these studies were published in 2019 and are part of the present thesis.[161]
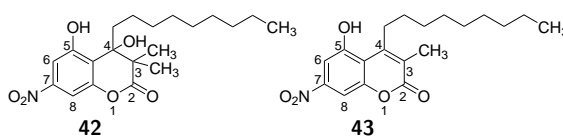
Figure 9. Chemical structures of myxocoumarin A (**42**) and B (**43**).[138]

The total synthesis of myxocoumarin B (**43**) features a Pechmann reaction and late stage palladium-catalyzed nitration as key steps (Scheme 11). The Pechmann reaction gives elegant access to the 3,4-substituted coumarin core by reacting a phenol with a β-keto ester in the presence of a catalyst. Solvent free microwave irradiation of the reactants and use of TFA as a catalyst were established as the optimal reaction conditions in an adaption of a protocol by Katkevičs *et al.*[146] (K. Kusserow). Alkyl substituents at C-3 and C-4 were introduced by the use of a β-keto ester (**55**), which in turn was available

3. Results and Discussion
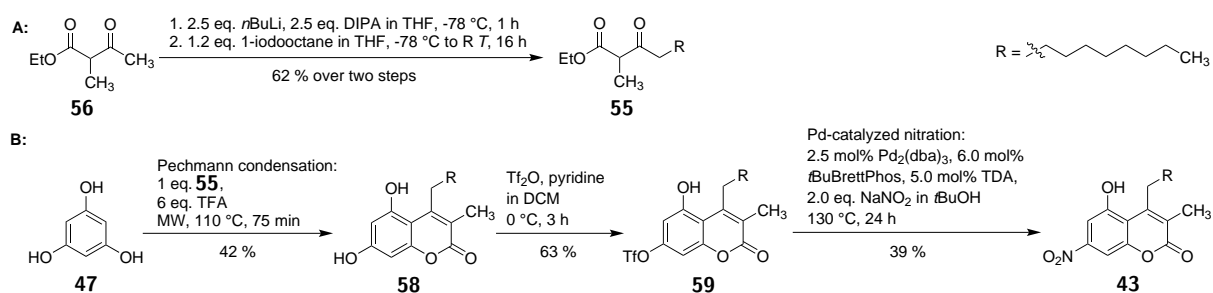
Scheme 11. Chemical total synthesis of myxocoumarin B (**43**). **A:** Synthesis of required β-keto ester **55**; **B:** synthesis of **43** via Pechmann reaction and palladium-catalyzed nitration with 10 % overall yield.

by regio-selective alkylation of ethyl 2-methylacetoacetate (**56**) with iodo-octane in 62 % yield (K. Kusserow). Simultaneous installation of the nitro-substituent at C-7 was not possible due to the moeities deactivating effect on the respective phenol (J. Müller). When an alternative strategy, involving later stage nitration of a C-7 iodo substituent at the coumarin core (**57**) by Ullmann-type copper catalyzed reaction as developed by Saito *et al.*,[162] was employed, only traces of **43** were detected by MS analysis (K. Kusserow). Instead, a triflate functionality was reagioselectively introduced at C-7 with 63 % yield. The triflate moiety served as the substrate in a palladium-catalyzed nitration as developed by the Buchwald laboratory,[163] and **43** was obtained as the direct product with 39 % yield (J. Müller, G. Hertrampf). The To. Gulder laboratory thereby established a three step total synthesis of **43** with approximately 10 % overall yield. The obtained material was subjected to *in vitro* as well as *in vivo* assays by the research group Nikodinovic-Runic. The planktonic growth of antifungal pathogens *Candida albicans* and *C. krusei* was not affected by **43** (A. Pavic). *In vitro* cytotoxicity of **43** against healthy human lung fibroblasts cell line MRC-5 and was found to be moderate (IC$_{50}$ at 100 μM) (A. Pavic). No toxic response (lethal nor teratogenic) was elicited by **43** in *in vivo* assays against zebrafish embryos upon treatment with doses up to 250 μM, with all embryos dying upon exposure to 500 μM (A. Pavic).

PAPER

Check for updates

Synthesis and initial biological evaluation of myxocoumarin B†

Jonas I. Müller,‡[a] Kalina Kusserow,‡[a] Gesa Hertrampf,[a] Aleksandar Pavic,[b] Jasmina Nikodinovic-Runic[b] and Tobias A. M. Gulder ⓘD *[a,c]

The myxocoumarins A and B from *Stigmatella aurantiaca* MYX-030 are natural products featuring unusual nitro- and long-chain alkyl substitution. While myxocoumarin A was shown to exhibit strong antifungal properties, the antifungal potential of myxocoumarin B was not yet assessed due to low production titers during initial isolation. We therefore developed a total synthesis of myxocoumarin B that involves a late-stage Pd-catalyzed nitration of the coumarin core. The availability of synthetic material facilitated the initial evaluation of the bioactivity of myxocoumarin B, which revealed a lack of activity against medically relevant *Candida* sp. and low cytotoxicity *in vitro* against human fibroblasts (MRC-5) and *in vivo* (zebrafish).

Introduction

Natural products have a huge impact as leads and drugs in medicine and agrochemical applications. Owing to the continued emergence of new and untreatable maladies and the evolution of pathogens exhibiting resistance against existing treatment options, the continued discovery of novel scaffolds with potent biological activities is of utmost importance. A rich source of such natural products with truly novel molecular architectures and activity profiles are myxobacteria. These mostly soil-dwelling δ-proteobacteria are particularly talented producers of unusual ribosomal and non-ribosomal peptides and polyketides with often unprecedented modes of actions.[1–5] It is thus not surprising that many myxobacterial natural products have intensely been studied in recent years. Intriguing examples include the antineoplastic pretubulusin (**1**),[6] the antifilarial corallopyronin A (**2**),[7,8] the antimalarial chlorotonil A (**3**),[9,10] the cystobactamids, *e.g.* **4**, as potent antibiotics against Gram-negative bacteria,[11] and the antifungal soraphen A1α (**5**) (Fig. 1).[12] In 2013, we reported the discovery of the myxocoumarins A (**6**) and B (**7**) from liquid cultures of *Stigmatella aurantiaca* MYX-030.[13] Compound **6** was shown to

exhibit promising inhibitory activities against a wide range of fungal pathogens, including *Botrytis cinerea*, *Magnaporthe grisea*, *Phaeospaeria nodorum*, *Blumeria graminis*, and *Fusarium culmorum*. Due to the initially low production titers of myxocoumarin B (**7**), combined with the unfortunate inability to regrow the producing strain from all existing stock cultures, the antifungal potential of **7** could not be evaluated during this study. Given the significant activity of **6**, we thus decided to develop a short synthetic access towards **7** to facilitate its biological evaluation.

Results and discussion

A broad range of synthetic approaches for the construction of coumarin core structures can be found in the literature, including Perkin,[14] Reformatsky,[15] Wittig[16] and Knoevenagel[17] reactions. The most widely used method is the Pechmann condensation[18] by which phenolic substrates are fused to β-keto esters catalysed by a (Lewis) acid. Disconnecting the respective building blocks accordingly in myxocoumarin B (**7**) leads to resorcinol **8** with substitution at *C*-5 and β-keto ester **9**, which in turn can readily be prepared from **10** by regio-selective alkylation with iodo-octane (Scheme 1A). Owing to the activation of the *ortho/para* aromatic positions by the phenolic functions in **8**, the introduction of suitable substituents at *C*-5 within this substrate is not directly possible. An elegant access to the corresponding nitro-substituted resorcinol **13** is provided by Pd-catalyzed nitration of aryl chlorides as developed by the Buchwald laboratory.[19] Following this approach, the commercially available substrate **11** was smoothly converted to **12** in 75% yield (Scheme 1B). BCl₃-promoted *O*-demethylation gave

[a]Biosystems Chemistry, Department of Chemistry and Center for Integrated Protein Science Munich (CIPSM), Technical University of Munich, Germany.
E-mail: tobias.gulder@ch.tum.de
[b]Institute of Molecular Genetics and Genetic Engineering, University of Belgrade, Vojvode Stepe 444a, Belgrade, Serbia
[c]Technische Universität Dresden, Chair of Technical Biochemistry, Bergstraße 66, 01062 Dresden, Germany
†Electronic supplementary information (ESI) available. See DOI: 10.1039/c8ob02273a
‡These authors contributed equally to this work.

1966 | *Org. Biomol. Chem.*, 2019, **17**, 1966–1969

This journal is © The Royal Society of Chemistry 2019
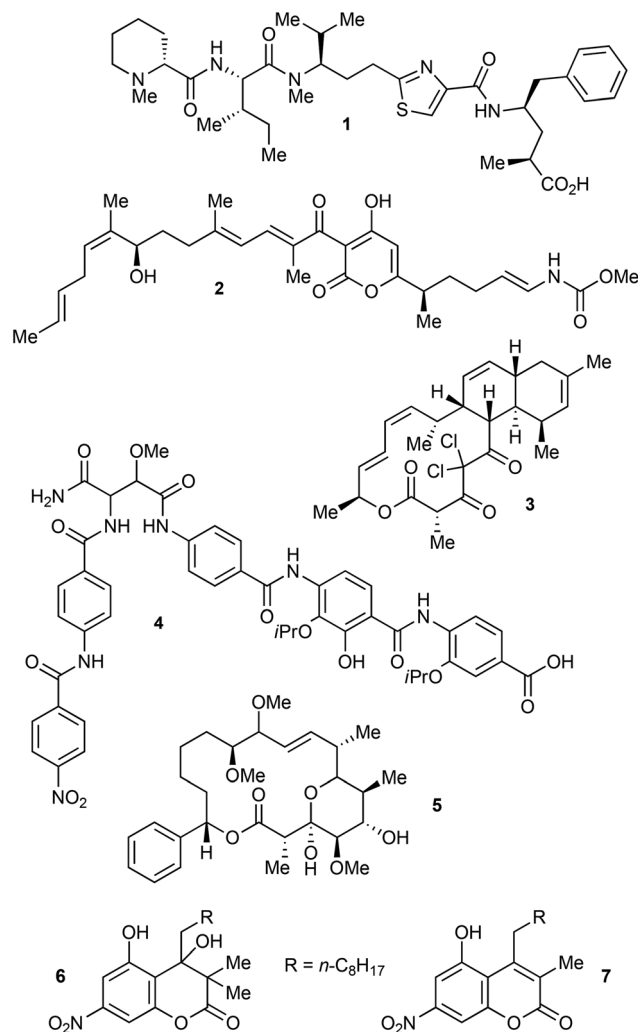
Fig. 1 Structures of myxobacterial compounds 1–7.

13 in 71% yield. Despite literature precedence for the utilization of nitro-substituted phenols in Pechmann reactions to yield the corresponding nitro coumarins,[20] our attempts to convert 13 to 7 under various condensation conditions failed to provide the desired product (data not shown). As this likely can be rationalized by the deactivation of resorcinol 13 due to the nitro substitution, we decided to use an alternative strategy that involves a later-stage nitration at the fully elaborated coumarin core (Scheme 1C). Following a protocol by Thorn *et al.* one of the hydroxy functions in phloroglucinol (14) was replaced by an amino group by stirring of this substrate in ammonium hydroxide.[21] The resulting crude hydrochloride 15 was directly used in a Sandmeyer reaction to generate 5-iodoresorcinol (16) in 49% yield over two steps. The latter was utilized in a Pechmann condensation reaction with 9 to deliver iodo coumarin 17, although only in unsatisfactory 5% yield. 17 was subjected to an Ullmann-type copper-catalyzed nitration utilizing a protocol by Saito *et al.*[22] However, only traces of myxocoumarin B (7) were detectable in the reaction mixture by MS analysis.
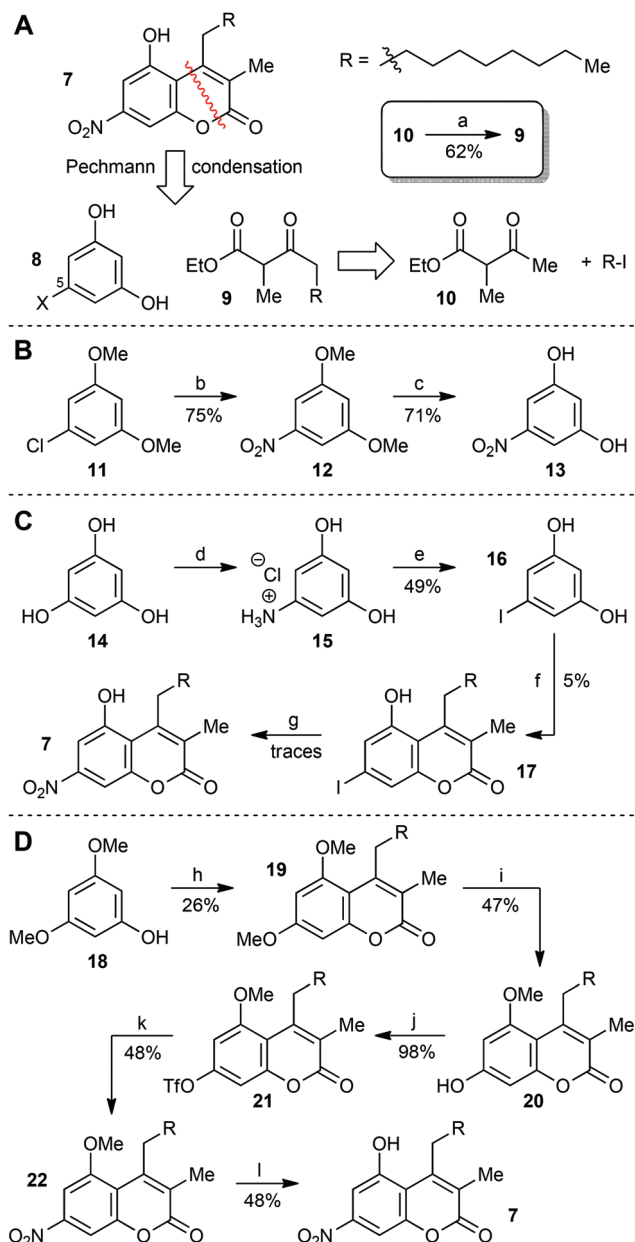
Scheme 1 A. Retro-synthetic analysis (A), unsuccessful synthetic routes (B, C) and first generation synthesis (D) of myxocoumarin B (7). Reagents and conditions: (a) 1. *n*BuLi (2.5 eq.), DIPA (2.5 eq.), THF, −78 °C, 1 h. 2. 10 (1.0 eq.), 0 °C, 1 h. 3. R–I (1.2 eq.), −78 °C to rt, 16 h. (b) Pd₂(dba)₃ (0.5 mol%), tBuBrettPhos (1.2 mol%), TDA (5.0 mol%), NaNO₂ (2 eq.), tBuOH, 130 °C, 24 h. (c) BCl₃ (2.0 eq.), toluene, 130 °C, 40 h. (d) 1. NH₄OH, RT, 18 h. 2. HCl (e) 1. H₂SO₄ (3.6 eq.), NaNO₂ (2.8 eq.), H₂O, 0 °C, 15 min. 2. KI (3.6 eq.), H₂O, rt, 5.5 h (49% over two steps d, e). (f) 9 (1.0 eq.), SSA (9.6 eq.), CHCl₃, 65 °C, 20 h. (g) CuI (0.2 eq.), KNO₂ (1.1 eq.), 18-crown-6 (1.0 eq.), *N,N*′-diethylethylenediamine (0.4 eq.), DMF, 100 °C, 26 h. (h) 9 (1.0 eq.), TFA (6.2 eq.), MW, 100 °C, 30 min. (i) BCl₃ (2.1 eq.), toluene, 110 °C, 18 h. (j) Tf₂O (1.3 eq.), pyridine (2.0 eq.), DCM, 0 °C to rt, 30 min. (k) Pd₂(dba)₃ (0.5 mol%), tBuBrettPhos (1.2 mol%), TDA (5.0 mol%), NaNO₂ (2 eq.), tBuOH, 130 °C, 24 h. (l) LiCl (6.0 eq.), DMF, 155 °C, 18 h. All yields are un-optimized.

This journal is © The Royal Society of Chemistry 2019

Org. Biomol. Chem., 2019, **17**, 1966–1969 | **1967**

Given the power of the Pd-catalyzed nitration utilized in route B for the synthesis of **12**, we decided to evaluate this reaction for the introduction of the desired nitro functionality later in the synthetic route. Coumarin **19** was constructed by a Pechmann condensation of 3,5-dimethoxyphenol (**18**) with **9** in 26% yield. Likely owing to a shielding effect of the long-alkyl chain R located at the coumarin core, a regioselective *O*-demethylation of the desired methoxy functionality using BCl₃ was possible in 47% yield. The resulting phenol **20** was converted into **21** by triflation in 98% yield. Triflate **21** served as the substrate in a Pd-catalyzed nitration again following the Buchwald protocol.[19] This indeed delivered the fully functionalized coumarin core **22** in 48% yield. The latter was *O*-deprotected in 48% yield to conclude the first total synthesis of **7**. Taken together, this sequence gave access to myxocoumarin B (**7**) in five steps from **18**, with an overall yield of approx. 3%.

To improve the unsatisfyingly low yield of the overall sequence, we set out to further streamline the synthetic route. As the yields of Pechmann condensation generally improve with the electron-richness of the employed phenols, we decided to first construct the corresponding dihydroxy derivative of **19**, coumarin **24**. This compound is available by condensation of phloroglucinol **23** with **9** in 42% yield. Given the apparent protective effect of the long-chain *n*-octyl group as observed in the selective *O*-demethylation of **19** to **20** shown above, we hypothesized that the desired activation by regioselective mono *O*-triflation of **24** should be possible, as well as the following Pd-catalyzed nitration reaction in the presence of the free phenol. Indeed, selective triflation proceeded smoothly to deliver **25** in 51% yield, along with >5% of the bis-triflated analog and 18% of re-isolated starting material **24**, thus leading to 63% of **25** brsm (Scheme 2). Compound **25** was subjected to Pd-catalyzed nitration with slightly modified conditions (5-fold increase of Pd-catalyst and ligand), furnishing 39% of the natural product **7**. Overall, this route thus reduced the number of required steps from five (Scheme 1D) to only three, accompanied by a more than 3-fold increase in overall yield.

Table 1 MIC values, IC₅₀ and LC₅₀ for myxocoumarin B (**7**)

Test	*C. albicans* MIC[a] [μg mL⁻¹]	*C. krusei* MIC[a] [μg mL⁻¹]	MRC-5 IC₅₀[b] [μg mL⁻¹]	Zebrafish LC₅₀[c] [μg mL⁻¹]
Compound 7 μM	>500	>500	35 100	120 344

[a] Minimum inhibitory concentration. [b] Calculated IC₅₀ value corresponds to the concentration required to inhibit 50% of cell growth. [c] Calculated LC₅₀ value corresponds to the concentration required to kill 50% of the embryos.
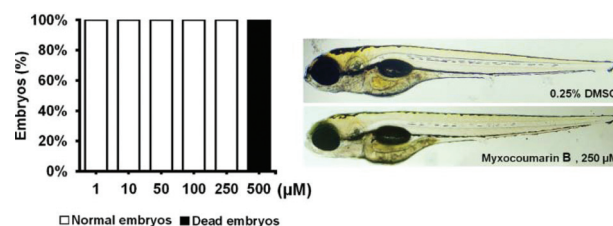
Fig. 2 Toxicity assessment of myxocoumarin B (**7**) in zebrafish embryos exposed to different concentrations and representative images of zebrafish embryos at 114 hpf upon treatment with 250 μM of myxocoumarin B (**7**) compared to a DMSO control.

Having sufficient amounts of synthetic myxocoumarin B (**7**) in hands we next aimed at the evaluation of its antifungal effects against fungal pathogens, *i.e.*, *Candida albicans* and *C. krusei* (see ESI† for details). Unfortunately, no effect on the planktonic growth of these strains was observed up to concentrations of 500 μg mL⁻¹ (Table 1).

Cytotoxicity of **7** *in vitro* was assessed against healthy human lung fibroblasts cell line MRC-5 and was found to be moderate (IC₅₀ at 100 μM). Toxicity of **7** *in vivo* was determined using zebrafish embryos and found to be at least 3-fold lower (IC₅₀ at 344 μM). Importantly, myxocoumarin B (**7**) elicited no toxic response (lethal nor teratogenic) in zebrafish embryos upon treatment with doses up to 250 μM, with all embryos dying upon exposure to 500 μM (Fig. 2).

Conclusions

In conclusion we developed a short total synthetic access to **7** with a late-stage Pd-catalyzed nitration reaction as the key step. Our work nicely showcases that the Pd-catalyzed nitration reaction developed by Buchwald *et al.*[19] can readily be applied to elaborate substrates such as the employed triflated coumarin derivatives **21** and **25** and therefore constitutes a valuable transformation for late-stage natural product functionalization. The obtained synthetic material facilitated initial assessment of the biological properties of **7**, which, in contrast to myxocoumarin A (**6**), despite only small structural differences, revealed a complete lack of activity against fungal pathogens and low toxicity both *in vitro* and *in vivo*. Access to **7** now permits investigations into the likely ecological functions of

Scheme 2 Alternative synthetic route to myxocoumarin B (**7**) *via* triflate **25**. Reagents and conditions: (a) **9** (1.0 eq.), TFA (6.2 eq.), MW, 110 °C, 75 min. (b) Tf₂O (1.2 eq.), pyridine (3.0 eq.), DCM, 0 °C, 4 h. (c) Pd₂(dba)₃ (2.5 mol%), *t*BuBrettPhos (6.0 mol%), TDA (5.0 mol%), NaNO₂ (2 eq.), *t*BuOH, 130 °C, 24 h.

1968 | *Org. Biomol. Chem.*, 2019, **17**, 1966–1969

This journal is © The Royal Society of Chemistry 2019

the myxocoumarin class of natural products in their natural producer. This work is currently ongoing in our laboratory.

Conflicts of interest

There are no conflicts to declare.

Acknowledgements

Notes and references

1 S. C. Wenzel and R. Müller, *Nat. Prod. Rep.*, 2007, **24**, 1211.
2 S. C. Wenzel and R. Müller, *Curr. Opin. Drug Discovery Dev.*, 2009, **12**, 220.
3 S. C. Wenzel and R. Müller, *Mol. Biosyst.*, 2009, **5**, 567.
4 T. F. Schäberle, F. Lohr, A. Schmitz and G. M. König, *Nat. Prod. Rep.*, 2014, **31**, 953.
5 J. Herrmann, A. Abou Fayad and R. Müller, *Nat. Prod. Rep.*, 2017, **34**, 135.
6 A. Ullrich, Y. Chai, D. Pistorius, Y. A. Elnakady, J. E. Herrmann, K. J. Weissmann, U. Kazmaier and R. Müller, *Angew. Chem., Int. Ed.*, 2009, **48**, 4422.
7 H. Irschik, R. Jansen, G. Höfle, K. Gerth and H. Reichenbach, *J. Antibiot.*, 1985, **38**, 145.
8 T. F. Schäberle, A. Schiefer, A. Schmitz, G. M. König, A. Hoerauf and K. Pfarr, *Int. J. Med. Microbiol.*, 2014, **304**, 72.
9 K. Gerth, H. Steinmetz, G. Höfle and R. Jansen, *Angew. Chem., Int. Ed.*, 2007, **47**, 600.
10 J. Held, T. Gebru, M. Kalesse, R. Jansen, K. Gerth, R. Müller and B. Mordmüller, *Antimicrob. Agents Chemother.*, 2014, **58**, 6378.
11 S. Baumann, J. Herrmann, R. Raju, H. Steinmetz, K. I. Mohr, S. Hüttel, K. Harmrolfs, M. Stadler and R. Müller, *Angew. Chem., Int. Ed.*, 2014, **53**, 14605.
12 K. Gerth, N. Bedorf, H. Irschik, G. Höfle and H. Reichenbach, *J. Antibiot.*, 1994, **47**, 23.
13 T. A. M. Gulder, S. Neff, T. Schüz, T. Winkler, R. Gees and B. Böhlendorf, *Beilstein J. Org. Chem.*, 2013, **9**, 2579.
14 W. H. Perkin, *J. Chem. Soc.*, 1877, **31**, 388.
15 R. L. Shriner, *Org. React.*, 1942, **1**, 1.
16 I. Yavari, R. Hekmat-Shoar and A. Zonouzi, *Tetrahedron Lett.*, 1998, **39**, 2391.
17 G. Brufola, F. Fringuelli, O. Piermatti and F. Pizzo, *Heterocycles*, 1996, **43**, 1257.
18 (*a*) H. v. Pechmann, *Ber. Dtsch. Chem. Ges.*, 1884, **17**, 929; (*b*) S. M. Sethna and N. M. Shah, *Chem. Rev.*, 1945, **36**, 1.
19 B. F. Fors and S. L. Buchwald, *J. Am. Chem. Soc.*, 2009, **131**, 12898.
20 (*a*) S. S. Bahekar and D. B. Shinde, *Tetrahedron Lett.*, 2004, **45**, 7999; (*b*) A. Hegedüs and Z. Hell, *Catal. Lett.*, 2006, **112**, 105; (*c*) E. Rafiee, A. Fakhri and M. Joshaghani, *J. Heterocycl. Chem.*, 2013, **50**, 1121.
21 M. A. Thorn, G. H. Denny and R. D. Babson, *J. Org. Chem.*, 1975, **40**, 1556.
22 S. Saito and Y. Koizumi, *Tetrahedron Lett.*, 2005, **46**, 4715.

3.1.2. Strong Antibiotic Activity of the Myxocoumarin Natural Product Family In Vivo and In Vitro

The synthesis of myxocoumarin B (**43**) via Pechmann reaction not only facilitated access to the natural product, but also to a wide range of derivatives. By variation of phenols and β-keto esters the To. Gulder research group introduced various phenol and alkyl substituents to the myxocoumarin B coumarine core. These substituents include hydroxy, methoxy, acyl, iodo, chloro, amine, dimethylamino, and nitrogen moeities at the aromatic ring as well as *n*-alkyl chains of diverse length (CH_3 to $C_{13}H_{27}$), one branched alkyl chain ($C_3H_6CH(CH_3)_2$), and one fluorinated alkyl chain ($C_3H_6C_6F_{13}$) at C-4. In total, 38 structural analogs and two simple coumarins (**62** and **63**) were synthesized. Compounds **64**, **65**, **66**, **67**, **68**, **69**, **70**, **71**, **72**, **73**, **57**, **62**, and **63** originated from this thesis. Subsequently, the biological potential of this library of compounds was investigated by the research group Nikodinovic-Runic in Belgrade. The results are currently evaluated for potential patenting and will be published in due course (Section 5.10.2).
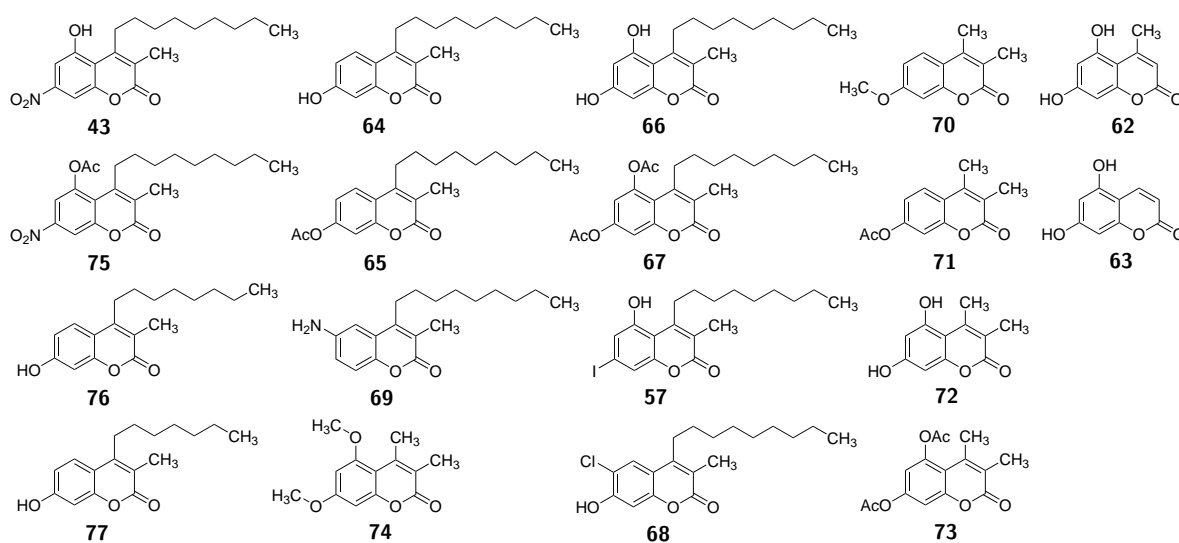
Figure 10. Myxocoumarin B (**43**) and selected derivatives. **43**, and derivatives **64** to **67**, **69** as well as **75** to **74** show strong biological activities; derivatives **64** to **63** were synthesized in this work (section 5.10.2).

The antimicorbial activity profile of the myxocoumarin B (**43**) library was assessed in minimum inhibitory concentration (MIC) assays and the compounds embryotoxicity determined in an *in vivo* zebrafish model. In these assays, **43** and several analogs exhibited a strong antibacterial activity and specificity against Gram-positive strains *S. aureus* (including clinical isolates), *S. aureus* MRSA, *B. subtilis*, and *Enterococcus faecium*. **43**

and several analogs also only showed toxicity against zebrafish embryos above the range of concentrations active against the tested microorganisms. For mono- and dihydroxylated compounds a clear structure-activity relationship could be observed, with the activity correlating with the length of the alkyl side chain. Mono-hydroxylated compounds exhibited an increased antibacterial activity when substituted with C_7 to C_9 alkyl chains, while dihydroxylated compounds showed significant activity with C_4 to C_{11} alkyl chains. When analysing the structure-acitivity relationships with regards to embryotoxicity, it becomes evident that longer side chains also lead to drastically decreased toxicity. Overall, the natural product **43**, the acetylated natural product **75**, and a structural analog of **77**, which carried two hydroxy groups at the aromatic ring in addition to an *n*-C_7 alkyl chain, showed the most promising activity profiles. However, **43** lost some antibacterial activity upon prolonged storage.

Based on these encouraning results, **75** and the cogener of **77** were used to combat *S. aureus* infections in an *in vivo* zebrafish embryo model. Analyses of zebrafish embryo survival and bacterial proliferation showed that both compounds could efficiently cure the infected zebrafish embryos and performed even better than vancomycin, which was used as the positive control. 2xMIC of **75** completely eliminated the infection. Moreover, multistep resistance selections of *S. aureus* against both compounds indicated a low likelihood that this bacterial strain will rapidly develop resistance to the tested myxocoumarins. (For further reference see Section 5.10.2.)

The results of the present study are especially promising since the investigated myxocoumarin B family represents a novel class of secondary metabolites, which can very easily and cheaply be accessed by chemical synthesis. With myxocoumarin B (**43**), compound **75** and the **77** cogener this study could thus identify promising new drug candidates for the treatment of *S. aureus* infections.

3.2. Kistamicin A

3.2.1. Genome Sequencing of *Actinomadura Parvosata*

To elucidate the biosynthesis of the antimicrobial peptides kistamicin A (**15**) and B (**16**) the genome of their producer, actinomycete strain *Actinomadura parvosata* subsp. *kistnae*, was sequenced and annotated. The results of these studies were published in 2017 and are part of the present thesis.[164] For this purpose, the genomic DNA (gDNA) of *A. parvosata* was isolated and its quality photometrically determined. gDNA of sufficient quantity and purity was sent to *GATC Biotech AG* and the genome sequenced by PacBio single molecule real-time (SMRT®) sequencing. From this, approximately 173,600 reads with an average size of 5.9 kb and a N50 read length of 10 kb were obtained. Assembly of this data by *GATC* gave 36 polished contigs with an average coverage of 61.3. In total, this leads to a size of the chromosome of this strain of approximately 13.56 Mbp and thus places it among the largest actinobacterial genome sequences known to date.[165] The G+C content is 71.7 %. The genome was annotated using the RAST server[166] and the software Geneious,[167] resulting in the annotation of 12,784 coding DNA sequences (CDSs) as well as 17 rRNA genes and 63 tRNA loci.

The assembled genome was analysed with the program antiSMASH,[73] whereby 32 biosynthetic gene clusters of secondary metabolites could be found (Table 1). *A. parvosata* thus belongs to the actinomycete strains that harbour the most biosynthetic gene clusters found in this group of bacteria.[165] The identified gene clusters[168] include six PKS clusters (three type I PKS, one type II PKS, one type III PKS, one unspecified), ranging from 41 kb to 105 kb in size, as well as four NRPS systems, ranging from 32 kb to 54 kb, and two mixed PKS-NRPS (both >100 kb). Moreover, seven terpene biosynthetic gene clusters (21 kb to 22 kb), four lassopeptide, three bacteriocin, two siderophore, one lantipeptide, one mixed lassopeptide-lantipeptide, one thiopeptide, and one unspecified cluster were detected. Only two of these clusters show 100 % similarity to already characterized pathways, namely those encoding geosmin and 2-methylisoborneol. All other biosynthetic loci have low similarity to previously characterized gene clusters. Together with the sheer number of biosynthetic gene clusters these findings underline the high potential of this organism for the discovery of novel bioactive secondary metabolites. The complete genome sequence was deposited at EMBL under Accession No. [PRJEB19374].

3. Results and Discussion

Table 1. Biosynthetic gene clusters identified with the program antiSMASH[73] in the genome of *Actinomadura parvosata* subsp. *kistnae.* Locus tags reference to the complete genome sequence deposited at EMBL under Accession No. [PRJEB19374].

Cluster	Predicted Product	Similarity to Characterized BGCs	Size [kb]	Locus Tag
1	lassopeptide	-	22.4	KIS93_00180 to KIS93_00195
2	bacteriocin	daptomycin (6 %)	44.8	KIS93_00382 to KIS93_00426
3	terpene	2-methylisoborneol (100 %)	21.1	KIS93_00682 to KIS93_00704
4	NRPS	oxazolomycin (9 %)	36.2	KIS93_00706 to KIS93_00740
5	lassopeptide	-	22.5	KIS93_01184 to KIS93_01215
6	bacteriocin	BE-14106 (7 %)	12.2	KIS93_01352 to KIS93_01361
7	lassopeptide	-	22.6	KIS93_02120 to KIS93_02139
8	PKS (unspecific)	calicheamicin (2 %)	42.3	KIS93_02170 to KIS93_02209
9	PKS (type II)	xantholipin (40 %)	50.1	KIS93_02405 to KIS93_02457
10	terpene	-	20.9	KIS93_02610 to KIS93_02626
11	PKS (type III)	alkylresorcinol (66 %)	41.0	KIS93_02758 to KIS93_02802
12	unspecified	-	43.8	KIS93_03416 to KIS93_03458
13	lantipeptide	AmfS (60 %)	22.6	KIS93_03479 to KIS93_03498
14	terpene	platensimycin (5 %)	21.0	KIS93_03500 to KIS93_03520
15	terpene	-	20.9	KIS93_04047 to KIS93_04063
16	NRPS	spinosad (5 %)	53.6	KIS93_04473 to KIS93_04516
17	NRPS	kistamicin (100 %) (Chapter 3.2.3)	48.0	KIS93_04799 to KIS93_04829
18	siderophore	-	13.1	KIS93_05212 to KIS93_05221
19	bacteriocin	-	10.8	KIS93_05408 to KIS93_05419
20	PKS (type I)	azicemicin (6 %)	45.5	KIS93_05794 to KIS93_05831
21	siderophore	-	13.2	KIS93_06152 to KIS93_06165
22	terpene	geosmin (100 %)	22.2	KIS93_06185 to KIS93_06206
23	PKS-NRPS	WS9326 (25 %)	104.8	KIS93_06483 to KIS93_06563
24	terpene	chlortetracycline (5 %)	21.0	KIS93_08896 to KIS93_08912
25	terpene	-	21.1	KIS93_10353 to KIS93_10375
26	thiopeptide	K-252a (5 %)	29.5	KIS93_10803 to KIS93_10831
27	PKS (type I)	herboxidiene (2 %)	48.2	KIS93_11563 to KIS93_11603
28	PKS-NRPS	marinophenazines (34 %)	133.0	KIS93_11709 to KIS93_11826
29	NRPS	pyridomycin (7 %)	69.1	KIS93_12224 to KIS93_12280
30	lassopeptide	-	14.5	KIS93_12303 to KIS93_12316
31	lassopeptide-lantipeptide	indigoidine (80 %)	86.0	KIS93_12452 to KIS93_12541
32	NRPS	coelichelin (54 %)	32.6	KIS93_12574 to KIS93_12597

Journal of Genomics

Short Research Paper

Complete Genome Sequence of *Actinomadura Parvosata* Subsp. *Kistnae*, A Rich Source of Novel Natural Product (Bio-)Chemistry

Kalina Kusserow and Tobias A. M. Gulder✉

Biosystems Chemistry, Department of Chemistry and Center for Integrated Protein Science Munich (CIPSM), Technical University of Munich, Lichtenbergstraße 4, 85748 Garching, Germany.

✉ Corresponding author: E.Mail: tobias.gulder@ch.tum.de

Abstract

The soil dwelling actinomycete strain *Actinomadura parvosata* subsp. *kistnae* is the producer of the antiviral antibiotics kistamicin A and B. Genome sequencing and bioinformatic analysis revealed the presence of the kistamycin biosynthetic gene cluster responsible for the formation of these non-ribosomal peptides as well as an impressive number of yet uncharacterized biosynthetic pathways. This includes polyketide, ribosomal and non-ribosomal peptide and a large number of terpenoid biosynthetic loci encoding yet unknown natural products. The genomic data of this strain is thus a treasure trove for genome mining for novel functional metabolites and new biocatalysts.

Key words: *Actinomadura parvosata* subsp. *kistnae*, whole-genome sequencing, Kistamicin.

Introduction

Actinomycetes are well known to produce a wealth of secondary metabolites with diverse biological activities and complex structures [1]. Included in this broad range of compounds are antibiotics, antivirals and anticancer agents from important natural product classes, such as peptides, polyketides or terpenes [2]. Unfortunately, many more promising secondary metabolites encoded in actinomycete genomes remain undiscovered because their biosynthetic gene clusters are not expressed under standard fermentation conditions [3, 4]. In recent years, these putatively silent gene clusters have become accessible by genome mining [5, 6]. In our search for yet undiscovered natural product chemistry and biochemistry we selected the actinomycete strain *Actinomadura parvosata* subsp. *kistnae* (strain designation S382-8) as a promising target organism. It was isolated from a soil sample collected near the Kistna River in India and shown to produce the potent antiviral antibiotics kistamicin A and B [7]. These secondary metabolites exhibit potent antiviral activity against influenza virus type A as well as antimicrobial activity against Gram-positive bacteria and putatively belong to the class of non-ribosomal peptides [7]. To get further insights into the kistamicin biosynthesis and to explore the strains whole metabolic potential we sequenced the genome of *Actinomadura parvosata* subsp. *kistnae* (Table 1).

In the draft genome sequence we indeed identified the 48 kb kistamicin biosynthetic gene cluster, showing the typical NRPS assembly line organization [8, 9]. Furthermore, *in silico* analysis with the program antiSMASH [8] revealed 33 other gene clusters for the biosynthesis of secondary metabolites. This places *Actinomadura parvosata* subsp. *kistnae*

among those actinomycete strains that harbour the most biosynthetic gene clusters found in this group of bacteria [10]. antiSMASH [8] revealed six ribosomal and non-ribosomal peptide Synthetase (NRPS) systems ranging from 30 kb to 69 kb in size as well as six polyketide synthase (PKS) clusters ranging from 34 kb to 51 kb (3 type I PKS, 1 type II PKS, 1 type III PKS, 1 unspecified) and two mixed NRPS-PKS (both >100 kb). Additionally, seven terpene biosynthetic gene clusters (21 kb to 22 kb), 4 lassopeptide, 3 bacteriocin, 2 lantipeptide, 1 mixed lassopeptide-lantipeptide, 2 siderophore and 1 unspecified cluster have been detected by antiSMASH. Only two of these clusters show 100 % similarity to already characterized pathways, namely those encoding geosmin and 2-methylisoborneol. All other biosynthetic loci have low similarity to previously characterized gene clusters. Together with the sheer number of biosynthetic gene clusters these findings underline the high potential of this organism for the discovery of novel chemistry and biochemical transformations useful in biomedicine and biotechnological applications.

Table 1. Genome features of *Actinomadura parvosata* subsp. *kistnae*.

Features	Chromosome
Length (bp)	13,559,781
G+C content (%)	71.7 %
CDS	12784
rRNA genes	17
tRNA genes	63
Biosynthetic gene clusters	34

The genomic sequence of *Actinomadura parvosata* subsp. *kistnae* was obtained by PacBio single molecule real-time (SMRT®) sequencing. The raw data was generated from three SMRT cells, resulting in a total of approx. 173.600 reads with an average size of 5.9 kb and a N50 read length of 10 kb. Assembly of this data by GATC resulted in 36 polished contigs with an average coverage of 61.3. In total this leads to a size of the chromosome of this strain of approx. 13.56 MBp and thus places it among the largest actinobacterial genome sequences known to date [10]. The G+C content is 71.7%. Importantly, approx. 10% of the very large genome of the strain is devoted to the biosynthesis of specialized metabolites, as shown by antiSMASH analysis [8] described above. The genome was annotated using the RAST server [11] and the software Geneious version 8.1.8 [12], resulting in the annotation of 12784 coding sequences (CDSs) as well as 17 rRNA genes and 34 tRNA loci.

The complete genome sequence was deposited at EMBL under Accession Np. [PRJEB19374].

Competing Interests

The authors have declared that no competing interests exist.

References

1. Nett M., Ikeda H., Moore B.S. Genomic basis for natural product biosynthetic diversity in the actinomycetes. Nat. Prod. Rep. 2009; 26: 1362-1384.
2. Nawani N., Aigle B., Mandal A., Bodas M., Ghorbel S., Prakash D. Actinomycetes: Role in biotechnology and medicine. Biomed. Res. Int. 2013; 2013: 687190.
3. Hertweck C. Hidden biosynthetic treasures brought to light. Nat. Chem. Biol. 2009; 5: 450-452.
4. Devine R., Hutchings M.I., Holmes N.A. Future directions for the discovery of antibiotics from actinomycete bacteria. Emerging Topics in Life Sciences 2017; [Epub ahead of print].
5. Rutledge P.J., Challis G.L. Discovery of microbial natural products by activation of silent biosynthetic gene clusters. Nat. Rev. Micro. 2015; 13: 509-523.
6. Ziemert N., Alanjary M., Weber T. The evolution of genome mining in microbes – a review. Nat. Prod. Rep. 2016; 33: 988-1005.
7. Naruse N., Tenmyo O., Kobaru S., Hatori M., Tomita K., Hamagishi Y., Oki T. New antiviral antibiotics, kistamicins A and B I. Taxonomy, production, isolation, physico-chemical properties and biological activities. J. Antibiot. 1993; 46: 1804-1811.
8. Weber T., Blin K., Duddela S., et al. antiSMASH 3.0 a comprehensive resource for the genome mining of biosynthetic gene clusters. Nucleic Acids Res. 2015; 43: W237-243.
9. Bachmann B.O., Ravel J. Methods for in silico prediction of microbial polyketide and nonribosomal peptide biosynthetic pathways from DNA sequencing data. Methods Enzymol. 2009; 458: 181-217.
10. Doroghazi J.R., Metcalf W.W. Comparative genomics of actinomycetes with a focus on natural product biosynthetic genes. BMC Genomics 2013; 14: 611-623.
11. Aziz R.K, Bartels D., Best A.A., et al. The RAST Server: Rapid Annotations using Subsystems Technology. BMC Genomics 2008; 9: 75-89.
12. Kearse M., Moir R., Wilson A., et al. Geneious Basic: an integrated and extendable desktop software platform for the organization and analysis of sequence data. Bioinformatics. 2012; 28: 1647-1649.

3.2.2. Isolation of Kistamicin A from *Actinomadura Parvosata*

To confirm the ability of actinomycete strain *Actinomadura parvosata* subsp. *kistnae* to produce the kistamicins A (**15**) and B (**16**), this work intended to isolate those secondary metabolites from the bacterial fermentation broth. For this purpose, a culture of *A. parvosata* in ISPI-I medium was incubated for 12 d at 28 °C and subsequently extracted with ethyl acetate. After removal of ethyl acetate, the residue was subjected to LC-MS analysis. However, **15** was found only in small quantities and **16** not at all. In a new attempt, a procedure published by Nazari *et al.*[132] was adapted: *A. parvosata* was precultured on oatmeal agar (4 d, 30 °C) and the grown mycellium used to inoculate modified R4 medium. Mycellium grown from those precultures (3 d, 30 °C) was then used to inoculate GFM medium. After incubating those cultures for 9 d at 30 °C, the mycellium was collected and extracted with acetone. After removal of acetone, the residue was dissolved in methanol. HPLC analysis of the crude extract showed exclusive production of a single compound (Figure 11) and purification by semi-preparative HPLC yielded 69 mg L^{-1} of a colourless solid. Isolation of **15** was confirmed by HR-MS and NMR. However, LC-MS analysis of the crude residue before purification did not detect **16**. This work finaly established the *A. parvosata* strain in our lab as producer of **15** and thus set the stage for the identification of the corresponding BGC.
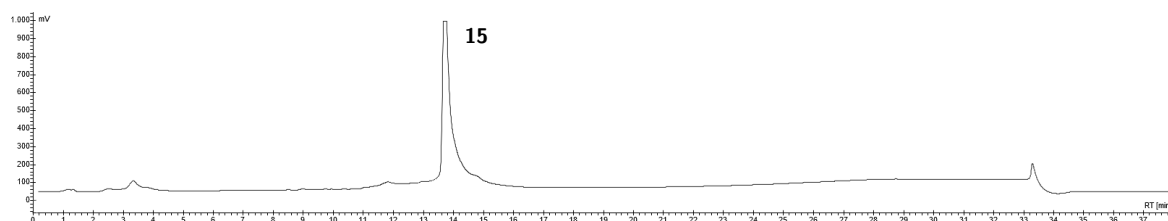
Figure 11. HPLC analysis of the crude extract of *Actinomadura parvosata* cultures showed exclusive production of kistamicin A (**15**).

3.2.3. Bioinformatic Analysis of the Kistamicin Biosynthetic Gene Cluster

In the search for the kistamicin A (**15**) and B (**16**) biosynthetic gene cluster the genome of the producer strain *A. parvosata* was analyzed *in silico.* Submission of the assembled genome to the program antiSMASH[73] led to the identification of 32 clusters for secondary metabolite biosynthesis, including six NRPS systems (Chapter 3.2.1). The principle of co-linearity[89] (as exemplified for complestatin in Chapter 1.2.1.1) suggests that the structure of nonribosomal peptides **15** and **16** directly corresponds to the structure of the encoding biosynthetic assembly line and *vice versa.* In this regard, one gene cluster appeared to be particularly relevant after antiSMASH[73] analyis and was further investigated. Since some open reading frames (ORFs) in the respective DNA region seemed to be disrupted, those DNA segments (390 bp to 1.2 kbp) were PCR amplified from gDNA and resequenced by Sanger sequencing at *GATC Biotech AG*. Alignment of the resequenced segments with the genome with the program Geneious[167] showed deletions of single bases in several cases. The respective DNA regions were corrected, CDSs annotated again with Geneious[167] and then submitted to the program BLAST®. Based on close homology to already known proteins derived from other organisms it was surmised which proteins were involved in the kistamicin biosynthesis. The identified 48.0 kb DNA region (Figure 12A, Table 2) shows the expected close similarity with the complestation biosynthetic gene cluster[82] (Chapter 1.2.1.1) in organisation and size. Besides the four genes forming the NRPS assembly line (*kisA*, *kisB*, *kisC*, *kisD*), all genes necessary for Hpg (**21**) (*hmaS*, *hmo*, *hpgT*, *pd*) and Dpg (**28**) biosynthesis (*dpgA*, *dpgB*, *dpgC*, *dpgD*, *hpgT*) were found.
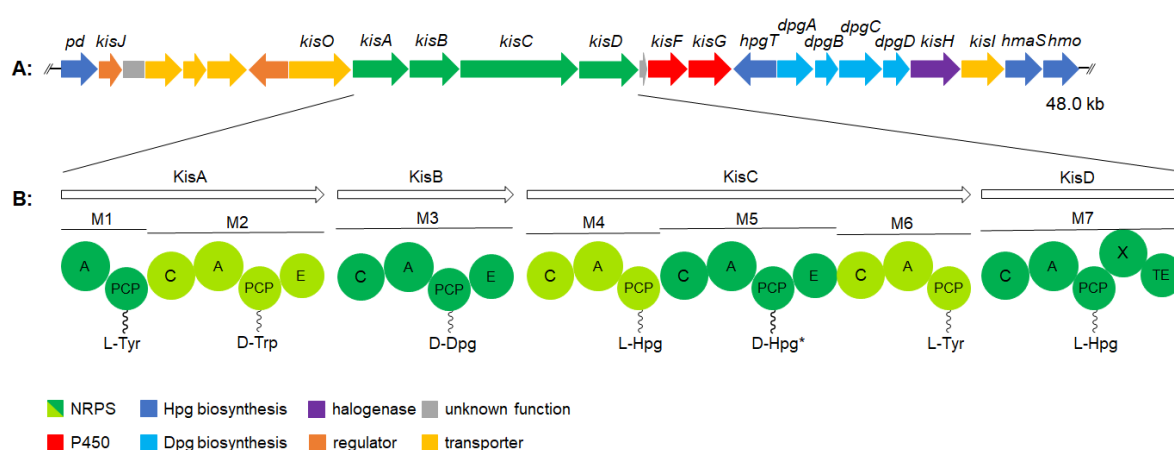
Figure 12. Organization of the kistamicin biosynthetic gene cluster (**A**) and the kistamicin NRPS assembly line (**B**). Amino acids intended for chlorination are indicated with *.

Moreover, a flavin-dependent halogenase (*kisH*), putatively responsible for the chlorination of one Hpg (**39**) building block, is encoded. Unexpectedly, genes corresponding to only two CYP enzymes (*kisF* and *kisG*), presumably responsible for the formation of biaryl and biarylether bonds, were detected. This result stands in opposition to the three biaryl and biarylether bonds characterizing the chemical structure of kistamicin A (**15**) and B (**16**). A search for a third CYP within the genome with sufficient homology was unsuccessful. These findings suggest that either *kisF* or *kisG* is responsible for the formation of two OPCRs. This would then be an unique and interesting feature of the kistamicin gene cluster since, to date, for all nonribosomal peptides a distinct CYP enzyme has been proposed for the formation of each biaryl and biarylether bond. In contrast to the complestatin cluster, genes encoding for proteins required in the catalytic cycle of CYPs, ferredoxin and ferredoxin oxidoreductase, are not included in the kistamicin gene cluster.[82] This points to the utilization of ferredoxin and ferredoxin oxidoreductase derived from other parts of the genome. Finally, several transporter (three ABC transporters (*kisM*, *kisN*, *kisP*), one NaH exchanger (*kisI*), one HylD family secretion protein (*kisL*)) and regulatory genes (a two-component response regulator (*kisJ*) coupled to a histidin kinase (*kisO*)), and one small gene for a MbtH protein (*kisE*) were detected. MbtH proteins can be found in almost all NRPS gene clusters and seem to be required for solubility and/or optimal activity of some A domains.[169–176]

The architecture of the kistamicin NRPS assembly line (Figure 12B, Scheme 12) was investigated more closely with the applications antiSMASH[73] and PKS/NRPS Analyzer.[168] It is composed of four enzymes (kisA, kisB, kisC, kisD), which in turn are divided into seven modules (M1 to M7). In total, seven A, T and six C domains correspond to the seven amino acid building blocks. Additionally, three E domains in M2, M3 and M5 amount to three epimerized amino acids. Module M7 contains an X domain, which is involved in biaryl and biarylether bond formation (Chapter 1.2.1.3). The NRPS systems is finally capped by a TE domain. The NRPS domain structure can be used to tentatively elucidate the as yet unknown absolute stereoconformation of amino acid building blocks in kistamicin A (**15**): The presence of an E domain in M2, M3 and M5 indicates that the amino acids tryptophane (**20**), Dpg (**28**), and 3-chloro-Hpg (**39**) are epimerized to D-amino acids, whereas the absence of an E domain in M1, M4, M6 and M7 implies that the other four building blocks (two tyrosine (**19**) and two Hpg (**21**) moeities) are L-amino acids. This important information shows that the kistamicin A (**15**) stereostructure should differ from the one of complestatin (**17**) (Chapters 1.2.1.1 and 1.2.2) and is the basis for the successful chemical total synthesis of the kistamicin A heptapeptide chain (**54**).

Table 2. Proteins encoded in the kistamicin biosynthetic gene cluster of *Actinomadura parvosata* subsp. *kistnae*. Locus tags reference to the complete genome sequence deposited at EMBL under Accession No. [PRJEB19374].

CDS No.	Protein	Predicted Function (NRPS Domains)	Size [AAs]	Locus Tag
1	PD	prephenate dehydrogenase	379	KIS93_04829
2	KisJ	two-component response regulator	217	KIS93_04828
3	KisK	hypothetical protein	165	KIS93_04827
4	KisL	HylD family secretion protein	352	KIS93_04826
5	KisM	ABC transporter	245	KIS93_04825
6	KisN	ABC transporter	389	KIS93_04824
7	KisO	histidin kinase	393	KIS93_04823
8	KisP	ABC transporter	627	KIS93_04822
9	KisA	NRPS (A-PCP-C-A-PCP-E)	1,680	KIS93_04821
10	KisB	NRPS (C-A-PCP-E)	1,186	KIS93_04818 to KIS93_04820
11	KisC	NRPS (C-A-PCP-C-A-PCP-E-C-A-PCP)	3,619	KIS93_04816 and KIS93_04817
12	KisD	NRPS (C-A-PCP-X-TE)	1,765	KIS93_04814 and KIS93_04815
13	KisE	MbtH protein	76	KIS93_04813
14	KisF	cytochrome P450 oxidase (CYP)	384	KIS93_04812
15	KisG	cytochrome P450 oxidase (CYP)	442	KIS93_04811
16	HpgT	Hpg transaminase	440	KIS93_04810
17	DpgA	DpgA synthase	1,106	KIS93_04808 and KIS93_04809
18	DpgB	DpgB synthase	220	KIS93_04807
19	DpgC	DpgC synthase	1,290	KIS93_04806
20	DpgD	DpgD synthase	271	KIS93_04805
21	KisH	flavin-dependent halogenase	495	KIS93_04804
22	KisI	NaH exchanger	427	KIS93_04803
23	HmaS	4-hydroxymandelate synthase	360	KIS93_04802
24	Hmo	L-4-hydroxymandelate oxidase	377	KIS93_04801
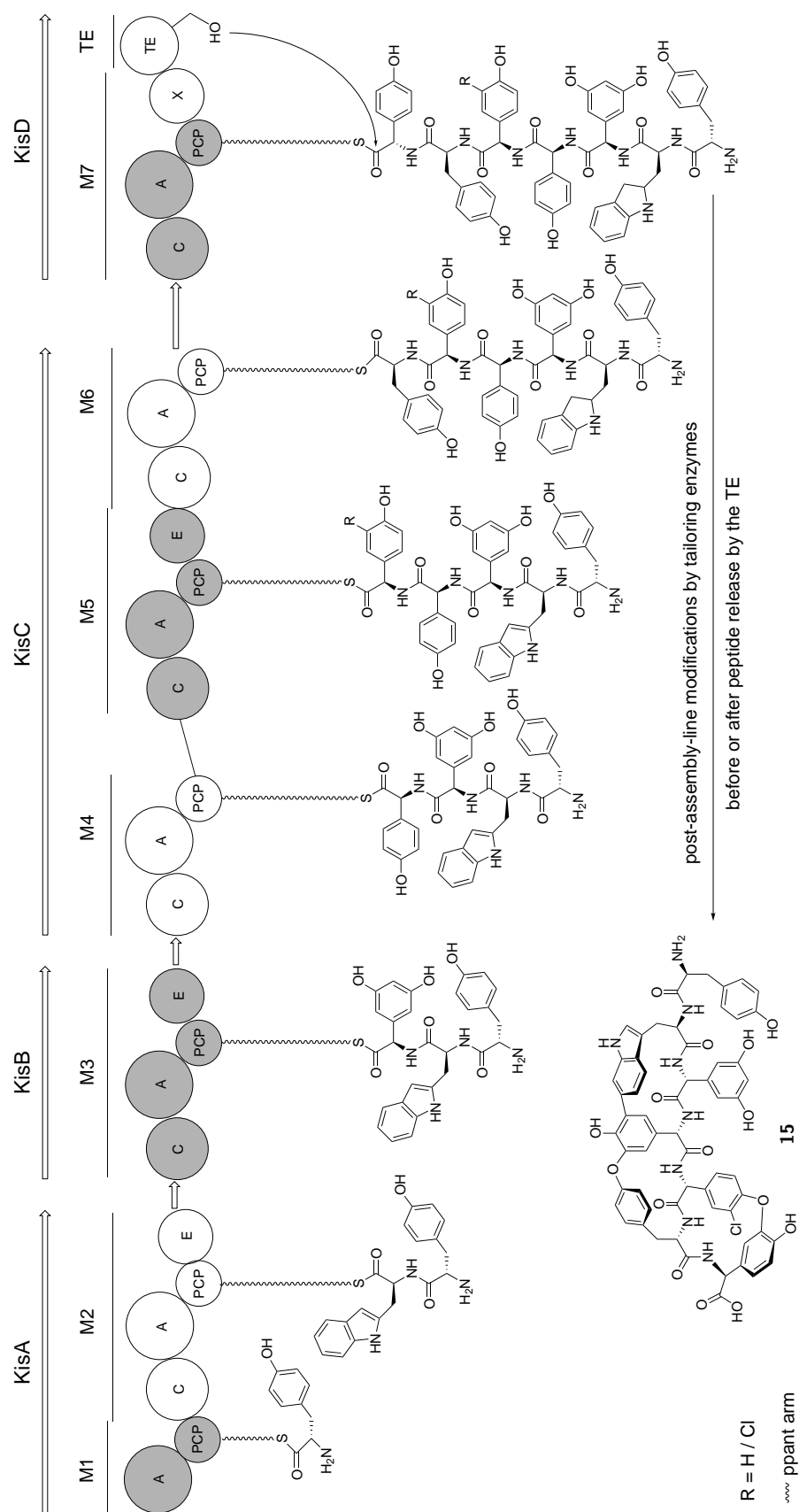
Scheme 12. Biosynthesis of kistamicin A (**15**) by the NRPS system KisABCD organised in the modules M1 to M7. The exact timing of the halogenation as well as the oxidative phenol coupling reactions is unknown. A: adenylation domain; PCP: peptidyl carrier protein domain; C: condensation domain; E: epimerization domain; X: X domain; TE: thioesterase domain.

3. Results and Discussion

In summary, the investigated 48.0 kb gene cluster contains all genes necessary for the biosynthesis of kistamicin A (**15**) with the to date unique limitation to two CYPs putatively catalyzing three OPCRs. The close structural similarity to the complestatin biosynthetic gene cluster suggests that the kistamicin cluster begins with gene *pd* (prephenate dehydrogenase) and ends with gene *hmo* (L-4-hydroxymandelate oxidase).
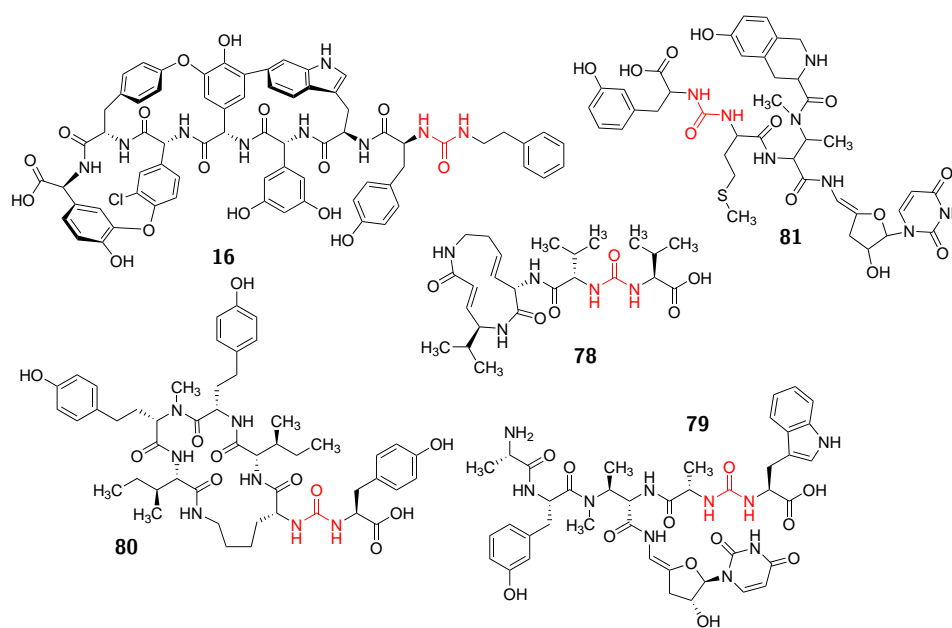
Figure 13. Nonribosomol peptides (-polyketide hybrides) containing ureido bonds (red): kistamicin B (**16**), syringoline A (**78**), pacidamycin 1 (**79**), anabaenopeptin G (**80**), and napsamycin A (**81**).

However, no genes responsible for the formation of the highly unusual ureido linkage in kistamicin B (**16**) could be found and the biosynthetic mechanism remains to be elucidated. Ureido bond formation was characterized for the NRPS-PKS hybrid syringoline A (**78**)[177–179] and the nonribosomal peptide family of pacidamycins (e.g. pacidamycin 1 (**79**)),[180,181] whereas it is still unknown for other groups of nonribosomal peptides such as the anabaenopeptins (e.g. anabaenopeptin G (**80**))[182] or napsamycins (e.g. napsamycin A (**81**)).[183] In the case of **78** - a cyclic tetrapeptide containing an ureido linkage between two side-chain valine residues - a free standing module activates both amino acids und joins the valine residues by incorporation of bicarbonate, thus forming an ureido bond. The respective module carries an unique 239 amino acid section between the A and C domain.[177–179] A similar process accounts for the ureido linkage in the pacidamycins.[180,181] However, the kistamicin assembly line does not contain an amino acid sequence with this characteristic, conserved motif. Moreover, in the case of **16** the *N*-terminal residue is not

an intact amino acid but rather an amine. A similar process as in the biosynthesis of **78**, featuring an additional decarboxylation to give the observed amine, is therefore unlikely to take place. The ureido bond thus most likely results from modifications taking place after the normal peptide bond was formed. Nevertheless, the kistamicin NRPS system only contains typical A and C domains with the characteristic conserved motifs[89] and no other genes putatively involved in the formation of the ureido linkage or decarboxylation could be identified. Moreover, **16** could not be detected in the extract of the fermentation broth of *A. parvosata* during this work, although an ample amount of **15** ($69\,\mathrm{mg\,mL^{-1}}$) was isolated (Chapter 3.2.2). Furthermore, the only reported detection of **16** was by Naruse *et al.* in 1993.[86] It may be that an unknown culture condition is required for the production of **16**. However, together with the lack of possible genes putatively encoding the formation of an ureido bond in the kistamicin gene cluster, this may also point to the inability of *A. parvosata* to produce **16** any longer. Possibly, the strain lost the respective genes since 1993 or **16** was a side product of the fermentation and isolation conducted by Naruse *et al.*[86]

3.2.4. Heterologous Expression of Enzymes Involved in OPCR Catalysis

Bioinformatic analysis of the kistamicin biosynthetic gene cluster (Chapter 3.2.3) revealed two genes encoding cytochrome P450 enzymes, *kisF* and *kisG*. Together with an X domain as well as an adjacent PCP domain, both encoded in gene *kisD*, the cytochrome P450 enzymes are putatively necessary for catalysis of OPCRs during kistamicin biosynthesis. All those enzymes were to be cloned and heterologously expressed in *E. coli* in this work, and thereby made available for later chemo-enzymatic total synthesis of kistamicin A (**15**) (Chapters 1.2.1.3 and 2).

3.2.4.1. Heterologous Expression of Cytochrome P450 Enzymes KisF and KisG

The two cytochrome P450 enzymes KisF and KisG, which are putatively involved in biaryl and biarylether bond formation during kistamicin biosynthesis, were to be cloned and heterologously expressed in *E. coli*. For this purpose, gDNA of *A. parvosata* was isolated and the respective sequences PCR amplified. In doing so, *Eco*RI and *Hind*III restriction sites were introduced into the PCR products. Each PCR product was then ligated by cohesive end ligation into pGS-21a as well as pHis8-TEV expression vectors. Both vectors have previously been used in our group for heterologous expression of

3. Results and Discussion
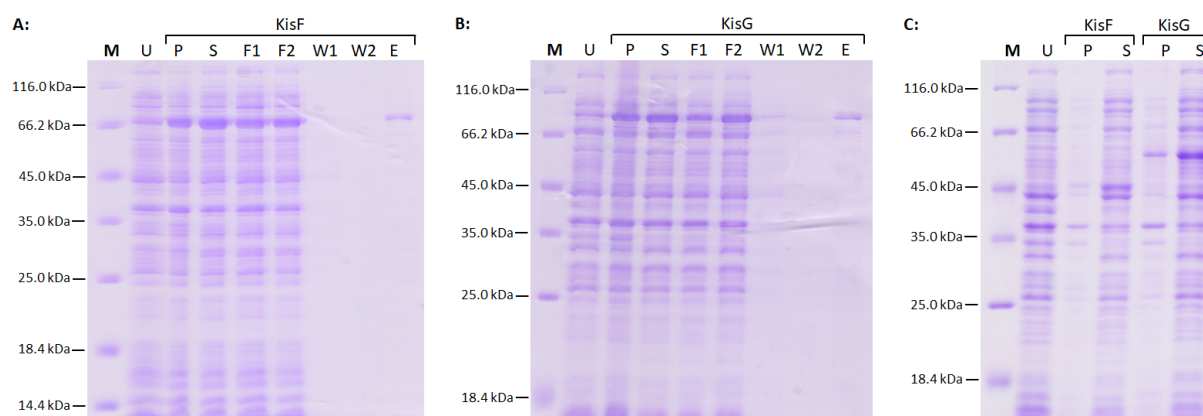
Figure 14. SDS gel (12 %) of the expression and purification of P450 enzymes KisF (72.3 kDa; **A**) and KisG (78.5 kDa; **B**) from pGS-21a plasmids. SDS gel (12 %) of the test expression of P450 enzymes KisF (45.5 kDa) and KisG (51.6 kDa) from pHis8-TEV plasmids (**C**). M: Pierce™Unstained Protein MW Marker; U: uninduced cells; P: pellet of the cell lysate after induction; S: supernatant of the cell lysate after induction; F1: first flow through after Ni-NTA column loading; F2: second flow through after Ni-NTA column loading; W1: first washing fraction; W2: second washing fraction; E: eluate.

cytochrome P450 enzymes ComI and ComJ, as well as the PCP domain of ComD from the complestatin biosynthetic gene cluster.[97] All cloned plasmids, pGS-21a::*kisF*, pHis8-TEV::*kisF*, pGS-21a::*kisG* and pHis8-TEV::*kisG*, were transformed into *E. coli* BL21(DE3) and heterologously expressed by inducing with 0.5 mM IPTG and incubation at 16 °C over night (LB medium). A small sample of each protein was purified using Ni-NTA columns. Protein expression as well as purification was analyzed by SDS-PAGE, and showed that KisF and KisG are both more strongly expressed utilizing pGS-21a plasmids (Figure 14).

3.2.4.2. Heterologous Expression of the PCP Domain, the X Domain and the PCP-X Didomain of KisD

In addition to cytochrome P450 enzymes KisF and KisG, the PCP-X didomain encoded in *kisD* is putatively involved in biaryl and biarylether bond formation during kistamicin biosynthesis. It is unknown, whether the fused didomain KisD-PCP+X is functional in this context or whether the isolated domains KisD-PCP and KisD-X are required. Therefore, KisD-PCP, KisD-X as well as KisD-PCP+X were to be heterologously expressed in this work. gDNA of *A. parvosata* was used for PCR amplification of the corresponding sequences and *Eco*RI and *Hind*III restriction sites introduced into the PCR products. All constructs were ligated into the pGS-21a vector by cohesive end ligation. DNA sequencing of the resulting plasmids confirmed successful cloning in case of *kisD-PCP* as well as *kisD-X*,
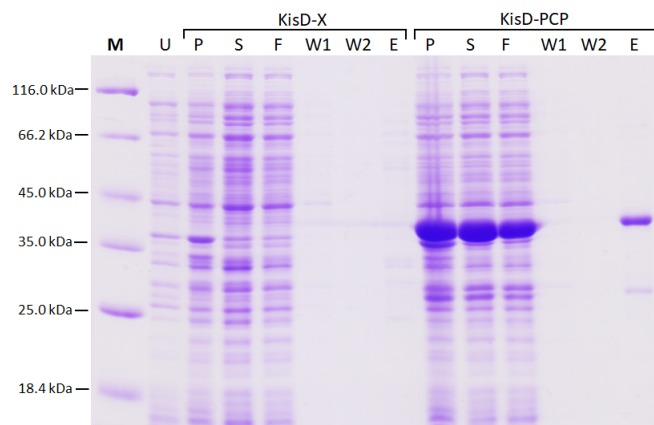
Figure 15. SDS gel (12 %) of the test expression and purification of KisD-X (72.3 kDa, not expressed) and KisD-PCP (72.3 kDa) from pGS-21a plasmids. M: Pierce™Unstained Protein MW Marker; U: uninduced cells; P: pellet of the cell lysate after induction; S: supernatant of the cell lysate after induction; F: flow through after Ni-NTA column loading; W1: first washing fraction; W2: second washing fraction; E: eluate.

but revealed mutations regarding *kisD-PCP+X*. The two correctly obtained plasmids (pGS-21a::*kisD-PCP*, pGS-21a::*kisD-X*) were transformed into *E. coli* BL21(DE3) and heterologously expressed by inducing with 0.5 mM IPTG and incubation at 16 °C over night (LB medium). Small samples of the proteins were purified using Ni-NTA columns. Unfortunately, SDS-PAGE analysis showed protein expression only in case of KisD-PCP, but no protein production in case of KisD-X (Figure 15). In a new approach to expression of KisD-X and KisD-PCP+X, the respective sequences were amplified from *A. parvosata* gDNA using Gibson primers. The PCR product resulting from amplification of *kisD-X* was introduced into vector pHis8-TEV by two fragment Gibson assembly and gave plasmid pHis8-TEV::*kisD-X*. Three fragment Gibson assembly was used for installation of the *kisD-PCP+X* PCR product into vector pHis8-TEV, yielding plasmid pHis8-TEV::*kisD-PCP+X*, but failed in case of vector pGS-21a. The two resulting vectors (pHis8-TEV::*kisD-X*, pHis8-TEV::*kisD-PCP+X*) were transformed into *E. coli* BL21(DE3). Unfortunately, initial tests for heterologous expression by inducing with 0.5 mM IPTG and incubation at 16 °C over night (LB medium) did not yield any protein. Inducing *E. coli* BL21(DE3) carrying pGS-21a::*kisD-X* with 0.5 mM IPTG as well as 1.0 mM IPTG, and protein production at 22 °C as well as 28 °C resulted in no protein, either. Since control of the plasmid sequences (pGS-21a::*kisD-X*, pHis8-TEV::*kisD-X*, pHis8-TEV::*kisD-PCP+X*) as well as control of *E. coli* BL21(DE3) clones directly before cultivation gave no unexpected results, all three plasmids were transformed into *E. coli* SoluBL21™. This strain carries uncharacteristic

3. Results and Discussion

mutations, which often allow the production of unsoluble proteins in soluble form. Again, inducing with 0.5 mM IPTG as well as 1.0 mM IPTG and incubation at 22 °C as well as 28 °C over night (LB medium) gave no protein. Additional induction of the *kisD-X* constructs with 0.5 mM IPTG and incubation at 22 °C over night (LB medium) also did not improve protein production. Due to those disappointing results, the gene coding for *kisD-PCP+X* was purchased in codon-optimized form for production in *E. coli* from *Eurofins Genomics* (*kisD-PCP+X$_{opt}$*). It was cut from plasmid pEX-K4::*kisD-PCP+X$_{opt}$* at the present restriction sites (*Eco*RI, *Hind*III) and ligated into vectors pHis8-TEV as well as pGS-21a by cohesive end ligation. Plasmid pGS-21a::*kisD-PCP+X$_{opt}$* was used as a template for PCR amplification of *kisD-X$_{opt}$*. In doing so, restriction sites *Eco*RI and *Hind*III were introduced and *kisD*-Xopt ligated into the vectors pGS-21a and pHis8-TEV by cohesive end ligation. The resulting plasmids (pGS-21a::*kisD-X$_{opt}$*, pGS-21a::*kisD-PCP+X$_{opt}$*, pHis8-TEV::*kisD-X$_{opt}$* and pHis8-TEV::*kisD-PCP+X$_{opt}$*) were transformed into *E. coli* BL21(DE3). Cultures were induced with 0.5 mM IPTG and incubated at 16 °C over night (LB medium). SDS-PAGE analysis showed that no proteins were produced in any case. These results were unexpected since the codon optimized (for expression in *E. coli*) version of the PCP-X didomain *comD-PCP+X$_{opt}$* encoded in the complestatin biosynthetic gene cluster shows similarity to its kistamicin equivalent, and was successfully heterologously expressed in *E.coli* BL21(DE3) under similar conditions.[97] Moreover, cultures grown for heterologous KisD-X and KisD-PCP+X expression did not show symptons of poisoning, but grew as expected. Instead of KisD-X and KisD-PCP+X, ComD-X$_{opt}$ and ComD-PCP+X$_{opt}$ may be tested in future chemo-enzymatic *in vitro* assays.

Table 3. Tested conditions for heterologous expression of proteins Kis-PCP, KisD-X, KisD-X$_{opt}$, KisD-PCP+X and KisD-PCP+X$_{opt}$ in *E. coli*. Strains were cultured in LB medium and incubated at 200 rpm over night. Protein was not expressed in any case.

Protein	Plasmid	*E. coli* Strain	c(IPTG) [mM]	T [°C]
KisD-X	pGS-21a	BL21(DE3), SoluBL21	0.5, 1.0	16, 22, 28 (all 0.5 mM); 22, 28 (all 1.0 mM)
KisD-X	pHis8-TEV	BL21(DE3), SoluBL21	0.5, 1.0	16, 22, 28 (all 0.5 mM); 22, 28 (all 1.0 mM)
KisD-X$_{opt}$	pGS-21a	BL21(DE3)	0.5	16
KisD-X$_{opt}$	pHis8-TEV	BL21(DE3)	0.5	16
KisD-PCP+X	pHis8-TEV	BL21(DE3), SoluBL2	0.5, 1.0	16, 22, 28 (all 0.5 mM); 22, 28 (all 1.0 mM)
KisD-PCP+X$_{opt}$	pGS-21a	BL21(DE3)	0.5	16
KisD-PCP+X$_{opt}$	pHis8-TEV	BL21(DE3)	0.5	16

3.2.5. Chemical Synthesis of the Kistamicin A Peptide Precursor

After elucidation of the absolute stereostructure of kistamicin A (**15**), its linear peptide precursor **54** was to be synthesized in one piece via solid phase peptide synthesis (SPPS).
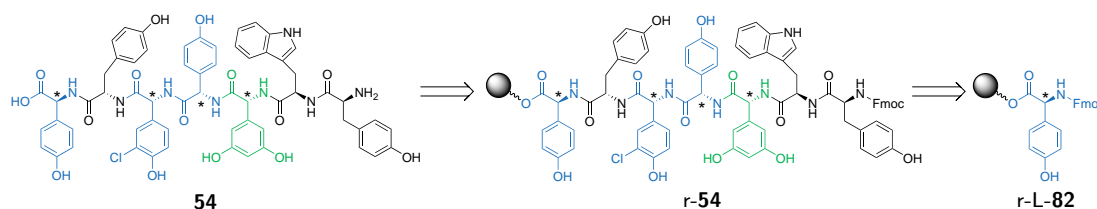
Scheme 13. Retrosynthesis of the kistamicin A linear peptide precursor (**54**): An SPPS strategy in combination with mild Fmoc chemistry was employed. Hpg (**21**) and Hpg-derived (**39**) units are marked as blue, Dpg (**28**) units in green, stereocenters prone to epimerization with *.

SPPS facilitates the effective and straightforward synthesis of long peptide chains, which are immobilized on a solid support resin.[184,185] The use of a solid support circumvents solubility problems frequently encountered in liquid phase peptide synthesis (LPPS) and renders laborious isolation procedures unnecessary, since reagents or soluable side products are removable after each step by simple washing and filtration. Moreover, the covalent attachment of a peptide chain to a resin via its *C*- or *N*-terminus reduces the amount of required protecting groups. Employed resins consist of polymer beads, which are insoluable in solvents commonly used for peptide synthesis, physically stable and therefore filterable, and equipped with functional linkers that allow the installation of amino acids. Their porous structure makes the beads permeable for reagents or swelling solvents, such as DCM and DMF, and improves interactions between reagents and substrate. SPPS procedures start with the covalent binding of a protected amino acid to the resin linker. Subsequently, unreacted binding sites on the resin are capped, which prevents coupling of amino acids
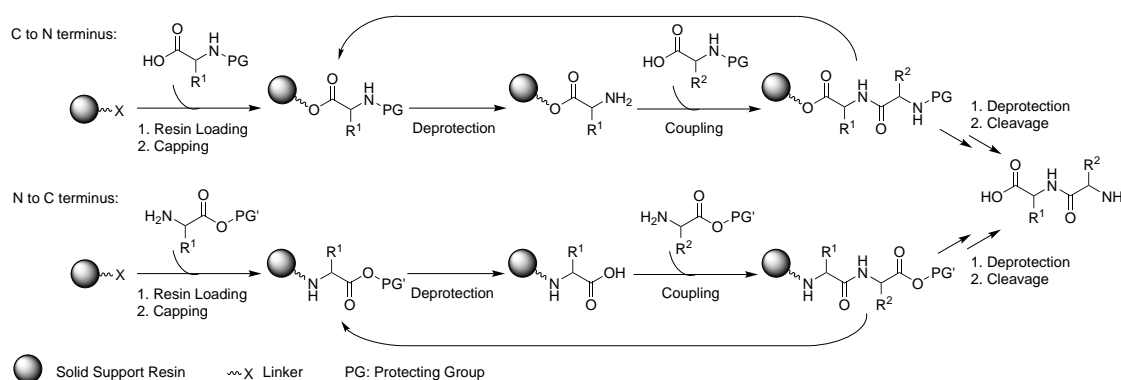
Scheme 14. The principle of solid phase peptide synthesis (SPPS).

3. Results and Discussion

during later stages of the synthesis, and reduces side product formation. The loaded amino acid is then deprotected, and the next protected amino acid attached. In this way, the peptide chain is elongated step by step until the desired peptide sequence is obtained. The crude product is subsequently cleaved off the resin, and remaining side products removed in a last step. SPPS most commonly starts at the *C*-terminus of the peptide chain and ends at its *N*-terminus. Amino acids are therefore protected at their *N*-terminus using appropiate groups, usually Alloc, Boc or Fmoc moieties.[184,185]

For the synthesis of **54** by SPPS, a known major challenge is the sensitivity of Hpg and Dpg building blocks to epimerization under traditionally applied conditions. Due to their electron-withdrawing aromatic system phenylglycins are especially susceptible to deprotonation in Cα position and therby to racemization (Scheme 15).[128]
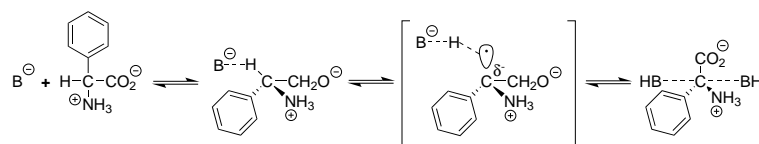
Scheme 15. Hydrogen exchange at Cα during racemization of L-phenylglycine.[128]

Racemization occurs depending on pH near the phenylglycins isoelectric point as well as on ionic strength at pH > 10.[128] Results of this work suggest that racemization is further enhanced by long reaction times (Chapter 3.2.5.3) and decreasing steric hindrance of protecting groups (Chapter 3.2.5.8). These properties render Hpg (**21**) and Dpg (**28**) incompatible with classic Boc and Fmoc chemistry,[120,129] which employs bases (and acids) in amino acid protection and deprotection. Instead, Alloc chemistry[120,121] has been used, requiering tedious synthesis of all protected building blocks as well as expensive palladium-mediated cleavage. However, **54** contains no less than one Dpg (**28**) and three Hpg (**21**) or Hpg-derived (**39**) building blocks, thus making cheaper Fmoc chemistry with its easy access to protected amino acids - commercially available in a large range or simple to synthesize - highly desirable. In addition, use of Fmoc groups would facilitate close monitoring of reactions by UV-detection (HPLC and LC-MS chromatography, Fmoc testing (Chapter 5.9.2.1)). In 2014 Brieke *et al.* published a mild Fmoc protecting strategy, and successfully employed it in the synthesis of vancomycin- and teicoplanin-type linear model peptide precursors (not halogentated).[122] This mild Fmoc chemistry protocol coupled with an SPPS resin featuring a sterically hindered linker appeared to be promising, and was applied for the synthesis of **54** in this work. In contrast to Brieke *et al.*, who used preloaded Fmoc-Tyr-Wang resin,[122] 2-chlorotrityl chloride (2-CTC) resin was chosen as the solid support. Trityl resins are highly acid labile, so that mild acidic conditions are sufficient for

peptide cleavage, thereby preventing epimerization through hydrolysis.[185,186] 2-CTC resin additionally possesses bulky linkers, which surpress undesirable diketopiperazine formation as well as epimerization of the first amino acid by steric hinderance.[185,187]

Before SPPS of **54** could commence, the not commercially available building blocks Fmoc-L-Hpg (L-**82**), Fmoc-3-chloro-D-Hpg (D-**83**), and Fmoc-D-Dpg (D-**84**) had to be synthesized as well as enantiomeres and derivatives for further investigation of all synthetic steps.

3.2.5.1. Synthesis of Hpg-Derived Building Blocks

Hpg-derived building blocks Fmoc-L-Hpg (L-**82**) and Fmoc-3-chloro-D-Hpg (D-**83**), which were to be synthesized for SPPS, were easily accessible. L-Hpg (L-**21**) was commercially purchased and Fmoc protected by stirring with 1.0 equivalent Fmoc hydroxysuccinimide ester in sodium bicarbonate (10 w/v % in water)/acetonitrile (1:2) over night at R T,[122] yielding 83 % of compound L-**82**. This method was used as standard for Fmoc protection in this thesis. Fmoc-3-chloro-D-Hpg (D-**83**) was synthesized in two steps. First, D-Hpg (D-**21**) was chlorinated by sulfuryl chloride in an electrophilic aromatic substitution with acetic acid as a solvent to facilitate heterolysis of sulfuryl chloride.[188] 3-Chloro-D-Hpg (D-**39**) was obtained in 68 % yield, and then used for standard Fmoc protection in a second step, giving D-**83** in 80 % yield. The respective enantiomeres, D-**21** and L-**83**, were synthesized in the same way, and applied to examine racemization during SPPS (Chapter 3.2.5.4). Later developments in the synthesis of the heptapeptide chain **54** necessitated the additional protection of L-Hpg (L-**21**) with an Alloc or a Cbz moiety (Chapter 3.2.5.8).
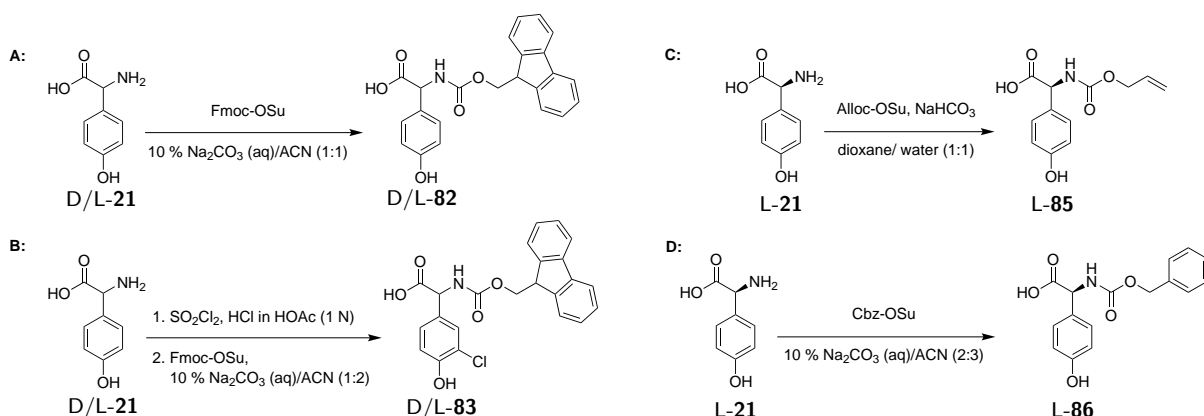
Scheme 16. Synthesis of Hpg derived building blocks. **A:** 83 % yield for Fmoc-L-Hpg (L-**82**); 94 % yield for Fmoc-D-Hpg (D-**82**). **B:** 54 % yield for Fmoc-3-chloro-D-Hpg (D-**83**) over two steps; 73 % yield for Fmoc-3-chloro-L-Hpg (L-**83**) over two steps. **C:** 100 % yield for Alloc-L-Hpg (L-**85**). **D:** 95 % yield for Cbz-L-Hpg (L-**86**).

3. Results and Discussion

The respective products, L-**85** and L-**86**, were synthesized with quantitative yields by stirring L-**21** with 1.0 equivalents of *N*-Alloc or *N*-Cbz hydroxysuccinimide ester, respectively, in sodium bicarbonate (10 w/v % in water)/dioxane or acetonitrile (1:1) at R*T*. Thus synthesized Hpg-derived building blocks were directly used in SPPS.

3.2.5.2. Synthesis of the D-Dpg Building Block

In contrast to the Hpg-derived building blocks, the approach to Fmoc-D-Dpg (D-**84**) was laborious and characterized by low yields due to construction of the required stereocenter as well as the extreme hydropholicity of the intermediates. Racemic Dpg (DL-**28**) was synthesized from 3,5-dimethoxybenzaldehyde (**87**) via Strecker synthesis followed by hydrolysis and deprotection of the methoxy groups.[189] For this purpose, **87** was stirred with trimethylsilyl cyanide in ammonia and methanol for 5 h at 45 °C. After work-up and column chromatography the respective α-aminonitrile **88** was obtained in 57 % yield. The reason for the low yield of this step was the formation of various side products, which could not be further reduced by careful reaction control, and were difficult to remove. Column chromatography with a mixture of DCM/methanol (20:1) proved to be the only feasible method for purification. Column chromatography with other eluents (ethyl acetate/pentane (4:1 or 3:2), DCM/pentane/acetone (4:1:1) or DCM/pentane/acetone (4:1:1) followed by acetone/methanol (5:1)) as well as MPLC left significant amounts of impurities, although those were not indicated by initial tests. Following purification, **88** was subjected to hydrolysis by refluxing in hydrochloric acid (6 M in water) for 4 h, yielding 54 % of compound **89**. Attempts to improve the yields of the first two synthetic steps by using another cyanide salt (sodium cyanide) for Strecker synthesis and direct hydrolysis by refluxing an acidic extract of **88** - thereby skipping lossy purification - resulted in the decomposition of compounds. At the next stage, **89** was deprotected to give racemic Dpg
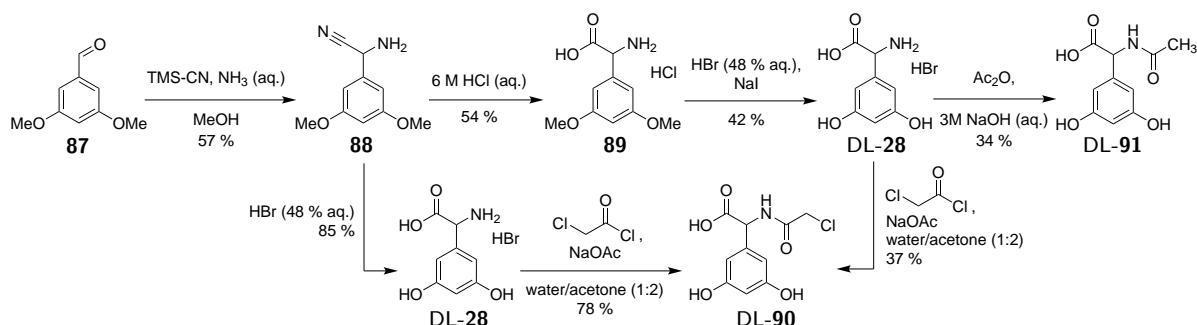
Scheme 17. Synthesis of racemic Dpg (DL-**28**) by Strecker synthesis and hydrolysis. DL-**28** is subsequently *N*-acetylated for later enzymatic chiral resolution.

(DL-**28**). Refluxing **89** with aluminium chloride in DCM led to decomposition, refluxing with hydrobromic acid (48 % in water) and sodium iodide for 2.5 h,[190] however, produced partially deprotected DL-**28**. By extending the reaction time to 16 h, DL-**28** was obatined with only 42 % yield after cation-exchange chromatography coupled with MPLC. To isolate D-Dpg (D-**28**) from the racemate, DL-**28** was *N*-acetylated and the product DL-**90** subjected to enzymatic chiral resolution.[191] For *N*-acetylation, DL-**28** was stirred with chloroacetyl chloride and sodium acetate in water/acetone (1:2) at R*T* over night, albeit yielding only 37 % DL-**90** after MPLC. Conversion of DL-**28** with acetic anhydride in 3 M sodium hydroxide solution at R*T* over night yielded only 34 % DL-**91**, too. However, attempts to simplify the synthesis of DL-**28** and DL-**90** were successful. To begin with, exclusion of sodium iodide from deprotecting **89** did not have a negative impact on the reaction, just as the exclusion of cation-exchange chromatography from purifying DL-**28** did not adversely influence *N*-acetylation. Finally, hydrolysis and deprotection were combined in one step by refluxing **88** in hydrobromic acid (48 % in water) for 16 h. After purification by MPLC, DL-**28** was gained with 85 % yield. *N*-acetylation of the resulting product now gave 78 % of compound DL-**90** after MPLC, possibly due to fewer remaining side products in DL-**28**.

For enzymatic chiral resolution, DL-**90** was dissolved in phosphate buffer (0.1 M) containg cobalt(II) chloride (2.5 mM in water) and sodium azide (154 mM in water).[191] The pH was adjusted to 7, the enzyme D-amano acylase added and the solution incubated for 1 h at 37 °C and 200 rpm. In this step, D-amano acylase selectively cleaved the *N*-acetyl moiety off the D-isomer, allowing for chromatographic separation of D-Dpg (D-**28**) from the remaining *N*-chloroacetyl-L-3,5-Dpg (L-**90**) by MPLC. The reaction was monitored by HPLC and stopped by addition of glacial acetic acid after conversion of 45 % DL-**28** to D-**28**. D-amano acylase proved to be a robust enzyme for this reaction, turning over up to 2.2 g of DL-**90** in 22 h using only 3.4 mg mmol^{-1} enzyme. The limitations of D-amano acylase were not reached in this work and it may be possible to convert larger amounts of compound with less enzyme. Concentration of compound or enzyme as well as longer than necessary reaction times did not influence enzymatic chiral resolution.
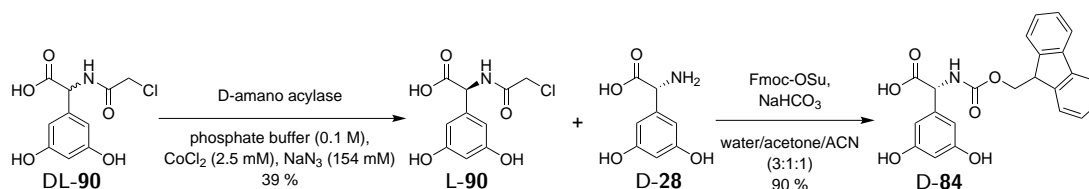
Scheme 18. Enzymatic chiral resolution of DL-**90** and synthesis of Fmoc-D-Dpg (D-**84**).
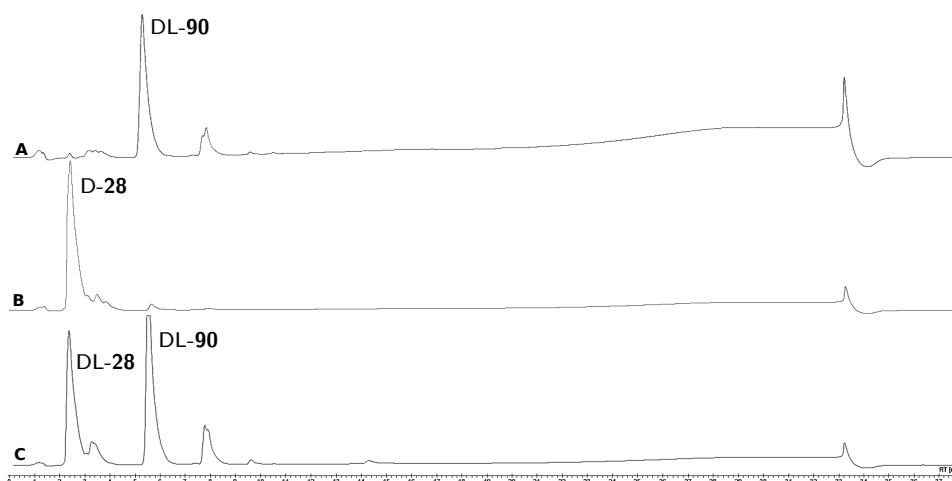
Figure 16. HPLC analysis of *N*-chloroacetyl-DL-3,5-Dpg (DL-**90**) (**A**), D-Dpg (D-**28**) (**B**), and the enzymatic chiral resolution of DL-**90** (**C**).

Regrettably, subsequent MPLC afforded D-**28** only highly contaminated with buffer salts due to its extreme hydropholicity. Nevertheless, crude D-**28** was used in a Fmoc protection reaction to obtain Fmoc-D-Dpg (D-**84**) (Table 4). Initially, standard Fmoc protection conditions such as for L-Hpg (L-**21**) (Chapter 3.2.5.1) were applied: stirring D-**28** with Fmoc hydroxysuccinimide ester in acetonitrile/sodium carbonate solution (10 % in water) (2:1) at R*T* for 38 h unexpectedly did not give any product. Using Fmoc hydroxysuccinimide ester in acetonitrile/dioxane (1:1) or Fmoc chloride in water/dioxane (1:1) produced some product (about 30 % of D-**84**), in case of the Fmoc chloride reaction containing major impurities even after MPLC. An obvious cause for such disappointing results was the high contamination of D-**28** with buffer salts. It was therefore attempted to purify D-**28** with diverse methods: recrystallization and precipitation with various solvents as well as extraction with *n*-butanol or continous extraction over 23 h with ethylacetate all failed to remove contaminating salts. Ultimately, laborious cation-exchange chromatography using water (pH 7) to remove salts and aqueous pyridine (10 v/v % in water, pH 8) as an eluent[191] proved to be the only successful purification method. Desalted D-**28** was then subjected to standard Fmoc protection conditions. However, after stirring with Fmoc hydroxysuccinimide ester and sodium carbonate in acetonitrile/water (1:1) at R*T* for 19 h reaction control with HPLC showed conversion of only a small part of D-**28**. Subsequently, DMF was added, which did not improve the reaction. It was therefore terminated without further workup after 84 h. In the next attempts, acetone/water was applied as another solvent as well as DIPEA as another base. The exchange of solvent led to a major decrease in side products as well as enhanced yields of D-**84** up to 82 %. The reaction could be

Table 4. Reaction conditions for Fmoc protection of D-Dpg (D-**28**) and DL-Dpg (DL-**28**).

Starting Material	Reagents	Solvents	Reaction Conditions	Yield
D-**28**, phosphate salt	Fmoc-OSu	ACN/Na$_2$CO$_3$ (10 % aq.) (2:1)	38 h at RT	could not be isolated
D-**28**, phosphate salt	Fmoc-OSu, NaHCO$_3$	ACN/dioxane (1:1)	18 h at RT	28 %
D-**28**, phosphate salt	Fmoc-Cl, NaHCO$_3$	water/dioxane (1:1)	18 h at RT	49 %[a]
D-**28**, desalted	Fmoc-OSu, NaHCO$_3$	water/ACN/DMF (1:1:1)	88 h at RT	incomplete conversion[b]
DL-**28**, desalted	Fmoc-OSu, DIPEA	acetone/water (8:3)	18 h at RT, 22 h at 40 °C	67 %
DL-**28**, desalted	Fmoc-OSu, NaHCO$_3$	acetone/water (1:1)	18 h at RT, 22 h at 40 °C	82 %
D-**28**, desalted	Fmoc-OSu, NaHCO$_3$	water/acetone/ACN (3:1:1)	84 h at RT	90 %

[a] Containing major impurities. [b] Reaction control with HPLC.

successfully reproduced on a larger scale in 90 % yield, although acetonitrile had to be added to aid solubility, and the reaction time extended to 88 h. In the end, Fmoc-D-Dpg (D-**84**) was synthesized in five steps with 13 % overall yield with Strecker synthesis and enzymatic chiral resolution as the key steps (Scheme 19). It is important to note, that this synthesis can not be scaled-up easily: purification of **88** was only satisfactory when using no more than 3 g of starting material **87** due to limitations imposed by equipment; an increase in side products was observed during hydrolysis and deprotection when more than 1.2 g of **88** were used resulting in yield loss; solubility of all compounds required for Fmoc
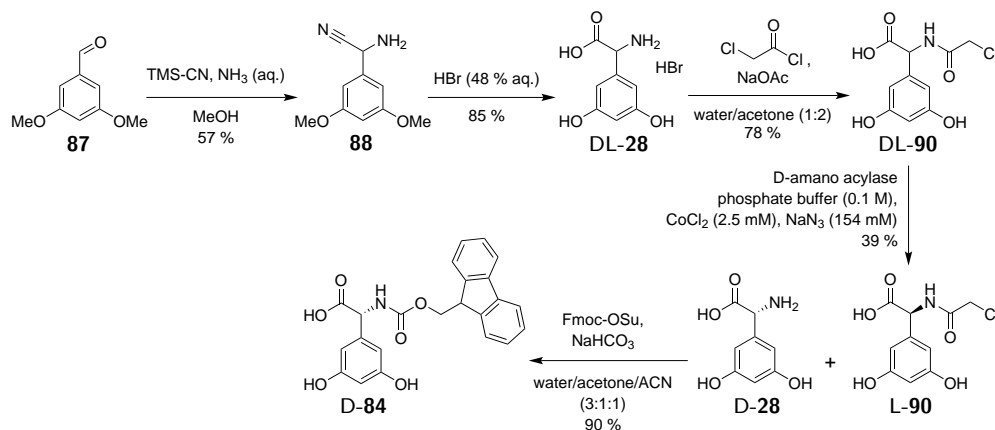
Scheme 19. Final synthetic route to Fmoc-D-Dpg (D-**84**).

protection of D-**28** had to be monitored very carefully and reaction times increased significantly for larger scale ($\geq 100\,\mathrm{mg}$) reactions.

3.2.5.3. Investigation into the Synthesis of the Heptapeptide and Synthesis of the Western Tetrapeptide on Solid Phase

The linear heptapeptide precursor of kistamicin A (**54**) was to be synthesized in one piece via SPPS. However, this approach is not trivial due to the high sensitivity of Hpg and Dpg building blocks to epimerization under conditions of standard Boc and Fmoc chemistry, the two classic SPPS strategies (Chapter 3.2.5). A protocol published in 2014[122] reported that a 1 % solution of DBU in DMF allows for effective deprotection of phenylglycine residues in less than 30 sec with very little epimerization. Moreover, four equivalents of COMU together with four equivalents of triethylamine with a coupling time of 30 min resulted in maximum coupling efficiency with scant epimerization.[122] This protocol was applied to the synthesis of the kistamicin A heptapeptide precursor (**54**) in this thesis. In contrast to the authors, who used preloaded Fmoc-Tyr-Wang resin,[122] 2-CTC resin was chosen as the solid support to further minimize epimerization of the first amino acid, Fmoc-L-Hpg (L-**82**), during loading as well as during final peptide cleavage.

Before use, 2-CTC resin was washed under argon atmosphere with DMF (3x) and DCM (3x), and then swollen for 30 min in DCM at RT. For activation, the resin was treated with 1.5 equivalents thionyl chloride in DCM under argon atmosphere and shaken for 1 h at RT. After removal of the solution, the resin was washed again with DMF (3x) and DCM (3x) under argon atmosphere. To load the first amino acid, 1.3 equivalents of Fmoc-L-Hpg (L-**82**) and 3.2 equivalents of NMM were dissolved in DCM/DMF (9:1), mixed with the activated resin under argon atmosphere, and shaken for 15 h at RT. After washing the loaded resin with DMF (3x), methanol (1x), DCM (1x), DMF (1x) and DCM (1x), and drying *in vacuo* to constant weight, the Fmoc test revealed a loading degree of 29 %. The loading was later improved to 79 % by incubating the activated resin with 2.3 equivalents of Fmoc-L-Hpg (L-**82**) and 3.2 equivalents of NMM in DCM/DMF (1:1) for 24 h. Afterwards, unreacted reaction sites of the freshly swollen resin were capped by shaking the resin with a solution of acetic anhydride, DIPEA and HOBt in DMF for 3 min at RT, and again for 7 min at RT. An alternative capping method, incubating the resin with DCM/methanol/DIPEA (80:15:5) for 15 min at RT, was also used. Both procedures capped unreacted reaction sites efficiently. Following washing with DCM (3x), loaded L-**82** was finally deprotected according to the published SPPS protocol,[122] utilizing 1 % DBU in DMF and shaking for 30 sec at RT. The next building block, Fmoc-L-Tyr
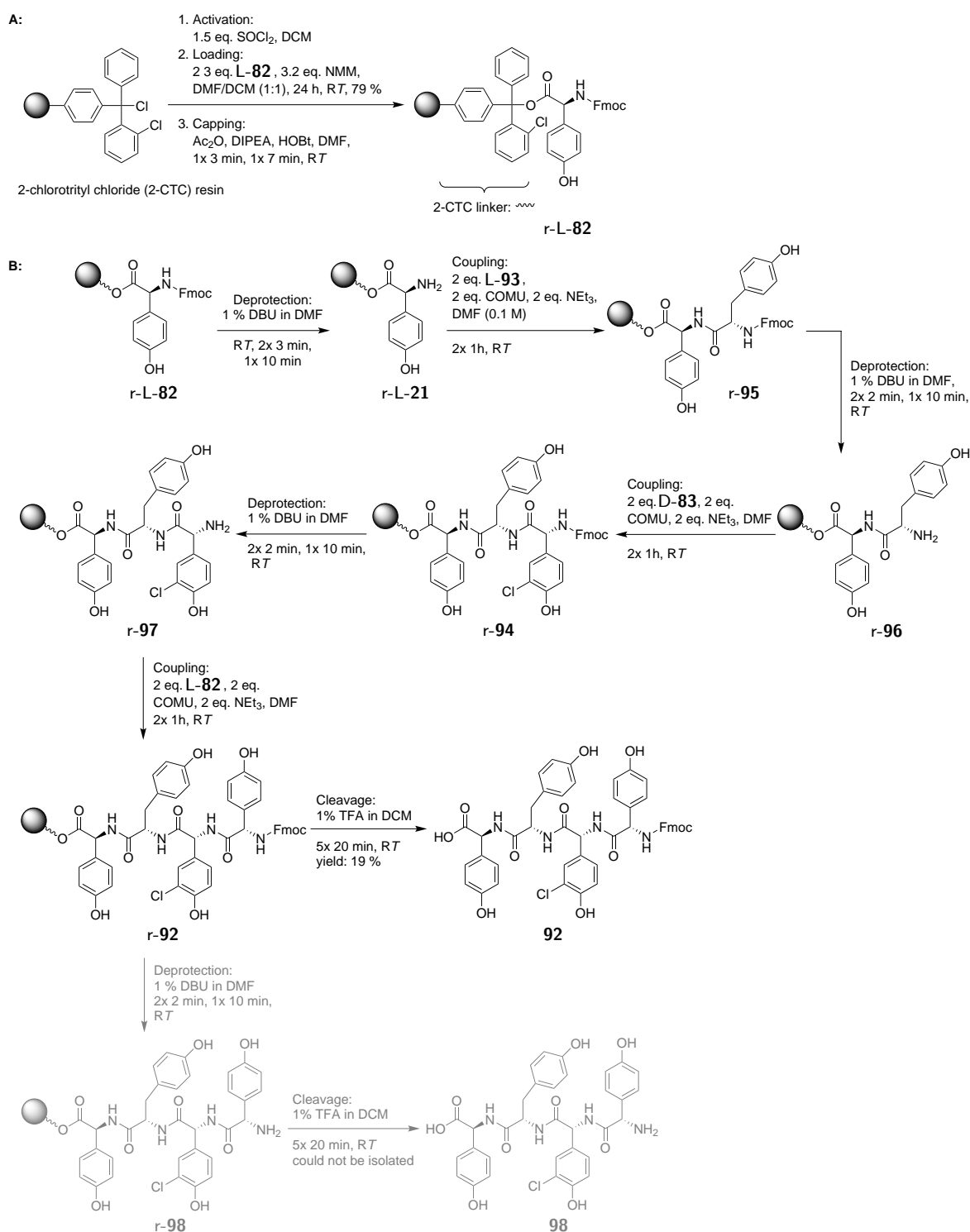
Scheme 20. SPPS of tetrapeptide **92** employed an optimized Fmoc strategy. **A:** loading of 2-CTC resin with the first amino acid, Fmoc-L-Hpg (**L-82**), and subsequent capping of unreacted reaction sites; **B:** Fmoc deprotection using 1 % DBU in DMF; coupling of subsequent building blocks using COMU and triethylamine in DMF; peptide cleavage from the resin using 1 % TFA in DCM; free tetrapeptide **98** was detected in LC-MS, but could not be isolated by semi-preparative HPLC due to low UV-activity.

3. Results and Discussion

(L-**93**), was coupled according to the published protocol,[122] as well: 4 equivalents of L-**93**, 4 equivalents of COMU and 4 equivalents of triethylamine were solubilized for 2 min in DMF, mixed with the resin, and shaken for 30 min at R*T*. Subsequent deprotection and coupling of each amino acid up to free tripeptide **r-97** was conducted as described and each step was followed by washing with DMF (3x), methanol (1x), DCM (1x), DMF (1x), and DCM (1x). Additionally, each step was monitored by LC-MS after cleaving the peptide off a small amount of resin by incubating with 1 % TFA in DCM for 20 min at R*T*. It was thus observed, that deprotection and coupling of the first three building blocks was not complete (Figure 17). Therefore, the resin was treated repeatedly (3x 3 min) with 1 % DBU in DMF for complete Fmoc removal. For synthesis in gram scale, reaction times had to be extended up to 10 min and the degree of Fmoc deprotection carefully monitored by LC-MS for all deprotection steps. Since coupling reactions remained incomplete under the applied conditions, as well, reaction time was extended to 16 h. However, coupling remained insufficient. Complete coupling was finally found when the resin was treated twice with 2.2 equivalents of Fmoc protected amino acid, 2.2 equivalents of COMU, and 2.2 equivalents of triethylamine in DMF for 1 h at R*T*. The amount of equivalents for the
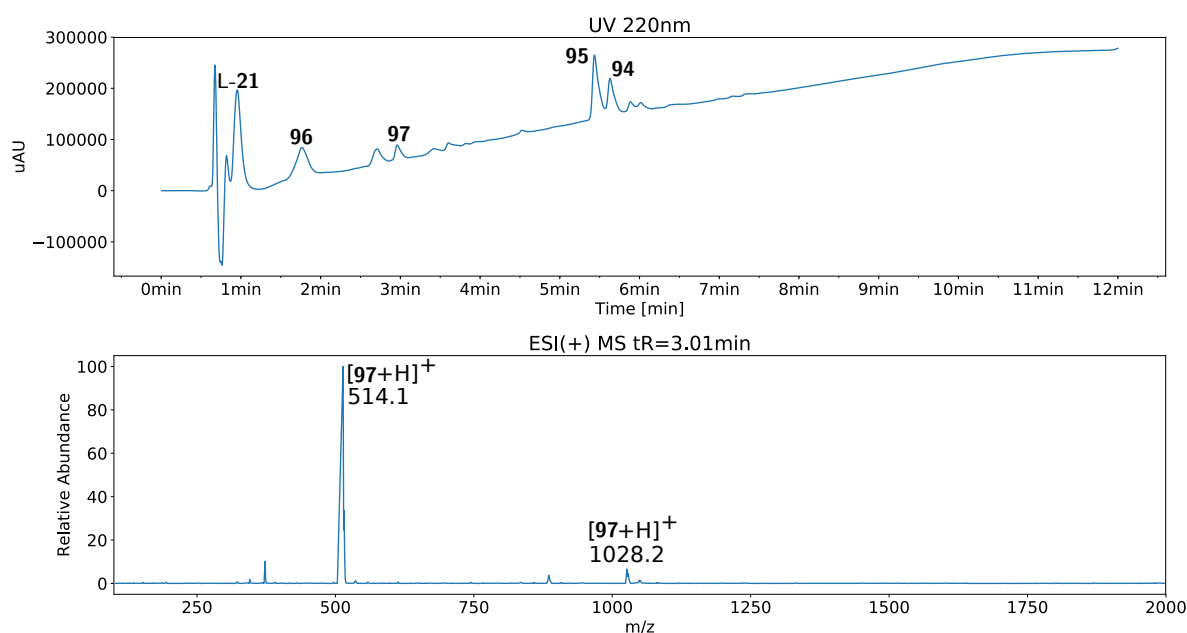
Figure 17. LC-MS analysis of free tripeptide **97** showed that deprotection as well as coupling reactions during SPPS remained incomplete when short deprotection (1x 30 sec) and coupling (1x 30 min) times were employed. The UV-spectrum (top) showed free amino acid L-**21** at tR = 0.77 min, free dipeptide **96** at tR = 1.8 min, free tripeptide **97** at tR = 3.0 min, Fmoc protected dipeptide **95** at tR = 5.5 min, Fmoc protected tripeptide **94** at tR = 5.7 min. MS-spectrum (bottom) of **97** at tR = 3.0 min.

58

third and fourth building blocks could be further reduced to 1.5 equivalents, although coupling should then be closely monitored by LC-MS. With this optimized strategy, Fmoc protected tetratpeptide **92** was easily and efficiently synthesized (Scheme 20 B; Figure 18). Cleavage of a larger amount of peptide by shaking the resin with 1 % TFA in DCM for 20 min at RT (5x), washing with DCM (5x), and timely purification by semi-preparative HPLC gave **92** in 19 % yield (341 mg) based on the resin's loading degree or 8 % based on the used quantity of L-**82**. The ^{1}H-NMR spectrum of compound **92** showed a single isomer, so that epimerization during its synthesis could be excluded. However, Fmoc removal before the free tetrapeptide **r-98** was cleaved off the resin significantly reduced UV-activity and made purification by semi-preparative HPLC impossible. It must also be noted that higher than usual reaction temperatures during summer (circa 30 °C) resulted in incomplete deprotection and coupling reactions, whereas lower than usual reaction temperatures (circa 18 °C) required extended deprotection times (2x 30 min). Extended deprotection times ultimately resulted in higher rates for epimerization, as observed in LC-MS spectra. The optimized SPPS protocol was applied to the synthesis of free heptapeptide **54** (Scheme 21).

While synthesis proceeded successfully to Fmoc protected tetrapeptide **92**, significant amounts of side products were formed during coupling of the fifth amino acid, Fmoc-D-Dpg (D-**84**). Formation of the desired product, Fmoc protected pentapeptide **99**, occured only
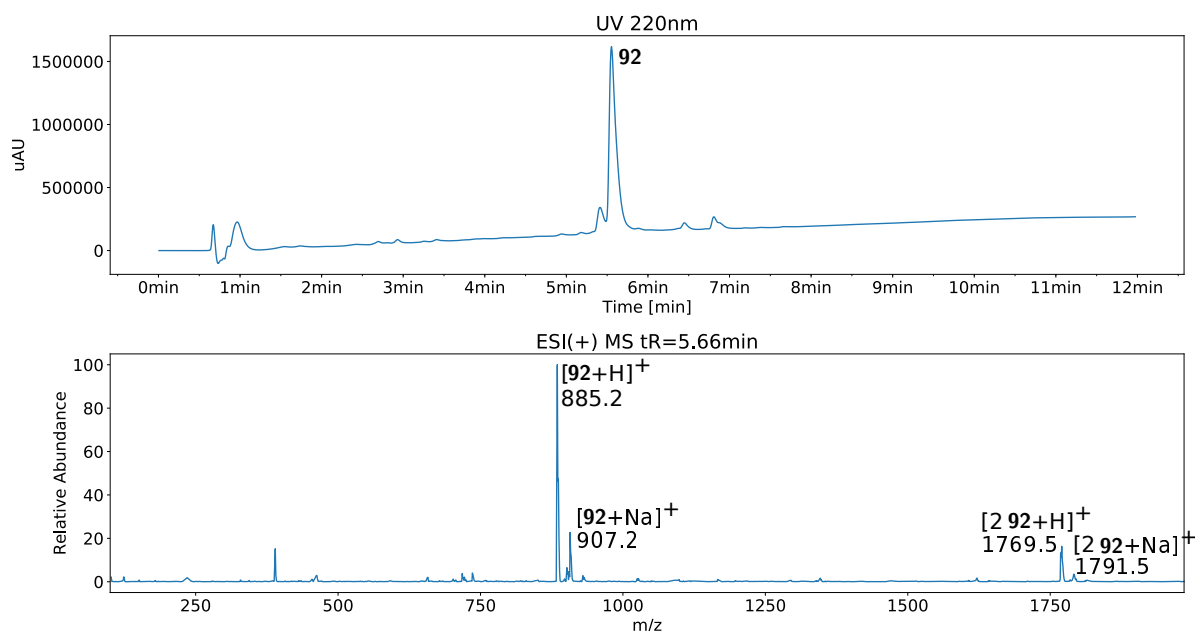
Figure 18. LC-MS analysis of crude, Fmoc protected tetrapeptide **92** (tR = 5.5 min), which was synthesized with an optimized SPPS protocol.

3. Results and Discussion

to a limited extent (Figure 19A). Side reactions also took place during consecutive coupling of the sixth and seventh amino acid, Fmoc-D-Trp (D-**100**) and Fmoc-L-Tyr (L-**93**), and only traces of final product **54** were found by LC-MS analysis. Repeated execution of the protocol gave the same results and the observed trace of **54** could not be isolated after cleavage from the resin. The interfering side reactions could not be identified based on the LC-MS spectra at hand. However, LC-MS spectra (Figure 19) showed that the formed side products always displayed the same mass differences (M-95, M-183, M-277) to the desired product, **99**, **101** or **102**. It can thus be speculated, that the same mechanism was responsible for side product formation during coupling of amino acids five, six, and seven. In a next step it was examined whether the observed side reactions were caused by inclusion of building block D-**84** or a more general problem. Therefore, three alternative amino acids were coupled to free tetrapeptide **r-98** as the fifth building block, Fmoc-L-Hpg (L-**82**), Fmoc-L-Tyr (L-**93**), and Fmoc-D-Trp (D-**100**) (Figure 20). No side reactions were observed for the coupling of L-**82**, but coupling of L-**93** resulted in formation of
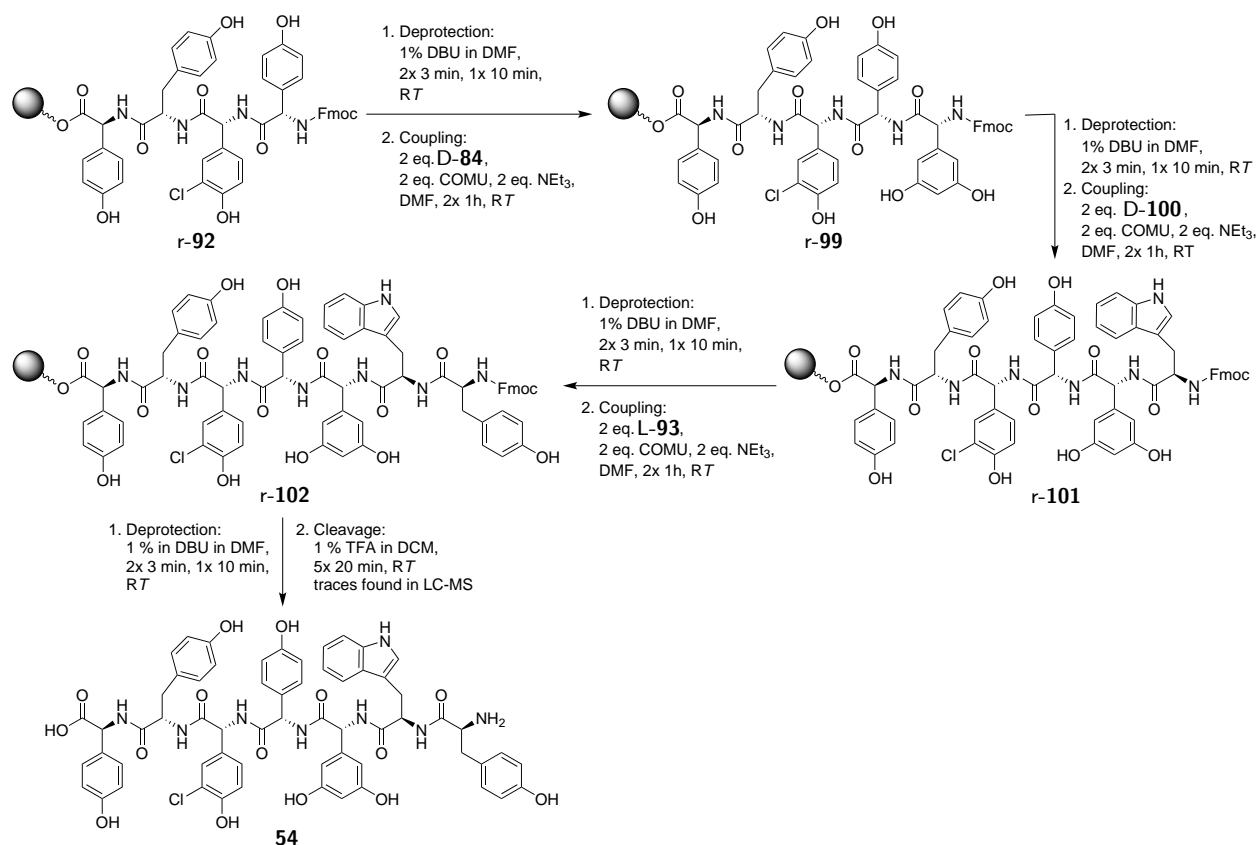
Scheme 21. Tetrapeptide **r-92** was elongated by SPPS to gain heptapeptide **54**. Significant side reactions took place during consecutive coupling of amino acids D-**84**, D-**100**, and L-**93**. Only traces of free heptapeptide **54** were found by LC-MS analysis, which could not be isolated.
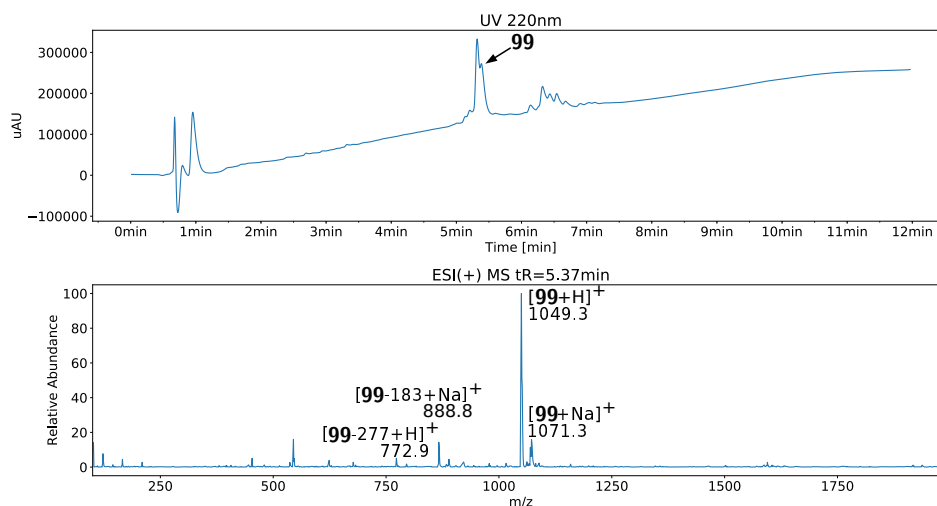
A LC-MS analysis of Fmoc protected pentapeptide **99** (tR = 5.4 min).
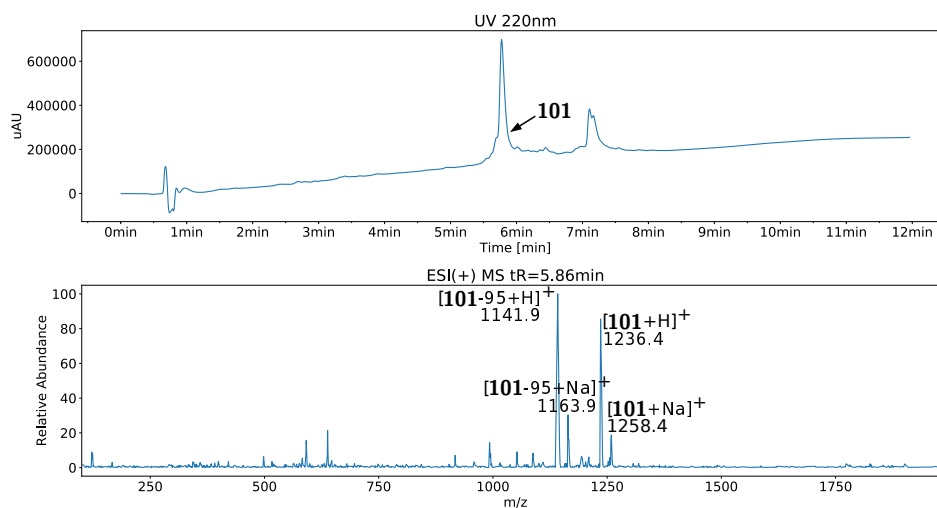
B LC-MS analysis of Fmoc protected hexapeptide **101** (tR = 5.9 min).
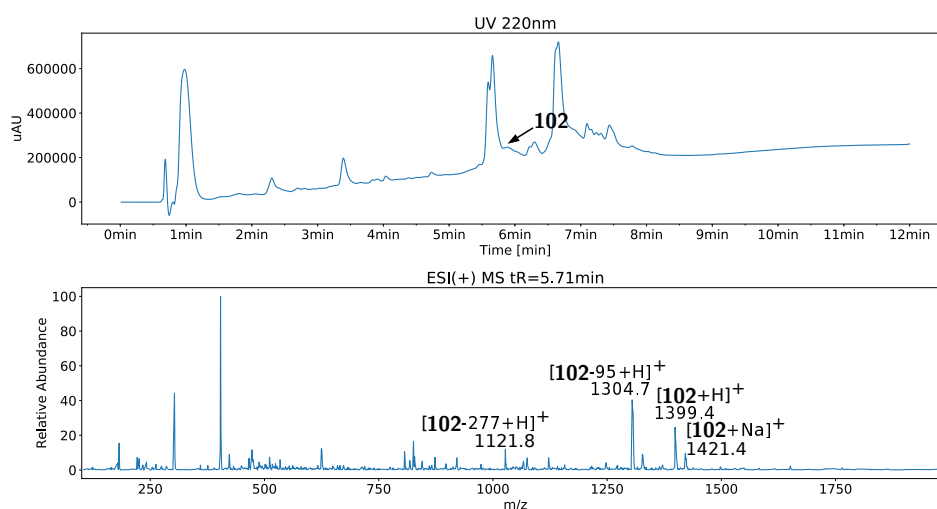
C LC-MS analysis of Fmoc protected heptapeptide **102** (tR = 5.7 min).

Figure 19. MS-spectra **A** to **C** show formation of side products during SPPS of **102**, which always exhibit the same mass differences to the respective product (M-95, M-183, M-277), at tR = 5.3 to 5.8 min (not displayed for all cases).

61
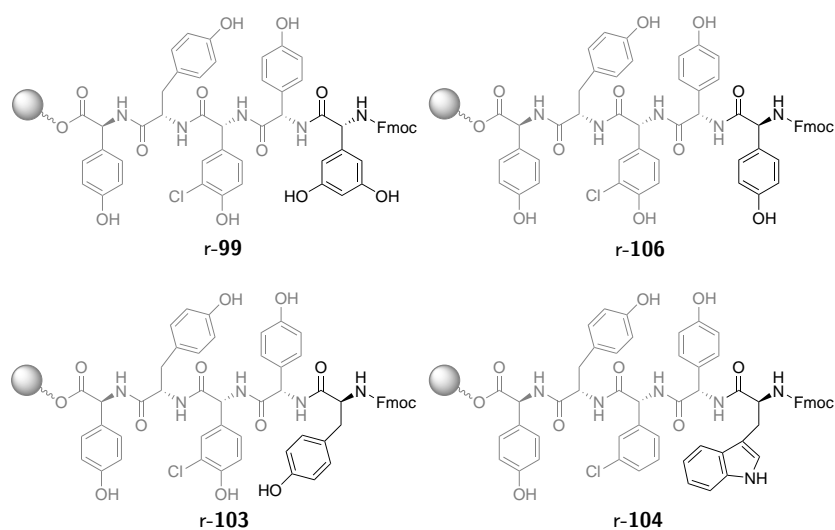
Figure 20. SPPS of Fmoc protected pentapeptide **r-99** was compared with those of derivatives **r-106**, **r-103**, and **r-104** to investigate side product formation during SPPS.

the previously observed side products as well as minor formation of Fmoc protected pentapeptide **103**. No Fmoc protected pentapeptide **104** was formed during coupling of D-**100**. These findings eliminated D-**84** as a cause for the disturbing side reactions. Instead, the hydrophilic nature of the growing peptide may have created a coiling chain, which was then difficult to attack by reagents and especially by sterically hindered amino acids. This suggests, that SPPS conditions had to be adjusted to prevent coiling of the peptide chain. Alternatively, heptapeptide **54** could be divided into two parts, the already synthesized western tetrapeptide **92** and the yet to be synthesized eastern tripeptide **105**, which would then be connected at later stage (Scheme 22). Both approaches were examined in the course of this thesis.
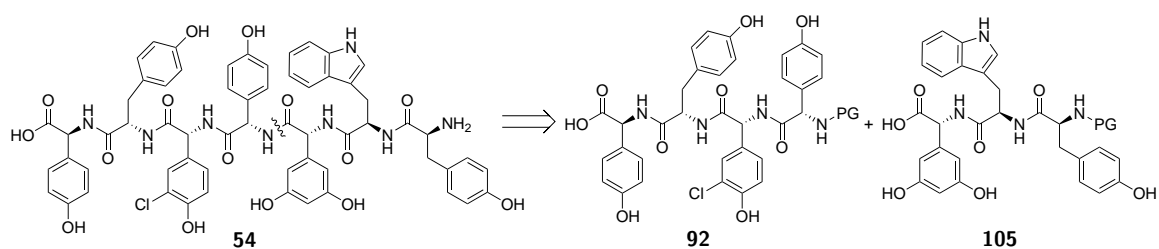
Scheme 22. Separation of the kistamicin A heptapeptide chain (**54**) into two parts, the already synthesized western tetrapeptide **92** (for PG = Fmoc) and the yet to be synthesized eastern tripeptide **105** (for PG = Fmoc).

3.2.5.4. Epimerization of Phenylglycin Building Blocks during SPPS

The use of phenylglycins as building blocks in SPPS is limited by their susceptibility to epimerization under reaction conditions classically employed in Fmoc chemistry (Chapter 3.2.5). Although epimerization did not occur during synthesis of tetrapeptide **92** - the respective ^{1}H-NMR showed a single isomer (Chapter 3.2.5.3) - it might have occured during other stages of peptide synthesis or under possibly altered reaction conditions. It was therefore decided to investigate, whether epimerization could be observed in LC-MS. For this purpose, diastereomeric di-, tri-, and tetrapeptides including different combinations of L-Hpg (L-**21**), D-Hpg (D-**21**), chloro-L-Hpg (L-**39**), and chloro-D-Hpg (D-**39**) were synthesized as previously described (Chapter 3.2.5.3). Synthesized diastereomers were cleaved off small amounts of resin and analyzed using LC-MS. The diastereomers were not isolated after cleavage. LC-MS analysis revealed that all diastereomeric Fmoc protected peptides did not differ in their respective retention times. After deprotection retention times slightly diverged (as exemplarily shown for free tripeptides **97**, **107**, **108**, **109** in Figure 22) and thereby allowed differentiation of each distinct diastereomer. This effect may be caused by the strong influence of the Fmoc moiety on the polarity of each peptide, which makes it impossible to discern small changes caused by stereochemistry. Comparision of LC-MS spectra off free dipeptides, tripetides, and tetrapeptides showed that racemization was minimal. More importantly, it can be assumed that LC-MS analysis of a free peptide would reveal occurance of diastereomers early in the synthesis. Indeed, after using racemic Fmoc-DL-Dpg (DL-**84**) in SPPS LC-MS analysis allowed for identification of both diastereomers (Chapter 3.2.5.5). To conclude, the developed mild, Fmoc based SPPS strategy (Chapter 3.2.5.3) fascilitates enantioselective synthesis of peptides containing phenylglycins.
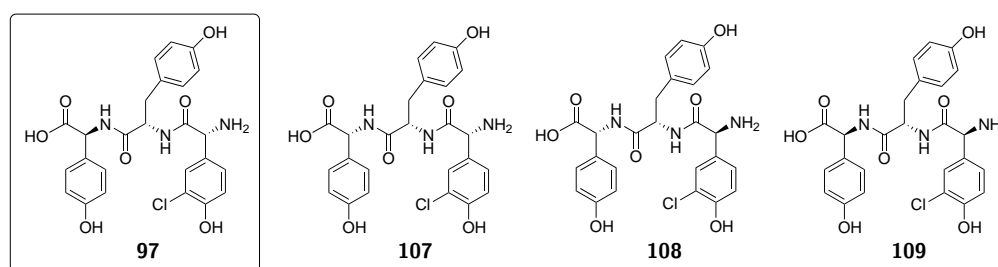
Figure 21. Various tripeptide diastereomers of the kistamicin-type tripeptide **97** were synthesized, which consisted of different combinations of L-Hpg (L-**21**), D-Hpg (D-**21**), chloro-L-Hpg (L-**39**), and chloro-D-Hpg (D-**39**).
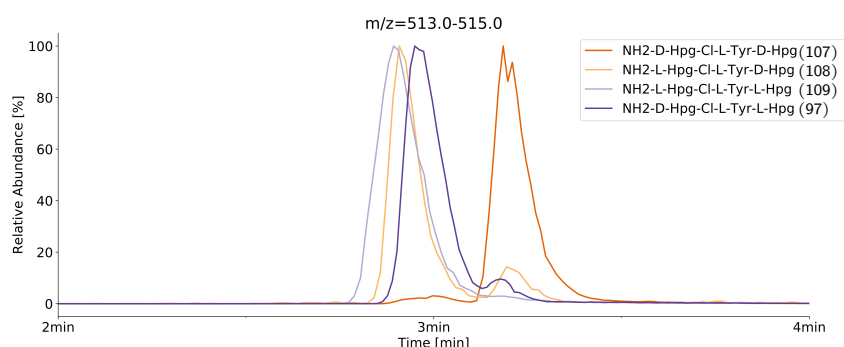
Figure 22. LC-MS analysis (extracted masses *m/z*=513.0-515.0) of tripeptide diastereomers with free *N*-termini showed a slight divergence in retention times.

3.2.5.5. Synthesis of the Eastern Tripeptide on Solid Phase

Due to the simple and straightforward synthesis of western tetrapeptide **92** by Fmoc chemistry based SPPS, the same strategy was applied to the synthesis of the other half of the kistamicin A heptapeptide chain (**54**), eastern tripeptide **105** (Scheme 23). As described above (Chapter 3.2.5.3), washed, swollen, and activated 2-CTC resin was mixed with 0.88 equivalents of Fmoc-D-Dpg (D-**84**) and 1.24 equivalents of NMM, solved in DCM/DMF (1:1) under argon atmosphere, and shaken for 24 h at R*T*. The amount of D-**84** used for loading of the resin was significantly reduced compared to that of Fmoc-L-Hpg
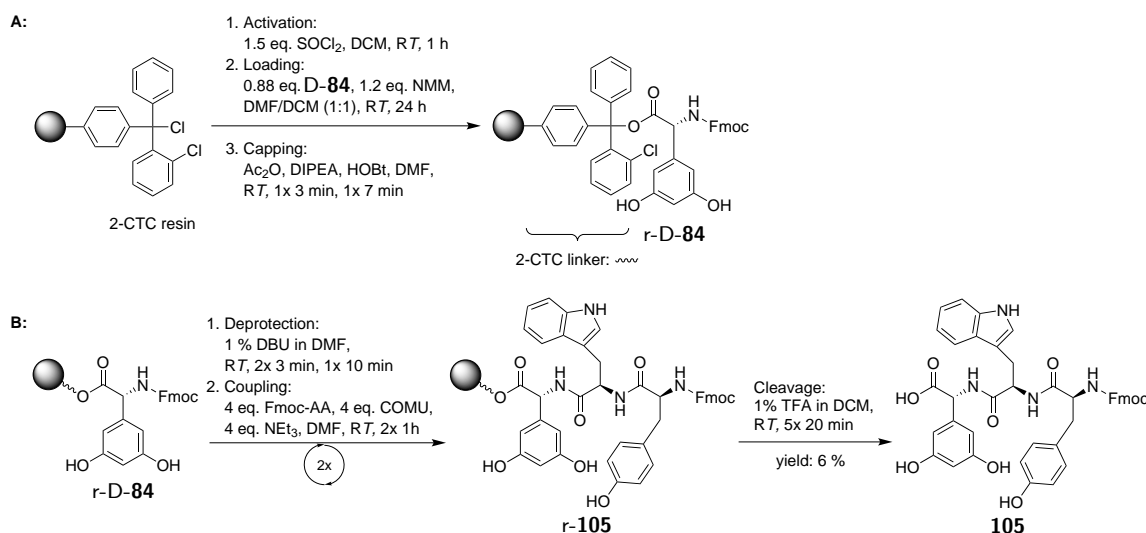
Scheme 23. SPPS of tripeptide **105** employing an optimized Fmoc strategy. **A:** loading of 2-CTC resin with the first amino acid, Fmoc-D-Dpg (D-**84**), and subsequent capping of unreacted reaction sites; **B:** Fmoc deprotection using 1 % DBU in DMF; coupling of subsequent building blocks, D-**100** and L-**93**, using COMU and triethylamine in DMF; peptide cleavage from the resin using 1 % TFA in DCM.

(L-**82**) (2.3 eq.) to economize on the laboriously synthesized compound. After washing (DMF (3x), methanol (1x), DCM (1x), DMF (1x), DCM (1x)), the loaded resin was dried *in vacuo* to constant weight and subjected to Fmoc testing. Unfortunately, the Fmoc test failed to produce a conclusive result (no UV-absorption was measured at 301 nm). In the next step, unreacted reaction sites of the freshly swollen resin were capped by incubating the resin with a solution of acetic anhydride, DIPEA, and HOBt in DMF at RT (1x 3 min, 1x 7 min), and subsequently washed with DCM (3x). Fmoc deprotection and coupling of each amino acid was conducted according to the established protocol, as well. For Fmoc deprotection, the resin was treated three times with 1 % DBU in DMF (shaking 2x 3 min and 1x 10 min at RT). For amino acid coupling, 4 equivalents of the respective building block, Fmoc-D-Trp (D-**100**) or Fmoc-L-Tyr (L-**93**), were dissolved together with 4 equivalents of COMU and 4 equivalents of triethylamine for 2 min in DMF, mixed with the resin, and shaken for 1.5 to 2.5 h at RT. This was repeated once to gain complete conversion. Again, the resin was washed after each step (DMF (3x), methanol (1x), DCM (1x), DMF (1x), DCM (1x)) and progress monitored by LC-MS after cleaving the peptide off of a small sample of resin with 1 % TFA in DCM (20 min at RT). Similar to the synthesis of the western Fmoc protected tetrapeptide (**92**), LC-MS showed successful progress for the synthesis of the eastern Fmoc protected tripeptide **105**. It was therefore cleaved off the resin by repeated incubation with 1 % TFA in DCM (20 min at RT), repeated washing with DCM, and promptly purified by semi-preparative HPLC. Thus, SPPS easily and efficiently yielded 45 mg of compound **105**. The yield was 6 %
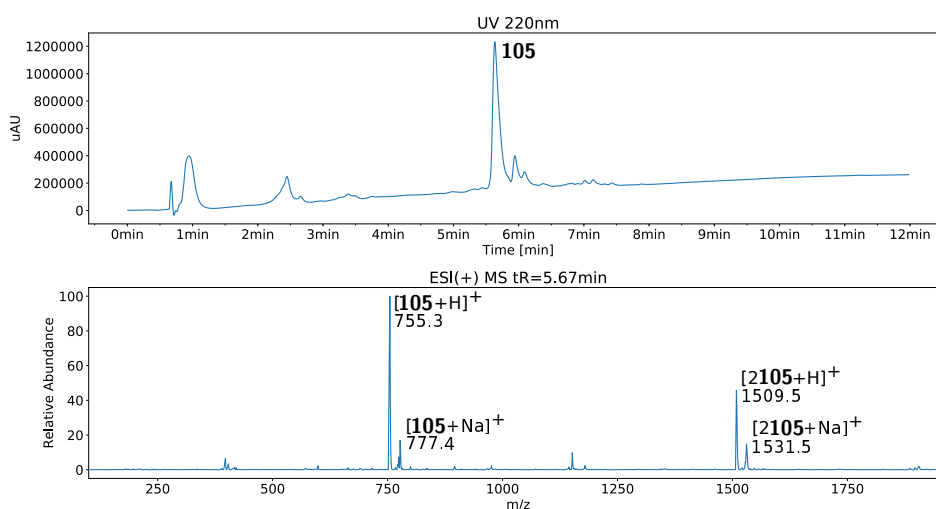
Figure 23. LC-MS analysis of crude, Fmoc protected tripeptide **105** (tR = 5.7 min), which was synthesized with an optimized SPPS protocol.

based on the used quantitity of D-**84**, which would be comparable to 8 % yield for tetrapeptide **92** based on the used quantity of L-**82**. Neither monitoring of SPPS by LC-MS nor the ^{1}H-NMR spectrum of product **105** showed epimerization.

3.2.5.6. Synthesis of the Eastern Tripeptide in Liquid Phase

The synthesis of the eastern tripeptide **105** was investigated in liquid phase as an alternative to SPPS. Due to the susceptibility of D-Dpg (D-**28**) to epimerization and already existing experience with the use of the Fmoc protecting group (Chapter 3.2.5.2), an Fmoc strategy was persued in this context, as well. However, it is important to note that the Fmoc group is not orthogonal to commonly applied carboxyl acid protecting groups, which are required in liquid phase peptide synthesis.
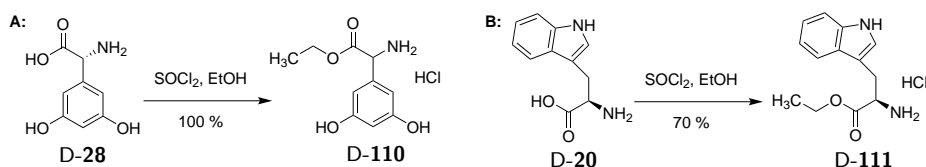
Scheme 24. *C*-terminal protection of D-Dpg (D-**28**) (**A**) and D-Trp (D-**20**) (**B**) as ethyl esters for later use in liquid phase peptide synthesis.

For protection of the *C*-terminus, D-Trp (D-**20**) as well as D-Dpg (D-**28**) were esterificated by refluxing with thionyl chloride in ethanol for 3 h. This yielded 70 % of D-tryptophan ethylester (D-**111**) and a quantitative amount of D-Dpg ethylester (D-**110**). Several coupling reagents were then applied to couple D-**111** to Fmoc-L-Tyr (L-**93**). After stirring with HBTU, TBTU, and DIPEA in DMF at R*T* for 31 h the desired dipeptide **112** could not be isolated, although the respective LC-MS signal had been observed during reaction control. Stirring with HOBt, EDCl, and NMM in DMF at R*T* for 16 h gave 45 % yield, but led to the precipitation of large amounts of a yellow solid during work-up and thus to yield loss during scale-up. Exchanging EDCl with DIC and adding THF as a solvent de-

Table 5. Reaction conditions for peptide coupling of D-tryptophane ethylester (D-**111**) and Fmoc-L-Tyr (L-**93**).

Starting Material	Reagents	Solvents	Reaction Conditions	Yield
D-**111**, L-**93**	HBTU, TBTU, DIPEA	DMF	31 h at R*T*	could not be isolated
D-**111**, L-**93**	HOBt, EDCl, NMM	DMF	16 h at R*T*	45 %
D-**113**, L-**93**	HOBt, DIC, NMM	DMF/THF (3:7)	18 h at R*T*	79 %
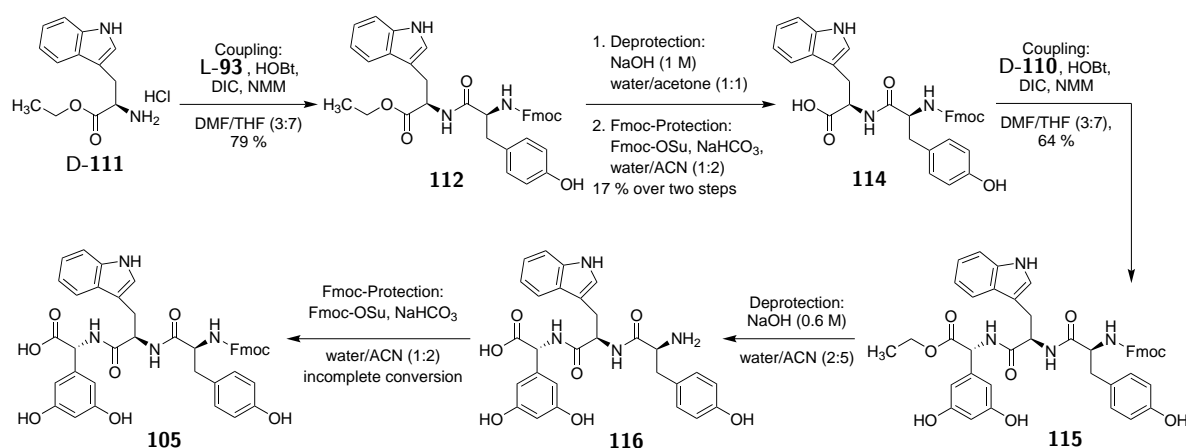
Scheme 25. Synthesis of eastern tripeptide **116** by liquid phase peptide synthesis.

reased the amount of precipitate during work-up and resulted in 79 % yield. To cleave the Fmoc moiety in **112** without saponification, **112** was subjected to various reagents. Stirring with acids (hydrochloric acid or TFA), nucleophiles (LiCl or TMS-Cl and soidum iodide) as well as the mild base lithium hydroxide resulted in no or only very limited conversion. Finally, it was resorted to stirring **112** in 1 M sodium hydroxide solution (acetone/water 1:1) at RT for 24 h, simultaneously loosing the Fmoc as well as the ethyl ester protecting group, and subsequent Fmoc restoration using Fmoc hydroxysuccinimide ester under standard conditions. This gave the desired dipeptide **114** in 17 % yield over two steps. However, massive solubility problems were encountered when larger amounts of **112** were subjected to deprotection, which could not be solved by exchange of solvents. In the next step, **114** was coupled to D-Dpg ethylester (D-**110**) by stirring with HOBt, EDCl, and NMM in DMF at RT over night, yielding 64 % **115**. Following the previously established procedure, the Fmoc as well as the ethyl ester moiety were removed by stirring **115** in a 0.6 M sodium hydroxide solution (acetonitrile/water 5:2) for 2 h (starting at 4 °C

Table 6. Reaction conditions for Fmoc deprotection of dipeptide **112**.

Reagents	Solvents	Reaction Conditions	Yield
TFA (20 v/v %)	methanol/ACN (5:1)	3 h at RT	no conversion
TFA (60 v/v %)	methanol/ACN (5:1)	120 h at RT	no conversion
HCl (3 M)	methanol	16 h at RT	traces
HCl (3 M)	methanol	24 h at 60 °C	traces
LiCl	DMF	10 min at 160 °C, MW	traces
TMS-Cl, NaI	solvent free	6 h and 27 h at 85 °C	traces
LiOH (0.08 M)	THF/water (1:4)	20 h at RT	traces
NaOH (1 M)	acetone/water (1:1)	24 h at RT	77 %

and warming up to R*T*). The Fmoc protecting group was reinstalled by conversion with Fmoc hydroxysuccinimide ester under standard conditions. However, HPLC monitoring of the Fmoc protection reaction revealed only incomplete conversion of starting material **116** to product **105**, possibly due to remaining salts. An even worse result was that HPLC analysis showed epimerization of **116** (Figure 24), probably occuring during protecting group removal or caused by racemization of D-**110** during esterification. Obtainment of diastereomers must also be assumed for **105**, although the strong influence of the Fmoc moiety on retention times most likely prevents separation of the respective diastereomers (Chapter 3.2.5.4) and the presence of several diastereomers could therefore not be proven. The previous experience with the synthesis of Fmoc-D-Dpg (D-**84**), which suggests that the laborious removal of salts from peptides with free *C*- and *N*-termini would be necessary for subsequent successfull Fmoc protection (Chapter 3.2.5.2), as well as the discouraging obeservation of epimerization, and problems during scale-up led to the rejection of the liquid phase synthetic route to tripeptide **105**. Instead, it was resorted to synthesize **105** by SPPS (Chapter 3.2.5.5).
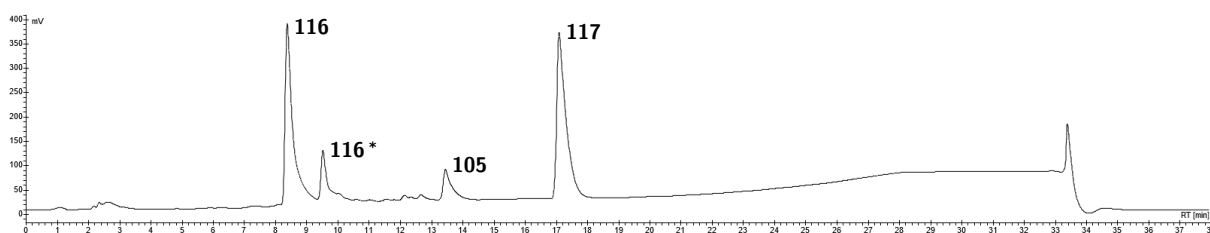
Figure 24. The reaction of dipeptide **116** with Fmoc hydroxysuccinimide ester (**117**) was monitored by HPLC. Starting material **116** occured as a scalemic mixture of diastereomers (diastereomer indicated with *). Only a small amount of - presumably racemic - product **105** was formed.

3.2.5.7. Investigation into the Coupling of the Western Tetrapeptide to the Eastern Tripeptide on Solid Phase

It was endeavored to find an easy and straightforward method to assemble Fmoc protected heptapeptide **102** from two halves, western tetrapeptide **98** and eastern tripeptide **105**. Therefore, different reaction conditions were applied to couple **105** to still resin bound **r**-**98**. In a first step, the Fmoc moiety was efficiently cleaved off resin bound tetrapeptide **r**-**92** using 1 % DBU in DMF and shaking at R*T* (3x 1 min, 2x 4 min). Next, standard peptide coupling reagents COMU and triethylamine were solubilized together with **105** for 2 min at R*T*, and then incubated with resin bound **r**-**98** for 3 days at R*T*. The resin was then washed (DMF (3x), methanol (1x), DCM (1x), DMF (1x), DCM (1x)), the
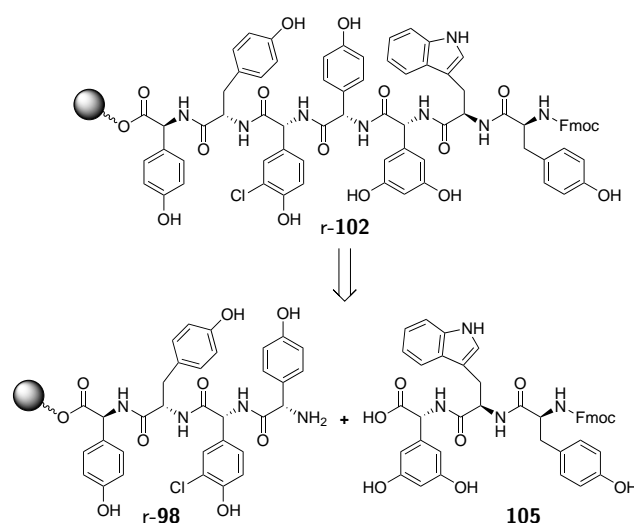
Scheme 26. The assembly of Fmoc protected heptapeptide **r-102** from two halves, **r-98** and **105**, was investigated. Only traces of **118** could be detected by LC-MS analysis.

product cleaved off a small amount of resin (1 % TFA in DCM for 20 min at R*T*), and analyzed by LC-MS. However, **102** could not be detected and no reaction seemed to have taken place. Subsequently, DMF was exchanged for a more polar solvent, NMP, which should improve solubility of the peptide chains. **102** could again not be found by LC-MS analysis. Therefore, the coupling reagents were exchanged for HOBt and DIC (with DMF as solvent). These reagents have previously been used for peptide coupling in liquid phase (Chapter 3.2.5.6), and also for assembling the complestatin linear peptide chain (**38**) from two halves in SPPS in the To. Gulder group.[192] Traces of **102** could be detected by LC-MS analysis, but there was no improvement compared to the previously investigated consecutive SPPS strategy (Chapter 3.2.5.3). These results were not surprising given that it has previously (Chapter 3.2.5.3) been assumed that the hydrophilic nature of the growing peptide might have created a coiling chain, which would have been difficult to attack by sterically hindered building blocks or reagents. However, the failure to assemble **102** on solid support created new challenges for the synthesis.

Table 7. Reaction conditions for coupling of tripeptide **105** to resin bound tetrapeptide **r-98** to give heptapeptide **102**.

Reagents	Solvent	Reaction Conditions	Yield
COMU, triethylamine	DMF	3 d at R*T*	no conversion
COMU, triethylamine	NMP	4 h at R*T*	no conversion
HOBt, DIC	DMF	3 d at R*T*	traces of **102**
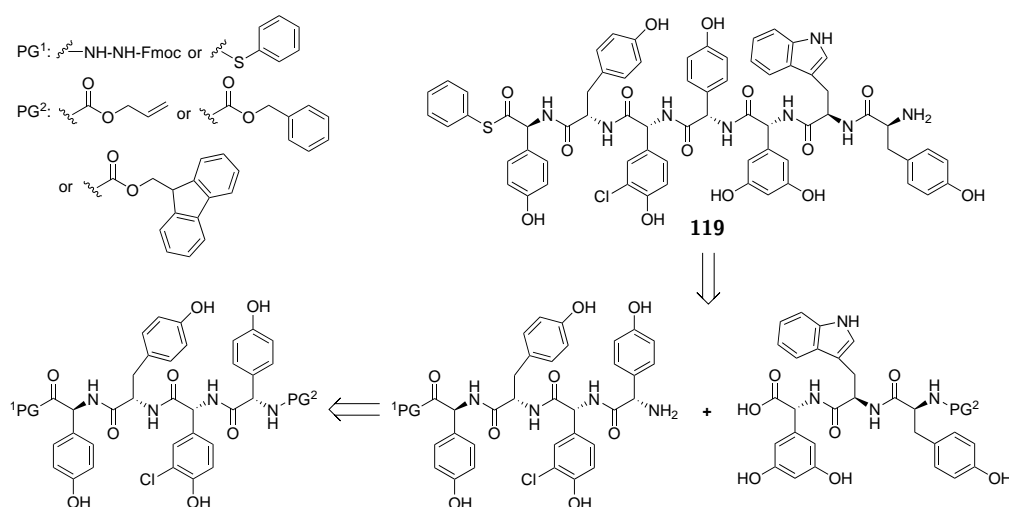
Scheme 27. The assembly of the kistamicin A linear peptide precursor **119** from two halves in liquid phase requires introduction of a carboxyl protecting group PG^1 as well as of orthogonal amine protecting groups PG^2.

To couple both halves of the heptapeptide chain in liquid phase required introduction of a carboxyl protecting group to the tetrapeptide. Utilization of classic ester protecting groups did not seem feasible due to the high sensitivity to epimerization of phenylglycin residues under basic (and acidic) conditions (Chapter 3.2.5) as well as the poor results observed during LPPS of **105** (Chapter 3.2.5.6). Since the ultimate use of the kistamicin A peptide chain in chemo-enzymatic assays requires introduction of a *C*-terminal thioester (Chapter 1.2.1.3, compound **119**), installation of a thioester or a masked thioester functioning as a carboxyl protecting group appeared to be more promising. However, this also required replacement of the Fmoc protecting group in the tetrapeptide as well as the tripeptide with a protecting group orthogonal to a thioester, such as an Alloc or Cbz moeity. The exchange of *N*-terminal protecting groups (Chapter 3.2.5.8) as well as the installation of a *C*-terminal thioester (Chapter 3.2.5.9), and a masked thioester (Chapters 3.2.5.10 and 3.2.5.11) was investigated in the course of this thesis.

3.2.5.8. Exchanging *N*-Terminal Protecting Groups in the Western Tetrapeptide

Utilization of a thioester as a *C*-terminal protecting group for the western tetrapeptide required adoption of an orthogonal *N*-terminal protecting group (Chapter 3.2.5.7). Both an Alloc as well as a Cbz moiety were considered to be suitable. Tripeptide **r-97** was therefore synthesized with the developed SPPS protocol (Chapter 3.2.5.3), and Alloc-L-Hpg (**L-85**) as well as Cbz-L-Hpg (**L-86**) were coupled as the fourth building block.
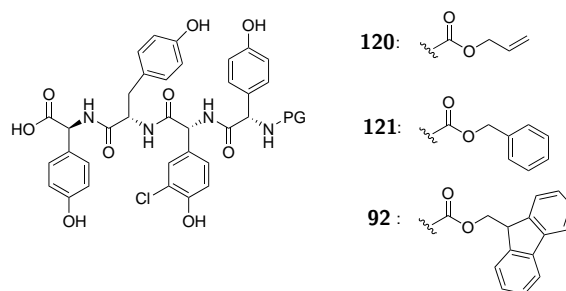
Figure 25. Adoption of an Alloc (**120**), a Cbz (**121**) as well as an Fmoc (**92**) moeity as *N*-terminal protecting groups for the western tetrapeptide chain.

Reaction conditions were the same as for the coupling of Fmoc protected amino acid building blocks: COMU and triethylamine were solubilized with the respective building block, L-**85** or L-**86**, in DMF for 2 min at R*T*, and the resin incubated for 1 h at R*T*. The resin was then washed (DMF (3x), methanol (1x), DCM (1x), DMF (1x), DCM (1x)), and the peptide cleaved off a small amount of resin (1 % TFA in DCM for 20 min at R*T*). Analysis by LC-MS confirmed formation of both **120** and **121** (Figure 27). Subsequently, each tetrapeptide - **120** and **121** - was cleaved off a larger amount of resin (incubating 5x with 1 % TFA in DCM for 20 min at RT and subsequent washing with DCM), and purified by semi-preparative HPLC. In both cases the respective HPLC chromatograms revealed epimerization, especially for **120**. At a first glance, this did not seem to negatively influence yields: 26 % of compound **120** and 43 % of compound **121** were apparently gained (based on the resin's loading degree). Those results were suspiciously high compared to 19 % yield for Fmoc protected tetrapeptide **92**. However, in contrast to **92**, which was lyophilized after purification by semi-preparative HPLC, **120** and **121** were dried *in vacuo* (the freeze dryer was not available at the given time). This method probably left water and TFA behind, and thereby led to errors in the determination of yields. Indeed, when the synthesis of the Cbz protected tetrapeptide (**121**) was later repeated in parallel to that of the Fmoc protected tetrapeptide (**92**), and both compounds were lyophilized after purification, only 2.6 % of compound **121** were obtained. Results for **92**, on the other hand, were reproduced in 18.3 % yield (based on the resin's loading degree). The cause for the surprising epimerization of compounds **120** and **121** presumably lay in the reduced sterical hindrance of the Alloc and Cbz moieties, which facilitated rotation. Alloc protected tetrapeptide **120** could not be completely separated from another diastereomer, as the respective ^{1}H-NMR spectrum showed. Therefore, **120** was not used in the further synthesis, which employed **121** and **92** instead.
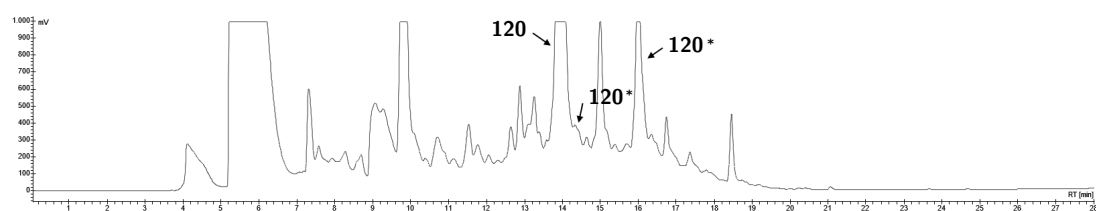
A Alloc protected tetrapeptide **120**. Diastereomers are indicated with *.
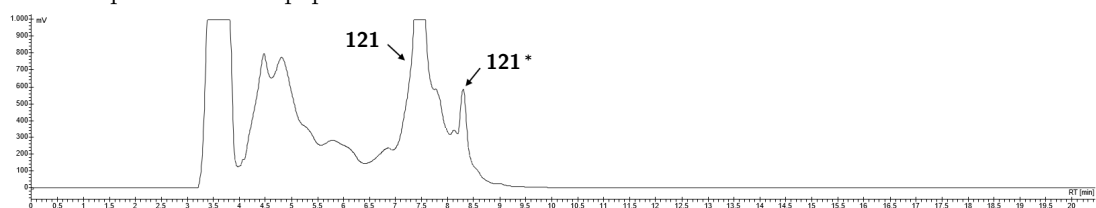
B Cbz protected tetrapeptide **121**. Diastereomers are indicated with *.
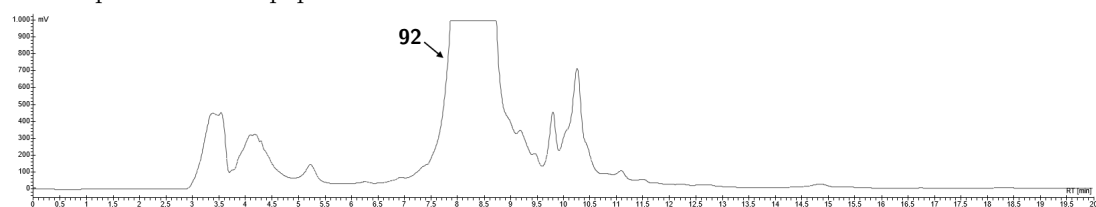
C Fmoc protected tetrapeptide **92**.

Figure 26. Semi-preparative HPLC analysis (different gradients) of the *N*-terminaly protected western tetrapeptides.
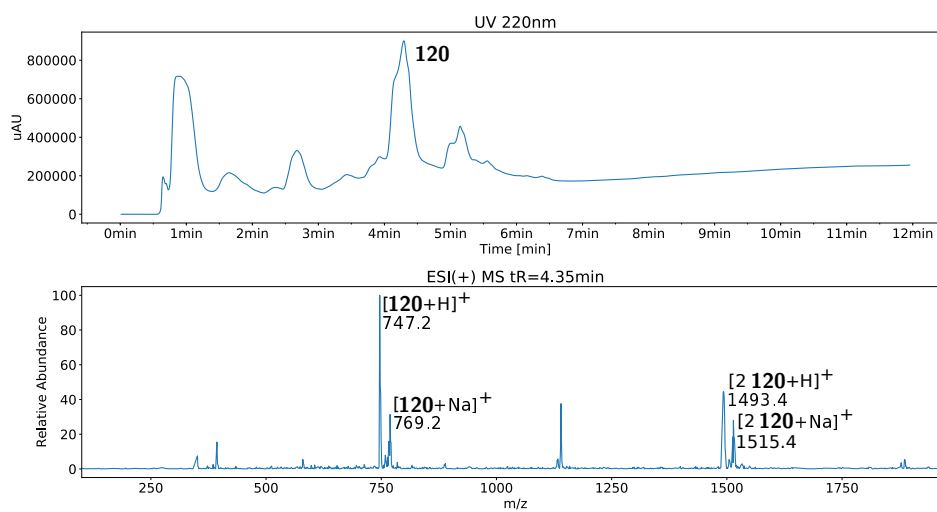
A LC-MS analysis of crude, Alloc protected tetrapeptide (**120**) (tR = 4.6 min).
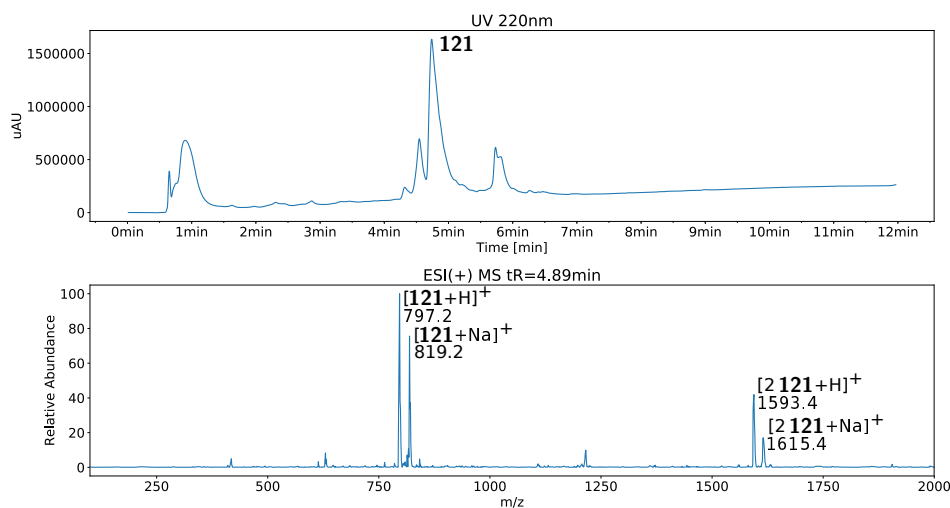
B LC-MS analysis of crude, Cbz protected tetrapeptide (**121**) (tR = 4.9 min).
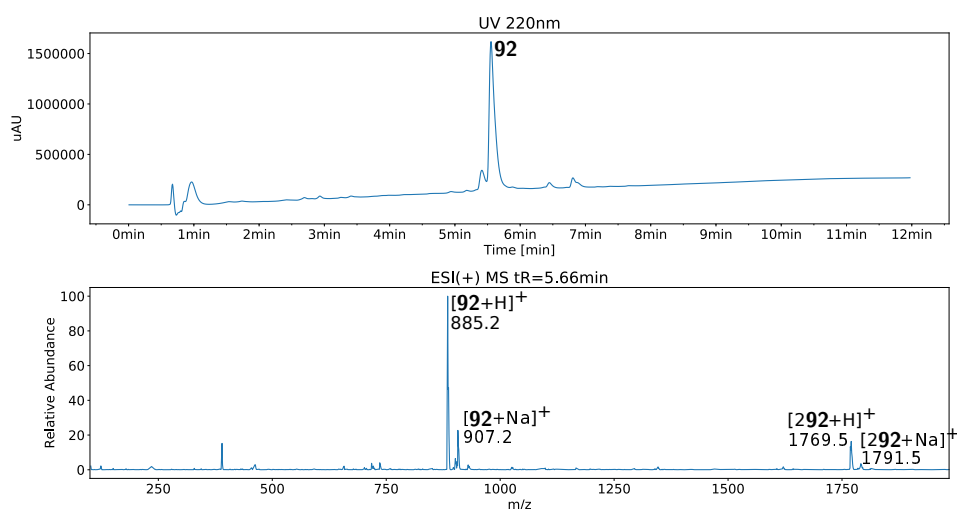
C LC-MS analysis of crude, Fmoc protected tetrapeptide (**92**) (tR = 5.5 min).

Figure 27. LC-MS analysis of western tetrapeptides with different *N*-terminal protecting groups.

3.2.5.9. Installation of a *C*-Terminal Thioester at the Western Tetrapeptide

To install a *C*-terminal thioester as a protecting group Fmoc as well as Cbz protected tetrapeptides **92** and **121** were reacted with thiophenol. For this purpose, a protocol previously used in the To. Gulder research group for the synthesis of the complestation thioester peptide chain[115] was employed: **92** and **121**, respectively, were stirred together with thiophenol as well as coupling reagents PyBOP and DIPEA in DMF for 30 h at R*T*, the reaction mixture then diluted with methanol, and directly purified by semi-preparative HPLC. Fmoc protected peptide **92** was converted to product **122** with a satisfactory yield of 72 %. However, thiophenylation of the Cbz protected peptide **121** under the same reaction conditions disappointed: conversion of **121** yielded only 16 % product **123**. These strongly deviating results in the *C*-terminal thiophenylation reactions of two tetrapeptides, which only slightly differ in their *N*-terminal protecting groups, were unexpected. In addition, epimerization of both products **122** and **123** was observed in the respective ^{1}H-NMR spectra.
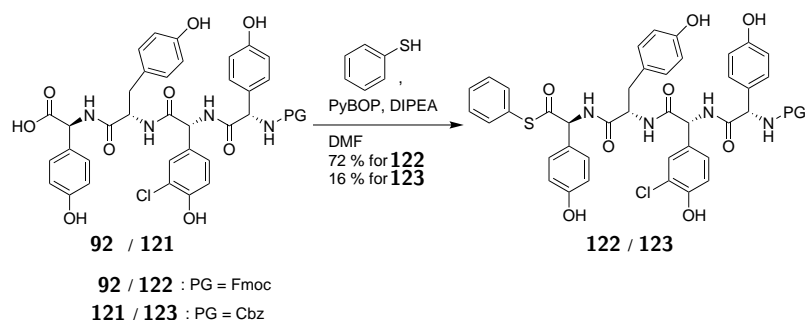
Scheme 28. Installation of a *C*-terminal thioester as a protecting group at the western tetrapeptide.

Nevertheless, attempts were made to remove the Fmoc protecting group from tetrapeptide **122** while keeping the thioester intact. (The minimal supply with **123** prevented similar attempts to remove the Cbz moeity.) For this purpose, a small sample of **122** was stirred with 1 % DBU in DMF at R*T* and the reaction monitored by LC-MS. After 20 min neither starting material **122** nor the desired product **124** could be observed in LC-MS spectra. The reaction was repeated using 1 % HOBt to suppress aminolysis. However, LC-MS spectra showed that the Fmoc moiety as well as the thioester were completely cleaved off **122** after stirring for 20 min at R*T*, and thus only free peptide **98** was formed. Exchanging DBU with another base, DIPEA (stirring **124** in DIPEA/DMF (1:2 and 1:1)), gave no conversion of **122** at all. In another try, **122** was stirred with 25 % 1-methylpyrrolidine,
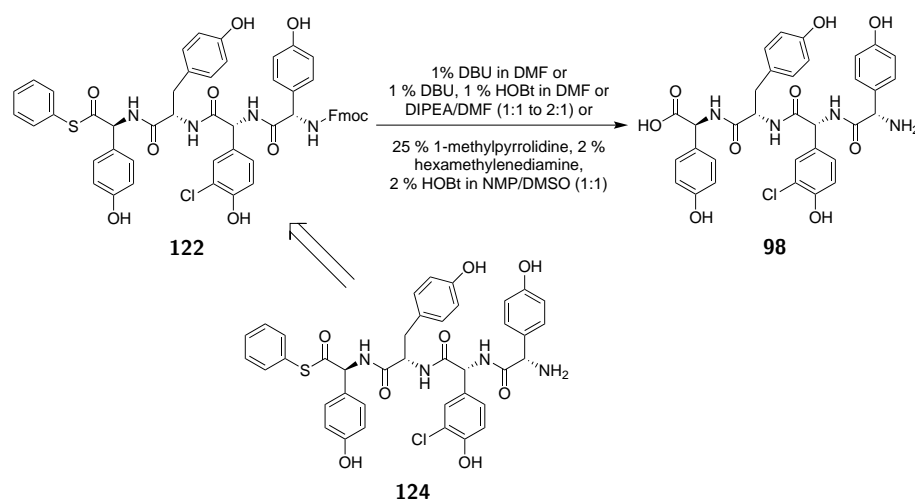
Scheme 29. Cleaving the Fmoc moeity off tetrapeptide **122** without simultaneous loss of the thioester was not possible.

2 % hexamethylenediamine, and 2 % HOBt in NMP/DMSO (1:1) for 2 h at RT according to a procedure of Li *et al.* The authors reported the use of this method for the removal of Fmoc moeities from several peptides while keeping the respective thioesters intact.[193] Again, LC-MS analysis only showed complete conversion to **98**. Considering those results, it seemed unlikely that cleavage of the Fmoc moeity from tetrapeptide **122** without simultaneous loss of the thioester was possible. Combined with the low yield in the thiophenylation of the Cbz protected tetrapeptide **121**, epimerization during thiophenylation, and the low yield in SPPS of starting material **121** (2.6 % for **121** as opposed to 19 % for **92**, Chapter 3.2.5.8) the direct introduction of a thioester as a carboxyl protecting group was consi-

Table 8. Reaction conditions for Fmoc deprotection of tetrapeptide **122** without cleavage of the *C*-terminal thioester.

Reagents	Solvents	Reaction Conditions	Result
1 % DBU	DMF	20 min at RT	no traces of **122** or **98**
1 % DBU, 1 % HOBt	DMF	20 min at RT	complete conversion to **98**
33 % DIPEA	DMF	20 h at RT	no conversion
50 % DIPEA	DMF	20 h at RT	no conversion
25 % 1-methylpyrrolidine, 2 % hexamethylenediamine, 2 % HOBt	NMP/DMSO (1:1)	2 h at RT	complete conversion to **98**

dered unserviceable. Instead, employing a masked thioester, which would only be converted to a thioester after removal of the *N*-terminal protecting group (Chapter 3.2.5.10), was deemed to be more promising.

3.2.5.10. Installation of a *C*-Terminal, Masked Thioester at the Western Tetrapeptide

In the endeavor to install a thioester as a carboxyl protecting group in the western tetrapeptide the use of a peptide hydrazide as a thioester surrogate was investigated. In this approach, Fmoc protected tetrapeptide **92** would be coupled with Fmoc hydrazide. Both the *C*- as well as the *N*-terminal Fmoc moeities would then be removed and the hydrazide subsequently oxidized to the azide and finally thiophenylated. To couple tetrapeptide **92** to Fmoc hydrazide, **92** and COMU were dissolved in DMF/THF (1:1) at 0 °C, triethylamine added to the solution, and after 10 min stirring at 0 °C Fmoc hydrazide was added, too. The reaction mixture was subsequently stirred over night at R*T*. However, no product could be isolatd after work-up. Exchanging coupling reagents with HATU and NMM gave no product, either, but use of HOAt, EDCl, and sodium bicarbonate in DMF/THF (1:2) finally yielded 36 % of product **125**. **125** was subsequently deprotected by stirring with 1 % DBU in methanol/acetonitrile (1:2) for 17 h at RT, giving 61 % of
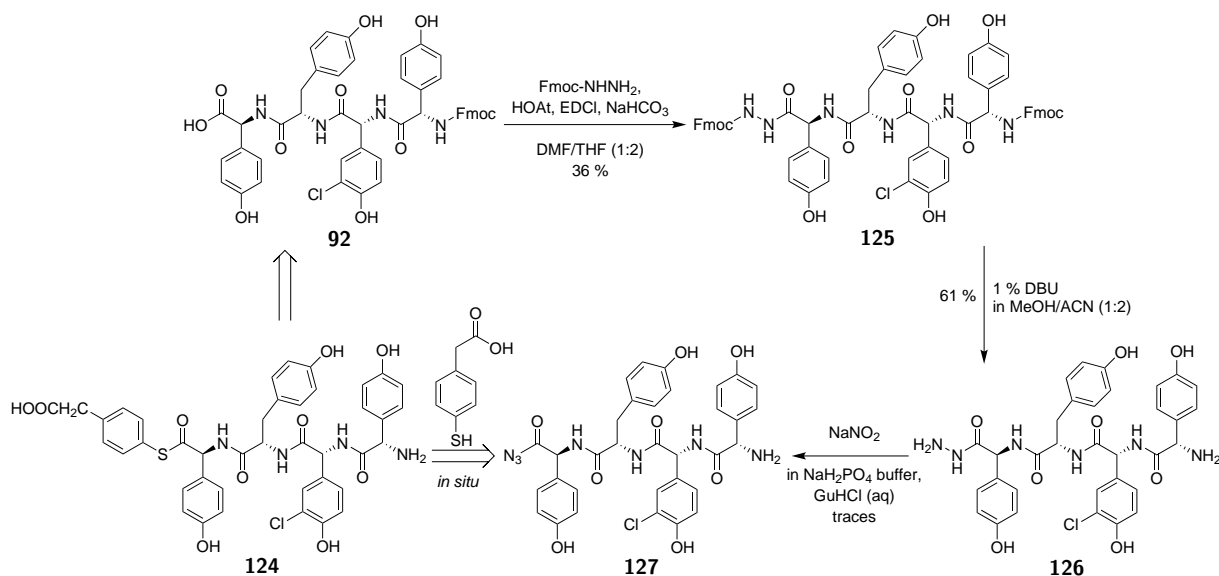
Scheme 30. Utilization of a peptide hydrazide as a thioester surrogate: Fmoc protected tetrapeptide **92** was coupled to Fmoc hydrazide, giving **125**. Both Fmoc groups were subsequently cleaved off and the resulting hydrazide **126** oxidized to azide **127**, which was not isolated. The final step would consist of an *in situ* conversion of azide **127** to thioester **124**, e.g. by addition of 4-mercaptophenylacetic acid, but could not be implemented.

Table 9. Reaction conditions for the oxidation of hydrazide tetrapeptide **126** to azide **127** with sodium nitrite in phosphate buffer (pH 3).

Concentration NaNO$_2$	Temperature	Reaction Time	ra(127)/ra(126)
0.05 M	−15 °C	20 min	0.88/1
0.05 M	0 °C	20 min	0.84/1
0.05 M	0 °C	1 h	0.7/1
0.05 M	0 °C	2 h	0.38/1
0.10 M	0 °C	4 h	0.38/1
0.10 M	0 °C	6 h	0.19/1

ra: relative abundance

product **126**. No epimerization was observed for compounds **125** and **126**. For oxidation of hydrazide **126** to azide **127** a protocol developed by Zheng *et al.*[194] for application in native chemical ligation procedures was adapted. To find the optimal reaction conditions, 1 mg of **126** was placed in an Eppendorf tube and solved in 200 µL 0.1 M monosodium phosphate buffer (pH 3), which was supplemented with 1.0 M guanidium chloride as a chaotropic salt. The Eppendorf tube was placed in an −15 °C ice/salt bath, to stabilize the product as well as to prevent side reactions, and 20 µL 0.5 M aqueous sodium nitrite solution were added. After stirring for 20 min a sample was analyzed by LC-MS (Figure 28). Indeed, approximately 0.88 parts of the desired product, azide **127**, were found besides one part of starting material **126**. Since the low temperature of the ice/salt bath led to freezing of the reaction mixture, the reaction was repeated while cooling to 0 °C. After stirring for 20 min, a 0.84/1 ratio of **127** to **126** was observed in the LC-MS spectra, a 0.7/1 ratio after 1 h, and a 0.38/1 ratio after 2 h. When the sodium nitrite concentration in the reaction mixture was doubled, the ratio of **127** to **126** remained at 0.38/1 after 4 h, and after 6 h only 0.19/1 were observed. Additionally, a significant increase in side products was observed with passing reaction time. These results indicate that azide **127** is unstable and decomposes over time. The oxidation reaction may thus be improved by an optimization of the reaction temperature, which is also depending on the salt content of the mixture, as well as the sodium nitrite concentration. Presumably, product **127** will need timely *in situ* thiophenylation, for example by direct addition of 4-mercaptophenylacetic acid to the reaction mixture (then pH 7).[194] However, due to a low supply with compound **126** as well as time limitations during this thesis, this approach was not further investigated. In parallel to the utilization of a peptide hydrazide in liquid phase, the employment of a solid support resin with a hydrazine linker in SPPS was examined (Chapter 3.2.5.11).
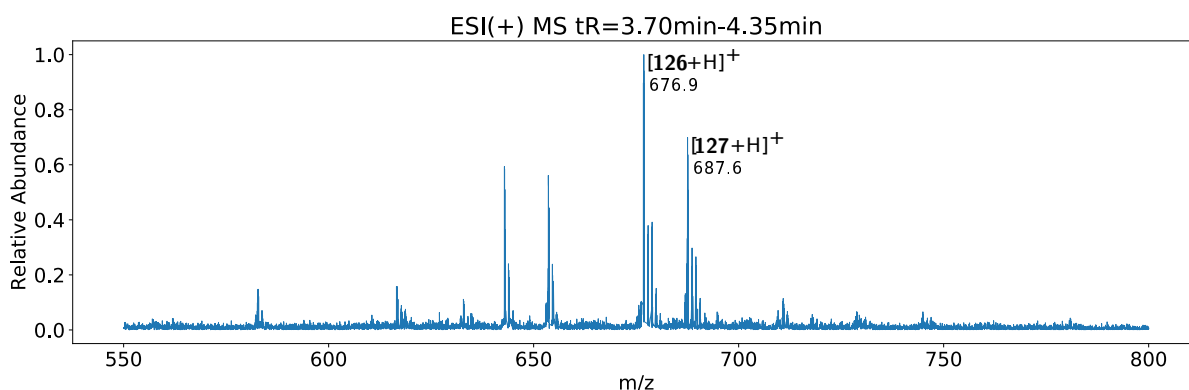
A Reaction control after 1 h (tR = 3.70 - 4.35 min).
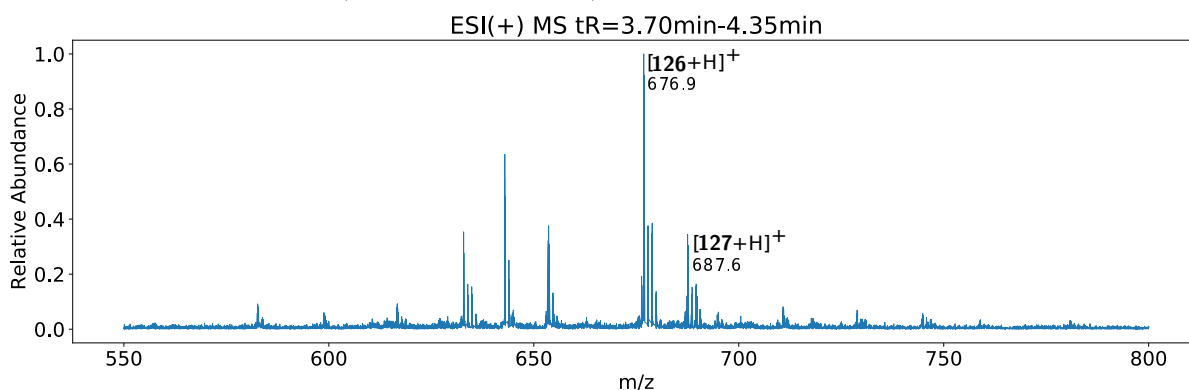
B Reaction control after 2 h (tR = 3.70 - 4.35 min).

Figure 28. The oxidation of hydrazide tetrapeptide **126** to azide **127** at 0 °C was monitored by LC-MS. The ratio of product **127** to starting material **126** decreased over time while formation of side products increased.

3.2.5.11. Investigation into the Synthesis of the Heptapeptide Hydrazide on Solid Phase

Another possible route to the *C*-terminaly thiophenylated heptapeptide **119** was SPPS of the respective peptide hydrazide (**128**) combined with oxidation to the azide (**129**) and thiophenylation. In this method, the conventional solid support resin 2-CTC resin carried a hydrazine linker to which the first amino acid, Fmoc-L-Hpg (L-**82**) was coupled. The synthesis of the peptide chain progressed by Fmoc based SPPS. After TFA mediated cleavage, the peptide was obtained as hydrazide **128**, which should then be converted to a thioester **119** by oxidation and thiophenylation.

For this purpose, the previously developed SPPS protocol (Chapter 3.2.5.3) was combined with an SPPS procedure by Zheng *et al.*,[194] which they developed for application in native chemical ligation. In the beginning of the synthesis, 2-CTC resin was washed with DMF
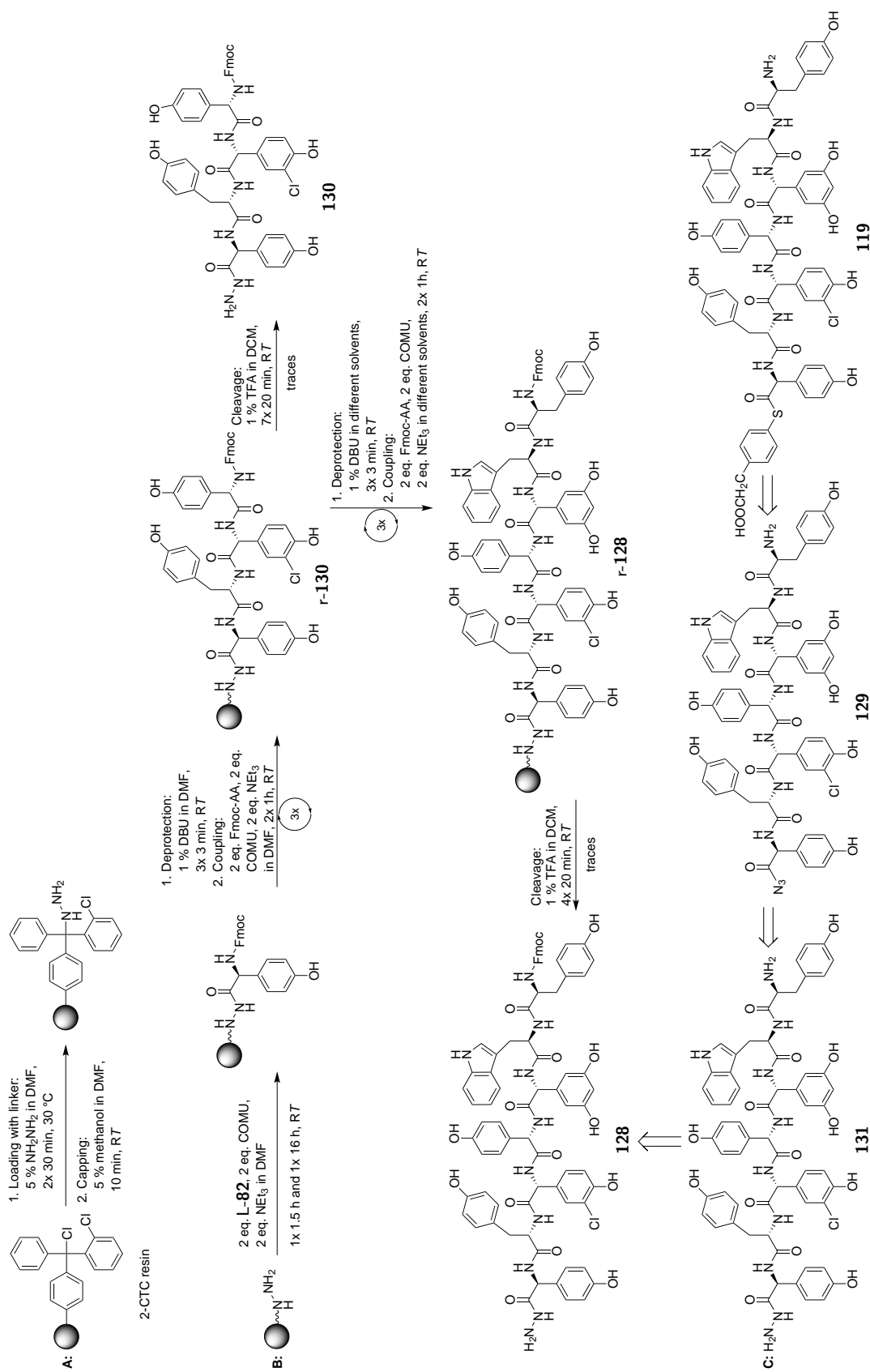
Scheme 31. **A**: Synthesis of 2-chlorotrityl hydrazine resin. **B**: SPPS of heptapeptide hydrazine **128** using 2-chlorotrityl hydrazine resin. DMF, NMP, NMP/DMSO (1:1) or a 3.0 M solution of guanidium chloride in DMF were applied as solvents for all Fmoc deprotection and amino acid coupling steps following formation of **r-130**. **C**: Retrosynthesis of thiophenylated heptapeptide **119** by Fmoc cleavage (**131**), oxidation to azide **129**, and subsequent thiophenylation.

3. Results and Discussion

(3x), DCM (3x), and DMF (3x), swollen with DCM/DMF (1:1) for 30 min at R T, and treated two times with hydrazine (5 v/v % in DMF) for 30 min at 30 °C to attach the linker. After capping unconverted reaction sites of the resin by incubation with MeOH (5 v/v % in DMF) for 10 min at R T, the resin was washed again (DMF (3x), DCM (3x), DMF (3x)). Subsequently, the first amino acid was coupled by solubilizing 2.0 equivalents Fmoc L-Hpg (L-**82**) with 2.0 equivalents COMU, and 2.0 equivalents triethylamine (0.1 M) in DMF for 2 min at R T, mixing with the resin, and incubation for 1.5 h at R T. This was repeated once with shaking for 16 h. After washing the loaded resin with DMF (3x), methanol (1x), DCM (1x), DMF (1x), and DCM (1x), and drying *in vacuo* to constant weight, the Fmoc test revealed a loading degree of only 17 %. Nevertheless, the freshly swollen resin was used for Fmoc deprotection and amino acid coupling according to the established protocol. The resin was washed after each step (DMF (3x), methanol (1x), DCM (1x), DMF (1x), DCM (1x)), and progress monitored by LC-MS after cleaving the peptide off a small amount of resin with 1 % TFA in DCM (20 min at R T). LC-MS spectra showed that SPPS progressed successfully to tetrapeptide hydrazide **130** (Figure 29A), and no signs for epimerization. Surprisingly, even SPPS of hepatapeptide hydrazide **128** appeared to be improved in LC-MS spectra: much less side products and a higher amount of product **128** were observed compared to SPPS with conventional 2-CTC resin. These results could be explained by the existence of the hydrazine linker, which sticked out of the resins bulky chlorotrityl moieties. The linker thereby might have reduced coiling of the peptide chain and improved access of coupling reagents as well as amino acids to the peptide. To further advance synthesis of **128**, three other, more polar solvents than DMF were applied to Fmoc deprotection and amino acid coupling. NMP, NMP/DMSO (1:1), and a 3.0 M solution of chaotropic salt guanidium chloride in DMF were employed for deprotection of **r-130** as well as all coupling and deprotecting reactions up to compound **r-128**. **r-128** formation remained strongly reduced in the guanidium chloride solution, while Utilization of NMP/DMSO (1:1) gave nearly no product. However, a single, high intensity peak was detected in LC-MS spectra for the formation of **128** when NMP was used as solvent (Figure 29B). Therefore, **128** was cleaved off the resin (1 % TFA in DCM, 20 min at R T, 4x) and subjected to semi-preparative HPLC. However, only a very small peak was identified in HPLC spectra for **128** (Figure 30A) and no product could be isolated. For better comparision, **130** was also cleaved off (1 % TFA in DCM, 20 min at R T, 7x) and purified by semi-preparative HPLC. Again, only a very small peak could by observed in HPLC spectra (Figure 30B) and no product could be isolated.
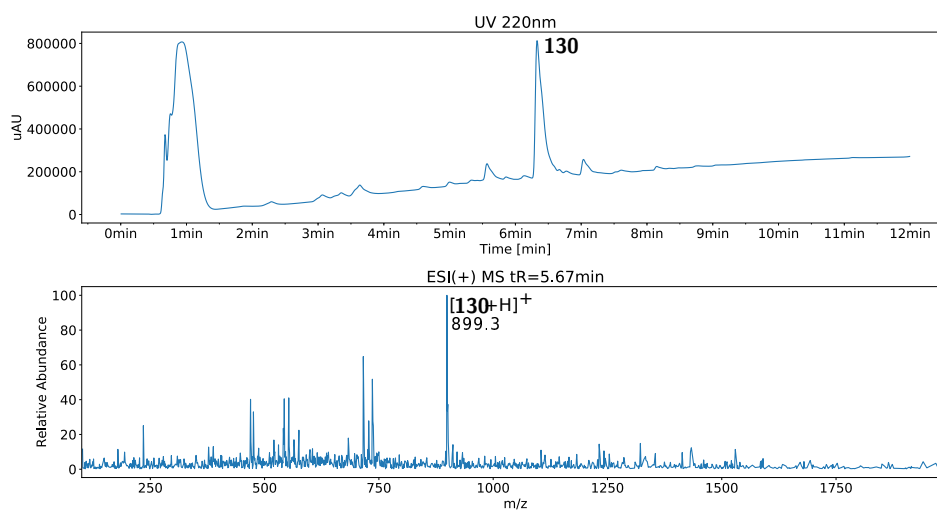
A Fmoc protected tetrapeptide hydrazide (**130**) (tR = 5.7 min) (DMF was used as solvent).
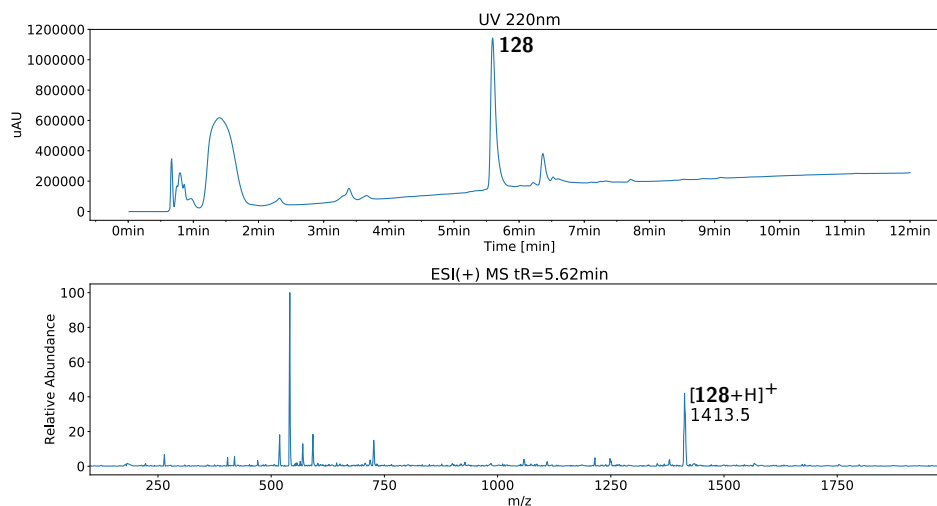
B Fmoc protected heptapeptide hydrazide (**128**) (tR = 5.6 min) (NMP was used as solvent).
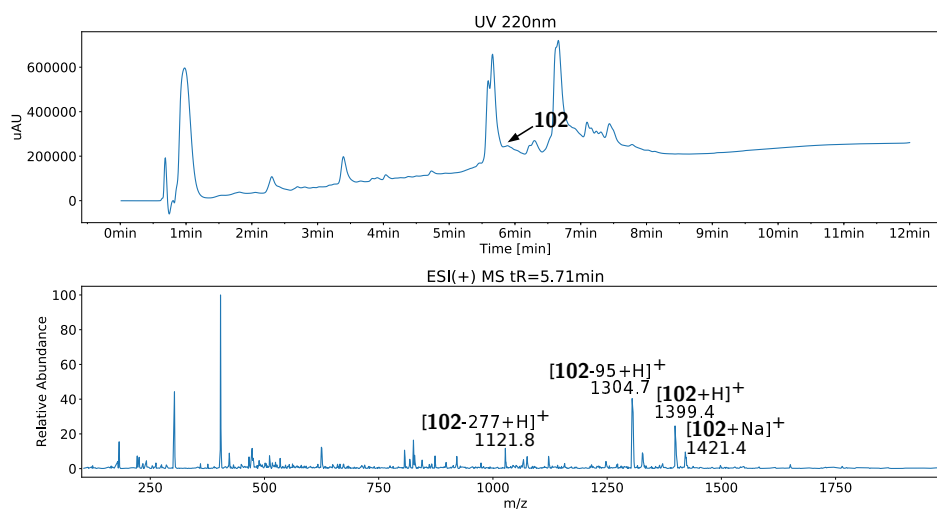
C Fmoc protected heptapeptide (**102**) (tR = 5.7 min) (Chapter 3.2.5.3) (DMF was used as solvent).

Figure 29. LC-MS analysis of heptapeptide synthesis with and without a hydrazine linker.

3. Results and Discussion

The main peak, which appeared in both cases in the HPLC spectra at 12.4 min and 9.0 min, respectively, could not be identified. It emerged even if the resin bound peptide was incubated once for 20 min with 1 % TFA in DCM, and immediately submitted to semi-preparative HPLC. Accordingly, the main peak could not be any artifact from excess treatement with TFA. Considering all collected data, a possible cause for the low yields seemed to be a poor loading of 2-CTC resin with Fmoc-L-Hpg (**L-82**). Indeed, the Fmoc test indicated a loading degree of only 17 % as opposed to 79 % when no linker was used (Chapter 3.2.5.3). Due to the fact that the Fmoc test can not be used to determine loading of a resin with a hydrazine linker, it remained unclear, whether the attachment of the hydrazine linker or the coupling with **L-82**, presented the obstacle. To exclude problems in the formation of the hydrazine linker, ready-made 2-chlorotrityl hydrazine resin (0.5 mmol/g hydrazine loading, 100-200 mesh) was purchased from *Sigma Aldrich* and **130** synthesized as described above. However, the amount of isolable peptide **130** remained the same. Therefore, other coupling reagents for the loading of **L-82** onto 2-chlorotrityl hydrazine resin were applied. In one try, the protocol of Zheng *et al.*[194] was adapted: 4 equivalents of **L-82** (0.34 M) were solubilized with 3.8 equivalents HBTU, 3.8 equivalents of HOBt, and 7.9 equivalents of DIPEA in DMF for 2 min at R*T*, and subsequently incubated for 1 h with 2-chlorotrityl hydrazine resin. This step was repeated
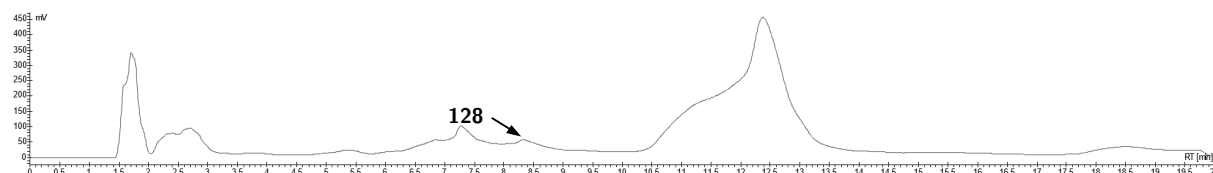
A Fmoc protected heptapeptide hydrazide (**128**) (tR = 8.35 min) (NMP was used as solvent).
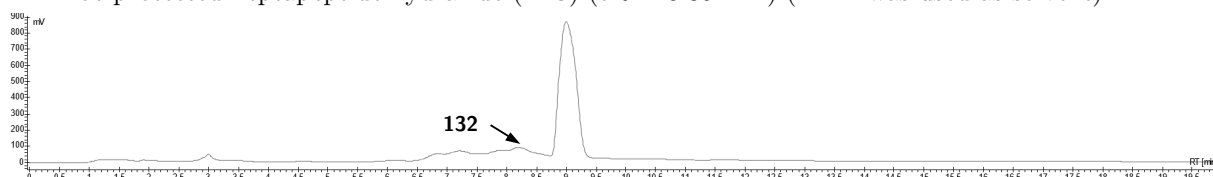
B Fmoc protected tetrapeptide hydrazide (**132**) (tR = 8.20 min) (DMF was used as solvent).
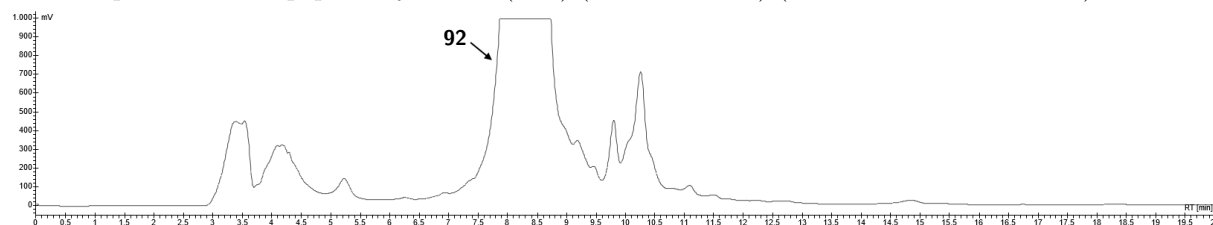
C Fmoc protected tetrapeptide (**92**) (tR = 7.60 to 8.90 min) (DMF was used as solvent) (Chapter 3.2.5.3).

Figure 30. Semi-preparative HPLC analysis of Fmoc protected peptides (various gradients).

once. In a second try, reagents also used in the coupling of Fmoc hydrazide to Fmoc protected tetrapeptide **92** (Chapter 3.2.5.10) were employed: 4 equivalents of L-**82** (0.2 M) were solubilized with 4.0 equivalents of HOAt in DMF at 0 °C, 6.0 equivalents of EDCl as well as 6.0 equivalents of sodium bicarbonate added, and shaken for 10 min at 0 °C. The mixture was then incubated once for 2.5 h with 2-chlorotrityl hydrazine resin, and again for 4.5 h. After washing and drying the treated resin to constant weight, the Fmoc test was repeated for both cases but showed no alterations in the degree of loading with Fmoc-L-Hpg (L-**82**). These severe problems in the attachment of the first amino acid to the hydrazine linker put a halt to attempts of synthesizing thiophenylated heptapeptide **119** via SPPS of the respective peptide hydrazide **128**.

Chapter 4

Conclusion

The present thesis focussed on the investigation of the (bio-)synthesis of natural products kistamicin A (**15**) and myxocoumarin B (**43**). These compounds combine intriguing molecular architectures with interesting antimicrobial activity profiles. Thus, they represent promising lead structures for drug development.
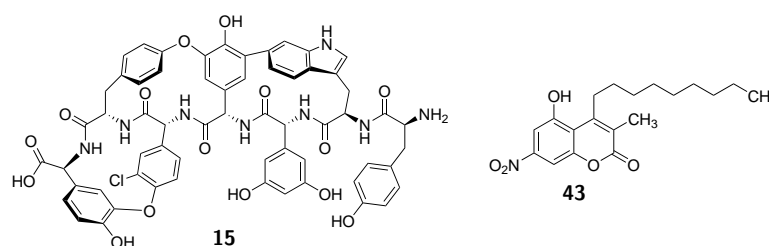
Figure 31. Chemical structures of the nonribosomal peptide kistamicin A (**15**) and the coumarin myxocoumarin B (**43**).

Myxocoumarin B (**43**) features a highly unusual 5-hydroxy-7-nitro substitution pattern as well as a long, saturated alkyl chain. Therefore, **43** is one of the few nitrogen containing coumarins found in nature and constitutes its own, novel class of secondary metabolites.[138] Co-workers of the To. Gulder laboratory (K. Kusserow, J. Müller, G. Hertrampf) synthesized myxocoumarin B (**43**) together with various derivatives, while the research group Nikodinovic-Runic at the Institute of Molecular Genetics and Genetic Engineering in Belgrade (A. Pavic) investigated the biological potential of **43**. Synthetic access to the 3,4-substituted myxocoumarin B (**43**) core was effectively provided by a Pechmann reaction, in which a phenol reacts with a β-keto ester in the presence of a catalyst. Solvent free microwave irradiation of the reactants and the use of TFA as a catalyst were established

4. Conclusion
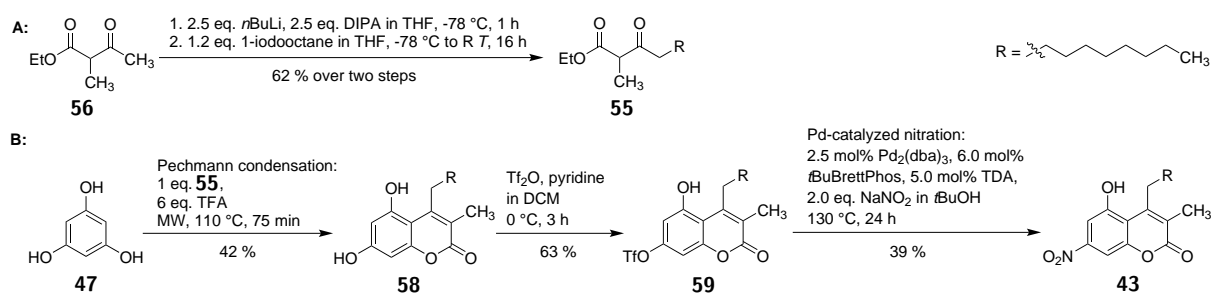
Scheme 32. Chemical total synthesis of myxocoumarin B (**43**). **A:** Synthesis of required β-keto ester **55**; **B:** synthesis of **43** via Pechmann reaction and palladium-catalyzed nitration in 10 % overall yield.

as the optimal reaction conditions. Alkyl substituents at C-3 and C-4 were introduced by the use of β-keto ester **55**, which in turn was available by regio-selective alkylation of **56** with iodo-octane in 62 % yield. Simultaneous installation of the nitro-substituent at C-7 was not possible due to its deactivating effect on the respective phenol. Instead, a triflate functionality was regioselectively introduced at C-7 (**59**) in 63 % yield via coumarin **58**, which in turn was gained in 42 % yield by Pechmann condensation of resorcinol with β-keto ester **55**. Triflate **59** served as the substrate in a palladium-catalyzed nitration as developed by the Buchwald laboratory and myxocoumarin B (**43**) was obtained as the direct product in 39 % yield. The To. Gulder laboratory thereby established the first, three step total synthesis of myxocoumarin B (**43**) in approximately 10 % overall yield, featuring a Pechmann reaction and late stage palladium-catalyzed nitration as the key steps. These results were published in *Org. Biomol. Chem.*[161]
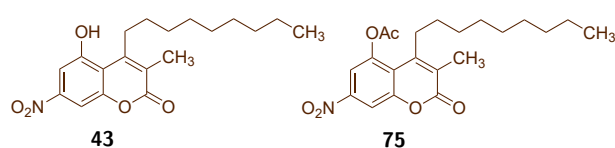
Scheme 33. Chemical structures of myxocoumarin B (**43**) and derivatives **75**, which show prominent antibacterial activity against *S. aureus* and *S. aureus* MRSA.

In the following work, variations of reactants in the Pechmann reaction allowed quick and easy generation of diverse myxocoumarin B derivatives for structure-activity relationship studies. By this approach, the To. Gulder laboratory introduced various phenol and alkyl substituents to the myxocoumarin B (**43**) core. In total, 38 structural myxocoumarin B analogs were synthesized. The biological potential of myxocoumarin B (**43**) and its derivatives was assessed in collaboration with the research group Nikodinovic-Runic. *In*

vitro tests showed strong antibacterial activity and specificity against Gram-positive strains *Staphylococcus aureus*, *S. aureus* MRSA, *Bacillus subtilis*, and *Enterococcus faecium*. In *in vivo* zebrafish assays **43** and several analogs only exhibited embryotoxicity above the range of concentrations active against the tested microorganisms. Overall, the natural product **43**, the acetylated natural product **75**, and a structural analog, which carried two hydroxy groups at the aromatic ring in addition to an n-C_7 alkyl chain, showed the most promising activity profiles. However, **43** lost some antibacterial activity upon prolonged storage. Based on these encouraning results, **75** and the 5,7-dihydroxy-4-heptaalkane analog were used to combat *S. aureus* infections in an *in vivo* zebrafish embryo model. Analyses of zebrafish embryo survival and bacterial proliferation showed that both compounds could efficiently cure the infected zebrafish embryos and performed even better than the glycopeptide antibiotic vancomycin, which was used as the positive control. Since the investigated compounds belong to a novel class of secondary metabolites, which can very easily and cheaply be accessed by chemical synthesis, those results were especially promising. They are currently evaluated for potential patenting and will be published in due course.

Similar to myxocoumarin B (**43**), the complex structural framework of the nonribosomal peptide kistamicin A (**15**) poses a big challenge to chemical synthesis. This does not only impede direct access to **15**, but also the generation of derivatives for structure-activity relationship studies. An innovative, straightforward approach to an efficient synthesis would be the combination of solid phase peptide synthesis (SPPS) of the kistamicin linear peptide precursor **54** with the use of cytochrome P450 enzymes to perform regio- and stereoselective oxidative phenol coupling reactions (OPCRs). With its interdisciplinary work, this thesis laid the foundation for the development of such a chemo-enzymatic synthesis.

As a first step, the genomic DNA of the kistamicin A (**15**) producer, bacterium *Actinomadura parvosata* subsp. *kistnae*, was isolated and subjected to *PacBio*® single molecule real-time (SMRT®) sequencing at *GATC*. Bioinformatic analysis of the assembled, 13.56 Mbp genome revealed 30 yet uncharacterized biosynthetic pathways, all of which display low similarity to previously characterized gene clusters. The *A. parvosata* genome thus not only belongs to the largest actinobacterial genome sequences known to date,[165] but also harbours the most biosynthetic gene clusters found in this group of bacteria.[165] These results were published in *Journal of Genomics*.[164]

Of the identified biosynthetic loci, one 48.0 kb DNA region shows close similarity to the

4. Conclusion

complestatin biosynthetic gene cluster in organisation and size, and could be assigned to the biosynthesis of **15**. Besides four genes (*kisA*, *kisB*, *kisC*, *kisD*) forming the expected NRPS assembly line, all genes necessary for Hpg (**21**) and Dpg (**28**) biosynthesis, as well
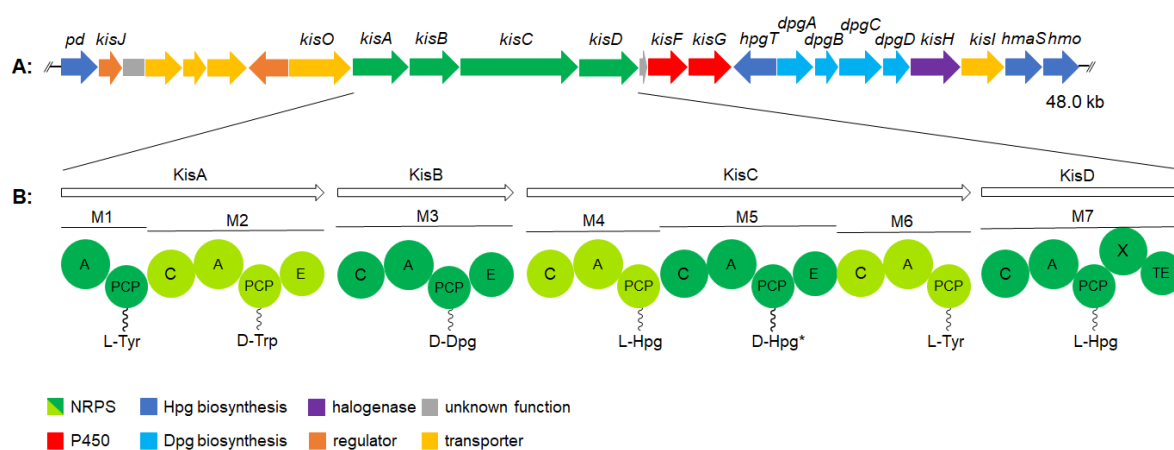
Figure 32. Gene organization of the kistamicin biosynthetic gene cluster (**A**) and the kistamicin NRPS assembly line (**B**). ∗: The timing of Hpg (**21**) halogenation is unknown.

as an FAD-dependent halogenase (*kisH*), putatively responsible for the chlorination of Hpg (**21**), were found. Surprisingly, only two genes corresponding to two cytochrome P450 enzymes (*kisF* and *kisG*), presumably responsible for the formation of the biaryl and biaryl ether bonds, were detected. This finding is in contrast to the three biaryl and biaryl ether bonds characterizing the kistamicin A (**15**) structure. The limitation to two cytochrome P450 enzymes catalyzing three OPCRs would be an unique and interesting feature of the kistamicin gene cluster since, to date, a distinct P450 enzyme has been proposed for each OPCR in all other nonribosomal peptides. Closer analysis of the NRPS assembly line revealed the presence of three epimerization (E) domains in modules M2, M3, and M5, indicating that the amino acids Dpg (**28**), 3-chloro-Hpg (**39**) as well as tryptophan (**20**) are epimerized to D-amino acids. In contrast, the absence of an E domain in modules M1, M4, M6, and M7 implies that the other four building blocks (two Hpg (**21**) and two tyrosin (**19**) moeities) are L-amino acids. This analysis of the NRPS domain architecture elucidated the kistamicin A (**15**) absolute stereostructure for the first time, and is the basis for a successful chemical total synthesis. Furthermore, an X domain is located in NRPS enzyme KisD before the terminating thioesterase domain (TE). Together with the adjacent peptidyl carrier protein domain (PCP) the X domain is putatively required for OPCR reactions catalyzed by the P450 enzymes KisF and KisG.

As an important step towards the utilization of the cytochrome P450 enzymes as biocatalysts in the synthesis of **15**, the genes encoding the P450 enzymes KisF and KisG,

the NRPS domains KisD-PCP and KisD-X as well as the fused didomain KisD-PCP+X were cloned into plasmids. The proteins KisF, KisG, and Kis-PCP were successfully heterologously expressed in *E. coli* BL21(DE3). However, neither the domain KisD-X, the didomain KisD-PCP-X nor their codon-optimized versions could be expressed in *E. coli*. In future chemo-enzymatic *in vitro* assays, the codon-optimized X domain or the codon-optimized PCP-X didomain from the complestatin biosynthetic gene cluster, which were heterologously expressed in the To. Gulder laboratory,[97,115] may be tested instead.

Subsequently, this thesis adressed the synthesis of the kistamicin A linear peptide precursor **54** via SPPS. For this purpose, not commercially available building blocks Fmoc-L-Hpg (L-**82**), Fmoc-3-chloro-D-Hpg (D-**83**), and Fmoc-D-Dpg (D-**84**) were synthesized, as well as enantiomers and derivatives for further investigation of all synthetic steps. Hpg derived units were gained in good yields in one or two steps, whereas Fmoc-D-Dpg (D-**84**) was synthesized in five steps in 13 % overall yield. In the latter case, Strecker synthesis followed by enzymatic chiral resolution with subsequent ion exchange chromatography represented the key synthetic steps. The susceptibility of Dpg and Hpg derived building blocks to epimerization under conditions traditionally employed in SPPS was adressed by the adaption of a mild Fmoc protocol, which was based on a procedure by Brieke *et al.*[122] and optimized for the synthesis of the kistamicin peptide precursor **54**. The optimized protocol employed highly acid labile 2-chlorotrityl chloride (2-CTC) resin as the solid support, which allowed for peptide cleavage under mild acidic conditions and thereby prevented epimerization through hydrolysis.[185,186] In addition, the bulky linkers of the resin suppressed epimerization of the first amino acid by steric hindrance.[185,187] Fmoc deprotection was achieved by employing 1 % DBU in DMF, whereas coupling reagents COMU and triethylamine in DMF were used for amino acid coupling. With this strategy, Fmoc protected tetrapeptide **92** was efficiently and enantioselectively synthesized (19 % yield based on the resin's loading degree or 8 % based on the used quantity of L-**82**). Additional synthesis of various peptide diastereomers confirmed that possible epimerization could be swiftly detected by LC-MS analysis and thus excluded in this approach.

After the successful synthesis of tetrapeptide **92**, the optimized SPPS protocol was applied to the synthesis of the complete heptapeptide chain (**54**). However, significant amounts of side products were formed during coupling of the fifth, sixth, and seventh amino acid. The desired peptides were formed only to a limited extent and heptapeptide **54** could only be detected in traces by LC-MS analysis. Closer inspection of the last three coupling reactions suggested that the hydrophilic nature of the growing peptide may have created a coiling
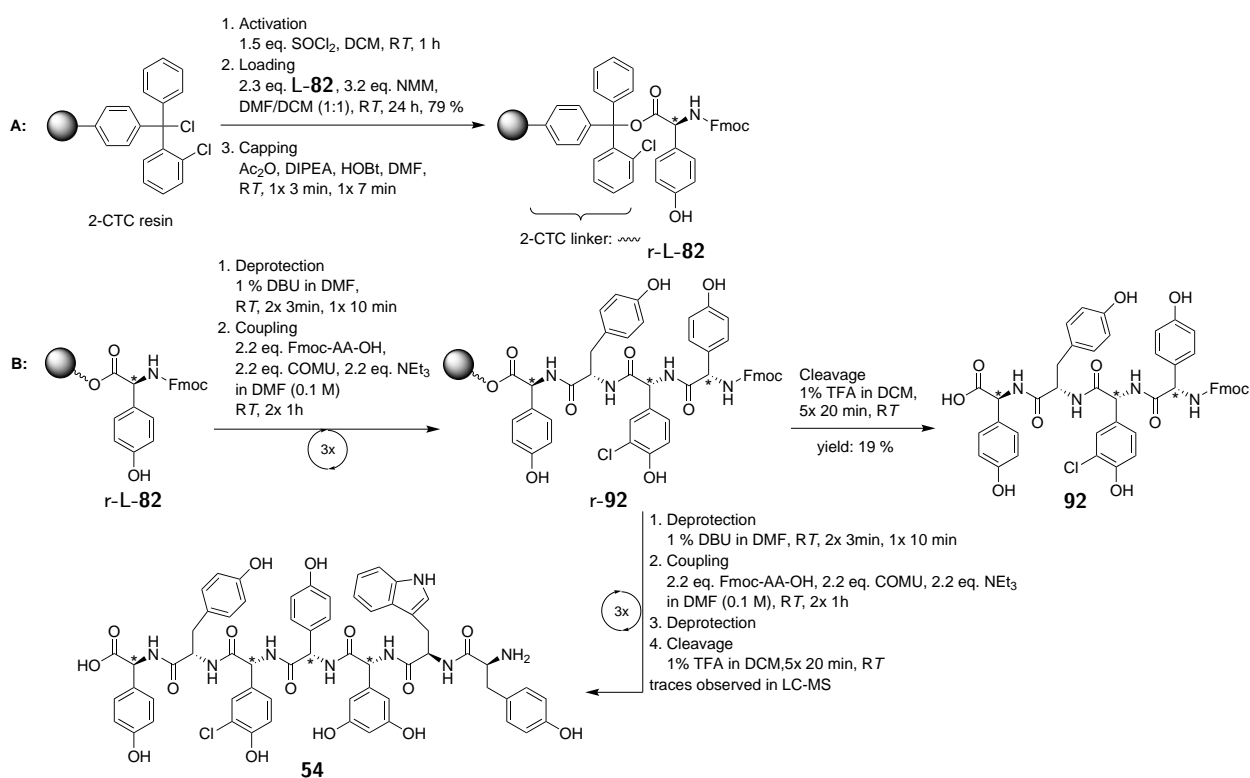
Scheme 34. SPPS of the kistamicin A linear peptide precursor (**54**) employed a mild Fmoc protection strategy. Tetrapeptide **92** was synthesized successfully, but only traces of **54** were found in LC-MS. Stereocenters prone to epimerization are marked with ∗.

chain, which was then difficult to attack by sterically hindered amino acids and reagents. Therefore, this work pursued the separation of heptapeptide **54** into two parts, western tetrapeptide **92** and eastern tripeptide **105**, and a final coupling of **92** and **105** to form **54**. Fmoc protected tripeptide **105** was efficiently and enantioselectively synthesized using the previously developed SPPS strategy (6 % yield based on the used quantity of D-**84**). However, it was not possible to couple **105** directly to the resin bound, *N*-terminaly unprotected tetrapeptide **r-98**, nor to couple both peptides in the liquid phase.
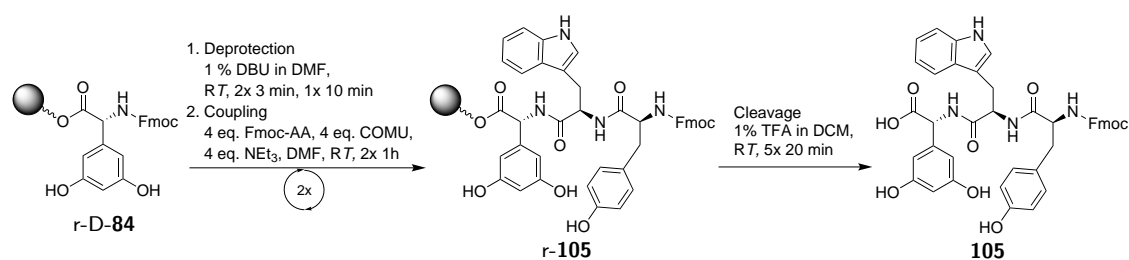
Scheme 35. SPPS of tripeptide **105** employed an optimized Fmoc strategy.

Instead, the employment of an SPPS resin equipped with a hydrazine linker was examined. In this approach, conventional 2-CTC resin carried a hydrazine linker to which the first amino acid Fmoc-L-Hpg (**L-82**) was coupled. The synthesis of the peptide chain progressed
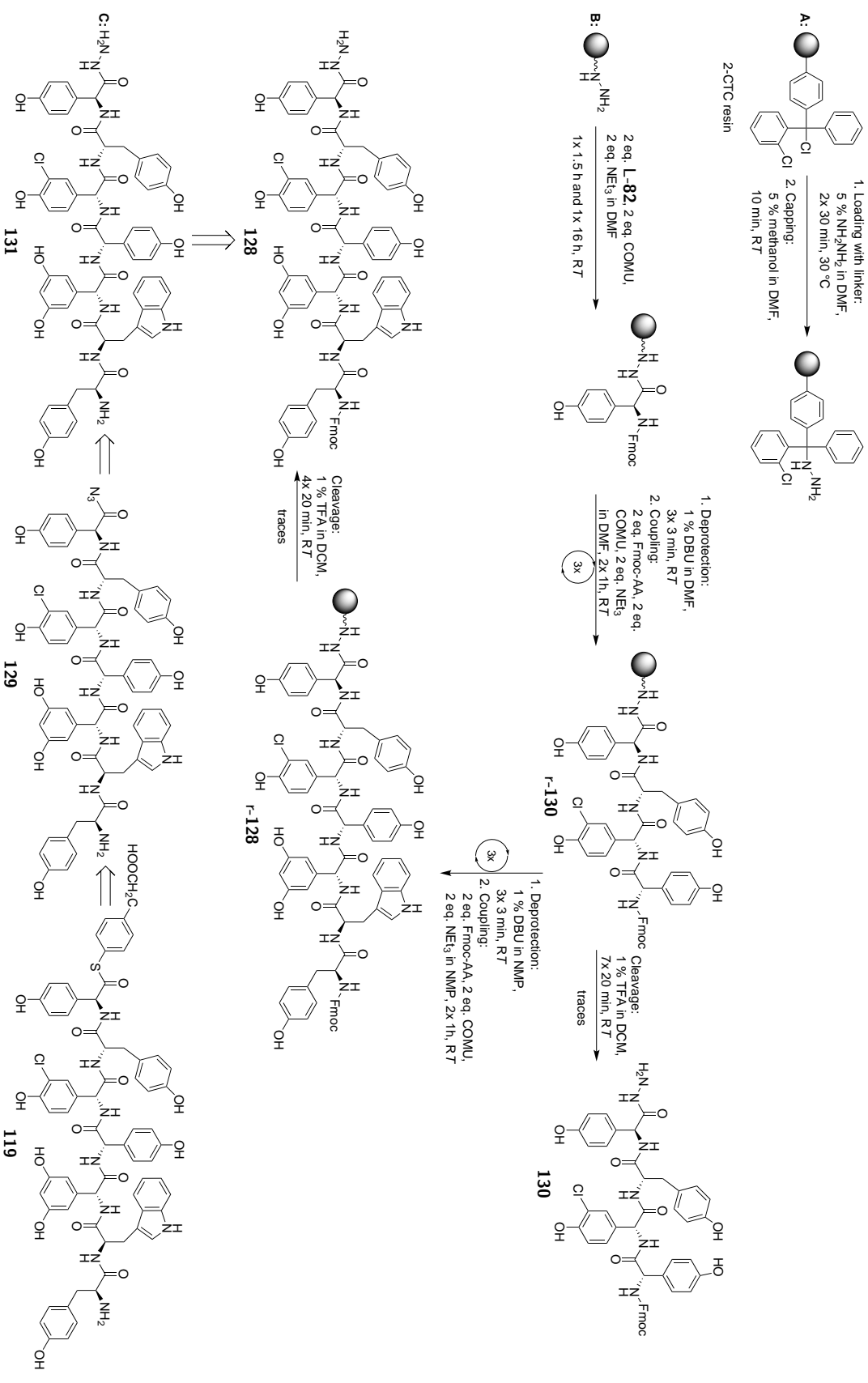
Scheme 36. Synthesis of *C*-terminaly thiophenylated heptapeptide **119** via SPPS using 2-chlorotrityl hydrazine resin. **A:** Synthesis of 2-chlorotrityl hydrazine resin. **B:** SPPS of heptapeptide hydrazide **128**. **C:** Retrosynthesis of thiophenylated heptapeptide **119** by Fmoc cleavage (**131**), oxidation to azide **129**, and subsequent thiophenylation.

using the previously developed Fmoc based SPPS strategy. After TFA mediated cleavage, the peptide was obtained as a hydrazide, which would allow conversion to a thioester by oxidation and thiophenylation. LC-MS analysis of SPPS showed successful formation of tetrapeptide hydrazide **130** and even of heptapeptide hydrazide **128**, when the very polar solvent NMP was employed. However, during semi-preparative HPLC of **130** and **128** only very small product peaks were identified and no product could be isolated. This phenomenon was caused by very low yields in the attachment of the first amino acid, L-**82**, to the hydrazine linker. Due to time limitations during this thesis, only few coupling reagents were employed for this reaction. Nevertheless, the use of 2-CTC hydrazine resin in combination with the solvent NMP significantly reduced coiling of the peptide chain and improved access of coupling reagents as well as amino acids. This led to the detection of a single, high intensity peak for **128** as well as very low amounts of side products in LC-MS spectra. Therefore, optimising the loading of Fmoc-L-Hpg (L-**82**) onto 2-CTC hydrazine resin and the subsequent conversion of the hydrazide to the desired thioester in future work is highly promising. This approach would constitute a straightforward synthesis of the thiophenylated kistamicin A linear peptide precursor **119**, which would then serve as the final substrate in chemo-enzymatic oxidative phenol coupling assays.

To conclude, this interdisciplinary thesis provided crucial insights into the yet unknown biosynthetic machinery encoding kistamicin A (**15**), and revealed the striking biological potential of the kistamicin producer *A. parvosata*. Of special significance is the elucidation of the putative kistamicin A (**15**) absolute stereostructure, which was tentatively assigned based on the NRPS architecture for the first time. Together with the heterologous expression of major enzymes for catalysis of oxidative phenol coupling reactions and the thorough investigation of the challenges characterizing SPPS of kistamicin A linear peptide precursors (**54/119**), this thesis laid the foundation for a future chemo-enzymatic total synthesis of kistamicin A (**15**). Moreover, this thesis provided innovative new approaches to the first total synthesis of myxocoumarin B (**43**) as well as various derivatives. In extensive structure-activity relationship studies conducted by the research group Nikodinovic-Runic in Belgrade, **43** and derivatives **64**, **75** as well as **77** were identified as promising new antibacterial drug leads for the treatment of *S. aureus* and *S. aureus* MRSA infections.

Chapter 5

Experimental Procedures

5.1. Chemicals, Materials, Equipment and Software

5.1.1. Solvents and Chemicals

Solvents

For HPLC, MPLC, and LC-MS methods HPLC-grade acetonitrile and HPLC-grade methanol were purchased from *VWR*. HPLC-grade water was purified and deionized by a TKA GenPure water treatment system. Trifluoroacetic acid (TFA for peptide synthesis) by *Carl Roth*®was used as buffer. For column chromatography acetone, dichloromethane, methanol, and pentane were purified by distillation. Ethyl acetate was purchased from *Fisher Scientific*™. Diethyl ether was purified by distillation. For peptide synthesis pure and, if necessary dry, solvents were purchased from *abcr*, *Acros Organics*, *Carl Roth*®, *Fisher Scientific*™, *Sigma Aldrich*, and *VWR*.

Other Chemicals

Unless otherwise noted, all reagents were purchased from *Acros Organics*, *Carbolution*, *Carl Roth*®, *Fisher Scientific*™, *Sigma Aldrich*, and *VWR*. 2-Chlorotrityl chloride resin ($1.60 \, \mathrm{mmol \, g^{-1}}$, 100-200 mesh) for solid phase peptide synthesis was purchased from *Carbolution*, 2-chlorotrityl hydrazine resin (ca. $0.5 \, \mathrm{mmol \, g^{-1}}$ loading, 100-200 mesh) from *Sigma Aldrich*.

5.1.2. Enzymes and Proteins

Enzymes, proteins or enzyme reaction mixtures were purchased by default from *New England Biolabs* (*NEB®*) and/or *Jena Bioscience*. The enzyme D-amano aclyase (from *Aspergillus Melleus*) was purchased from *Sigma Aldrich*.

5.1.3. Kits

Kits for microbiological methods, for example preparation of plasmids or genomic DNA, were purchased from *Jena Bioscience*, *Peqlab*, and *Promega*.

5.1.4. Equipment

Autoclave
Autoclave 3170 ELV (*Biomedis®*) was used for sterilizing media and consumable supplies.

Cell Disruption
Ultrasonic homogenizer Sonopuls HD2070 (*BandeliBacteria*) was utilized for disruption of bacteria cells.

Centrifugation
Centrifuges Heraeus Multifuge X3R Centrifuge (*Thermo Scientific*™), 24/6 (*VWR*) and Centrifuge 5418R (*Eppendorf*) were used.

Electrophoresis
Electrical voltage for electrophoresis was applied by Electrophoresis Power Supply EV243 (*Consort*). SDS-PAGE was conducted in Mini Protean® Tetra System (*Bio-Rad*) gel chambers.

Electroporation
MicroPulser (*Bio-Rad*) was used for electroporation of electrocompetent cells.

Gel Documentation
The Bio-Imaging-System Gene Genius from *SynGene* was utilized for documentation of agarose gels. The instrument was controled by the software GeneSnap (*SynGene*). SDS polyacrylamid gels were documented using a costum-made flatbed scanner.

Heating Block and Water Bath

For heating of small DNA, protein, and cell samples ThermoMixer C (*Eppendorf*) or water bath FBH 604 (*Fisherbrand*) were used.

Electrospray Ionization Mass Spectrometry (ESI-MS)

ESI-MS analysis was carried out using an UltiMate 3000 LC System coupled to a LCQ Fleet Ion Trap Mass Spectrometer (both *Thermo Scientific*™). The *Thermo* Xcalibur™software was used to control the system and interpretation of the recorded data was carried out using the *Thermo* Xcalibur™Qual Browser 2.2 SP1.48 software. High resolution ESI-MS spectra were recorded by mass spectrometer *Thermo* LTQ FT Ultra. Interpretation of the recorded data was conducted with *Thermo* Xcalibur™Qual Browser 2.2 SP1.48 software. Measured molecular fragments were indicated as mass/charge ratios *m/z*.

Incubation Shakers

Incubation shakers Multitron Standard and Ecotron (both *Infors HT*) were used.

Lyophilization

Aqueous solutions were lyophilized using an Alpha 2-4 device (*Christ*) coupled with a Chemistry-Hybrid-Pump-RC6 (*Vacuubrand*).

Nuclear Magnetic Resonance (NMR) Spectroscopy

NMR spectra were recorded using Bruker AVHD300, Bruker AVHD400, and Bruker AVHD500 instruments at R*T*. In the case of kistamicin A, NMR spectra were recorded at the BNMRZ by PD Dr. G. Gemmecker using Bruker AV900 and Bruker AV950 instruments. Chemical shifts δ are listed as parts per million [ppm] and refer to δ(TMS) = 0 ppm. Spectra were calibrated using residual undeuterated solvent as an internal reference δ(DMSO-d$_6$) = 2.50 ppm, δ(methanol-d$_4$) = 3.31 ppm for ^{1}H-NMR; δ(DMSO-d$_6$) = 39.5 ppm, δ(methanol-d$_4$) = 49.0 ppm for ^{13}C-NMR). The following abbreviations (or combinations thereof) were used to explain multiplicities: s = singlet, d = doublet, dd = doublet of doublets, t = triplet, q = quartet, m = multiplet, br = broad. Coupling constants *J* are stated in Hertz [Hz]. Spectra were interpreted using MestReNova (*Mestrelab Research S.L.*).

pH Meter

pH 211 Microprocessor pH Meter (*HANNA Instruments*®) was used for pH adjustment.

Photometer

The optical density of a cell culture at 600 nm was measured with a photometer from *Eppendorf.* DNA concentrations were measured with Nanophotometer P330 (*Implen*).

Polymerase Chain Reaction (PCR)

DNA amplification was conducted with Life Eco-PCR (*Bioer*) or TC-5000-PCR (*Techne*) PCR cyclers.

Software

Listed below are all independent programs and internet-based applications used in this work. LC-MS data were plotted using custom scripts.

Table 10. Independent programs.

Software	Version	Producer	Analytical Application
Galaxie Chromatography	1.10.2006	*Agilent Technologies*	HPLC chromatograms
Geneious[167]	9.1.2	*Biomatters*	DNA sequences
MestReNova[195]	10.0.2	*Mestrelab Research S. L.*	NMR spectra
SnapGene® Viewer	3.1.1	*GSL Biotec*	DNA & protein sequences
Xcalibur™Qual Browser	2.2 SP1.48	*Thermo Fisher Scientific™*	MS & LC-MS spectra

Table 11. Internet-based applications.

Software	Website	Date	Application
antiSMASH v4.2.0[73]	https://antismash.secondarymetabolites.org	02.12.2018	prediction of BGCs
NCBI BLAST®	http://blast.ncbi.nlm.nih.gov/Blast.cgi	02.12.2018	DNA & protein sequence analysis
NEBuilder® v1.12.18	http://nebuilder.neb.com	02.12.2018	PCR primer design
NEBcloner® v1.3.8	https://nebcloner.neb.com/#!/redigest	02.12.2018	restriction digest design
NEB®Tm Calculator v1.9.13	http://tmcalculator.neb.com/#!/main	02.12.2018	estimation of PCR annealing temperatures
OligoAnalyzer[196]	http://eu.idtdna.com/calc/analyzer	01.01.2016	PCR primer design
PKS/NRPS Analysis[168]	http://nrps.igs.umaryland.edu	02.12.2018	protein sequence analysis

5.2. Bacterial Strains, Plasmids and Primer

5.2.1. Bacterial Strains

For this work, bacterial strains noted in Table 12 were utilized. *Actinomadura parvosata* subsp. *kistnae* was used for production of kistamicin A and isolation of genomic DNA for genome sequencing and PCR amplification. *E. coli* DH5α was used for cloning and storage of plasmids/vectors. *E. coli* BL21(DE3) and *E. coli* SoluBL21™ were used for heterologous protein expression.

Table 12. Utilized bacterial strains.

Bacterial Strain	Genotype	Origin/Reference
A. parvosata	wild type	*ATCC*® 55076™
E. coli DH5α	F⁻ *endA1 glnV44 thi-1 recA1 relA1 gyrA96 deoR nupG purB20 φ80dlacZ*Δ*M15* Δ*(lacZYA-argF)*U169, hsdR17$(r_K{}^- m_K{}^+)$, λ⁻	laboratory stock
E.coli BL21(DE3)	F⁻ *ompT gal dcm hsdS$_B$(r$_B{}^-$ m$_B{}^-$)* (DE3)	laboratory stock
*E. coli*SoluBL21™	F⁻ *ompT gal dcm hsdS$_B$(r$_B{}^-$ m$_B{}^-$)* (DE3) This strain carries uncharacteristic mutations, which were generated by specific selection criteria. These mutations often allow the production of unsoluble proteins in soluble form.	*Genlantis*

5.2.2. Plasmids and Vectors

In this work, plasmids and vectors noted in Table 13 were utilized. They were commercially aquired, previously produced in the laboratory or generated during this work.

5.2.3. Primers

All primers (Table 14 and Table 15) in this work were produced from Sigma-Aldrich. Lyophilized oligonucleotides were resuspended in sterile, double distilled water to generate stock solutions with concentrations of 100 µM. Stock solutions were stored at −20 °C.

5. Experimental Procedures

Table 13. Utilized plasmids and vectors. Resistance genes: $ampR$ = ampicillin, $kanR$ = kanamycin.

Plasmid/Vector	Size [bp]	Features/Function	Origin
pEX-K4::$kisD$-PCP+X_{opt}	1,191	$kanR$, $kisD$-PCP+X (codon optimized) integrated into pEX-K4	*eurofins Genomics*
pGS-21a	6,169	$ampR$, pBR322 origin of replication, $lacI$, His6-tag (*N*-terminal and *C*-terminal), GST-tag (*N*-terminal)/expressions vector (T7)	*GenScript*
pHis8-TEV	5,330	$kanR$, pBR322 origin of replication, $lacI$, His8-tag (*N*-terminal), His6-tag (*C*-terminal), TEV protease cleavage site/expression vector (T7)	R. Richarz[97]
pGS21a::$kisD$-PCP	6,382	$ampR$, $kisD$-PCP integrated into pGS21a	this work
pGS21a::$kisD$-PCP+X_{opt}	7,336	$ampR$, $kisL$-PCP+X (codon optimized) integrated into pGS21a	this work
pGS21a::$kisD$-X	7,096	$ampR$, $kisD$-X integrated into pGS21a	this work
pGS21a::$kisD$-X_{opt}	7,087	$ampR$, $kisD$-X (codon optimized) integrated into pGS21a	this work
pGS21a::$kisF$	7,312	$ampR$, $kisF$ integrated into pGS21a	this work
pGS21a::$kisG$	7,486	$ampR$, $kisG$ integrated into pGS21a	this work
pHis8-TEV::$kisD$-PCP+X	6,496	$kanR$, $kisD$-PCP+X integrated into pHis8-TEV	this work
pHis8-TEV::$kisD$-PCP+X_{opt}	6,496	$kanR$, $kisD$-PCP+X (codon optimized) integrated into pHis8-TEV	this work
pHis8-TEV::$kisD$-X	6,256	$kanR$, $kisD$-X integrated into pHis8-TEV	this work
pHis8-TEV::$kisD$-X_{opt}	6,247	$kanR$, $kisD$-X (codon optimized) integrated into pHis8-TEV	this work
pHis8-TEV::$kisF$	6,472	$kanR$, $kisF$ integrated into pHis8-TEV	this work
pHis8-TEV::$kisG$	6,646	$kanR$, $kisG$ integrated into pHis8-TEV	this work

Table 14. Utilized primers for PCR screening and DNA sequencing.

Designation	Sequence (5'-3')	Restriction Site	Application
T7	TAATACGACTCACTATAGGG	-	sequencing/screening
pGEX-5	CTGGCAAGCCACGTTTGG	-	sequencing/screening
pET-RP	CTAGTTATTGCTCAGCGG	-	sequencing/screening
pRSET-RPnew	GGGTTATGCTAGTTATTGC	-	sequencing/screening
KC-NRPS-19,799_f	GTACGGCGCTGGTGATCG	-	sequencing
KC-NRPS-19,799_r	ACAGCTCGCGGAAGACCC	-	sequencing
KC-NRPS-24,865_f	ATGACGAGGTGGAGGCAC	-	sequencing
KC-NRPS-24,865_r	GTCGAGAGCTCCGTCGAT	-	sequencing
KC-NRPS-26,513_f	CCGGGTGGAAGCGATGAT	-	sequencing
KC-NRPS-26,513_r	CATCACATACGCCGCATCC	-	sequencing
KC-NRPS-27,339_f	GTGACGTGGTCCCGCTTG	-	sequencing
KC-NRPS-27,339_r	CACGTAACCGACCAGCCG	-	sequencing
KC-NRPS-29,424_f	CGACCGATCCGAGCTGAC	-	sequencing
KC-NRPS-29,424_r	CCGACGATGACCTGCACG	-	sequencing
KC-NRPS-30,925_f	TGGAACAGCTGGCCGACC	-	sequencing
KC-NRPS-30,925_r	ACACTCCCGCATCAGCCAG	-	sequencing
KC-NRPS-40,228_f	GATCATCTCGATGCGGCTGG	-	sequencing
KC-NRPS-40,228_r	CAGGGAATCTTGACCTCGCG	-	sequencing
KC-NRPS-40,331_f	ATCGACGCGCTGATCGAC	-	sequencing
KC-NRPS-40,331_r	GAAACACGCTCGCAGGGC	-	sequencing
KC-NRPS-42,019_f	CGGATCGGCGTGGTGATG	-	sequencing
KC-NRPS-42,019_r	GACCAGCGGTACCCAGGT	-	sequencing
KC-NRPS-43.545_f	CAGCTGTTCTCGACGCCG	-	sequencing/screening
KC-NRPS-43.545_r	CAGGTCCTGATGGCGGTG	-	sequencing
kisD-PCP+X$_{opt}$_f	GGCAGATGAACGTGACT	-	screening
kisD-X_screen	CTGGGACCAGATCGAGTT	-	screening
kisF_screen	TGGTCATGAACTCCAGC	-	screening
kisG_screen	CTAGTTATTGCTCAGCGG	-	screening

101

Table 15. Utilized primers for cloning and Gibson assembly. Underlined sequences indicate restriction sites for enzymes or DNA regions for Gibson assembly. Sequences marked in bold indicate stop codons. Lower cases indicate nucleobases, which were changed in the primer compared to the original sequence.

Designation	Sequence (5'-3')	Restriction Site	Application
kisD-PCP_f	ACATAGAATTCGGGCGGAGGTCGAGGAGC	EcoRI	kisD-PCP cloning
kisD-PCP_r	TACGAAGCTTT**TAA**CGGGACTTGGCGGC	HindIII	kisD-PCP cloning
kisD-PCP_GA_f	ATCTTTATTTTCAGGGAGGATCCGAATTCGAGGAGCGGGCTGTGCGCG	-	kisD-PCP Gibson assembly with pHis8-TEV
kisD-PCP_GA_r	GGCAGCGGGCGGCCATCCGGGTC	-	kisD-PCP Gibson assembly with pHis8-TEV
kisD-X_f	CGATTGAATTCCCGGATGGCCCGCTG	EcoRI	kisD-X cloning
kisD-X_r	ATATAAGCTTT**TAG**GGATCGCCCGACACAGGTCGA	HindIII	kisD-X cloning
kisD-X_GA_f	GGATGGCCCGCTGCCGGGTCAC	-	kisD-X Gibson assembly with pHis8-TEV
kisD-X_GA_r	TCGAGTGCGGCGCGCAAGCTTT**TA**CGACACAGGTCGACGGGCGGCAGGGGCGGAGCCA	-	kisD-X Gibson assembly with pHis8-TEV
kisD-X$_{opt}$_f	AATTGAATTCCCCGACGGGCCCGTTAC	EcoRI	kisD-X$_{opt}$ cloning
kisD-X$_{opt}$_r	GCCGCAAGCTTT**TAG**GACAGGTCGA	HindIII	kisD-X$_{opt}$ cloning
kisF_f	tatagaattcATGGTCGCGCCGGAGCA	EcoRI	kisF cloning
kisF_r	attaagcttTCACCCAGGTCAACGGCAG	HindIII	kisF cloning
kisG_f	tatagaattcGTGGACGCGGTACGGAACG	EcoRI	kisG cloning
kisG_r	attaagcttTCATCGGGTCGCGGGCTGA	HindIII	kisG cloning

5.3. Strain Cultivation, Media and Buffers

5.3.1. Strain Cultivation

Conditions for strain cultivation in liquid culture or on agar plate are noted in Table 16. Indicated rotation speeds refer to liquid cultures.

Table 16. Culture conditions for bacterial strains.

Bacterial Strain	Medium	Temperature [°C]	rpm	Time
Actinomadura parvosata subsp. *kistnae*	ISP-I	30	-	3 days
Actinomadura parvosata subsp. *kistnae*	oatmeal agar	30	200	3 days
E. coli DH5α	LB	37	200	over night
E. coli BL21(DE3)	LB	37	200	over night
E. coli SoluBL21™	LB	37	200	over night

Starter cultures were inoculated from single clones on agar plates or cryo cultures. For inoculation from cryo cultures a small part of the frozen cell suspension was used. Standard volumina for starter cultures were 5 mL to 10 mL for *E. coli* and 50 mL for *A. parvosata*. *E. coli* starter cultures were incubated at 37 °C and 200 rpm over night, *A. parvosata* starter cultures for six days at 30 °C and 200 rpm. Main cultures were inoculated at a ratio of 1:100 (*E. coli*) or 1:1000 (*A. parvosata*) from starter cultures. Culture conditions for protein expression are noted in the respective experiments. Culture conditions for *A. parvosata* for kistamicin A production are described in Chapter 5.4.

5.3.2. Cryoconservation

For storage of strains 700 µL fresh over night culture (LB) (*E. coli*) or three days culture (ISP-I) (*A. parvosata*) were mixed with 300 µL of aqueous (50 v/v %) glycerol solution under sterile conditions. All cryo cultures were stored at −80 °C.

5.3.3. Culture Media and Buffers

The following culture media were used in this work. They were prepared with distilled water and sterilized by autoclaving.

Luria Bertani (LB) Medium

LB medium by Miller[197] was used as a standard medium for *E. coli* cultivation (e.g., for transformation, plasmid preparation or protein expression). It was purchased as a ready-made powder from *Roth®*, 25 g dissolved in 1 L distilled water and autoclaved. For preparation of agar plates 15 g agar were added to the medium before autoclaving.

Table 17. Composition of LB medium.

Component	Amount
tryptone	10 g
yeast extract	5 g
NaCl	5 g
distilled water	ad 1 L

SOC Medium (Super Optimal Broth with Catabolite Repression)

SOC medium by Hanahan[198] was used for *E. coli* cultivation after transformation or for preparation of competent cells.

Table 18. Composition of SOC medium.

Component	Amount
tryptone	20 g
yeast extract	5 g
NaCl	0.58 g
KCl	0.19 g
$MgSO_4$ (1 M)	10 mL
$MgCl_2$ (1 M)	10 mL
D-glucose (40 w/v %)	9 mL
distilled water	ad 1 L

Solutions of $MgSO_4$, $MgCl_2$, and D-glucose were sterile-filtered separately and added after autoclaving.

ISP-I Medium

ISP-I medium by Shirling and Gottlieb[199] was used for cultivation of *A. parvosata* for gDNA preparation.

Table 19. Composition of ISP-I medium.

Component	Amount
tryptone	5 g
yeast extract	3 g
distilled water	ad 1 L

Oatmeal Agar

Oatmeal agar by Shirling and Gottlieb[199] was used for cultivation of *A. parvosata* on agar plates. Oatmeal (Hafer Gold) was purchased from *Holo*®.

Table 20. Composition of oatmeal agar.

Component	Amount
oatmeal	20 g
agar	18 g
trace salts solution	1 mL
distilled water	ad 1 L

The pH was adjusted to pH 7.0 before autoclaving. Trace salts solution (Table 21) was sterile-filtered separately and added after autoclaving.

Table 21. Composition of trace salts solution.

Component	Amount
$FeSO_4 \cdot 7\ H_2O$	0.1 g
$MnCl_2 \cdot 4\ H_2O$	0.1 g
$ZnSO_4 \cdot 7\ H_2O$	0.1 g
distilled water	ad 100 mL

5. Experimental Procedures

Modified R4 Medium

Modified R4 medium[132] was used for precultivation of *A. parvosata* for kistamicin A (**15**) production. TES was purchased from *AppliChem.*

Table 22. Composition of modified R4 medium.

Component	Amount
D-glucose	5 g
MgCl$_2$ · 6	5 g
TES	2.8 g
CaCl$_2$ · 2	2 g
L-proline	1.5 g
L-valine	1.18 g
yeast extract	0.5 g
K$_2$SO$_4$	0.1 g
casamino acids	0.05 g
trace salts solution	1 mL
distilled water	ad 1 L

The pH was adjusted to pH 7.2 before autoclaving. Trace salts solution (Table 21) was sterile-filtered separately and added after autoclaving.

Glucose Fish Meal (GFM) Medium

GFM Medium[132] was used for cultivation of *A. parvosata* for kistamicin A (**15**) production. Fish meal was purchased from *Karpfen Hans.*

Table 23. Composition of GFM medium.

Component	Amount
D-glucose	20 g
fish meal	10 g
CaCO$_3$	1 g
distilled water	ad 1 L

The pH was adjusted to pH 7.0 before autoclaving.

5.3.4. Antibiotics

In this work, antibiotics ampicillin and kanamycin were used as media supplements to select clones carrying specific plasmids and avoid contamination of pure cultures. Stock solutions were prepared by solving ampicillin in aqueous (50 v/v %) ethanol ($100\,\mathrm{mg\,mL^{-1}}$) and kanamycin in double distilled water ($50\,\mathrm{mg\,mL^{-1}}$). These stock solutions were used to supplement media with a final concentration of $100\,\mathrm{\mu g\,mL^{-1}}$ ampicillin and $50\,\mathrm{\mu g\,mL^{-1}}$ kanamycin, respectively.

5.3.5. Buffers

For buffer preparation double distilled water was used.

DNA Loading Buffer (10x)

Table 24. Composition of tenfold DNA loading buffer.

Component	Concentration
sucrose	20 w/v %
orange G	0.15 w/v %
xylen cyanol	0.05 w/v %
bromphenol blue	0.05 w/v %

Lysis Buffer for Heterologous Protein Purification

Table 25. Composition of lysis buffer for protein purification.

Component	Concentration
glycerol	10 w/v %
NaCl	300 mM
NaH_2PO_4	50 mM
imidazole	10 mM

The pH was adjusted to pH 8.0.

Washing and Elution Buffers for Protein Purification

Table 26. Composition of washing and elution buffers for protein purification.

Component	Concentration	
	Washing Buffer	Elution Buffer
NaH_2PO_4	50 mM	50 mM
NaCl	300 mM	300 mM
imidazole	20 mM	250 mM
glycerole	10 v/v %	10 v/v %

The pH of all buffers was adjusted to pH 7.5.

SDS-PAGE Sample Buffer (5x)

Table 27. Composition of fivefold SDS-PAGE sample buffer.

Component	Concentration
gylcerol	50 v/v %
Tris (1 M, pH 6.8)	25 v/v %
SDS	10 w/v %
2-mercaptoethanol	5 v/v %
bromphenol blue	0.2 w/v %

SDS-PAGE Separating Buffer (4x)

Table 28. Composition of fourfold SDS-PAGE separating buffer.

Component	Concentration
Tris	1.5 M
SDS	0.8 w/v %

The pH was adjusted to pH 8.8.

SDS-PAGE Stacking Buffer (4x)

Table 29. Composition of fourfold SDS-PAGE stacking buffer.

Component	Concentration
Tris	0.5 M
SDS	0.8 w/v %

The pH was adjusted to pH 6.8.

5.4. Isolation of Kistamicin A (15) from *Actinomadura parvosata*

Actinomadura parvosata subsp. *kistnae* was precultured on oatmeal agar for 4 d at 30 °C based on a procedure by Nazari *et al.*[132] . The collected mycellium from two agar plates was used to inoculate 2x 0.2 L of modified R4 medium. The starter cultures were then incubated at 200 rpm at 28 °C for 3 d. The mycellium was collected by centrifugation (15,000 xg, 10 min, 4 °C) and used to inoculate 6x 1 L flasks, each containing 0.2 L GFM medium, in a ratio of 1:100 (w/v). Those cultures were grown at 250 rpm for 9 d at 30 °C. The mycellium was again collected by centrifugation (15,000 xg, 10 min, 22 °C). Each pellet was redissolved in 30 mL acetone, vortexed vigorously for 1 min, and the supernatant collected after centrifugation (15,000 xg, 10 min, 22 °C). Extraction was repeated twice, all organic extracts combined, and the solvent removed *in vacuo*. The residue was dissolved in methanol and purified by semi-preparative HPLC (A: water + 0.05 % TFA, B: ACN + 0.05 % TFA, 0.0-2.0 min 95 % A, 2.0-7.0 min 55 % A, 7.0-17.0 min 55 % A, 17.0-17.1 min 95 % A, 17.1-20.0 min; column: Eurospher II 100-5 C18 250x8 mm; flow rate: 5 mL/min; tR = 14 min). In this way, 69.3 mg (or 69 mg mL^{-1}) kistamicin A (**15**) were isolated.

Analytics

Molecular formula: $C_{61}H_{51}ClN_8O_{15}$
Molecular weight: 1171.57 g/mol
HR-ESI(+)-MS: *m/z* = calc. for $C_{61}H_{52}ClN_8O_{15}$ 1172.32407 [M+H]$^+$, found 1172.32418.
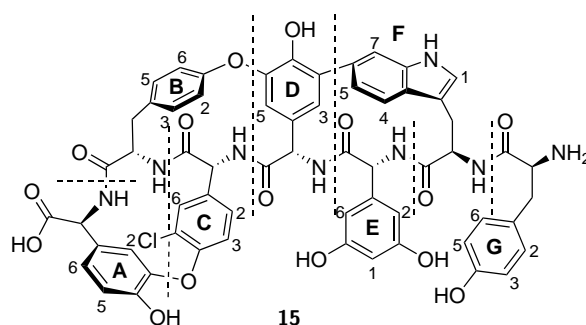
Figure 33. Chemical structure of kistamicin A (**15**). NMR signals were assigned to units A to G.

The following NMR spectra were recorded (900 MHz, DMSO-d$_6$, RT): 1D ^{1}H; 1D ^{13}C; 2D ^{1}H-DQF-COSY; 2D ^{1}H,^{13}C-HMBC; 2D ^{1}H,^{13}C-HMQC; 2D ^{1}H,^{13}C-HSQC; 2D ^{1}H,^{13}C-edited HSQC; 2D ^{1}H-NOESY.

Signals of ^{1}H nuclei were assigned to correlating ^{13}C nuclei by interpretation of the HSQC spectrum. Signals of quarternary ^{13}C could not be securely assigned despite HMBC measurements due to their very similar chemical shifts. NMR signales were assigned to the peptide backbone (NH, CH$_\alpha$, CH$_2$) by interpretation of DQF-COSY and NOESY spectra. Coupling of ^{1}H nuclei in DQF-COSY are listed in Table 31 only for nuclei of the peptide backbone, since strong coupling occured through the whole cage structure of kistamicin A (**15**).

Table 30. 1D ^{1}H and 2D ^{1}H,^{13}C-HSQC NMR data for kistamicin A (**15**) in DMSO-d$_6$ at RT (900 MHz).

Unit	^{1}H			HSQC
	δ_H [ppm]	Multiplicity	Integration	Coupling with δ_C [ppm]
A-NH	9.40	d	1 H	
A-CH$_{ar,5}$	7.09	m	1 H	124.3
A-CH$_{ar,6}$	7.05	m	1 H	119.4
A-CH$_\alpha$	5.47	d	1 H	54.0
A-CH$_{ar,2}$	5.17	s	1 H	111.2
B-NH	8.17	d	1 H	
B-CH$_{ar,6}$	7.87	m	1 H	130.6
B-CH$_{ar,5}$	7.56	d	1 H	133.1
B-CH$_{ar,2}$	7.23	d	1 H	124.2
B-CH$_{ar,3}$	7.03	m	1 H	117.4
B-CH$_\alpha$	4.56	m	1 H	56.5
B-CH$_2$	3.43	d	1 H	40.4
B-CH$_2$	2.78	m	1 H	40.4
C-NH	9.28	s	1 H	
C-CH$_{ar,6}$	7.90	s	1 H	133.8
C-CH$_{ar,2}$	7.31	d	1 H	129.2
C-CH$_{ar,3}$	6.70	d	1 H	126.0
C-CH$_\alpha$	4.86	d	1 H	53.3
D-NH	8.86	d	1 H	
D-CH$_{ar,5}$	7.38	d	1 H	122.5
D-CH$_\alpha$	6.18	m	1 H	54.3
D-CH$_{ar,3}$	5.51	s	1 H	107.7
E-NH	8.35	d	1 H	
E-CH$_{ar,2}$, E-CH$_{ar,6}$	6.01	s	2 H	103.5
E-CH$_{ar,4}$	5.79	s	1 H	100.9
E-CH$_\alpha$	5.07	d	1 H	55.5
F-NH	9.39	d	1 H	
F-NH$_{Indol}$	8.75	s	1 H	
F-CH$_{ar,4}$	7.88	m	1 H	120.6
F-CH$_{ar,1}$	7.33	s	1 H	114.9
F-CH$_{ar,7}$	6.99	d	1 H	130.5
F-CH$_{ar,5}$	6.60	d	1 H	121.2
F-CH$_\alpha$	6.10	s	1 H	52.3
F-CH$_2$	3.37	d	1 H	29.1
F-CH$_2$	2.87	m	1 H	29.1
G-NH$_2$	7.74	s	2 H	
G-CH$_{ar,2}$, G-CH$_{ar,6}$	6.46	d	2 H	129.8
G-CH$_{ar,3}$, G-CH$_{ar,5}$	6.21	d	2 H	115.2
G-CH$_\alpha$	4.02	m	1 H	44.4
G-CH$_2$	3.22	d	1 H	36.2
G-CH$_2$	2.57	m	1 H	36.2

5. *Experimental Procedures*

Table 31.   2D ^{1}H-DQF-COSY and 2D ^{1}H-NOESY NMR data for kistamicin A (**15**) in DMSO-d$_6$ at RT (900 MHz).

Unit	^{1}H	DQF-COSY	Selected NOESY
	δ_H [ppm]	Coupling with δ_H [ppm]	Coupling with δ_H [ppm]
A-NH	9.40	5.47	5.17; 4.86; 4.56; 5.47
A-CH$_{ar,5}$	7.09	6.70	
A-CH$_{ar,6}$	7.05	5.47; 5.17	
A-CH$_\alpha$	5.47	9.40; 7.05; 5.17	9.40; 8.17
A-CH$_{ar,2}$	5.17	7.05; 5.47	
B-NH	8.17	4.56	
B-CH$_{ar,6}$	7.87	7.56; 7.23	
B-CH$_{ar,5}$	7.56	7.87; 7.38; 7.23; 7.03	
B-CH$_{ar,2}$	7.23	7.90; 7.87; 7.38; 7.03	
B-CH$_{ar,3}$	7.03	7.56; 7.23	
B-CH$_\alpha$	4.56	8.17; 3.43; 2.78	9.40; 9.28; 8.86; 8.17
B-CH$_2$	3.43	2.78	
B-CH$_2$	2.78	4.56; 3.43	
C-NH	9.28	4.86	6.18; 6.10; 5.07; 4.86; 4.56
C-CH$_{ar,6}$	7.90	7.31	
C-CH$_{ar,2}$	7.31	7.90; 6.70	
C-CH$_{ar,3}$	6.70	7.90; 7.31	
C-CH$_\alpha$	4.86	9.28; 7.90	9.40; 9.28; 8.86; 8.35; 8.17
D-NH	8.86	6.18	
D-CH$_{ar,5}$	7.38	7.56; 7.23; 6.60	
D-CH$_\alpha$	6.18	8.86; 5.51	9.28; 8.86; 8.35
D-CH$_{ar,3}$	5.51	6.18	
E-NH	8.35	5.07	
E-CH$_{ar,2}$, E-CH$_{ar,6}$	6.01	6.46; 6.21; 5.79	
E-CH$_{ar,4}$	5.79	6.01; 5.51	
E-CH$_\alpha$	5.07	8.35; 6.01	9.39; 9.28; 8.86; 8.35
F-NH	9.39		6.10; 4.02
F-NH$_{Indol}$	8.75		
F-CH$_{ar,4}$	7.88	6.60	
F-CH$_{ar,1}$	7.33	6.60; 3.37	
F-CH$_{ar,7}$	6.99	6.60	
F-CH$_{ar,5}$	6.60	7.88; 7.33	
F-CH$_\alpha$	6.10	9.39; 3.37; 2.87	9.39; 9.28; 8.35; 8.17
F-CH$_2$	3.37	6.10; 2.87	
F-CH$_2$	2.87	6.10; 3.37	
G-NH$_2$	7.74	4.02; 2.56	9.39
G-CH$_{ar,2}$, G-CH$_{ar,6}$	6.46	6.21; 6.01	
G-CH$_{ar,3}$, G-CH$_{ar,5}$	6.21	6.46; 6.01; 5.79	
G-CH$_\alpha$	4.02	7.74; 3.21; 2.56	9.39; 8.35; 7.74
G-CH$_2$	3.22	6.46; 4.02; 3.57	
G-CH$_2$	2.57	4.02; 3.22; 6.01	

5.5. Micro- and Molecularbiological Methods

5.5.1. Isolation of Genomic DNA

Genomic DNA (gDNA) of *Actinomadura parvosata* subsp. *kistnae* was isolated with the help of Bacteria DNA Preparation Kit (*Jena Bioscience*). The protocol was based on the manufacturers' specifications. In contrast to the manufacturers' guidelines, three main cultures of *A. parvosata* (50 mL each) were used for harvesting cells. The cultures were centrifuged (20,000 xg, 15 min, RT), the supernatant discarded, and residue centrifuged again (13,000 xg, 1 min, RT). This residue was then split into five fractions and each fraction used for gDNA isolation. For cell lysis the cell suspension was treated with 4 µL Lysozyme Solution. In the final step, DNA was hydrated by incubation with 50 µL to 150 µL double distilled water over night at 4 °C.

5.5.2. Preparation of Plasmid DNA

Preparation of plasmid DNA was conducted with the help of peqGOLD Plasmid Miniprep Kit I (*Peqlab*). 3 mL to 5 mL over night *E. coli* cultures were used as standard for purification as definded by the manufacturer.

5.5.3. Polymerase Chain Reaction (PCR)

DNA can be selectivly amplified by PCR. For this purpose, gDNA of *A. parvosata* as well as miscellaneous plasmids were used as templates. Desired genes or DNA sections were amplified utilizing Taq polymerase (*Jena Bioscience*) or Q5™ High-Fidelity DNA Polymerase (*New Englands Biolabs, NEB®*). The latter enzyme possesses an exonuclease function for repair of incorrect incorporated base pairs. The propability of mutations in amplified DNA is thereby significantly reduced.

5.5.3.1. Q5 PCR

PCR reactions utilizing Q5™ High-Fidelity DNA Polymerase (*NEB®*) were conducted according to Table 32. Addition of GC Enhancer was optional and was done due to the high GC content of DNA templates.

Table 32. A PCR reaction utilizing Q5™ High-Fidelity DNA Polymerase (*NEB*®).

Component	Amount
Q5 polymerase (200 U/mL)	$0.125\,\mu\text{L}$
Q5 buffer (5x)	$5\,\mu\text{L}$
GC Enhancer (5x)	$5\,\mu\text{L}$
dNTPS (10 mM)	$0.5\,\mu\text{L}$
forward primer ($20\,\text{pmol}\,\text{mL}^{-1}$)	$0.125\,\mu\text{L}$
reverse primer ($20\,\text{pmol}\,\text{mL}^{-1}$)	$0.125\,\mu\text{L}$
template	ca. $200\,\text{ng}$
double distilled water	ad $50\,\mu\text{L}$

In Table 33 the standard temperature program for PCR reactions with Q5™ polymerase was noted.

Table 33. Temperature program for PCR reactions with Q5™ High-Fidelity DNA Polymerase (*NEB*®).

	Segment	Temperature	Time
1	initial temperature	$98\,°\text{C}$	$1\,\text{min}$
2	denaturation	$98\,°\text{C}$	$10\,\text{s}$
3	primer hybridization	primer dependent: $47\,°\text{C}$ to $72\,°\text{C}$	$20\,\text{s}$
4	elongation	$72\,°\text{C}$	$20\,\text{s}$ to $30\,\text{s/kb}$
5	final elongation	$72\,°\text{C}$	$2\,\text{min}$

Steps 2 to 4 were repeated 30 times.

5.5.3.2. Taq PCR

PCR reactions utilizing Taq polymerase (*Jena Bioscience*) were conducted according to Table 34. Taq polymerase was frequently used to search bacterial colonies for the presence or absence of a desired insert in plasmid constructs by (colony) screening PCR. Single colonies were picked with sterile tooth picks from agar plates, and resuspended in $5\,\mu\text{L}$ sterile double distilled water. Those suspensions were then used as a templates for PCR. For cultivation of positive colonies a part of the respective cell suspension was used to inoculate $5\,\text{mL}$ LB medium supplemented with the respective antibiotic, and cultivated under standard conditions (Chapter 5.3.1).

Table 34. A PCR reaction utilizing Taq polymerase.

Component	Amount
Taq polymerase (2.5 U/mL)	0.125 µL
Taq buffer (10x)	2.5 µL
DMSO (100 %)	1 µL
dNTPS (10 mM)	0.25 µL
forward primer (20 µM)	0.125 µL
reverse primer (20 µM)	0.125 µL
template	ca. $8\,ng\,µL^{-1}$ gDNA or 5 µL cell suspension
double distilled water	ad 25 µL

In Table 35 the standard temperature program for PCR reactions with Taq polymerase was noted.

Table 35. Temperature program for Taq screening PCR.

	Segment	Temperature	Time
1	initial temperature	95 °C	2 min
2	denaturation	95 °C	45 s
3	primer hybridization	primer dependent: 47 °C to 72 °C	30 s
4	elongation	72 °C	70 s/kb
5	final elongation	72 °C	5 min

Steps 2 to 4 were repeated 33 times.

5.5.4. Visualization of DNA

Agarose gel electrophoresis was used for the analysis of PCR reactions, plasmid, and gDNA extraction as well as restriction digests. Moreover, DNA fragments were purified and isolated with its help (Chapter 5.5.6). By default, 1 (w/v) % agarose was dissolved in 1x TAE buffer by heating in a microwave. After cooling to ca. 60 °C Clear G DNA stain (*Serva*) was added and the solution poured into a casting tray with gel combs. After hardening, the gel was placed in an electrophoresis chamber and filled with 1x TAE buffer until it was completely submerged. DNA samples were blended with DNA loading buffer (Table 24) to increase their weight before loading them into the slots of the agarose gel. For size reference 2 µL of GeneRuler™1 kb plus DNA Ladder (*Thermo Scientific*™) (Figure 34) was used. By application of an electric voltage (90 V to 120 V) migration of the evenly
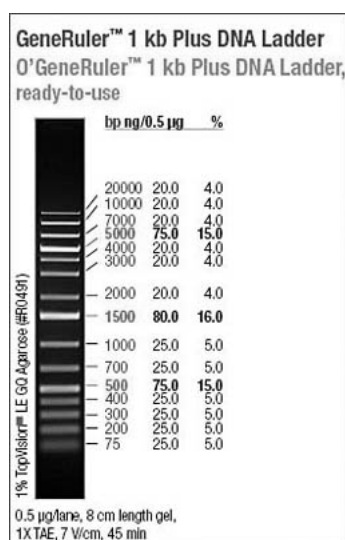
Figure 34. DNA fragments incorporated in the size standard GeneRuler™1 kb plus DNA Ladder from *Thermo Scientific*™. Fragment size (bp) and quantitative (ng/0.5 µg) as well as percentage ratios are indicated. This figure was obtained from the manufacturers' website. [200]

negatively charged samples from anode to cathode was caused. After 20-30 min agarose gels could by analyzed and documented under UV light.

5.5.5. Determination of DNA Concentration and Purity

Concentration and purity of PCR products, plasmid DNA, and gDNA was determined photometrically with Nanophotometer P330 (*Implen*). For this purpose, menu options 'NanoVolume Applications', 'Nucleic Acids' and 'dsDNA' as well as the following settings were choosen: LID-factor: 10; Dilution: 1,000; Background: ON; Units $ng\,\mu L^{-1}$; Factor: 50.0. Blank values were measured with double distilled water or the buffer, in which the DNA sample was dissolved. DNA concentration and ratios of absorption at 260 nm to absorption at 280 nm (A260/A280) or at 230 nm (A260/230) were given as results. Both ratios provide information about contamination with proteins or salts and should range about ≥ 1.8.

5.5.6. Preparation of PCR Products

5.5.6.1. Direct Purification of PCR Products

PCR products were purified with the help of PCR Purification Kit (*Jena Bioscience*) according to the manufacturers' specifications.

5.5.6.2. Purification of PCR Products by Agarose Gel Extraction

For purification of PCR products by agarose gel extraction the respective PCR product was cleanly cut from the agarose gel after electrophoresis (Chapter 5.5.4). Subsequent isolation of the PCR product from agarose was conducted with Gel Extraction Kit, peqGOLD (*Peqlab*) according to the manufacturers' specifications.

5.5.7. Enzymatic DNA Modifications

5.5.7.1. DNA Restriction Digest for Subsequent Ligation

DNA was subjected to restriction digest for preparation of cloning experiments and analysis of plasmids. PCR products were previously purified by direct PCR purification or agarose gel extraction (Chapter 5.5.6). Restriction enzymes were purchased from *Jena Bioscience* and *NEB*®. Reactions were incubated for 1.5 h to 2.5 h at 37 °C, and enzymes then inactivated for 20 min at a temperature specified by the manufacturer. In case of subsequent use in cloning experiments, DNA was extracted by direct purification (Chapter 5.5.6) after restriction digest and possibly dephosphorylation (Chapter 5.5.7.2). Table 36 and Table 37 indicate the standard composition of a restriction digest.

Table 36. Composition of a restriction digest for a vector.

Component	Amount
vector	1 µg to 2 µg
restriction enzyme(s)	2.5 µL each
buffer (10x)	5 µL
double distilled water	ad 50 µL

Table 37. Composition of a restriction digest for a purified PCR product.

Component	Amount
purified PCR product	0.5 µg to 2 µg
restriction enzyme(s)	2.5 µL each
buffer (10x)	5 µL
double distilled water	ad 50 µL

5.5.7.2. DNA Dephosphorylation

After restriction digest (Chapter 5.5.7.1), linearized vectors were dephosphorylized at their 5' and 3' ends to reduce the probability of recirculation during subsequent ligation. For this purpose, the enzyme Antarctic Phosphatase (*NEB®*) was used. Reactions were incubated for at least 2 h or over night, and the enzyme then inactivated for 20 min at 80 °C. Linear dephosphorylized vectors were subsequently purified by direct purification (Chapter 5.5.6).

Table 38. Composition of a dephosphorylation reaction.

Component	Amount
restriction digest	50 µL
Antarctic Phosphatase buffer (10x)	2 µL
Antarctic Phosphatase (5 U/µL)	2 µL
double distilled water	ad 60 µL

5.5.7.3. DNA Cohesive End Ligation by T4 Ligase

For ligation of compatible DNA ends the enzyme T4 ligase (*Jena Bioscience*) was used. The composition of each ligation reaction was calculated independently based on the concentration of PCR fragments and vectors. For this purpose, the molar ratio of vector to insert ideally amounted to 1/5, and the reaction mixture contained at least 0.02 pmol of the respective vector. Moreover, 5 % T4 ligase (2.5 U/µL) and 10 % T4 ligase buffer were used. Ligation reactions were incubated over night at 16 °C. The enzyme was inactivated for 20 min at 65 °C, and reaction mixtures subsequently transformed into chemically competent *E. coli* DH5α cells (Chapter 5.5.11).

5.5.7.4. Gibson Assembly

For cloning of DNA fragments by Gibson assembly primers were designed with the help of the online application NEBuilder®(Table 11). Overhangs were at least 7 bp long, and primers were utilized in Q5™PCR reactions (Chapter 5.5.3.1) to amplify the sequences of *kisD-PCP* and *kisD-X*. The resulting products were purified by direct PCR purification (Chapter 5.5.6). Vector pHis8-TEV was linearized by restriction digest (Chapter 5.5.7.1), dephosphorylized (Chapter 5.5.7.2), and purified by direct PCR purification (Chapter 5.5.6). Subsequent Gibson assembly of the respective PCR products (*kisD-PCP* and

kisD-X) with vector pHis8-TEV was carried out using 10 µL HiFi DNA Assembly Mix (2x) (HiFi DNA Assembly Cloning Kit by *NEB*®) and a 10 µL mixture of insert and vector. The latter one consisted of a vector/insert ratio of 1/2 and at least 0.02 pmol of the respective vector. The 20 µL reactions were incubated for 1 h at 50 °C, and 10 µL reaction mixture then transformed into chemically competent *E. coli* DH5α cells (Chapter 5.5.11).

5.5.7.5. Analytical Restriction Digest

Colonies which appeared to be positive in screening PCRs (Chapter 5.5.3.2) were cultivated under standard conditions (Chapter 5.3.1) and subjected to plasmid preparation (Chapter 5.5.2). A portion of the plasmid solution was then submitted to an analytical restriction digest with one or several restriction enzymes. This should generate characteristic band patterns which allowed clear identification of vectors with the desired insert. Plasmids which seemed to be positive in the analytical restriction digest, too, were used for DNA sequencing (Chapter 5.5.10).

Table 39. Composition of an analytical restriction digest for a new construct.

Component	Amount
plasmid	ca. 240 ng
restriction enzyme(s)	0.125 µL each
buffer (10x)	1 µL
double distilled water	ad 10 µL

5.5.8. DNA Sequencing

5.5.9. SMRT® Genome Sequencing

For genome sequencing, the gDNA of *Actinomadura parvosata* subsp. *kistnae* was isolated (Chapter 5.5.1), and its quality photometrically determined. 1.7 µg gDNA of sufficient purity (A260/A280 ≥1.4, A260/A230 ≥2.1) was sent to *GATC Biotech AG*, and the genome sequenced by *PacBio*® single molecule real-time (SMRT®) sequencing. Assembly of those data was performed by *GATC*.

5.5.10. Sanger Sequencing

To verify the DNA sequence of inconclusive segments in the kistamicin gene cluster the corresponding segments were PCR amplified using Taq or Q5™ polymerase (Chapter 5.5.3) and *A. parvosata* gDNA as a template. PCR products were purified (Chapter 5.5.6) and sent to *GATC Biotech AG* for Sanger sequencing (20 µL sample with $10\,\text{ng}\,\text{µL}^{-1}$ to $50\,\text{ng}\,\text{µL}^{-1}$ PCR fragment). For PCR product sequencing self designed primers (Table 14) were used.

Successful and mutation free cloning of a DNA sequence was controlled by sending the respective plasmid in purified form (20 µL sample with $30\,\text{ng}\,\text{µL}^{-1}$ to $100\,\text{ng}\,\text{µL}^{-1}$ plasmid) to *GATC Biotech AG* for Sanger sequencing. For plasmid sequencing various standard primers (Table 14) were used.

Analysis of sequencing results was carried out using the 'Alignment' option ('Geneious Alignment' with standard settings) of the Geneious software (Table 10). Only if mutation free cloning was proven, a primary culture of the respective clone was created and used for further experiments. Additionally, the respective clone was stored as a cryo culture (Chapter 5.3.2). In all other cases, the clone was discarded and other plasmids or PCR products sequenced or cloning repeated.

5.5.11. Transformation into Chemically Competent *E. coli* Cells

Chemically competent *E. coli* DH5α, *E. coli* BL21(DE3) or *E. coli* SoluBL21™cells were obtained from stocks produced in the laboratory. For transformation 5 µL to 10 µL ligation reaction, 1 µL to 5 µL Gibson assembly mix or 5 µL plasmid were suspended in 100 µL chemically competent cell culture, and incubated for 15 min to 30 min on ice. The cells were then subjected to heat shock for 90 s at 42 °C, and again cooled on ice for 2 min. Subsequently, 900 µL SOC medium (Chapter 5.3.3) were added and the solution incubated for 60 min at 37 °C. The 150 µL cell culture was spread onto LB agar supplemented with an appropriate antibiotic and incubated over night at 37 °C. The remaining culture was centrifuged (4,000 xg, 2 min, RT) and 600 µL supernatant discarded. The residue was resuspended and also spread onto LB agar supplemented with an appropiate antibiotic, and incubated over night at 37 °C. For future applications, clones were picked from the agar plate on which they could be identified as single colonies.

5.6. Heterologous Protein Expression and Protein Purification

5.6.1. Testing Conditions for Protein Expression in *E. coli*

All cloned plasmids (Table 13) were subjected to heterologous test expressions to verify whether the corresponding protein could be expressed and to find the optimal conditions for protein production. If various plasmids coding for the desired protein had been successfully cloned previously, test expressions were conducted for all plasmids. Plasmids were based on expression vectors pGS-21a and pHis8-TEV (Table 13).

For heterologous expression 250 mL LB medium were inocuated with a starter culture of *E. coli* BL21(DE3) or *E. coli* SoluBL21™, which carried the respective plasmid. Cultures were grown at 37 °C and 200 rpm until an OD$_{600nm}$ of 0.5 to 0.6 was reached, and then cooled on ice for 30 min. Subsequently, 1 mL culture was taken as an uninduced sample (sample [U]), centrifuged (4,000 xg, 2 min, RT), the pellet resuspended in 20 µL double distilled water, and stored at −20 °C. The remaining culture was induced with 0.5 mM or 1.0 mM IPTG, and incubated at 16 °C, 22 °C or 28 °C and 200 rpm over night. IPTG was available as an 1.0 M, sterile-filtered stock solution in double distilled water. At the next day, the culture was cooled on ice for 30 min, and then centrifuged (5,000 xg, 5 min, 4 °C). The pellet was resuspended in 4 mL to 5 mL lysis buffer (Chapter 5.3.5) per g pellet, and disrupted using an ultrasonic homogenizer. The lysate was centrifuged (14,000 xg, 10 min, 4 °C), and the pellet resuspended in 8 mL to 10 mL double distilled water per g pellet (sample [P]). The supernatant provided sample [S]. The sample of the uninduced cells ([U]), the pellet ([P]) as well as of the supernatant ([S]) were subjected to SDS-PAGE analysis (Chapter 5.7).

5.6.2. Protein Purification for Proteins with His-Tag

Small samples of protein were purified after heterologous test expression using Ni-NTA Spin Columns (*Qiagen*). For this purpose, a Ni-NTA column was activated by loading with 600 µL lysis buffer (Chapter 5.3.5) and centrifugation (2,000 xg, 2 min, 4 °C). The column was then loaded with 600 µL lysate (Chapter 5.6.1), centrifuged (2000 xg, 2 min, 4 °C), and the flow through collected in an 2 mL *Eppendorf* tube (sample [F1]). This was repeated once and the second flow through collected as well (sample [F2]). The loaded Ni-NTA column was treated with 600 mL washing buffer (Chapter 5.3.5), centrifuged (2000 xg, 2 min, 4 °C), and the washing fraction collected in an 2 mL *Eppendorf* tube (sample [W1]).

This was repeated once and the second washing fraction collected as well (sample [W2]). Finally, the washed Ni-NTA column was treated with 200 mL elution buffer (Chapter 5.3.5), centrifuged (2000 xg, 2 min, 4 °C), and the eluate collected in a 2 mL *Eppendorf* tube (sample [E]). Samples of the flow through ([F1] and [F2]), the washing fractions ([F1] and [F2]) as well as of the eluate ([E]) were subjected to SDS-PAGE analysis (Chapter 5.7).

5.7. Sodium Dodecyl Sulfate–Polyacrylamide Gel (SDS-PAGE) Electrophoresis

For analysis of heterologously expressed proteins SDS-PAGE was utilized.

In this process negatively charged sodium dodecyl sulfate binds stoichiometrically to proteins and covers their intrinsic charges. All treated proteins thereby exhibit a very similar ratio of molecular weight to negative total charge. This can be used to separate different proteins according to their weight by application of an electric voltage, since small proteins migrate at a faster pace through the gel than larger proteins. For separation vertical multigel electrophoresis systems (Mini-Protean® Tetra Cell (*Biorad*) were used. Gels were produced with 12 % acrylamide. In the first step, the separating gel (Table 40) was cast and poured between two glas plates, wich were fixed with clips. It was then coated with isopropanol, thereby creating an even horizontal surface. After polymerization of the separating gel, isopropanol was removed and the stacking gel (4 %) (Table 41) as well as a gel comb added. The separating gel was used for separation of proteins, the stacking gel for sample application.

Table 40. Composition of two 12 % separating gels for SDS-PAGE.

Component	Amount
separating gel buffer (4x) (Table 28)	3.75 mL
water	6.75 mL
acrylamide (40 v/v %)	4.5 mL
APS (10 w/v %)	150 µL
TEMED	15 µL

Table 41. Composition of two 4 % stacking gels for SDS-PAGE.

Component	Amount
stacking gel buffer (4x) (Table 29)	1.25 mL
water	3.25 mL
acrylamide (40 v/v %)	0.5 mL
APS (10 w/v %)	50 µL
TEMED	5 µL

The finished gel was placed in an electrophoresis chamber, which was then filled with SDS running buffer (1x) (*Roth*). 20 µL of each sample (for sample preperation see Chapter 5.6.1 and Chapter 5.6.2) were mixed with 5 µL SDS-PAGE sample buffer (Table 27), vortexed, denatured for 5 min at 95 °C, and vortexed again. 10 µL of each sample was transferred into a separate well in the stacking gel. 6 µL Pierce™Unstained Protein Molecular Weight Marker (*Thermo Scientific*) (Figure 35) was used as reference. Subsequently, separation of proteins was achieved by application of a voltage of 35 A per gel and was finalized when the dye front reached the end of the gel. Gels were stained with a Coomassie Brilliant Blue solution (10 v/v % acetic acid, 30 v/v % methanol, 0.25 w/v % Coomassie Brilliant Blue R-250) for 30 min to 60 min, and bleached over night with bleaching solution (10 v/v % acetic acid and 30 v/v % methanol in water). During staining and bleaching the gel was slightly shaken. Documentation was carried out using a customary faltbed scanner.
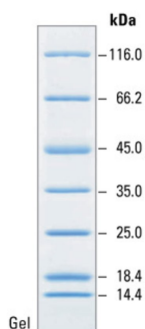

Figure 35. Pierce™Unstained Protein Molecular Weight Marker (*Thermo Scientific*™) was used as a size standard for protein gels in this work. This figure was obtained from the manufacturers' website.[201]

5.8. Chromatographic Methods

5.8.1. High Performance Liquid Chromatography (HPLC)

HPLC analyses were carried out using computer-controlled *Jasco* systems (system 1: MD-2010 Plus Multiwavelength Detector, DG-2080-53 3-Line Degaser, two PU-2086 Plus Intelligent Prep. Pumps, AS-2055 Plus Intelligent Sampler, MIKA 1000 Dynamic Mixing Chamber, 1000 µL *Portmann Instruments AG* Biel-Benken, LC-NetII/ADC; system 2: UV-1575 Intelligent UV/VIS Detector, DG-2080-53 3-Line Degaser, two PU-1580 Intelligent HPLC Pumps, AS-1550 Intelligent Sampler, HG-1580-32 Dynamic Mixer, LC-NetII/ADC). Program control and interpretation of the recorded data was carried out using the *Jasco* ChromPass Chromatography Data System software and Galaxie-Chromatography software. An Eurospher II 100-3 C18 A (150 x 4.6 mm) column (*Knauer*) with integrated pre-column was used with the solvents A: water + 0.05 % TFA and B: ACN + 0.05 % TFA. Except where otherwise specified, the following gradient was applied: 0.0-2.0 min 95 % A, 2.0-25.0 min 5 % A, 25.0-30.0 min 5 % A, 30.0-31.0 95 % A, 31.0-38.0 95 % A with a flow rate of 1 mL/min.

Product isolation with semi-preparative HPLC separation was carried out using a computer-controlled *Jasco* system (UV-1575 Intelligent UV/VIS Detector, two PU-1580 Intelligent HPLC Pumps, MIKA 1000 Dynamic Mixing Chamber, 1000 µL *Portmann Instruments AG* Biel-Benken, LC-NetII/ ADC, *Rheodyne* injection valve). Program control and interpretation of the recorded data was carried out using Galaxie software. Eurosphere II 100-5 C18 A columns (*Knauer*) with integrated pre-columns in different sizes were used with the solvents A: water + 0.05 % TFA and B: ACN + 0.05 % TFA. Applied column sizes and solvent gradients are noted in the respective experimental procedures.

After preparative product-isolation the respective fractions were combined and acetonitrile removed *in vacuo*. The aqueous layer was then lyophilized.

5.8.2. High Performance Liquid Chromatography-Mass Spectrometry (LC-MS)

LC-MS analyses were carried out using an UltiMate 3000 LC System coupled to a LCQ Fleet Ion Trap Mass Spectrometer (both by *Thermo Scientific*™). The *Thermo* Xcalibur™software was used to control the system and interpretation of the recorded data was carried out using the *Thermo* Xcalibur™Qual Browser 2.2 SP1.48 software. A C18

Hypersil GOLD™AQ (150 x 2.1 mm) column with integrated pre-column and the solvents A: water + 0.1 % formic acid as well as B: ACN + 0.1 % formic acid were used for chromatographic separation. Except where otherwise specified, the following gradient was applied: -2.5-0.0 min 95 % A, 0.0-8.0 min 95 % B, 8.0-8.4 min 100 % B, 8.4-10.8 min 100 % B, 10.8-11.2 min 95 % A, 11.2-12.0 min 95 % A with a flow rate of 0.7 mL/min. Measured molecular fragments were indicated as mass/ charge ratios *m/z*.

5.8.3. Medium Pressure Liquid Chromatography (MPLC)

The Reveleris®X2 MPLC system (*Grace*) was employed for MPLC purification. Miscellaneous Reveleris®Reverse Phase (RP) C18 finished columns (*Grace*) in different sizes were used as required. The system was run with the Reveleris®Navigator™software (*Grace*). UV detection was carried out at 220 nm, 254 nm, and 250 nm. Applied column sizes and solvent gradients are noted in the respective experimental procedures.
After preparative product-isolation the respective fractions were combined and acetonitrile removed *in vacuo.* The aqueous layer was then lyophilized.

5.8.4. Thin Layer Chromatography (TLC)

TLC aluminium foils (TLC silica gel 60 F$_2$4) (*Merck*) were used for TLC. Applied substances were observed with UV light at 254 nm. For the detection of UV inactive substances TLC foils were stained with ninhydrin (0.35 % in ethanol) or anisaldehyde (3.7 mL 4-anisaldehyde, 1.5 mL glacial acetic acid, 5 mL conc. sulfuric acid, 135 mL ethanol) and developed at 250 °C in a hot airflow.

5.8.5. Column Chromatography

Silica gel 60 Geduran®Si 60 (40 µm to 60 µm) (*Merck*) was used as the stationary phase in column chromatography. Applied solvent systems are noted in the respective experimental procedures.

5.8.6. Cation-Exchange Chromatography

Dowex™50X8-100 ion exchange resin (*Acros Organics*) was applied as the stationary phase in cation-exchange chromatography. The resin was equilibrated to pH 3 with HCl (0.01 M in water) before use. Employed solvent systems are noted in the respective experimental procedures. Removal of chloride salts from synthesized compounds was monitored by the addition of two drops of silver nitrate (0.1 M in water) and two drops of concentrated nitric acid to samples of cation-exchange chromatography fractions. If a colourless precipitate was formed in the process chloride salts were still present in the respective sample.

5.9. Chemical Peptide Synthesis

Air or moisture sensitive reactions were carried out under Schlenck conditions in argon atmosphere. For this purpose, glasware was heated in high vacuum and filled with argon repeatedly.

5.9.1. Amino Acid Building Blocks

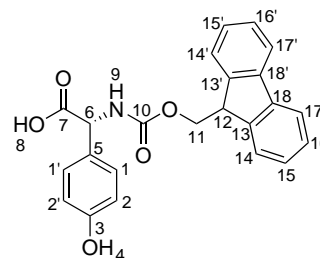### 5.9.1.1. *N*-Fmoc-D-4-Hpg (D-82)
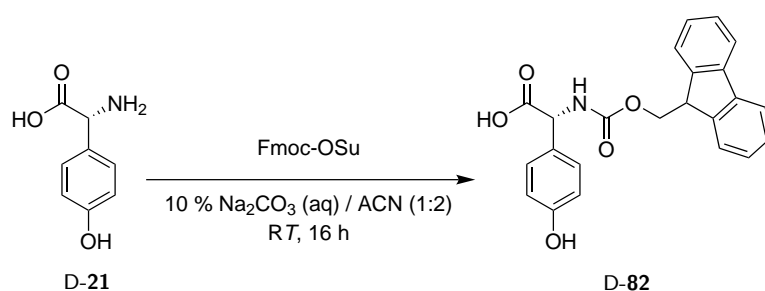
0.50 g D-4-Hpg (D-**21**) (2.99 mmol, 1.0 eq.) were dissolved in 5 mL Na_2CO_3 solution (10 w/v % in water) and 5 mL acetonitrile. 1.01 g *N*-Fmoc hydroxysuccinimide ester (2.99 mmol, 1.0 eq.), dissolved in 5 mL acetonitrile, were added drop-wise while stirring. After 16 h of vigorous stirring at R*T* the colourless precipitate was dissolved in water. The solution was subsequently washed with Et_2O (2x), the aqueous layer acidified to pH 2 with HCl (10 v/v % in water), and extracted with EtOAc (3x). The combined EtOAc layers were washed with brine (2x), dried over $MgSO_4$, and the solvent removed *in vacuo.* Product D-**82** was obtained as a colourless solid (1.10 g, 2.82 mmol) in 94.2 % yield.

Analytics

Molecular formula: $C_{23}H_{19}NO_5$

Molecular weight: 389.41 g/mol

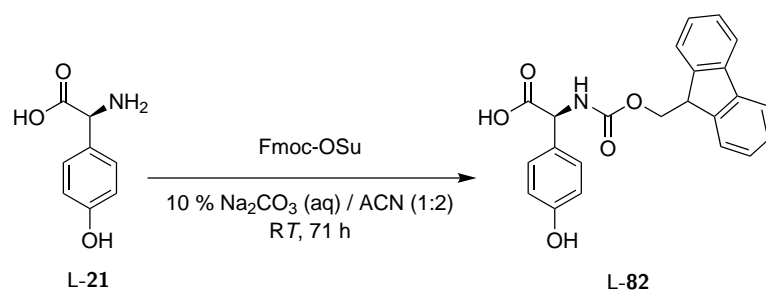HR-ESI(+)-MS: m/z = calc. for $C_{23}H_{20}NO_5$ 390.13415 [M+H]$^+$, found 390.13370.

^{1}H-NMR (300 MHz, DMSO-d$_6$, RT) δ = 9.47 (s, 1 H, H-4), 8.05 (d, J = 7.8 Hz, 1 H, H-9), 7.88 (d, J = 7.4 Hz, 2 H, H-17, H-17'), 7.75 (d, J = 7.4 Hz, 2 H, H-14, H-14'), 7.41-7.44 (m, 2 H, H-16, H-16'), 7.28-7.35 (m, 2 H, H-15, H-15'), 7.20 (d, J = 8.5 Hz, 2 H, H-1, H-1'), 6.73 (d, J = 8.5 Hz, 2 H, H-2, H-2'), 5.01 (d, J = 7.8 Hz, 1 H, H-6), 4.18-4.28 (m, 3 H, H-11, H-12) ppm.

The spectroscopic data are in agreement with the literature.[122]

### 5.9.1.2. *N*-Fmoc-L-4-Hpg (L-82)

L-21   →   L-82

5.0 g L-4-Hpg (L-**21**) (29.93 mmol, 1.0 eq.) were dissolved in 50 mL Na$_2$CO$_3$ solution (10 w/v % in water) and 50 mL acetonitrile. 10.09 g *N*-Fmoc hydroxysuccinimide ester (29.91 mmol, 1 eq.), dissolved in 50 mL acetonitrile, were added drop-wise while stirring. After 71 h of vigorous stirring at RT the colourless precipitate was dissolved in water. The solution was subsequently washed with Et$_2$O (2x), the aqueous layer acidified to pH 3 with HCl (10 w/v % in water), and extracted with EtOAc (3x). The combined EtOAc layers were washed with brine (2x), dried with MgSO$_4$, and the solvent removed *in vacuo*. Product L-**82** was obtained as a colourless solid (9.63 g, 24.75 mmol) in 82.8 % yield.

Analytics

Molecular formula: C$_{23}$H$_{19}$NO$_5$

Molecular weight: 389.41 g/mol
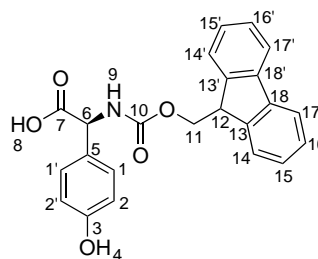
HR-ESI(+)-MS: m/z = calc. for C$_{23}$H$_{20}$NO$_5$ 390.13415 [M+H]$^+$, found 390.13369; calc. for C$_{46}$H$_{39}$N$_2$O$_{10}$ 779.26047 [2M+H]$^+$, found 779.25943

^{1}H-NMR (300 MHz, DMSO-d$_6$, RT) δ = 9.50 (brs, 1 H, H-4), 8.06 (d, J = 7.9 Hz, 1 H,

H-9), 7.88 (d, $J = 7.4$ Hz, 2 H, H-17, H-17'), 7.75 (d, $J = 7.4$ Hz, 2 H, H-14, H-14'), 7.39-7.44 (m, 2 H, H-16, H-16'), 7.27-7.34 (m, 2 H, H-15, H-15'), 7.20 (d, $J = 8.5$ Hz, 2 H, H-1, H-1'), 6.73 (d, $J = 8.5$ Hz, 2 H, H-2, H-2'), 5.01 (d, $J = 7.8$ Hz, 1 H, H-6), 4.18-4.27 (m, 3 H, H-11, H-12) ppm.

The spectroscopic data are in agreement with the literature.[122]

### 5.9.1.3. 3-Chloro-D-4-Hpg (D-39)
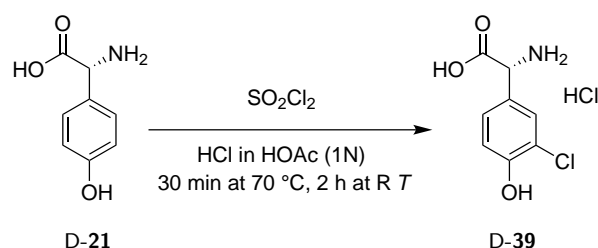
5.0 g D-4-Hpg (D-**21**) (29.92 mmol, 1.0 eq.) were dissolved in 75 mL hydrochlorid acid (1 N in acetic acid), and 5.57 mL sulforyl chloride (68.92 mmol, 2.30 eq.) added drop-wise over 30 min while stirring and cooling. The reaction mixture was subsequently stirred for 30 min at 70 °C, and then for 2 h at RT. The solution was then poured into 2x 300 mL Et$_2$O, and cooled for 16 h at 4 °C. The resulting colourless precipitate was filtered and washed with ice cold water and acetone. The filtrate was adjusted to pH 5 with ammonia solution, and the resulting colourless precipitate filtered and washed with ice cold water and acetone. The combined precipitates were dried *in vacuo*. The hydrochloride salt of D-**39** was obtained as a colourless solid (4.82 g, 20.26 mmol) in 67.7 % yield.

Analytics

Molecular formula: C$_8$H$_8$ClNO$_3$

Molecular weight: 201.61 g/mol
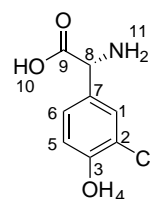
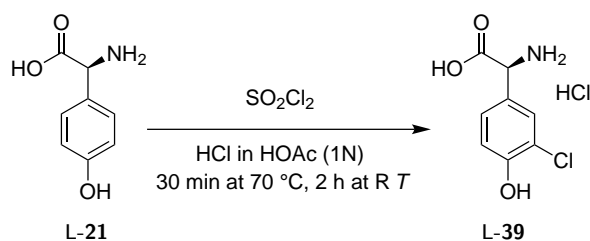HR-ESI(+)-MS: m/z = calc. for C$_8$H$_9$ClNO$_3$ 202.02708 [M+H]$^+$, found 202.02660.

^{1}H-NMR (300 MHz, DMSO-d$_6$, RT) $\delta = 8.70$ (brs, 2 H, H-11), 7.36 (d, $J = 2.1$ Hz, 1 H, H-1), 7.12 (dd, $J = 2.1$ Hz, $J = 8.4$ Hz, 1 H, H-6), 6.92 (d, $J = 8.4$ Hz, 2 H, H-5), 4.20 (s,

1 H, H-8) ppm.

The spectroscopic data are in agreement with the literature.[202]

5.9.1.4. 3-Chloro-L-4-Hpg (L-39)

L-21   SO$_2$Cl$_2$, HCl in HOAc (1N), 30 min at 70 °C, 2 h at R*T*   L-39

1.0 g L-4-Hpg (**L-21**) (5.97 mmol, 1.0 eq.) were dissolved in 15.0 mL hydrochlorid acid in acetic acid (1 N) and 1.12 mL sulforyl chloride (13.86 mmol, 2.32 eq.) added drop-wise over 15 min while stirring and cooling. The reaction mixture was subsequently stirred for 30 min at 70 °C and then for 2 h at R*T*. The solution was poured into 250 mL Et$_2$O. and cooled for 16 h at 4 °C. The resulting colourless precipitate was filtered, washed with ice cold acetone and dried *in vacuo*. The hydrochloride salt of **L-39** was obtained as a colourless solid (1.93 g) and used without further purification.

Analytics

Molecular formula: C$_8$H$_8$ClNO$_3$

Molecular weight: 201.61 g/mol
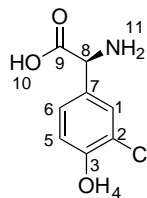
HR-ESI(+)-MS: m/z = calc. for C$_8$H$_9$ClNO$_3$ 202.02710 [M+H]$^+$, found 202.02663.

^{1}H-NMR (500 MHz, methanol-d$_4$, R*T*) δ = 7.46 (d, J = 2.3 Hz, 1 H, H-1), 7.26 (dd, J = 2.3 Hz, J = 8.5 Hz, 1 H, H-6), 7.0 (d, J = 8.4 Hz, 2 H, H-5), 5.01 (s, 1 H, H-8) ppm.

The spectroscopic data are in agreement with the literature.[202]
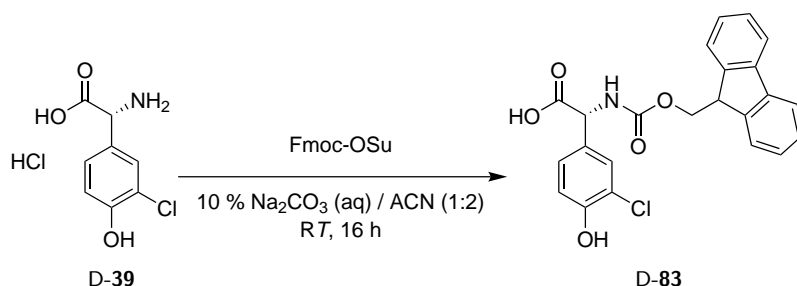
5.9.1.5. *N*-Fmoc-3-Chloro-D-4-Hpg (D-83)

4.50 g 3-chloro-D-4-Hpg (D-**39**) (18.91 mmol, 1.0 eq.) were dissolved in 35 mL Na_2CO_3 solution (10 w/v % in water) and 35 mL acetonitrile. 7.53 g *N*-Fmoc hydroxysuccinimide ester (22.32 mmol, 1.18 eq.), dissolved in 35 mL acetonitrile, were added drop-wise while stirring. After 16 h of vigorous stirring at R*T* the colourless precipitate was dissolved in water. The solution was subsequently washed with Et_2O (2x), the aqueous layer acidified to pH 3 with HCl (10 w/v % in water), and extracted with EtOAc (3x). The combined EtOAc layers were washed with brine (2x), dried over $MgSO_4$, and the solvent removed *in vacuo.* Product D-**83** was obtained as a colourless solid (6.40 g, 15.11 mmol) in 79.9 % yield.

Analytics

Molecular formula: $C_{23}H_{18}ClNO_5$

Molecular weight: 423.85 g/mol
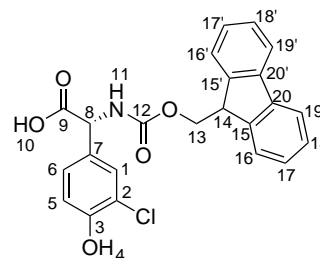
HR-ESI(+)-MS: m/z = calc. for $C_{23}H_{19}ClNO_5$ 424.09518 $[M+H]^+$, found 424.09462.

^{1}H-NMR (300 MHz, DMSO-d$_6$, R*T*) δ = 10.27 (s, 1 H, H-4), 8.15 (d, J = 7.9 Hz, 1 H, H-11), 7.89 (d, J = 7.5 Hz, 2 H, H-19, H-19'), 7.74 (d, J = 7.4 Hz, 2 H, H-16, H-16'), 7.39-7.44 (m, 3 H, H-1, H-18, H-18'), 7.28-7.35 (m, 2 H, H-17, H-17'), 7.18 (dd, J = 1.8 Hz, J = 8.4 Hz, 1 H, H-6), 6.94 (d, J = 8.3 Hz, 1 H, H-5), 5.06 (d, J = 7.9 Hz, 1 H, H-8), 4.19-4.29 (m, 3 H, H-13, H-14) ppm.

5. Experimental Procedures

5.9.1.6. *N*-Fmoc-3-Chloro-L-4-Hpg (L-83)
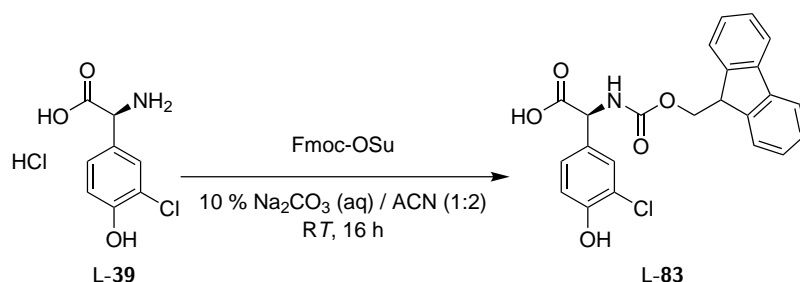
1.93 g of 3-chloro-L-4-Hpg (L-**39**) were dissolved in 40 mL Na_2CO_3 solution (10 w/v % in water) and 40 mL acetonitrile. 2.01 g *N*-Fmoc hydroxysuccinimide ester (5.96 mmol), dissolved in 40 mL acetonitrile, were added drop-wise while stirring. After 16 h of vigorous stirring at R*T* the colourless precipitate was dissolved in water. The solution was subsequently washed with Et_2O (2x), the aqueous layer acidified to pH 3 with HCl (10 w/v % in water), and extracted with EtOAc (3x). The combined EtOAc layers were washed with brine (2x), dried over $MgSO_4$, and the solvent removed *in vacuo*. Product L-**83** was obtained as a colourless solid (1.84 g, 4.33 mmol) in 72.5 % yield over two steps.

Analytics

Molecular formula: $C_{23}H_{18}ClNO_5$

Molecular weight: 423.85 g/mol
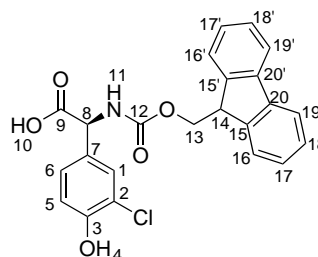
HR-ESI(+)-MS: m/z = calc. for $C_{23}H_{19}ClNO_5$ 424.09518 $[M+H]^+$, found 424.09470.

^{1}H-NMR (300 MHz, DMSO-d$_6$, R*T*) δ = 10.28 (s, 1 H, H-4), 8.14 (d, J = 7.9 Hz, 1 H, H-11), 7.88 (d, J = 7.5 Hz, 2 H, H-19, H-19'), 7.74 (d, J = 7.3 Hz, 2 H, H-16, H-16'), 7.39-7.44 (m, 3 H, H-1, H-18, H-18'), 7.28-7.35 (m, 2 H, H-17, H-17'), 7.18 (dd, J = 1.8 Hz, J = 8.4 Hz, 1 H, H-6), 6.93 (d, J = 8.3 Hz, 1 H, H-5), 5.05 (d, J = 7.9 Hz, 1 H, H-8), 4.19-4.29 (m, 3 H, H-13, H-14) ppm.

5.9.1.7. *N*-Alloc-L-4-Hpg (L-85)
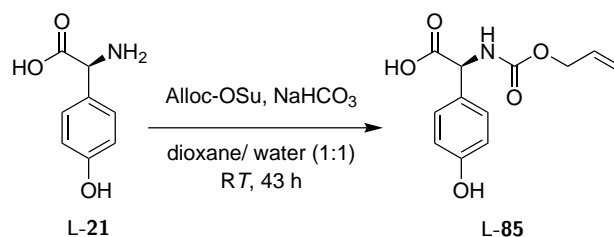
5.06 g L-4-Hpg (**L-21**) (30.26 mmol, 1.0 eq.) were dissolved in 200 mL dioxane/water 1:1, and 2.5 g $NaHCO_3$ (30.30 mmol, 1.0 eq.) as well as 4.68 mL *N*-Alloc hydroxysuccinimide ester (30.24 mmol, 1.0 eq.) were added to the solution. After 43 h of vigorous stirring at R*T* the pH was adjusted to pH 8-9 with aqueous $NaHCO_3$ (10 w/v %), the solution subsequently extracated with EtOAc (2x), acidified with aqueous $KHSO_4$ (1 M) to pH 1-2, and again extracted with EtOAc (3x). The combined organic layers were washed with brine (1x), dried over $MgSO_4$, and the solvent removed *in vacuo*. Product **L-85** was obtained as a colourless solid (7.95 g, 30.26 mmol) in quantitative yield and used without further purification.

Analytics

Molecular formula: $C_{12}H_{13}NO_5$

Molecular weight: 251.24 g/mol
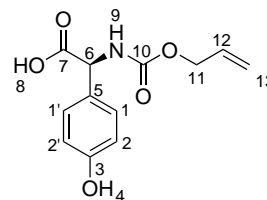
HR-ESI(+)-MS: m/z = calc. for $C_{12}H_{14}NO_5$ 252.08720 $[M+H]^+$, found 252.08670; calc. for $C_{24}H_{27}N_2O_{10}$ 503.16657 $[2M+H]^+$, found 503.16608.

^{1}H-NMR (300 MHz, DMSO-d$_6$, R*T*) δ = 9.45 (brs, 1 H, H-4), 7.87 (d, J = 7.9 Hz, 1 H, H-9), 7.18 (d, J = 8.6 Hz, 2 H, H-1, H-1'), 6.72 (d, J = 8.6 Hz, 2 H, H-2, H-2'), 5.83-5.96 (m, 1 H, H-12), 5.30 (d, J = 17.2 Hz, 1 H, H-13), 5.17 (d, J = 10.5 Hz, 1 H, H-13), 5.00 (d, J = 7.9 Hz, 1 H, H-6), 4.48 (d, J = 5.2 Hz, 2 H, H-11) ppm.

The spectroscopic data are in agreement with the literature.[120]

5.9.1.8. *N*-Cbz-L-4-Hpg (L-86)
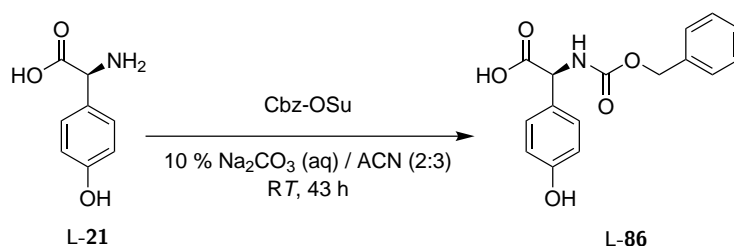
5.0 g L-4-Hpg (**L-21**) (29.93 mmol, 1.0 eq.) were dissolved in 150 mL NaHCO$_3$ (10 % in water)/ACN 1:1 and 7.46 g *N*-Cbz hydroxysuccinimide ester (29.93 mmol, 1.0 eq.), dissolved in 30 mL ACN, were added drop-wise while stirring. After 43 h of vigorous stirring at R*T* the resulting colourless precipitate was dissolved in water, and the solution subsequently washed with Et$_2$O (2x), acidified with HCl (10 % in water) to pH 2, and extracted with Et$_2$O (3x). The combined organic layers were dried over MgSO$_4$, and the solvent removed *in vacuo*. Product L-**86** was obtained as a light pink solid (8.60 g, 28.54 mmol) in 95.4 % yield.

Analytics

Molecular formula: C$_{16}$H$_{15}$NO$_5$

Molecular weight: 301.30 g/mol
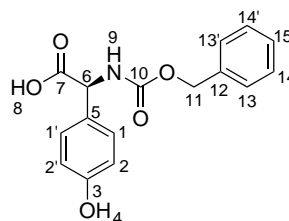
HR-ESI(+)-MS: *m/z* = calc. for C$_{16}$H$_{16}$NO$_5$ 302.10285 [M+H]$^+$, found 302.10240; calc. for C$_{32}$H$_{31}$N$_2$O$_{10}$ 603.19787 [2M+H]$^+$, found 603.19718.

^{1}H-NMR (300 MHz, DMSO-d$_6$, R*T*) δ = 9.46 (s, 1 H, H-4), 7.93 (d, *J* = 7.9 Hz, 1 H, H-9), 7.28-7.37 (m, 5 H, H-13, H-13', H-14, H-14', H-15), 7.18 (d, *J* = 8.6 Hz, 2 H, H-1, H-1'), 6.71 (d, *J* = 8.6 Hz, 2 H, H-2, H-2'), 5.04 (s, 2 H, H-11), 5.02 (d, *J* = 8.0 Hz, 1 H, H-6) ppm.

The spectroscopic data are in agreement with the literature.[203]

5.9.1.9. 2-Amino-2-(3,5-dimethoxyphenyl)acetonitrile (88)
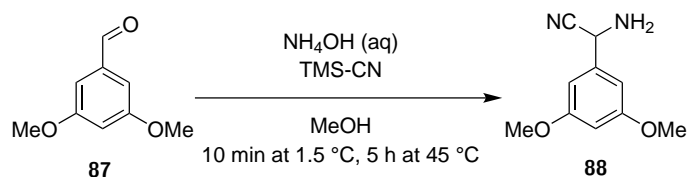
3.00 g 3,5-dimethoxybenzaldehyde (**87**) (18.07 mmol, 1.0 eq.) were dissolved in 40 mL methanol, and 50 mL ammonia solution (28 % in water) were added. Subsequently, 3.34 mL trimethylsilyl cyanide (26.70 mmol, 1.48 eq.) were added drop-wise while stirring and cooling to 1.5 °C. After 10 min, the solution was heated to 45 °C for 5 h. The solvents were then removed *in vacuo*, and the raw product purified by column chromatography on silica gel (dichloromethane/methanol 20:1, $R_f = 0.52$). Product **88** was obtained as an orange oil (1.97 g, 10.27 mmol) in 56.8 % yield.

Analytics

Molecular formula: $C_{10}H_{12}N_2O_2$
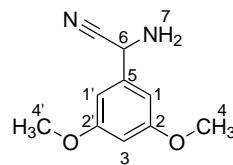
Molecular weight: 192.22 g/mol

^{1}H-NMR (300 MHz, DMSO-d$_6$, RT) δ = 8.91 (brs, 2 H, H-7), 6.71 (d, J = 2.2 Hz, 2 H, H-1, H-1'), 6.55 (t, J = 2.2 Hz, 1 H, H-3), 4.97 (s, 1 H, H-6), 3.75 (s, 6 H, H-4, H-4') ppm.

The spectroscopic data are in agreement with the literature.[189]

5. Experimental Procedures

5.9.1.10. 3,5-Dimethoxy-DL-phenylglycine (89)
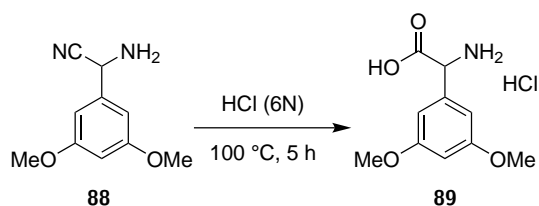
1.97 g **88** (10.27 mmol, 1.0 eq.) were dissolved in 50 mL hydrochloric acid (6 N in water) and refluxed for 5 h. After cooling to RT the mixture was poured into Et$_2$O, the resulting colourless precipitate filtrated, washed with Et$_2$O, and dried *in vacuo*. The raw product was purified by MPLC on C18 silica gel (A: water + 0.05 % TFA, B: ACN + 0.05 % TFA, 0.0-1.5 min 95 % A, 1.5-26.8 min 5 % A, 26.8-29.0 min 5 % A; column: Reveleris®C18 40 g; flow rate: 40 mL/min), and the hydrochloride salt of **89** obtained as a colourless solid (1.36 g, 5.50 mmol) in 53.6 % yield.

Analytics

Molecular formula: C$_{10}$H$_{13}$NO$_4$
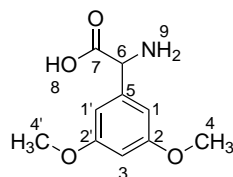
Molecular weight: 211.22 g/mol

^{1}H-NMR (300 MHz, DMSO-d$_6$, RT) δ = 8.79 (brs, 2 H, H-9), 6.68 (d, J = 2.1 Hz, 2 H, H-1, H-1'), 6.55 (t, J = 2.1 Hz, 1 H, H-3), 4.97 (s, 1 H, H-6), 3.75 (s, 6 H, H-4, H-4') ppm.

The spectroscopic data are in agreement with the literature.[189]

5.9.1.11. DL-3,5-Dpg (DL-28)
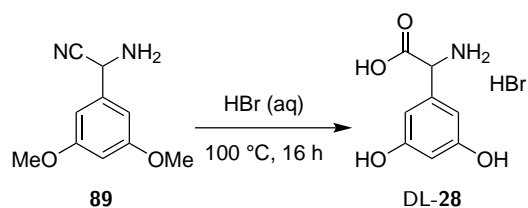
115 mg **89** (0.60 mmol, 1.0 eq.) were dissolved in 5 mL hydrobromic acid (48 % in water) and refluxed for 16 h. After cooling to RT the solvent was removed *in vacuo*, and the raw product purified by MPLC on C18 silica gel (A: water + 0.05 % TFA, B: ACN + 0.05 % TFA, 0.0-2.0 min 95 % A, 2.0-12.0 min 80 % A, 12.0-17.0 min 50 % A; column: Reveleris®C18 12 g; flow rate: 30 mL/min). The hydrobromide salt of DL-**28** was obtained as a colourless solid (134 mg, 0.51 mmol) in 84.8 % yield.

A small portion of the raw product was redissolved in aqueous HCl (0.01 M, pH 3), and further purified by cation-exchange chromatography on Dowex 50X8-100 (column subsequently eluted with aqueous HCl (0.01 M, pH 3), water (pH 7), aqueous pyridine (10 v/v % in water, pH 8)). Pyridine and water were removed *in vacuo*, and salt-free DL-**28** was obtained as a colourless solid (0.16 g, 0.89 mmol).

Analytics

Molecular formula: $C_8H_9NO_4$

Molecular weight: 183.16 g/mol
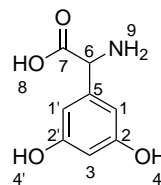
HR-ESI(+)-MS: *m/z* = calc. for $C_8H_{10}NO_4$ 184.06098 [M+H]$^+$, found 184.06049.

^{1}H-NMR (300 MHz, DMSO-d$_6$, RT) δ = 9.24 (brs, 2 H, H-4, H-4'), 7.90 (brs, 2 H, H-9), 6.26 (d, J = 2.1 Hz, H-1, H-1'), 6.12 (t, J = 2.1 Hz, 1 H, H-3), 3.98 (s, 1 H, H-6) ppm.

The spectroscopic data are in agreement with the literature.[204]

5. Experimental Procedures

### 5.9.1.12. *N*-Chloroacetyl-DL-3,5-Dpg (DL-90)
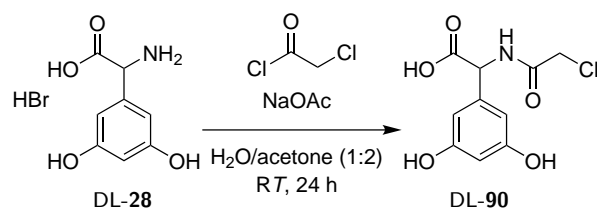
0.96 g of the hydrobromic salt of DL-**28** (3.63 mmol, 1.0 eq.) and 0.56 g NaOAc (7.2 mmol, 2.0 eq.) were dissolved in 30 mL water/acetone 1:2, and 0.35 mL chloroacetyl chloride (4.36 mmol, 1.20 eq.) were added drop-wise. The solution was stirred at RT for 24 h. Acetone was removed *in vacuo*, the aqueous layer extracted with EtOAc (5x), and the combined organic layers dried over $MgSO_4$. After removal of the solvent *in vacuo*, the raw product was purified by MPLC on C18 silica gel (A: water + 0.05 % TFA, B: ACN + 0.05 % TFA, 0.0-1.8 min 95 % A, 1.8-19.9 min 80 % A, 19.9-28.0 min 50 % A; column: Releris®C18 40 g; flow rate: 40 mL/min). Product DL-**90** was obtained as a light yellow solid (0.73 g, 2.82 mmol) in 77.7 % yield.

Analytics

Molecular formula: $C_{10}H_{10}ClNO_5$
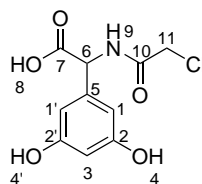
Molecular weight: 259.64 g/mol

HR-ESI(+)-MS: m/z = calc. for $C_{10}H_{11}ClNO_5$ 260.03258 [M+H]$^+$, found 260.03209; calc. for $C_{20}H_{21}Cl_2N_2O_{10}$ 519.05733 [2M+H]$^+$, found 519.05669.

^{1}H-NMR (300 MHz, DMSO-d$_6$, RT) δ = 12.87 (brs, 1 H, H-8), 9.35 (s, 2 H, H-4, H-4'), 8.80 (d, J = 7.2 Hz, 1 H, H-9), 6.23 (d, J = 2.1 Hz, 2 H, H-1, H-1'), 6.16 (t, J = 2.1 Hz, 1 H, H-3), 5.02 (d, J = 7.2 Hz, 1 H, H-6), 4.15 (s, 2 H, H-11) ppm.

The spectroscopic data are in agreement with the literature.[191]

5.9.1.13. *N*-Acetyl-DL-3,5-Dpg (DL-91)
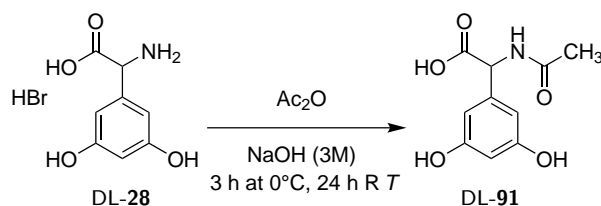
To a suspension of 0.10 g of the hydrobromic salt of DL-**28** (0.38 mmol, 1.0 eq.) in 4.0 mL aqueous NaOH (3 M) were added 32 µL acetic anhydride (0.34 mmol, 0.9 eq.) while stirring and cooling in an ice bath. The mixture was subsequently stirred at R*T* for 1 h, whereupon additional 32 µL acetic anhydride (0.34 mmol, 0.9 eq.) were added. This was repeated twice an hour apart, until DL-**28** dissolved completely. The reaction was then stirred for 16 h at R*T*, and subsequently acidified with aqueous hydrochloric acid (10 v/v %) to pH 3. Since no precipitate was formed, the solvent was removed *in vacuo*, and the crude product purified by MPLC on C18 silica gel (A: water + 0.05 % TFA, B: ACN + 0.05 % TFA, 0.0-1.9 min 95 % A, 1.9-11.3 min 80 % A, 11.3-16.0 min 50 % A; column: Reveleris®C18 12 g; flow rate: 30 mL/min). Product DL-**91** was obtained as a colourless solid (0.03 g, 0.13 mmol) in 34.2 % yield.

Analytics

Molecular formula: $C_{10}H_{11}NO_5$

Molecular weight: 225.20 g/mol
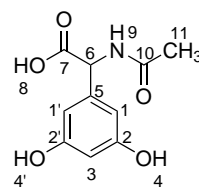
^{1}H-NMR (300 MHz, DMSO-d$_6$, R*T*) δ = 12.71 (br, 1 H, H-8), 9.33 (brs, 2 H, H-4, H-4'), 8.45 (d, J = 7.4 Hz, 1 H, H-9), 6.22 (d, J = 2.1 Hz, 2 H, H-1, H-1'), 6.15 (t, J = 2.1 Hz, 1 H, H-3), 5.06 (d, J = 7.4 Hz, 1 H, H-6), 1.97 (s, 3 H, H-11) ppm.

5.9.1.14. D-3,5-Dpg (D-28)
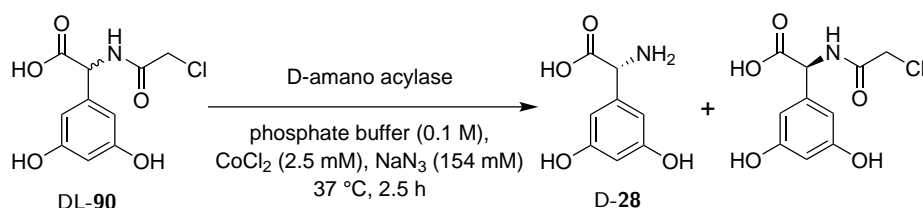
1.31 g DL-**90** (5.06 mmol) were dissolved in 32 mL phosphate buffer (0.1 M K_2HPO_4, 0.1 M KH_2PO_4, pH 7) and 9.40 mL aqueous $CoCl_2$ (2.5 mM) were added. The pH was adjusted to pH 7 with aqueous NaOH (8 M) and 0.21 mL aqueous NaN_3 (154 mM). 0.80 mL D-amano acylase (25 mg/L in phosphate buffer (0.1 M K_2HPO_4, 0.1 M KH_2PO_4, pH 7)) were added to the solution. The mixture was incubated for 2.5 h at 37 °C and 200 rpm. The enzymatic conversion was terminated by acidification to pH 4 with glacial acetic acid, and the mixture poured into 200 mL ice cold EtOH. After incubation for 16 h at 4 °C, the resulting precipitate of enzyme-related protein was filtered, washed with ice cold EtOH, and the solvent removed from the filtrate *in vacuo*. The salt of product D-**28** was isolated from the resulting colourless solid by MPLC on C18 silica gel (A: water + 0.05 % TFA, B: ACN + 0.05 % TFA, 0.0-3.0 min 100 % A, 3.0-6.0 min 95 % A, 6.0-14.0 min 80 % A, 14.0-19.0 min 50 % A; column: Reveleris®C18 12 g; flow rate: 30 mL/min). 88.03 % of the raw product were redissolved in aqueous HCl (0.01 M, pH 3) and further purified by cation-exchange chromatography on Dowex 50X8-100 (column subsequently eluted with aqueous HCl (0.01 M, pH 3), water (pH 7), aqueous pyridine (10 v/v % in water, pH 8)). Pyridine and water were removed *in vacuo*, and salt-free D-**28** was obtained as a colourless solid (0.32 g, 0.17 mmol) in 39.0 % yield.

Analytics

Molecular formula: $C_8H_9NO_4$
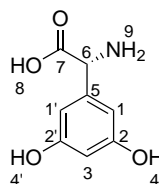
Molecular weight: 183.16 g/mol

HR-ESI(+)-MS: m/z = calc. for $C_8H_{10}NO_4$ 184.06098 [M+H]$^+$, found 184.06048.

^{1}H-NMR (300 MHz, DMSO-d$_6$, RT) δ = 9.33 (brs, 2 H, H-4, H-4'), 8.80 (d, J = 7.2 Hz, 2 H, H-9), 6.23 (d, J = 2.1 Hz, 2 H, H-1, H-1'), 6.16 (t, J = 2.1 Hz, 1 H, H-3), 5.07 (d,

$J = 7.2$ Hz, 1 H, H-6) ppm.

The spectroscopic data are in agreement with the literature.[204]

5.9.1.15. *N*-Fmoc-D-3,5-Dpg (D-84)
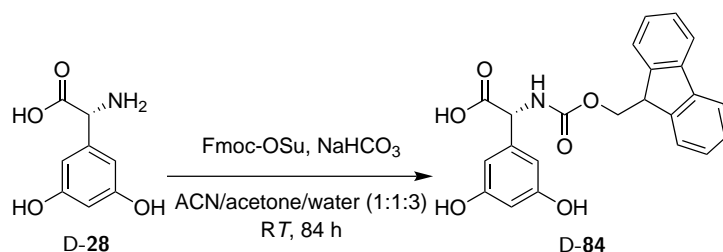
0.10 g D-**28** (0.56 mmol, 1.0 eq.) were dissolved in 6 mL water/acetone 1:1. 0.10 g NaHCO$_3$ (1.19 mmol, 2.13 eq.) were added to the solution, and the pH adjusted to pH 8 with 4 mL of aqueous NaHCO$_3$ (10 w/v % in water). 0.23 g *N*-Fmoc hydroxysuccinimide ester (0.68 mmol, 1.22 eq.), dissolved in 3 mL acetone, were slowly added drop-wise while stirring. The resulting colourless precipitate was dissolved by additon of 9 mL water and 5 mL ACN. After 84 h of vigorous stirring at R*T* the organic layer was removed *in vacuo* and the aqueous layer washed with Et$_2$O (2x). The aqueous layer was subsequently acidified to pH 3 with HCl (10 w/v % in water) and extracted with EtOAc (4x). The combined EtOAc layers were washed with brine (2x), dried over MgSO$_4$, and the solvent removed *in vacuo*. The product D-**84** was obtained as a colourless solid (0.20 g, 0.50 mmol) in 89.5 % yield.

Analytics

Molecular formula: C$_{23}$H$_{19}$NO$_6$

Molecular weight: 405.41 g/mol
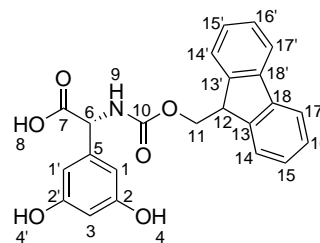
HR-ESI(+)-MS: m/z = calc. for C$_{23}$H$_{20}$NO$_6$ 406.12906 [M+H]$^+$, found 406.12854; calc. for C$_{46}$H$_{39}$N$_2$O$_{12}$ 811.250303 [2M+H]$^+$, found 811.25010.

^{1}H-NMR (300 MHz, DMSO-d$_6$, R*T*) δ = 12.73 (brs, 1 H, H-8), 9.29 (s, 2 H, H-4, H-4'), 8.09 (d, $J = 7.7$ Hz, 1 H, H-9), 7.88 (d, $J = 7.5$ Hz, 2 H, H-17, H-17'), 7.78 (d, $J = 7.5$ Hz,

2 H, H-14, H-14'), 7.39-7.44 (m, 2 H, H-16, H-16'), 7.28-7.35 (m, 2 H, H-15, H-15'), 7.27 (d, J = 2.1 Hz, 2 H, H-1, H-1'), 6.16 (t, J = 2.1 Hz, 1 H, H-3), 4.92 (d, J = 7.9 Hz, 1 H, H-6), 4.18-4.24 (m, 3 H, H-11, H-12) ppm.

The spectroscopic data are in agreement with the literature.[122]

5.9.1.16. *N*-Fmoc-DL-3,5-Dpg (DL-84)
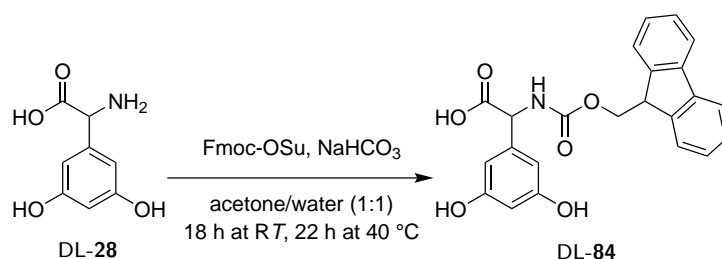
50 mg DL-**28** (0.27 mmol, 1.0 eq.) and 48 mg $NaHCO_3$ (0.57 mmol, 2.01 eq.) were dissolved in 4 mL water. 111 mg *N*-Fmoc hydroxysuccinimide ester (0.33 mmol, 1.20 eq.), dissolved in 4 mL acetone, were slowly added drop-wise while stirring. After 18 h of vigorous stirring at R*T* and additional 22 h stirring at 40 °C, the organic layer was removed *in vacuo* and the aqueous layer washed with Et_2O (2x). The aqueous layer was subsequently acidified to pH 3 with HCl (1 N in water) and extracted with EtOAc (3x). The combined EtOAc layers were washed with brine (2x), dried over $MgSO_4$, and the solvent removed *in vacuo*. The raw product was purified by MPLC on C18 silica gel (A: water + 0.05 % TFA, B: ACN + 0.05 % TFA, 0.0-1.1 min 95 % A, 1.1-14.2 min 5 % A, 14.2-16.0 min 5 % A; column: Reveleris®C18 12 g; flow rate: 30 mL/min), and DL-**84** obtained as a colourless solid (89 mg, 0.22 mmol) in 80.0 % yield.

Analytics

Molecular formula: $C_{23}H_{19}NO_6$

Molecular weight: 405.41 g/mol
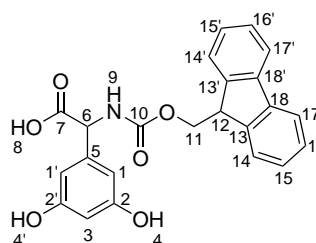
HR-ESI(+)-MS: m/z = calc. for $C_{23}H_{20}NO_6$ 406.12906 [M+H]$^+$, found 406.12858; calc. for $C_{46}H_{39}N_2O_{12}$ 811.250303 [2M+H]$^+$, found 811.25003.

^{1}H-NMR (300 MHz, DMSO-d$_6$, RT) δ = 12.79 (brs, 1 H, H-8), 9.33 (s, 2 H, H-4, H-4'), 8.13 (d, J = 7.8 Hz, 1 H, H-9), 7.89 (d, J = 7.5 Hz, 2 H, H-17, H-17'), 7.77 (d, J = 7.5 Hz, 2 H, H-14, H-14'), 7.39-7.44 (m, 2 H, H-16, H-16'), 7.28-7.35 (m, 2 H, H-15, H-15'), 7.27 (d, J = 2.1 Hz, 2 H, H-1, H-1'), 6.16 (t, J = 2.1 Hz, 1 H, H-3), 4.92 (d, J = 7.8 Hz, 1 H, H-6), 4.19-4.25 (m, 3 H, H-11, H-12) ppm.

The spectroscopic data are in agreement with the literature.[122]

5.9.2. Solid Phase Peptide Synthesis (SPPS)

5.9.2.1. General Procedures for Solid Phase Peptide Synthesis

2-Chlorotrityl chloride (2-CTC) resin (1.60 mmol g^{-1}, 100-200 mesh) from *Carbolution* was used for SPPS. For amounts of less than 0.6 g resin reactions were run in syringes (reactors for peptide synthesis from *Roth*®). For larger amounts, glass reactors with a glass frit and vaccuum stopper were used. Each washing and swelling step was conducted with 5 mL g^{-1} to 10 mL g^{-1} resin of the respective solvent, unless stated otherwise. Special attention was paid to ensure that the resin was sufficiently swollen with solvent before a reaction was run. All steps were conducted at R*T*.

Resin Activation

2-CTC resin was washed by filling the SPPS reactor with dry DMF (3x), shaking for 10 sec at R*T* under argon atmosphere, and filtrating. The procedure was repeated with dry DCM (3x). The resin was then swollen by shaking with dry DCM under argon atmosphere for 30 min at R*T*. After filtration, the resin was mixed with not-distilled thionyl chloride (1.5 eq) in dry DCM (5 mL g^{-1} to 10 mL g^{-1} resin) under argon atmosphere for 1 h at R*T*. After filtration, the resin was washed subsequently with dry DMF (3x) and dry DCM (3x) under argon atmosphere.

Loading of the First Amino Acid

The first amino acid was loaded onto 2-CTC resin by adding a solution of the amino acid (2.3 eq.) and NMM (3.2 eq.) in DCM/DMF (1:1) (7.5 mL g^{-1} resin) to the activated resin, and shaking under argon atmosphere for 24 h at R*T*. After filtration, the resin was washed (see below).

Resin Washing

The resin was washed by filling the SPPS reactor with DMF (3x), methanol (1x), DCM (1x), DMF (1x), and DCM (1x), shaking for 10 sec at R*T* and filtrating.

Fmoc Test

The substitution of the resins reaction sites with the first amino acid building block was determined using the Fmoc test.[185] This method is based on the formation of a dibenzofulvene-piperidine adduct during a Fmoc deprotection reaction, which shows an absorption maximum at 301 nm. The concentration of dibenzofulvene-piperidine adduct,

and thereby the concentration of cleaved Fmoc groups as well as resin bound amino acid building blocks, can be calculated based on UV absorption at 301 nm. For this purpose, loaded resin was dried under reduced pressure until weight constancy. 5 mg to 10 mg resin were then mixed with 1 mL piperidine (20 % in DMF), and shaken for 20 min at R*T*. The suspension was filtrated using a syringe filter holder (cellulose acetate, 0.2 µm, *VWR*), and 100 µL supernatant were mixed with 10 mL DMF. Subsequently, the UV absorption of the sample was measured at 301 nm and the subsitituion calculated according to:

$$Substitution/1 \ g \ resin = (101 * Absorbance_{301nm})/(7.8 * weight \ in \ mg)$$

The Fmoc test was perfomed in triplicate and DMF used as a reference.

Resin Swelling

Dry resin was swollen by shaking with DCM for 30 min at R*T* and subsequently filtrated.

Capping of Unreacted Reaction Sites

Two methods were used for capping of unreacted reaction sites:
The SPPS reactor was filled with DCM/methanol/DIPEA (80:15:5) ($5 \, \mathrm{mL \, g^{-1}}$ to $10 \, \mathrm{mL \, g^{-1}}$ resin) and shaken for 15 min at R*T*. After filtration, the resin was washed (see above).
In another method, a capping solution was prepared out of acetic acid anhydride (0.5 M), DIPEA (0.125 M), HOBt (0.015 M) and DMF. $5.5 \, \mathrm{mL \, g^{-1}}$ resin capping solution were the filled into the SPPS reactor, and shaken for 3 min at at R*T*. After filtration, the SPPS reactor was filled again with $5.5 \, \mathrm{mL \, g^{-1}}$ resin capping solution, and shaken for 7 min at R*T*. After filtration, the resin was washed (see above).

Fmoc Deprotection

The *N*-terminal Fmoc protecting group was cleaved off of the growing peptide chain by shaking the resin with DBU (1 % in DMF) ($5 \, \mathrm{mL \, g^{-1}}$ to $12 \, \mathrm{mL \, g^{-1}}$ resin) for 3 min at R*T*. After filtration, the procedure was repeated (2x 3 min) and the resin washed (see above) after the last step. For reactions in gram scale, the reaction time of the final step had to be extended to 10 min for complete deprotection.

Chain Elongation

An amino acid was coupled to the unprotected peptide chain by mixing the Fmoc protected amino acid (2.2 eq.), COMU (2.2 eq.), and triethylamine (2.2 eq.) in DMF (0.1 M) for 2 min at R*T*. The reaction mixture was added to the resin and shaken for 1 h at R*T*. After

filtration, the procedure was repeated once and the resin subsequently washed (see above).

Analytical Peptide Cleavage

Coupling and deprotection reactions were monitored by collecting a small amount of resin and shaking it with $1\,\text{mL}$ TFA (1 % in DCM) for $20\,\text{min}$ at RT. The suspension was filtrated using a syringe filter holder (cellulose acetate, $0.2\,\text{µm}$, *VWR*), and $10\,\text{µL}$ supernatant were mixed with $90\,\text{µL}$ methanol. The sample was then submitted to LC-MS analysis (Chapter 5.8.2).

Preparative Peptide Cleavage

The completed peptide chain was cleaved off the resin by filling the SPPS reactor with TFA (1 % in DCM) ($10\,\text{mL}\,\text{mmol}^{-1}$ to $25\,\text{mL}\,\text{mmol}^{-1}$ resin) and shaking for $20\,\text{min}$ at RT. The resin was filtrated and the supernatant collected. The procedure was repeated four times and the resin subsequently washed with DCM (5x $10\,\text{mL}\,\text{mmol}^{-1}$ to $25\,\text{mL}\,\text{mmol}^{-1}$ resin). The supernatants and washing fractions were combined, and the solvent removed *in vacuo* at $30\,°\text{C}$. The light yellow precipitate was resuspended in methanol, filtrated using a syringe filter holder (cellulose acetate, $0.2\,\text{µm}$, *VWR*), and purified by semi-preparative HPLC (Chapter 5.8.1).

5.9.2.2. Tetrapeptide HO-L-Hpg-L-Tyr-D-3-chloro-Hpg-L-Hpg-Fmoc (92)

92
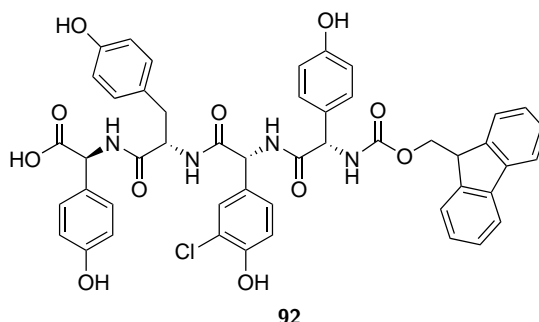
Tetrapeptide **92** was synthesized according to the general procedures for SPPS as described in Chapter 5.9.2.1. The Fmoc test revealed substitution of 79.0 % of reaction sites with the first building block Fmoc-L-Hpg (L-**82**). The crude product was purified by semi-preparative HPLC (A: water + 0.05 % TFA, B: ACN + 0.05 % TFA, 0.0-2 min 70 % A, 2.0-5.0 min 40 % A, 5.0-18.0 min 37 % A, 18.0-18.1 min 70 % A, 18.10-20.0 70 % A; column: Eurospher II 100-5 C18 250x20 mm; flow rate: 12 mL/min) and **92** obtained as a colourless solid (340.8 mg, 0.385 mmol) in 19.0 % yield.

Analytics

Molecular formula: $C_{48}H_{41}ClN_4O_{11}$

Molecular weight: 885.32 g/mol

HR-ESI-MS(+): m/z = calc. for $C_{48}H_{42}ClN_4O_{11}$ 885.25386 $[M+H]^+$, found 885.25275.

^{1}H-NMR (500 MHz, DMSO-d_6, RT) δ = 12.68 (br, 1 H, COOH), 9.98 (s, 1 H, Ar-OH), 9.52 (s, 1 H, Ar-OH$_{Cl-Hpg}$), 9.35 (s, 1 H, Ar-OH), 9.09 (s, 1 H, Ar-OH), 8.73 (d, 1 H, NH), 8.58-8.62 (dd, 2 H, NH, NH), 7.92 (d, 1 H, NH), 7.87 (d, 2 H, Ar-CH$_{Fmoc}$), 7.75 (dd, 2 H, Ar-CH$_{Fmoc}$), 7.39-7.42 (m, 2 H, Ar-CH$_{Fmoc}$), 7.27-7.32 (m, 2 H, Ar-CH$_{Fmoc}$), 7.21-7.25 (dd, 4 H, Ar-CH), 6.97 (s, 1 H, Ar-CH$_{Cl-Hpg}$), 6.92 (d, 2 H, Ar-CH), 6.76 (d, 2 H, Ar-CH), 6.65-6.67 (m, 4 H, Ar-CH), 6.52 (d, 2 H, Ar-CH), 5.44 (d, 1 H, CH$_\alpha$), 5.39 (d, 1 H, CH$_\alpha$), 5.19 (d, 1 H, CH$_\alpha$), 4.48-4.52 (m, 1 H, CH$_\alpha$), 4.24-4.28 (m, 1 H, CH$_{Fmoc}$), 4.16-4.21 (m, 2 H, CH$_{2,Fmoc}$), 2.63-2.89 (m, 2 H, CH$_{2,Tyr}$) ppm.
The ^{1}H-NMR spectrum showed the presence of a single conformer.

5.9.2.3. Tetrapeptide HO-L-Hpg-L-Tyr-D-3-chloro-Hpg-L-Hpg-Alloc (120)

120
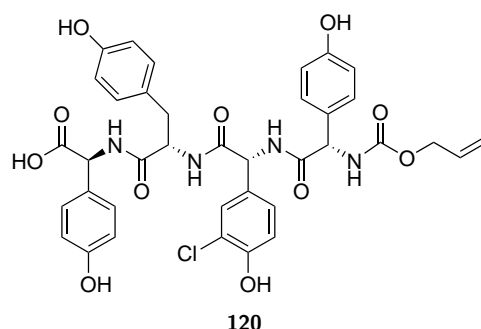
Tetrapeptide **120** was synthesized according to the general procedures for SPPS as described in Chapter 5.9.2.1. Weight measurement of the resin after drying under reduced pressure until weight constancy revealed substitution of 92.4 % of reaction sites with the first building block Fmoc-L-Hpg (**L-82**). The crude product was purified by semi-preparative HPLC (A: water + 0.05 % TFA, B: ACN + 0.05 % TFA, 0.0-2 min 95 % A, 2.0-25.0 min 5 % A, 25.0-26.0 min 5 % A, 26.0-26.1 min 95 % A, 26.1-28.0 95 % A; column: Eurospher II 100-5 C18 250x20 mm; flow rate: 12 mL/min), the solvent removed *in vacuo*, and **120** obtained as a colourless solid (71.7 mg, 0.096 mmol) in 26.0 % yield.

Analytics

Molecular formula: $C_{37}H_{35}ClN_4O_{11}$

Molecular weight: 747.15 g/mol

HR-ESI-MS(+): m/z = calc. for $C_{37}H_{36}ClN_4O_{11}$ 747.20691 $[M+H]^+$, found 747.20612; calc. for $C_{37}H_{35}ClN_4O_{11}Na$ 769.18885 $[M+Na]^+$, found 769.18791.

^{1}H-NMR (500 MHz, DMSO-d$_6$, RT) δ = 9.70 (br, 1 H, COOH), 8.59 (d, 1 H, NH), 8.02 (d, 1 H, NH), 7.76 (d, 1 H, NH), 7.61-7.72 (dd, 1 H, NH), 7.19 (d, 2 H, Ar-CH), 7.11 (d, 2 H, Ar-CH), 7.00 (s, 1 H, Ar-CH$_{Cl-Hpg}$), 6.85-6.98 (dd, 2 H, Ar-CH), 6.76 (d, 2 H, Ar-CH), 6.62-6.68 (m, 4 H, Ar-CH), 6.51 (d, 2 H, Ar-CH), 5.85-5.91 (m, 1 H, CH$_{Alloc}$), 5.33-5.36 (m, 2 H, CH$_\alpha$, CH$_\alpha$), 5.24-5.32 (m, 2 H, CH$_{2,Alloc}$), 5.14 (d, 1 H, CH$_\alpha$), 4.75 (d, 1 H, CH$_\alpha$), 4.45 (d, 2 H, CH$_{2,Alloc}$), 2.63-2.73 (m, 2 H, CH$_{2,Tyr}$) ppm.
The ^{1}H-NMR spectrum showed the presence of different conformers.

5.9.2.4. Tetrapeptide HO-L-Hpg-L-Tyr-D-3-chloro-Hpg-L-Hpg-Cbz (121)

121
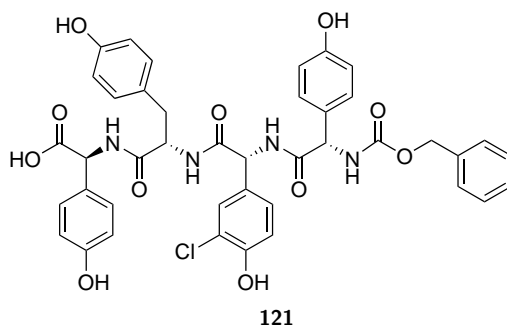
Tetrapeptide **121** was synthesized according to the general procedures for SPPS as described in Chapter 5.9.2.1. Weight measurement of the resin after drying under reduced pressure until weight constancy revealed substitution of 92.4 % of reaction sites with the first building block Fmoc-L-Hpg (L-**82**). The crude product was purified by semi-preparative HPLC (A: water + 0.05 % TFA, B: ACN + 0.05 % TFA, 0.0-2 min 95 % A, 2.0-25.0 min 5 % A, 25.0-26.0 min 5 % A, 26.0-26.1 min 95 % A, 26.1-28.0 95 % A; column: Eurospher II 100-5 C18 250x20 mm; flow rate: 12 mL/min) and **121** obtained as a colourless solid (26.2 mg, 0.033 mmol) in 2.6 % yield.

Analytics

Molecular formula: $C_{41}H_{37}ClN_4O_{11}$

Molecular weight: 797.21 g/mol

HR-ESI-MS(+): m/z = calc. for $C_{41}H_{38}ClN_4O_{11}$ 797.22256 [M+H]$^+$, found 797.22200; calc. for $C_{41}H_{37}ClN_4O_{11}Na$ 819.20451; [M+Na]$^+$, found 819.20394.

^{1}H-NMR (500 MHz, DMSO-d$_6$, RT) δ = 12.70 (br, 1 H, COOH), 9.98 (s, 1 H, Ar-OH), 9.52 (s, 1 H, Ar-OH$_{Cl-Hpg}$), 9.34 (s, 1 H, Ar-OH), 9.09 (s, 1 H, Ar-OH), 8.72 (d, 1 H, NH), 8.61 (d, 1 H, NH), 8.53 (d, 1 H, NH), 7.74 (d, 1 H, NH), 7.30-7.35 (m, 5 H, Ar-CH$_{Cbz}$), 7.21 (d, 4 H, Ar-CH), 6.49-6.91 (m, 3 H, Ar-CH), 6.77 (d, 2 H, Ar-CH), 6.61-6.65 (m, 4 H, Ar-CH), 6.52 (d, 2 H, Ar-CH), 5.41 (d, 1 H, CH$_\alpha$), 5.38 (d, 1 H, CH$_\alpha$), 5.19 (d, 1 H, CH$_\alpha$), 5.02 (s, 2 H, CH$_{2,Cbz}$), 4.47-4.51 (m, 1 H, CH$_\alpha$), 2.60-2.89 (m, 2 H, CH$_{2,Tyr}$) ppm. The ^{1}H-NMR spectrum showed the presence of a single conformer.

5.9.2.5. Tripeptide HO-D-Dpg-D-Trp-L-Tyr-Fmoc (105)
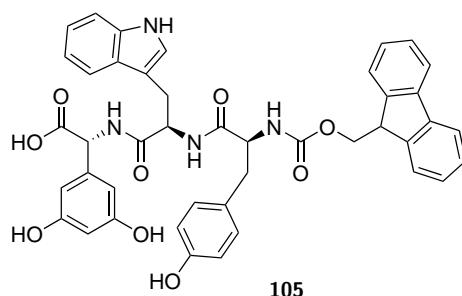
Tripeptide **105** was synthesized according to the general procedures for SPPS as described in Chapter 5.9.2.1. For resin loading only 0.88 eq. of Fmoc-D-Dpg (D-**84**) (0.97 mmol) and 1.24 eq. NMM (150 µL, 1.36 mmol) in 2 mL dry DMF/DCM (1:1) were used. The Fmoc test was conducted, but failed to produce a conclusive result. The crude product was purified by semi-preparative HPLC (A: water + 0.05 % TFA, B: ACN + 0.05 % TFA, 0.0-2.0 min 70 % A, 2.0-5.0 min 46 % A, 5.0-15.0 min 44 % A, 15.0-18.0 min 30 % A, 18.0-18.5 min 70 % A, 18.5-20.0 min 70 % A; column: Eurospher II 100-5 C18 250x8 mm; flow rate: 5 mL/min), and **105** obtained as a light brown solid (44.7 mg, 0.059 mmol) (6.1 % yield based on the used quantity of D-**84**).

Analytics

Molecular formula: $C_{43}H_{38}N_4O_9$
Molecular weight: 754.80 g/mol

HR-ESI-MS(+): m/z = calc. for $C_{43}H_{39}N_4O_9$ 755.27170 [M+H]$^+$, found 755.27011; calc. for $C_{43}H_{33}N_4O_9Na$ 777.25364 [M+Na]$^+$, found 777.25254.

^{1}H-NMR (500 MHz, DMSO-d$_6$, RT) δ = 12.76 (br, 1H, COOH), 10.78 (s, 1 H, Ar-NH$_{Trp}$), 9.34 (s, 2 H, Ar-OH$_{Dpg}$), 9.08 (s, 1 H, Ar-OH$_{Tyr}$), 8.81 (d, 1 H, NH$_{Dpg}$), 8.20 (d, 1 H, NH$_{Trp}$), 7.86 (d, 2 H, Ar-CH$_{Fmoc}$), 7.72 (d, 1 H, NH$_{Tyr}$), 7.58-7.62 (m, 2 H, Ar-CH$_{Fmoc}$), 7.37-7.40 (m, 3 H, Ar-CH$_{Fmoc}$, Ar-CH$_{Trp}$), 7.24-7.30 (m, 3 H, Ar-CH$_{Fmoc}$, Ar-CH$_{Trp}$), 7.16 (d, 1 H, Ar-CH$_{Trp}$), 7.01-7.05 (m, 1H, Ar-CH$_{Trp}$), 6.49-6.98 (m, 1H, Ar-CH$_{Trp}$), 6.87 (d, 2 H, Ar-CH$_{Tyr}$), 6.51 (d, 2 H, Ar-CH$_{Tyr}$), 6.30 (m, 2 H, Ar-CH$_{Dpg}$), 6.17 (m, 1 H, Ar-CH$_{Dpg}$), 5.10 (d, 1 H, CH$_{\alpha,Dpg}$), 4.75-4.79 (m, 1 H, CH$_{\alpha,Trp}$), 4.05-4.19 (m, 4 H, CH$_{\alpha,Tyr}$, CH$_{2,Fmoc}$, CH$_{Fmoc}$), 2.91-3.18 (m, 2 H, CH$_{2,Trp}$), 2.36-2.63 (m, 2 H,

$CH_{2,Tyr}$) ppm.

The ^{1}H-NMR spectrum showed the presence of a single conformer.

5.9.2.6. Tripeptide HO-L-Hpg-L-Tyr-D-3-chloro-Hpg-NH$_2$ (97)
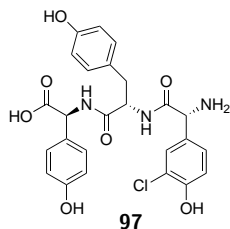
Tripeptide **97** was synthesized according to the general procedures for SPPS as described in Chapter 5.9.2.1. A sample of **97** was cleaved off by collecting a small amount of resin and shaking it with 1 mL TFA (1 % in DCM) for 20 min at RT. The suspension was filtrated using a syringe filter holder (cellulose acetate, 0.2 µm, *VWR*), and 10 µL supernatant were mixed with 90 µL methanol. The sample was then submitted to LC-MS analysis.

Analytics

Molecular formula: $C_{25}H_{24}ClN_3O_7$

Molecular weight: 513.93 g/mol

ESI-MS(+): m/z = calc. for $C_{26}H_{24}ClN_3O_7$ 514.94 [M+H]$^+$, found 515.13.
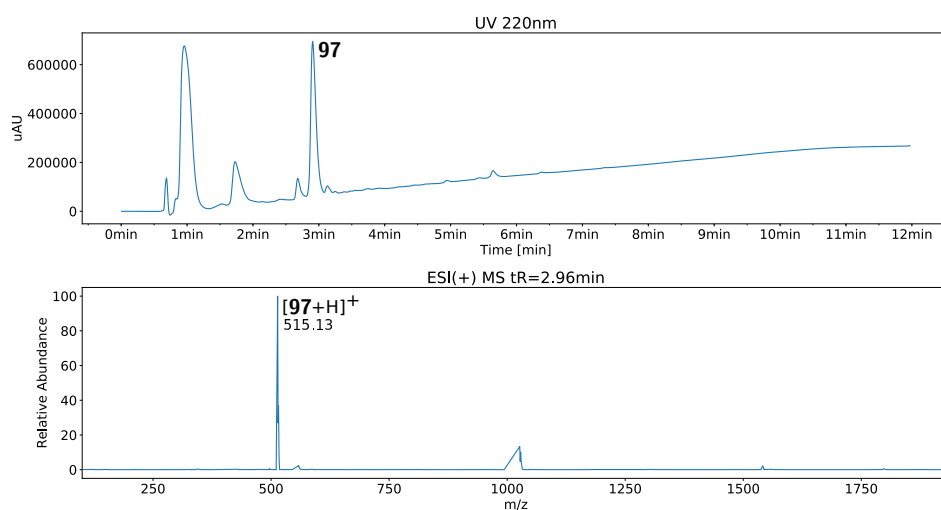
5.9.2.7. **Tripeptide HO-D-Hpg-L-Tyr-D-3-chloro-Hpg-NH$_2$ (107)**
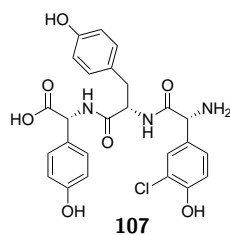
Tripeptide **107** was synthesized according to the general procedures for SPPS as described in Chapter 5.9.2.1. A sample of **107** was cleaved off by collecting a small amount of resin and shaking it with 1 mL TFA (1 % in DCM) for 20 min at RT. The suspension was filtrated using a syringe filter holder (cellulose acetate, 0.2 µm, *VWR*), and 10 µL supernatant were mixed with 90 µL methanol. The sample was then submitted to LC-MS analysis.

Analytics

Molecular formula: C$_{25}$H$_{24}$ClN$_3$O$_7$

Molecular weight: 513.93 g/mol

ESI-MS(+): m/z = calc. for C$_{26}$H$_{24}$ClN$_3$O$_7$ 514.94 [M+H]$^+$, found 514.29.
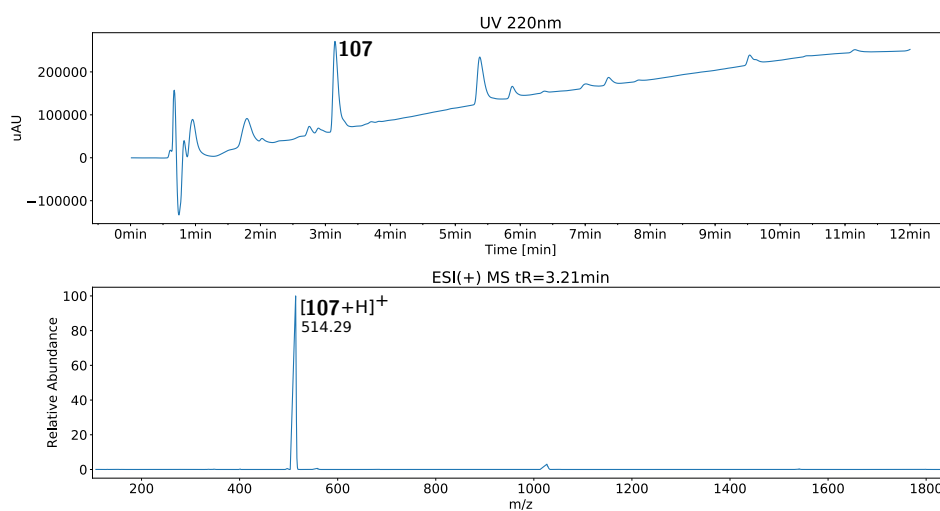
5.9.2.8. Tripeptide HO-D-Hpg-L-Tyr-L-3-chloro-Hpg-NH₂ (108)

108
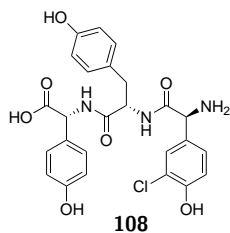
Tripeptide **108** was synthesized according to the general procedures for SPPS as described in Chapter 5.9.2.1. A sample of **108** was cleaved off by collecting a small amount of resin and shaking it with 1 mL TFA (1 % in DCM) for 20 min at R*T*. The suspension was filtrated using a syringe filter holder (cellulose acetate, 0.2 µm, *VWR*), and 10 µL supernatant were mixed with 90 µL methanol. The sample was then submitted to LC-MS analysis.

Analytics

Molecular formula: $C_{25}H_{24}ClN_3O_7$

Molecular weight: 513.93 g/mol

ESI-MS(+): m/z = calc. for $C_{26}H_{24}ClN_3O_7$ 514.94 [M+H]$^+$, found 515.93.
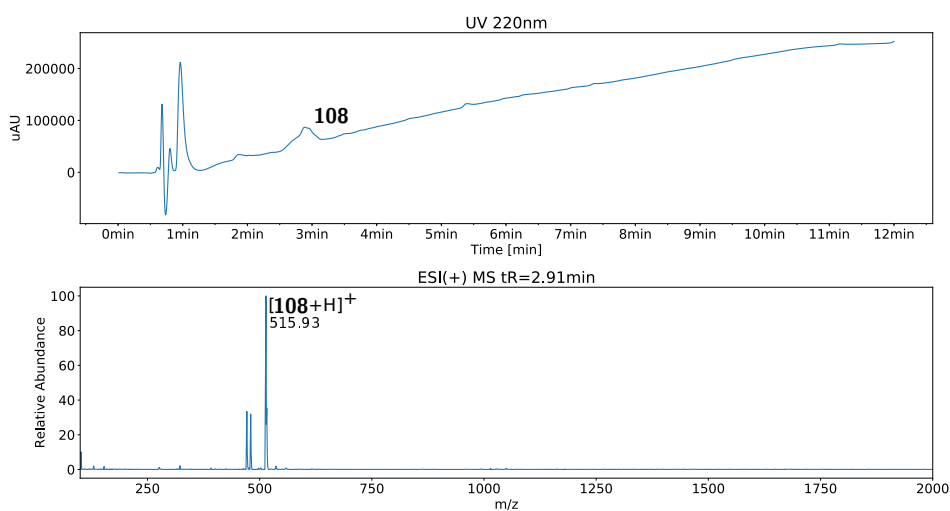
5.9.2.9. Tripeptide HO-L-Hpg-L-Tyr-L-3-chloro-Hpg-NH$_2$ (109)
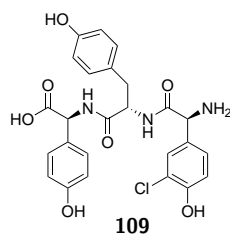
Tripeptide **109** was synthesized according to the general procedures for SPPS as described in Chapter 5.9.2.1. A sample of **109** was cleaved off by collecting a small amount of resin and shaking it with 1 mL TFA (1 % in DCM) for 20 min at R*T*. The suspension was filtrated using a syringe filter holder (cellulose acetate, 0.2 µm, *VWR*), and 10 µL supernatant were mixed with 90 µL methanol. The sample was then submitted to LC-MS analysis.

Analytics

Molecular formula: C$_{25}$H$_{24}$ClN$_3$O$_7$

Molecular weight: 513.93 g/mol

ESI-MS(+): m/z = calc. for C$_{26}$H$_{24}$ClN$_3$O$_7$ 514.94 [M+H]$^+$, found 515.75.
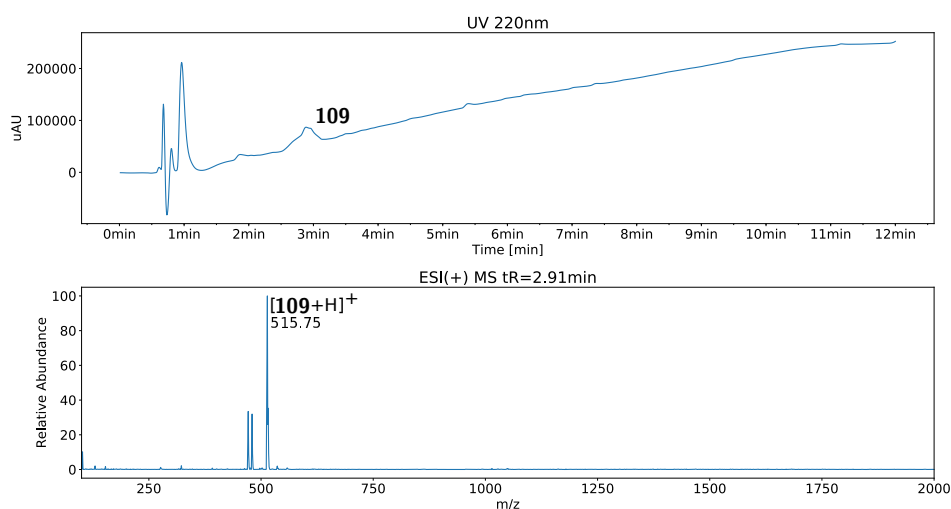
5.9.3. Liquid Phase Peptide Synthesis (LPPS)

5.9.3.1. EtO-D-Tryptophan (D-111)
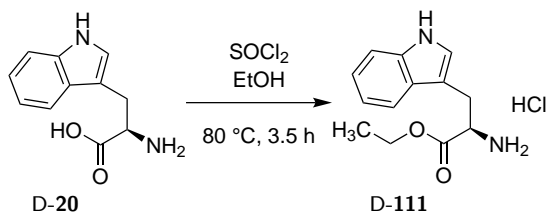
2.13 mL thionyl chloride (29.33 mmol, 2.0 eq.) were added drop-wise to a colloidal suspension of 3.0 g D-tryptophan (**D-20**) (14.73 mmol, 1.0 eq.) in 30 mL EtOH under argon atmosphere while stirring and cooling. The starting material dissolved when thionyl chloride was added and the solution was refluxed for 3.5 h. After cooling to R*T*, the resulting colourless precipitate was filtrated, washed with Et_2O, and dried *in vacuo*. The hydrochloric salt of **D-111** was obtained as a colourless solid (2.78 g, 10.35 mmol) in 70.3 % yield.

Analytics

Molecular formula: $C_{13}H_{16}N_2O_2$

Molecular weight: 232.28 g/mol
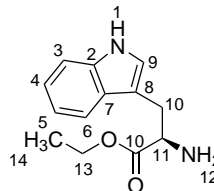
^{1}H-NMR (300 MHz, DMSO-d$_6$, R*T*) δ = 11.07 (s, 1 H, H-1), 8.48 (br, 2 H, H-12), 7.51 (d, J = 7.8 Hz, 1 H, H-6), 7.37 (d, J = 7.8 Hz, 1 H, H-3), 7.23 (d, 1 H, H-9), 7.07-7.12 (m, 1 H, H-4), 6.98-7.04 (m, 1 H, H-5), 4.20 (t, J = 9.0, 1 H, H-11), 4.05-4.12 (m, 2 H, H-13), 3.22-3.34 (m, 2 H, H-10), 1.09 (t, J = 6.0 Hz, 3 H, H-14) ppm.

The spectroscopic data are in agreement with the literature.[205]

5.9.3.2. **EtO-D-Dpg (D-110)**
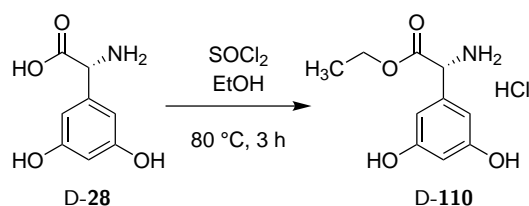
0.08 mL thionyl chloride (1.10 mmol, 2.0 eq.) were added drop-wise to a colloidal suspension of 0.10 g D-**28** (0.55 mmol, 1.0 eq.) in 3 mL EtOH under argon atmosphere while stirring and cooling. The starting material dissolved when thionyl chloride was added and the solution was refluxed for 3 h. After cooling to RT, the solution was diluted with 10 mL water, washed with EtOAc (5x), and water removed *in vacuo*. The crude product (D-**110**) was obtained as a colourless solid (4.18 g), and used without purification.

Analytics

Molecular formula: $C_{10}H_{13}NO_4$
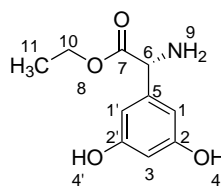
Molecular weight: 211.23 g/mol

HR-ESI(+)-MS: m/z = calc. for $C_{10}H_{14}NO_4$ 212.09228 [M+H]$^+$, found 212.09178.

^{1}H-NMR (500 MHz, DMSO-d$_6$, RT) δ = 9.20 (s, 2 H, H-4, H-4'), 6.20 (d, J = 2.1 Hz, 2 H, H-1, H-1'), 6.09 (t, J = 2.1 Hz, 1 H, H-3), 4.29 (s, 1 H, H-6), 4.05-4.12 (m, 2 H, H-10), 1.09 (t, J = 6.0 Hz, 3 H, H-11) ppm.

5.9.3.3. EtO-D-Trp-L-Tyr-Fmoc (112)
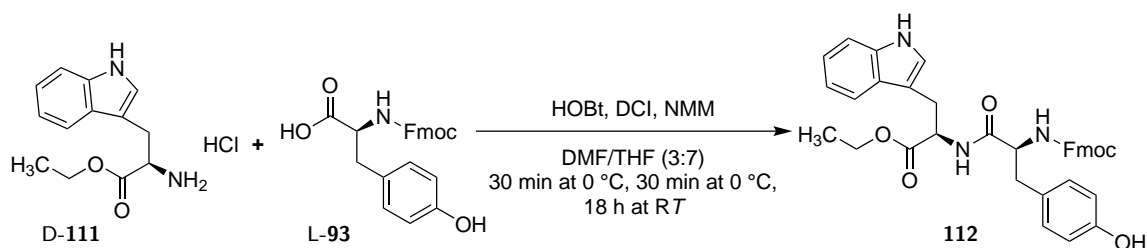
0.60 g Fmoc-L-Tyr (L-**93**) (1.49 mmol, 1.0 eq.) and 0.23 g HOBt monohydrate (1.50 mmol, 1.0 eq.) were dissolved in 4.0 mL THF. 0.16 mL NMM (1.48 mmol, 1.0 eq.) were added while stirring and cooling at 0 °C, and 0.23 mL DIC (1.48 mmol, 1.0 eq.) were added drop-wise, too. After stirring for 30 min at 0 °C, an ice cold solution of 0.40 g D-**111** (1.49 mmol, 1.0 eq.) in 6 mL DMF/THF 1:1 as well as 0.16 mL NMM (1.48 mmol, 1.0 eq.) were slowly added. After stirring for further 30 min at 0 °C, the mixture was warmed up to R*T*, and stirred for 18 h at R*T*. Finally, 50 mL ice cold KHCO$_3$ (90 % in water) were added, and again stirred for 30 min at 0 °C. The resulting light yellow precipitate was filtered, washed with ice cold KHCO$_3$ (90 % in water), and redissolved in chloroform. The organic layer was washed with Na$_2$CO$_3$ (10 % in water) (2x), water (2x), cold hydrochloric acid (1 N) (2x), and brine (2x). The combined organic layers were dried over MgSO$_4$, the solvent removed *in vacuo*, and the crude product purified by column chormatography (pentane/acetone 1:1, R$_f$ = 0.76). Product **112** was obtained as a colourless solid (0.72 g, 1.17 mmol) in 78.7 % yield.

0.35 g Fmoc-L-Tyr (L-**93**) (0.77 mmol, 1.0 eq.) and 0.13 g HOBt monohydrate (0.87 mmol, 1.1 eq.) were dissolved in 5.0 mL DMF. 0.10 mL NMM (0.87 mmol, 1.0 eq.) were added while stirring and cooling at 0 °C; then 0.14 mg EDCl (0.72 mmol, 0.9 eq.) were added portion-wise. After stirring for 10 min at 0 °C, an ice cold solution of 0.21 g D-**111** (0.87 mmol, 1.1 eq.) and 0.10 mL NMM (0.87 mmol, 1.1 eq.) in 5 mL DMF were slowly added. After stirring for further 20 min at 0 °C, the pH was adjusted with 0.15 mL NMM (1.34 mmol, 1.7 eq.) to pH 7-8, the mixture then warmed up to R*T*, and stirred for 16 h at R*T*. Finally, ice cold KHCO$_3$ (90 % in water) were added, and again stirred for 30 min at 0 °C. The resulting light yellow precipitate was filtered, washed with ice cold KHCO$_3$ (90 % in water), and redissolved in chloroform. The organic layer was washed with NaHCO$_3$ (10 % in water) (2x), water (2x), cold hydrochloric acid (1 M) (2x), and brine (2x). The

combined organic layers were dried over $MgSO_4$, the solvent removed *in vacuo*, and the crude product purified by MPLC on C18 silica gel (A: water + 0.05 % TFA, B: ACN + 0.05 % TFA, 0.0-1.0 min 55 % A, 1.0-9.0 min 5 % A; column: Reveleris®C18 12 g; flow rate: 30 mL/min). Product **112** was obtained as a yellow solid (0.21 g, 0.34 mmol) in 44.5 % yield.

Analytics

Molecular formula: $C_{37}H_{35}N_3O_6$

Molecular weight: 617.70 g/mol
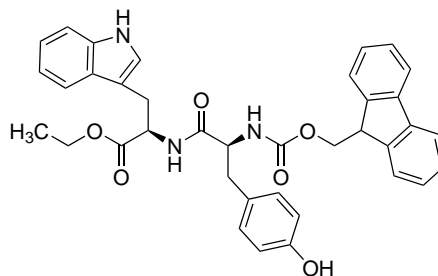
ESI(+)-MS: m/z = calc. for $C_{37}H_{36}N_3O_6$ 618.26 $[M+H]^+$, found 618.06; calc. for $C_{37}H_{35}N_3O_6Na$ 640.24 $[M+Na]^+$, found 640.31; calc. for $C_{74}H_{71}N_6O_{12}$ 1235.51 $[2M+H]^+$, found 1234.56; calc. for $C_{74}H_{70}N_6O_{12}Na$ 1257.49 $[2M+Na]^+$, found 1256.53.

^{1}H-NMR (500 MHz, DMSO-d$_6$, R T) δ = 10.87 (s, 1 H, Ar-NH$_{Trp}$), 9.15 (s, 1 H, Ar-OH$_{Tyr}$), 8.42 (d, 1 H, NH$_{Trp}$), 7.87 (d, 2 H, Ar-CH$_{Fmoc}$), 7.61-7.66 (dd, 2 H, Ar-CH$_{Fmoc}$), 7.51 (t, 2 H Ar-CH$_{Fmoc}$), 7.38-7.42 (m, 2 H, Ar-CH$_{Trp}$), 7.26-7.34 (m, 3 H, Ar-CH$_{Fmoc}$, Ar-CH$_{Trp}$), 7.17 (d, 1 H, Ar-CH$_{Trp}$), 7.07 (d, 2 H, Ar-CH$_{Tyr}$), 7.05 (d, 1 H, NH$_{Tyr}$), 6.98 (t, 1 H, Ar-CH$_{Trp}$), 6.63 (d, 2 H, Ar-CH$_{Tyr}$), 4.51-4.53 (m, 1 H, CH$_{\alpha,Tyr}$), 4.09-4.25 (m, 4 H, CH$_{2,Fmoc}$, CH$_{Fmoc}$, CH$_{\alpha,Trp}$), 3.99 (q, 2 H, CH$_2$), 3.07-3.19 (m, 2 H, CH$_{2,Trp}$), 2.62-2.89 (m, 2 H, CH$_{2,Tyr}$), 1.06 (t, 3 H, CH$_3$) ppm.
The ^{1}H-NMR spectrum showed the presence of a single conformer.

5.9.3.4. HO-D-Trp-L-Tyr-NH₂ (133)
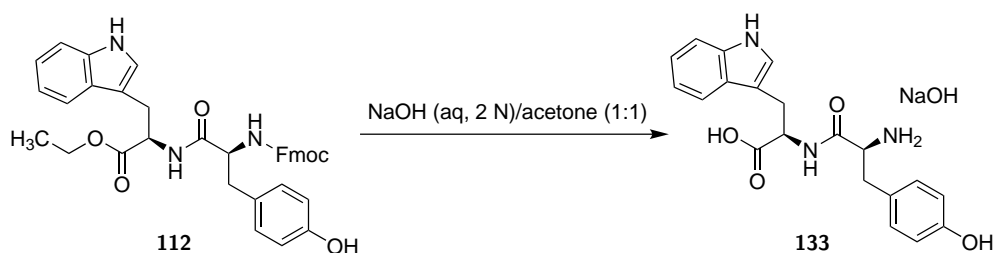
0.84 g **112** (1.36 mmol, 1.0 eq.) were dissolved in 40 mL acetone and 40 mL aqueous NaOH (2 N) were added. The solution was stirred for 24 h at R *T*. Afterwards, 40 mL EtOAc were added, the organic layer separated, and the pH of the aqueous layer adjusted to pH 6-7 with HCl (2N in water). The aqueous layer was then extracted with EtOAc (3x), all organic layers combined, and the solvent removed *in vacuo*. The crude product was purified by MPLC on C18 silica gel (A: water + 0.05 % TFA, B: ACN + 0.05 % TFA, 0.0-1.0 min 55 % A, 1.0-9.0 min 5 % A; column: Reveleris®C18 12 g; flow rate: 30 mL/min), and the sodium hydroxide salt of **133** obtained as an orange oil (0.43 g, 1.05 mmol) in 77.1 % yield. Unfortunately, massive solubility problems during NMR preparation prevented recording of NMR spectra. Presumably, remaining impurities were responsible.

Analytics

Molecular formula: $C_{20}H_{21}N_3O_4$

Molecular weight: 367.41 g/mol
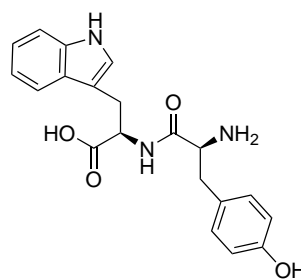
ESI(+)-MS: m/z = calc. for $C_{20}H_{22}N_3O_4$ 368.16 [M+H]⁺, found 368.09; calc. for $C_{40}H_{43}N_6O_8$ 735.31 [2M+H]⁺, found 734.62.

¹H-NMR (500 MHz, DMSO-d₆, R *T*) δ = 10.87 (s, 1 H, Ar-NH$_{Trp}$), 9.15 (s, 1 H, Ar-OH$_{Tyr}$), 7.58 (m, 2 H, Ar-CH$_{Trp}$), 7.32 (d, 1 H, Ar-CH$_{Trp}$), 7.17 (d, 1 H, NH$_{Trp}$), 7.07 (d, 2 H, Ar-CH$_{Tyr}$), 7.05 (d, 1 H, Ar-CH$_{Trp}$), 6.72 (t, 1 H, Ar-CH$_{Trp}$), 6.51 (d, 2 H, Ar-CH$_{Tyr}$), 4.51 (t, 1 H, CH$_{\alpha,Trp}$), 3.95 (m, 1 H, CH$_{\alpha,Tyr}$), 3.07-3.19 (m, 2 H, CH$_{2,Trp}$), 2.62-2.89 (m,

2 H, $CH_{2,Tyr}$) ppm.

The spectroscopic data are in agreement with the literature.[206]

5.9.3.5. **HO-D-Trp-L-Tyr-Fmoc (114)**
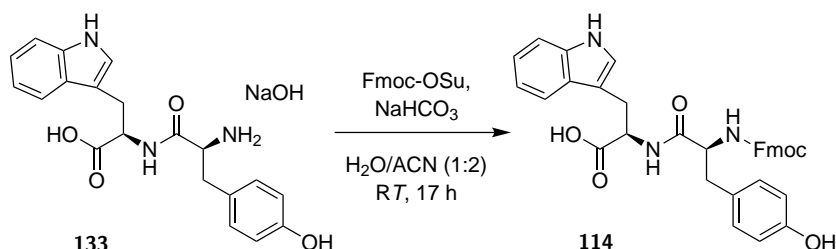
0.43 g of the sodium hydroxide salt of **133** (1.05 mmol, 1.0 eq.) and 0.20 g NaHCO₃ (2.37 mmol, 2.3 eq.) were dissolved in 4.0 mL water/acetonitrile 1:1. 0.40 g *N*-Fmoc hydroxysuccinimide ester (1.17 mmol, 1.1 eq.), dissolved in 2.0 mL acetonitrile, were added drop-wise while stirring. After 17 h of vigorous stirring at R*T* the solution was washed with Et₂O (2x), the aqueous layer acidified to pH 2 with HCl (10 w/v % in water), and extracted with EtOAc (3x). The combined EtOAc layers were washed with brine (2x), dried over MgSO₄, and the solvent removed *in vacuo*. Product **114** was obtained as an orange solid (0.15 g, 0.26 mmol) in 22.0 % yield.

Analytics

Molecular formula: $C_{35}H_{31}N_3O_6$

Molecular weight: 589.65 g/mol
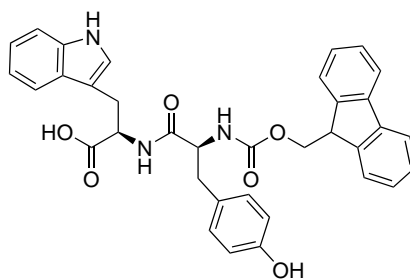
The exact mass of **114** could not be detected in LC-MS or HR-MS spectra.

¹H-NMR (500 MHz, DMSO-d₆, R*T*) δ = 10.87 (s, 1 H, Ar-NH$_{Trp}$), 9.13 (s, 1 H, Ar-OH$_{Tyr}$), 8.45 (d, 1 H, NH$_{Trp}$), 7.87 (d, 2 H, Ar-CH$_{Fmoc}$), 7.61-7.66 (dd, 2 H, Ar-CH$_{Fmoc}$), 7.44-7.53 (dd, 2 H, Ar-CH$_{Fmoc}$), 7.38-7.42 (m, 2 H, Ar-CH$_{Trp}$), 7.32 (d, 1 H, Ar-CH$_{Trp}$), 7.26-7.32 (m, 2 H, Ar-CH$_{Fmoc}$), 7.15 (d, 1 H, Ar-CH$_{Trp}$), 7.06 (t, 1 H, NH$_{Tyr}$), 7.01 (d, 2 H, Ar-CH$_{Tyr}$), 6.98 (d, 1 H, Ar-CH$_{Trp}$), 6.60 (d, 2 H, Ar-CH$_{Tyr}$), 4.49-4.53 (m, 1 H, CH$_{\alpha,Tyr}$), 4.08-4.25 (m, 4 H, CH$_{2,Fmoc}$, CH$_{Fmoc}$, CH$_{\alpha,Trp}$), 3.01-3.18 (m, 2 H, CH$_{2,Trp}$), 2.54-2.70 (m, 2 H,

$CH_{2,Tyr}$) ppm.

The ^{1}H-NMR spectrum showed the presence of a single conformer.

5.9.3.6. EtO-D-Dpg-D-Trp-L-Tyr-Fmoc (115)
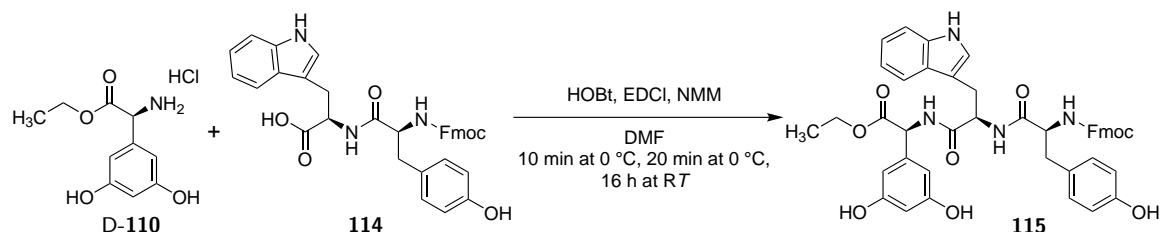
68.9 mg **114** (0.12 mmol, 1.0 eq.) and 15.5 mg HOBt monohydrate (0.10 mmol, 0.9 eq.) were dissolved in 2.5 mL DMF. 0.12 mL NMM (0.11 mmol, 0.9 eq.) were added while stirring and cooling at 0 °C and 23.5 mg EDCl (0.12 mmol, 1.0 eq.) were added portion-wise, too. After stirring for 10 min at 0 °C, an ice cold solution of 1.05 g D-**110** (0.14 mmol, 1.2 eq.) in 3 mL DMF as well as 0.12 mL NMM (0.11 mmol, 0.9 eq.) were added drop-wise and again stirred for 20 min at 0 °C. The pH was adjusted with additional 0.12 mL NMM (0.11 mmol, 0.9 eq.) to pH 7-8. The mixture was then stirred for 16 h at R*T*. Finally, DMF was removed *in vacuo*, 5 mL ice cold KHCO$_3$ (90 % in water) were added to the remaining solution and stirred for 30 min at 0 °C. The resulting light yellow precipitate was filtered, washed with ice cold KHCO$_3$ (90 % in water) and redissolved in chloroform. The organic layer was washed with Na$_2$CO$_3$ (10 % in water) (2x), water (2x), cold hydrochloric acid (0.1 N) (2x) and brine (2x). The combined organic layers were dried over MgSO$_4$, the solvent removed *in vacuo* and product **115** obtained as a yellow solid (59.0 mg, 0.08 mmol) in 64.4 % yield.

Analytics

Molecular formula: $C_{45}H_{42}N_4O_9$

Molecular weight: 782.85 g/mol
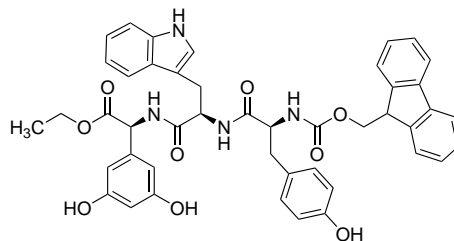
ESI(+)-MS: m/z = calc. for $C_{45}H_{43}N_4O_9$ 783.30 [M+H]$^+$, found 782.98; calc. for $C_{45}H_{42}N_4O_9Na$ 805.28 [M+Na]$^+$, found 805.38; calc. for $C_{90}H_{85}N_8O_{18}$ 1565.60 [2M+H]$^+$, found 1565.47; calc. for $C_{90}H_{84}N_8O_{18}Na$ 1587.58 [2M+Na]$^+$, found 1586.54.

The ^{1}H-NMR spectrum (500 MHz, DMSO-d$_6$, RT) showed a mixture of different conformers, which hindered the unambiguous peak assignment.

5.9.3.7. HO-D-Dpg-D-Trp-L-Tyr-NH$_2$ (116)

115   NaOH (aq, 2 N)/ACN (2:5)   **116**
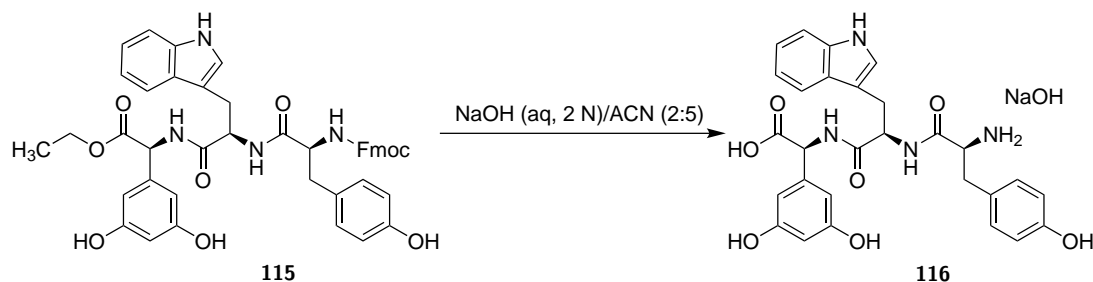
59.0 mg **115** (0.08 mmol, 1.0 eq.) were dissolved in 5 mL acetonitrile and 2 mL aqueous NaOH (2 M) were added drop-wise at 0 °C. The solution was stirred for 2 h, while the solution was slowly warmed to RT. The solvents were then removed *in vacuo* and the crude product purified by MPLC on C18 silica gel (A: water + 0.05 % TFA, B: ACN + 0.05 % TFA, 0.0-1.0 min 55 % A, 1.0-9.0 min 5 % A; column: Reveleris®C18 12 g; flow rate: 30 mL/min). The sodium hydroxide salt of **116** was obtained as a yellow solid (72.2 mg) and used without further purification. Unfortunately, massive solubility problems during NMR preparation prevented recording of NMR spectra. Presumably, remaining impurities were responsible.

Analytics

Molecular formula: C$_{28}$H$_{28}$N$_4$O$_7$

Molecular weight: 532.55 g/mol
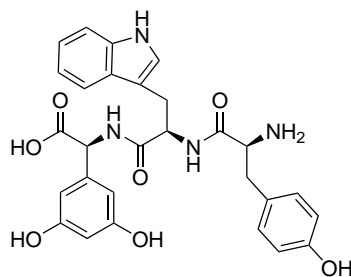
ESI(+)-MS: m/z = calc. for C$_{28}$H$_{29}$N$_4$O$_7$ 533.20 [M+H]$^+$, found 533.10; calc. for C$_{56}$H$_{57}$N$_8$O$_{14}$ 1065.40 [2M+H]$^+$, found 1064.71.

The ^{1}H-NMR spectrum (500 MHz, DMSO-d$_6$, RT) showed a mixture of different conformers, which hindered the unambiguous peak assignment.

5.9.4. Modifications of Peptides in Liquid Phase

5.9.4.1. PhS-L-Hpg-L-Tyr-D-3-chloro-Hpg-L-Hpg-Fmoc (122)
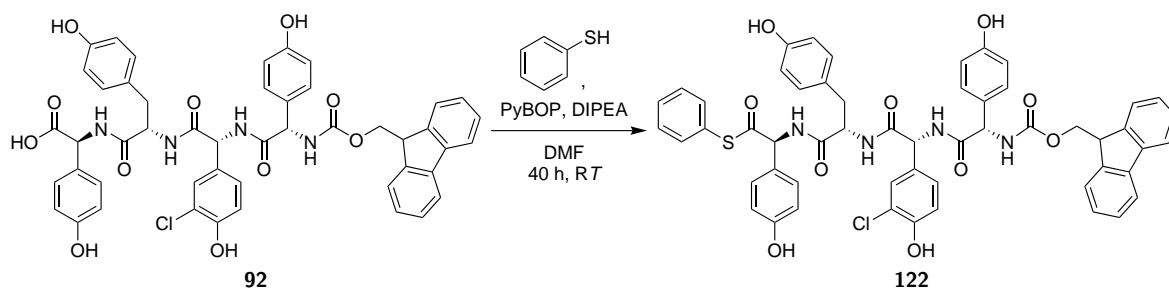
20.5 mg tetrapeptide **92** (0.023 mmol, 1.0 eq.), 5.53 µL thiophenol (0.054 mmol, 2.3 eq.), 4.7 µL DIPEA (0.028 mmol, 1.2 eq.), and 14.1 mg PyBOP (0.027 mmol, 1.2 eq.) were dissolved in 200 µL DMF under argon atmosphere. The reaction mixture was stirred for 40 h at R*T*. The solution was diluted with 400 µL methanol and directly purified by semi-preparative HPLC (A: water + 0.05 % TFA, B: ACN + 0.05 % TFA, 0.0-2 min 70 % A, 2.0-5.0 min 37 % A, 5.0-18.0 min 34 % A, 18.0-18.1 min 70 % A, 18.10-20.0 70 % A; column: Eurospher II 100-5 C18 250x20 mm; flow rate: 12 mL/min). Product **122** was obtained as a colourless solid (16.3 mg, 0.017 mmol) in 71.9 % yield.

Analytics

Molecular formula: $C_{54}H_{45}ClN_4O_{10}S$

Molecular weight: 977.48 g/mol
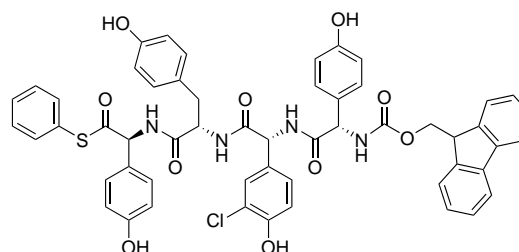
The exact mass of **114** could neither be detected in LC-MS nor HR-MS spectra.

The ^{1}H-NMR spectrum showed signs of different conformers. Listed below are the peaks of the main conformer:
^{1}H-NMR (500 MHz, DMSO-d$_6$, R*T*) δ = 9.98 (s, 1 H, Ar-OH), 9.62 (s, 1 H, Ar-OH$_{Cl-Hpg}$), 9.35 (s, 1 H, Ar-OH), 9.11 (s, 1 H, Ar-OH), 8.75 (d, 1 H, NH), 8.65 (d, 1 H, NH), 8.59 (d, 1 H, NH), 7.93 (d, 1 H, NH), 7.87 (d, 2 H, Ar-CH$_{Fmoc}$), 7.71-7.77 (m, 2 H, Ar-CH$_{Fmoc}$), 7.39-7.45 (m, 6 H, Ar-CH$_{Fmoc}$, Ar-CH), 7.22-7.33 (m, 7 H, Ar-CH$_{Fmoc}$, Ar-CH), 6.99 (d, 1 H, Ar-CH$_{Cl-Hpg}$), 6.94 (s, 2 H, Ar-CH), 6.76-6.83 (d, 2 H, Ar-CH), 6.63-6.71 (m, 4 H,

Ar-CH), 6.54 (d, 2 H, Ar-CH), 5.53-5.55 (m, 1 H, CH$_\alpha$), 5.44-5.47 (m, 1 H, CH$_\alpha$), 5.38-5.41 (m, 1 H, CH$_\alpha$), 4.52-4.64 (m, 1 H, CH$_\alpha$), 4.16-4.29 (m, 3 H, CH$_{Fmoc}$, CH$_{2,Fmoc}$), 2.60-2.74 (m, 2 H, CH$_{2,Tyr}$) ppm.

5.9.4.2. PhS-L-Hpg-L-Tyr-D-3-chloro-Hpg-L-Hpg-Cbz (123)
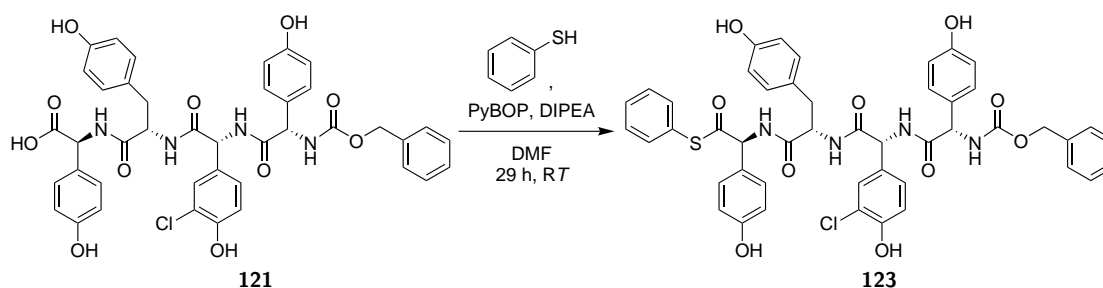
18.2 mg tetrapeptide **121** (0.023 mmol, 1.0 eq.), 5.44 µL thiophenol (0.053 mmol, 2.3 eq.), 4.62 µL DIPEA (0.027 mmol, 1.2 eq.) and 14.1 mg PyBOP (0.027 mmol, 1.2 eq.) were dissolved in 200 µL DMF under argon atmosphere. The reaction mixture was stirred for 29 h at RT. The solution was diluted with 400 µL methanol and directly purified by semi-preparative HPLC (A: water + 0.05 % TFA, B: ACN + 0.05 % TFA, 0.0-2 min 95 % A, 2.0-25.0 min 5 % A, 25.0-26.0 min 5 % A, 26.0-26.1 min 95 % A, 26.1-28.0 95 % A; column: Eurospher II 100-5 C18 250x20 mm; flow rate: 12 mL/min). Product **123** was obtained as a colourless solid (3.2 mg, 0.004 mmol) in 15.8 % yield.

Analytics

Molecular formula: C$_{47}$H$_{41}$ClN$_4$O$_{10}$S

Molecular weight: 889.37 g/mol
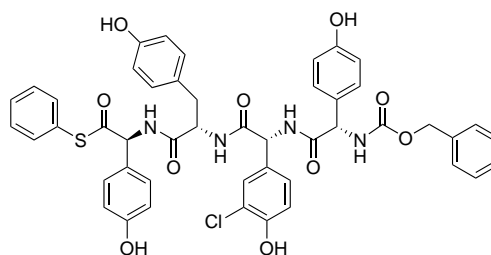
The exact mass of **114** could neither be detected in LC-MS nor HR-MS spectra.

The ^{1}H-NMR spectrum (500 MHz, DMSO-d$_6$, RT) showed a mixture of different conformers, which hindered the unambiguous peak assignment.

5.9.4.3. Fmoc-NHNH-L-Hpg-L-Tyr-D-3-chloro-Hpg-L-Hpg-Fmoc (125)
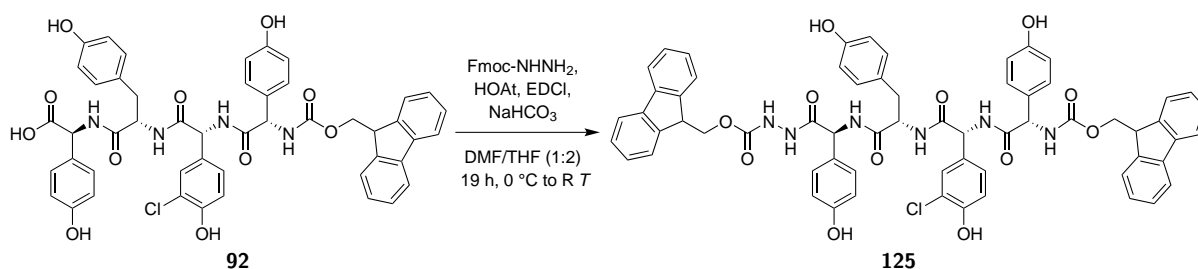
101.1 mg tetrapeptide **92** (0.114 mmol, 1.0 eq.) were dissolved in 0.5 mL DMF, 23.1 mg HOAt (0.170 mmol, 1.5 eq.) in 1.0 mL THF added, and the solution cooled to 0 °C. 33.5 mg EDCl (0.175 mmol, 1.5 eq.) and 16 mg sodium bicarbonate (0.190 mmol, 1.7 eq.) were added; after 10 min stirring at 0 °C 28.7 mg Fmoc-hydrazide (0.113 mg, 1.0 eq.) were added, too. The reaction mixture was subsequently stirred for 19 h at R T. THF was removed under reduced pressure, the resulting light yellow precipitate dissolved in ethyl acetate as well as methanol, and the solution washed with water (1x). The watery phase was reextracted using ethyl acetate (4x). The combined organic phases were washed with 40 % citric acid (4x) as well as brine (1x), and dried over $MgSO_4$. After removal of the solvent *in vacuo*, the crude product was purified by semi-preparative HPLC (A: water + 0.05 % TFA, B: ACN + 0.05 % TFA, 0.0-2.0 min 90 % A, 2.0-8.0 min 40 % A, 8.0-18.0 min 37 % A, 18.0-18.1 min 90 % A, 18.5-20.0 min 90 % A; column: Eurospher II 100-5 C18 250x8 mm; flow rate: 5 mL/min). Product **125** was obtained as a yellow solid (46.0 mg, 0.041 mmol) in 36.0 % yield.

Analytics

Molecular formula: $C_{63}H_{53}ClN_6O_{12}$

Molecular weight: 1121.32 g/mol
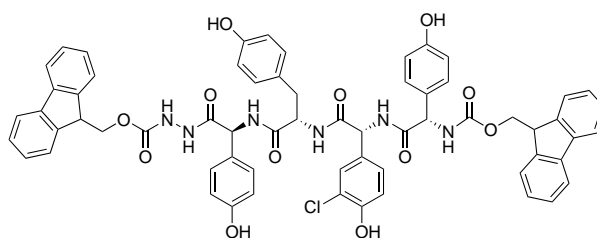
ESI(+)-MS: m/z = calc. for $C_{63}H_{54}ClN_6O_{12}$ 1121.35 [M+H]$^+$, found 1120.61; calc. for $C_{63}H_{53}ClN_6O_{12}Na$ 1143.33 [M+Na]$^+$, found 1143.20.

The ^{1}H-NMR spectrum (500 MHz, DMSO-d$_6$, R T) showed contamination with Fmoc-hydrazide, which hindered an unambiguous peak assignment. Clearly identifiable are:

^{1}H-NMR (500 MHz, DMSO-d$_6$, RT) δ = 11.29 (s, 1 H, NH$_{hydrazide}$), 10.21 (s, 1 H, NH$_{hydrazide}$), 10.02 (s, 1H, Ar-OH), 9.35 (br, 2 H, Ar-OH, Ar-OH), 9.09 (br, 1 H, Ar-OH), 8.47 (d, 1 H, NH), 8.38-8.40 (dd, 2 H, NH, NH), 8.28 (d, 1 H, NH), 5.81 (d, 1 H, CH$_\alpha$), 5.31-5.33 (m, 1 H, CH$_\alpha$), 4.85-4.88 (m, 2 H, CH$_\alpha$, CH$_\alpha$), 4.13-4.21 (m, 3 H, CH$_{2,Fmoc}$, CH$_{Fmoc}$) ppm.

5.9.4.4. NH$_2$NH-L-Hpg-L-Tyr-D-3-chloro-Hpg-L-Hpg-NH$_2$ (126)
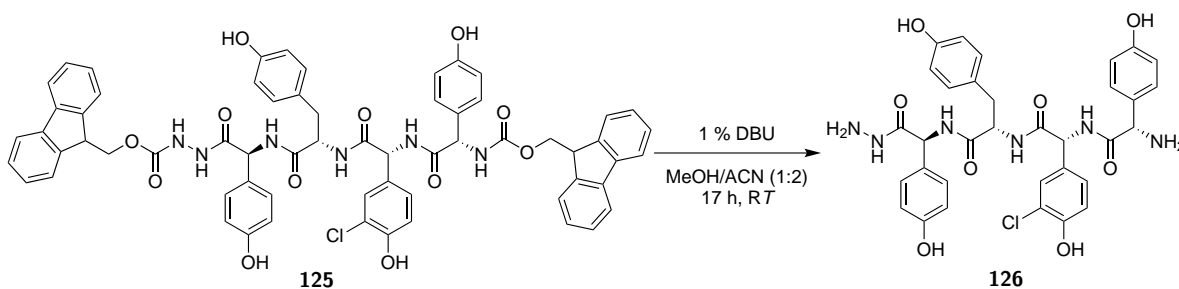
46.0 mg tetrapeptide **125** (0.041 mmol, 1.0 eq.) were dissolved in 3 mL methanol/acetonitrile (1:2) and 30 µL 10 % DBU in methanol/acetonitrile (1:2) added. The reaxtion mixture was stirred for 17 h at RT. Subsequently, the solution was washed with cyclohexane (3x), the combined cyclohexane phases reextracted with acetonitrile (3x) and a colourless solid precipitated from the combined acetonitrile phases using Et$_2$O. The precipitate was collected by centrifugation (8,000 xg, 15 min), and remaining solvent removed *in vacuo*. Product **126** was obtained as a yellow solid (16.9 mg, 0.025 mmol) in 60.9 % yield.

Analytics

Molecular formula: C$_{33}$H$_{33}$ClN$_6$O$_8$

Molecular weight: 677.11 g/mol
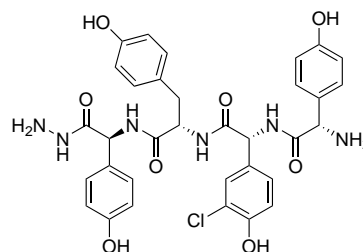
ESI(+)-MS: m/z = calc. for C$_{33}$H$_{34}$ClN$_6$O$_8$ 677.21 [M+H]$^+$, found 676.94; calc. for C$_{66}$H$_{67}$Cl$_2$N$_{12}$O$_{16}$ 1353.41 [2M+H]$^+$, found 1352.50.

^{1}H-NMR (500 MHz, DMSO-d$_6$, RT) δ = 9.98 (s, 1 H, Ar-OH), 9.52 (s, 1 H, Ar-OH$_{Cl-Hpg}$), 9.35 (s, 1 H, Ar-OH), 9.09 (dd, 2 H, Ar-OH, NH$_{hydrazine}$), 8.73 (d, 1 H, NH), 8.58-8.62 (dd, 2 H, NH, NH), 7.92 (d, 1 H, NH), 7.21-7.25 (dd, 4 H, Ar-CH), 6.97 (s, 1 H, Ar-CH$_{Cl-Hpg}$),

6.92 (d, 2 H, Ar-CH), 6.76 (d, 2 H, Ar-CH), 6.65-6.67 (m, 4 H, Ar-CH), 6.52 (d, 2 H, Ar-CH), 5.44 (d, 1 H, CH$_\alpha$), 5.39 (d, 1 H, CH$_\alpha$), 5.19 (d, 1 H, CH$_\alpha$), 4.48-4.52 (m, 1 H, CH$_\alpha$), 4.22 (m, 1 H, NH$_{hydrazide}$), 2.63-2.89 (m, 2 H, CH$_{2,Tyr}$) ppm.

5.10. Supporting Information of Publication

5.10.1. Synthesis and Initial Biological Evaluation of Myxocoumarin B

The supporting information is related to the following publication which was highlighted in Chapter 3.1.1:

Müller, J. I.*; **Kusserow, K.***; Hertrampf, G.; Pavic, A; Nikodinovic-Runic, J.; Gulder, T.A.M. Synthesis and Initial Biological Evaluation of Myxocoumarin B. *Org. Biomol. Chem.* **2019**, *17*, 1966-1969.

*equally contributing authors

Supporting Information

Synthesis and Initial Biological Evaluation of Myxocoumarin B

Jonas I. Müller,[a,†] Kalina Kusserow,[a,†] Gesa Hertrampf,[a] Aleksandar Pavic,[b] Jasmina Nikodinovic-Runic,[b] Tobias A. M. Gulder[a,*]

[a.] Biosystems Chemistry, Department of Chemistry and Center for Integrated Protein Science Munich (CIPSM), Technical University of Munich, Germany.
[b.] Institute of Molecular Genetics and Genetic Engineering, University of Belgrade, Vojvode Stepe 444a, Belgrade, Serbia.
* Corresponding author: tobias.gulder@ch.tum.de
† These authors contributed equally to this work.

Table of Contents

1. General Information

All solvents used in the reactions were p.A. grade. Solvents for chromatography were technical grade and distilled prior to use. If necessary, solvents were dried over suitable molecular sieves (3 Å, 4 Å) purchased from AppliChem GmbH (Darmstadt, Germany). Commercial materials were purchased at the highest available quality from the providers Acros Organics, Alfa Aesar, Carbolution, Carl Roth, Sigma Aldrich, Thermo Fisher Scientific and Tokyo Chemical Industry. These chemicals were used without further purification. Silica sulfuric acid was prepared according to the literature[1] and the H+ content determined prior to use according to the literature.[2] Reactions under microwave irradiation were carried out in 10 mL pressure vials equipped with a stirring bar using a Discover LabMate microwave from CEM (Matthews, USA). Reactions conducted under high pressure were conducted in glas pressure tubes sealed with Teflon screw caps. Silica gel Geduran® Si 60 (particle size 0.40 – 0.60 mm) purchased from Merck was used for flash column chromatography. Solvent mixtures are given as volume/volume. For TLC analysis, TLC-silica gel 60 F254 plates were purchased from Merck. Applied substances were observed using a UV lamp at 254 nm and 365 nm. For UV-inactive substances, dyeing reagents, such as 2.4 % anisaldehyde solution in ethanol, were used. NMR spectra were recorded on Bruker AVHD300, Bruker AVHD400, Bruker AVHD500 (only ^{1}H NMR spectra), or Bruker AV500-cryo spectrometers. The chemical shifts δ are listed as parts per million [ppm] and refer to δ(TMS) = 0. The spectra were calibrated using residual undeuterated solvent as an internal reference ($\delta(CDCl_3)$ = 7.26 ppm, $\delta((CD_3)_2CO)$ = 2.05 ppm, $\delta((CD_3)_2SO)$ = 2.50 ppm $\delta(CD_3OD)$ = 3.31 for ^{1}H NMR; $\delta(CDCl_3)$ = 77.0 ppm, $\delta((CD_3)_2CO)$ = 29.8 ppm, $\delta((CD_3)_2SO)$ = 39.5 ppm, $\delta(CD_3OD)$ = 49.0 for ^{13}C NMR). The following abbreviations (or combinations thereof) are used to explain the multiplicities: s = singlet, d = doublet, dd = doublet of doublets, t = triplet, q = quartet, m = multiplet, br = broad. In addition, the following abbreviations for chemicals are used: DCM = dichloromethane, DIPA = diisopropylamine, DMF = dimethylformamide, EtOAc = ethyl acetate, *n*BuLi = *n*buthyllithium, $Pd_2(dba)_3$ = tris(dibenzylideneacetone)dipalladium(0), SSA = silica sulfuric acid, *t*BuBrettPhos = 2-(di-*t*butylphosphino)-2',4',6'- triisopropyl-3,6-dimethoxy-1,1'-biphenyl, *t*BuOH = *t*butanol, TDA = tris-(3,5-dioxaheptyl)-amine, TFA = trifluoroacetic acid, Tf_2O = triflic anhydride, THF = tetrahydrofuran, TLC = thin layer chromatography, rt = room temperature. EI MS spectra were recorded on a Thermo Finnigan MAT 90 instrument. For High resolution mass spectrometry (HRMS) a Thermo LTQ FT Ultra mass spectrometer was used and analyses of the recorded spectra were performed using Thermo Xcalibur Qual Browser 2.2 SP1.48 Software.

2. Biological Activity Tests

2.1 Antifungal activity

The minimal inhibitory concentrations (MICs) of myxocoumarin B (**7**) against *Candida albicans* ATCC 10231 and *C. krusei* ATCC 6258 were determined according to the standard broth microdilution assay, recommended by the American National Committee for Clinical Laboratory Standards (M07-A8) for bacteria and Standard of European Committee on Antimicrobial Susceptibility Testing (v 7.3.1: Method for the determination of broth dilution minimum inhibitory concentrations of antifungal agents for yeasts) for fungal strain. Myxocoumarin B (**7**) was dissolved in DMSO. The highest concentration tested was 500 µg/mL and the inocula were 10^5 cfu/mL for *Candida* sp.

2.2 Cytotoxicity

Cytotoxicity in terms of antiproliferative effects was tested by the 3-(4,5-dimethylthiazol-2-yl)-2,5-diphenyltetrazolium bromide (MTT) assay[3]. The assay was carried out using a human lung fibroblasts (MRC5) cell line after 48 h of cell incubation in the medium, containing **7** at concentrations ranging from 1 to 200 µg/mL. Briefly, MRC5 cells were maintained in RPMI-1640 medium supplemented with 100 µg/mL streptomycin, 100 U/mL penicillin and 10% (v/v) fetal bovine serum (FBS) (Gibco) as a monolayer (1×10^4 cells per well). All cell lines were grown in humidified atmosphere of 95% air and 5% CO_2 at 37 °C. The MTT assay was performed two times in four replicates. The extent of MTT reduction was measured spectrophotometrically at 540 nm using a Tecan Infinite 200 Pro multiplate reader (Tecan Group Ltd., Mannedorf, Switzerland), and the cell survival was expressed as percentage of the control (untreated cells). Cytotoxicity was expressed as the concentration of the compound inhibiting cell growth by 50% (IC_{50}) in comparison to untreated control.

2.3 Embryotoxicity using the zebrafish (*Danio rerio*) model

The evaluation of the toxicity of myxocoumarin B (**7**) on zebrafish embryos was carried out according to the general rules of the OECD Guidelines for the Testing of Chemicals.[4] All experiments involving zebrafish were performed in compliance with the European directive 2010/63/EU and the ethical guidelines of the Guide for Care and Use of Laboratory Animals of the Institute of Molecular Genetics and Genetic Engineering, University of Belgrade. Adult zebrafish (*Danio rerio*, wild type) were obtained from a commercial supplier (Pet Center, Belgrade, Serbia), housed in a temperature- and light-controlled facility with 28 °C and standard 14:10-hour light-dark photoperiod, and regularly fed with commercially dry flake food (TetraMin™ flakes; Tetra Melle, Germany) twice a day and *Artemia nauplii*

once daily. Zebrafish embryos were produced by pair-wise mating, collected and distributed into 24-well plates containing 10 embryos per well and 1 mL distilled water with 0.2 g/L of Instant Ocean® Salt, and raised at 28 °C. For assessing lethal and developmental toxicity, embryos at 6 hours post fertilization (hpf) stage were treated with six concentrations of myxocoumarin B (**7**) (1, 10, 50, 100, 250 and 500 μM). DMSO (0.25%) was used as a negative control. Experiments were performed three times using 20 embryos per concentration. Apical endpoints for the toxicity evaluation were recorded at 24, 48, 72, 96 and 114 hpf using an inverted microscope (CKX41; Olympus, Tokyo, Japan). Dead embryos were counted and discarded every 24 h. At 114 hpf, embryos were inspected for heartbeat rate, anesthetized by addition of 0.1% (w/v) tricaine solution (Sigma-Aldrich, St. Louis, MO), photographed and killed by freezing at -20 °C for ≥ 24 h.

3. Experimental Data
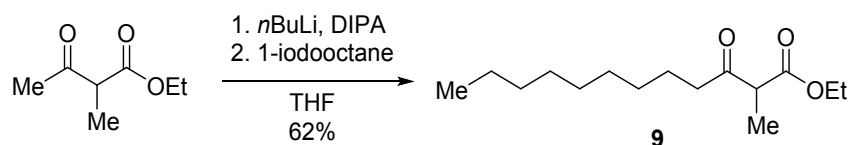
Scheme S1. Synthesis of ethyl 2-methyl-3-oxododecanoate (**9**).

3.1 Synthesis of ethyl-2-methyl-3-oxododecanoate (**9**):

Lithium diisopropylamide was freshly prepared by the addition of nBuLi (20.0 mL, 2.5 M in hexane, 50.0 mmol, 2.5 eq.) to a solution of DIPA (7.0 mL, 5.0 g, 50.0 mmol, 2.5 eq.) in THF (20.0 mL) at -78 °C under argon atmosphere and stirred for 1 h. To this solution, ethyl 2-methylacetoacetate (2.9 g, 20.0 mmol, 1.0 eq.) was added at 0 °C. The resulting deep yellow clear solution was stirred for 1 h at 0 °C. After cooling the solution to -78 °C 1-iodooctane (5.7 g, 24.0 mmol, 1.2 eq.) was added slowly over 15 min. The reaction mixture was allowed to warm to rt over 14 h and was then stirred for two additional hours at rt. The reaction was quenched by adding 10% aqueous HCl (20.0 mL) and the mixture was then extracted with Et_2O (3 x). The combined organic layers were dried over $MgSO_4$ and concentrated under reduced pressure. Column chromatography (cyclohexane: EtOAc 10:1, R_f = 0.7) afforded a yellow oil (3.2 g, 12.4 mmol, 62 %). ^{1}H-NMR (300 MHz, $CDCl_3$) δ= 4.15 (q, J = 7.1 Hz, 2H), 3.48 (q, J = 7.1 Hz, 1H), 2.64 - 2.35 (m, 2H), 1.58 - 1.53 (m, 2H), 1.30 (d, J = 7.1 Hz, 3H), 1.26 - 1.21 (m, 15H), 0.85 (t, J = 6.3 Hz, 3H) ppm. ^{13}C-NMR (101 MHz, $CDCl_3$) δ= 206.1, 170.7, 61.3, 53.0, 41.5, 32.0, 29.5, 29.5, 29.4, 29.2, 23.7, 22.7, 14.2, 12.9 ppm. HRMS (ESI+): m/z = 257.2112 [M+H]$^+$, calc.: 257.2111.
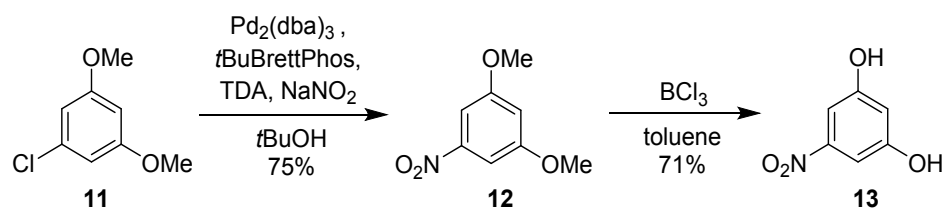
Scheme S2. Synthesis of 5-nitroresorcinol (**13**).

3.2 Synthesis of 1,3-dimethoxy-5-nitrobenzene (**12**):

An oven dried glass pressure tube was flushed with argon and charged with 1,3-dimethoxy-5-chlorobenzene (**11**, 942.0 mg, 5.5 mmol, 1.0 equiv.), $Pd_2(dba)_3$ (25.0 mg, 0.5 mol%), tBuBrettPhos (33.0 mg, 1.2 mol%), TDA (87.0 mg, 5 mol%) and $NaNO_2$ (753.0 mg, 10.9 mmol, 2.0 eq.). After addition

of *t*BuOH (11.0 mL) the pressure tube was sealed with a Teflon screw cap and heated to 130°C for 24 h. The dark red reaction mixture was cooled to rt, diluted with EtOAc and washed with H_2O. The solvent was removed under reduced pressure and the obtained raw product was purified by column chromatography (pentane: EtOAc 10:1, R_f = 0.5 in pentane: EtOAc 5:1) to give a yellow solid (755.0 mg, 4.1 mmol, 75 %). ^{1}H-NMR (400 MHz, CDCl$_3$) δ= 7.35 (d, *J* = 2.3 Hz, 2H), 6.73 (t, *J* = 2.3 Hz, 1H), 3.85 (s, 6H) ppm. ^{13}C-NMR (101 MHz, CDCl$_3$) δ= 161.0, 150.0, 107.3, 101.6, 56.0 ppm. The spectroscopic data were in agreement with those described in the literature.[5]

3.3 Synthesis of 5-nitroresorcinol (**13**):

An oven dried glass pressure tube was flushed with argon and **12** (175.0 mg, 1.0 mmol, 1.0 eq.) dissolved in 2 mL toluene was added. At 0°C BCl$_3$ in toluene (2.0 mL, 1 M, 2.0 mmol, 2.0 eq.) was added to the solution, the pressure tube sealed with a Teflon screw cap and the reaction mixture was heated to 130 °C. After 20 h BCl$_3$ in toluene (2.0 mL, 1 M, 2.0 mmol, 2.0 eq.) was added and the mixture was kept stirring at 130 °C for additional 20 h. The solution was cooled to rt and water was added carefully. After neutralization with 10% aqueous NaHCO$_3$ (10.0 mL) the solution was extracted with EtOA (3 x). The combined organic layers were washed with brine, dried over MgSO$_4$ and the solvent was removed under reduced pressure. Purification of the raw product by column chromatography (pentane: EtOAc 5:1, R_f = 0.5) gave a yellow solid (106.0 mg, 0.68 mmol, 71 %). ^{1}H-NMR (500 MHz, CD$_3$OD) δ= 7.10 (d, *J* = 2.2 Hz, 2H), 6.58 (t, *J* = 2.2 Hz, 1H) ppm. ^{13}C-NMR (101 MHz, CD$_3$OD) δ= 160.5, 151.2, 109.6, 102.7 ppm. HRMS (ESI-): m/z = 309.0365 [2M-H]$^-$, calc.: 309.0364. The spectroscopic data were in agreement with those described in the literature.[6]
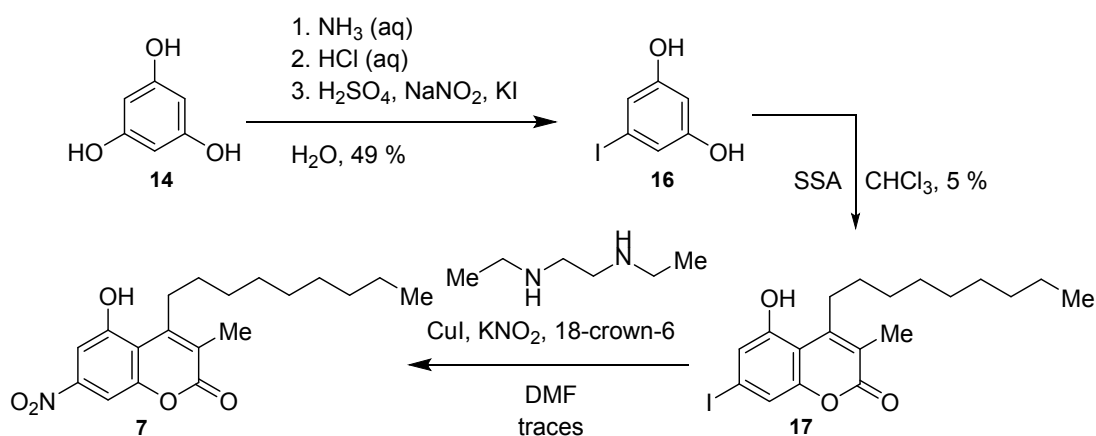
Scheme S3. Initial route to myxocoumarin B (**7**).

3.4 Synthesis of 5-iodoresorcinol (**16**)

Ammonia solution (60.0 mL, 1.6 mol, 26 % in H_2O, 19.6 eq.) was added slowly to phloroglucinol (**14**) (10.0 g, 79.3 mmol, 1.0 eq.), while stirring and cooling at 0 °C. Upon completion of the addition, the mixture was stirred for 30 min at 0 °C and then for 18 h at rt. Concentration under reduced pressure gave a brown solid, to which aqueous HCl (40.0 mL, 200.0 mmol, 5 N, 2.5 eq.) was added. The mixture was concentrated under reduced pressure to give a light brown solid (15.58 g). This solid (1.0 g, 6.2 mmol, 1.0 eq.) was then dissolved in H_2O (25.0 mL, 0.2 M), cooled to 0 °C and H_2SO_4 (1.2 mL, 22.1 mmol, 95 %, 3.6 eq.) was added slowly. After addition of an aqueous solution of $NaNO_2$ (1.2 g, 17.4 mmol, 3.5 M, 2.8 eq.) the mixture was stirred for 15 min at 0 °C and then EtOAc (6.2 mL) was added. An aqueous solution of KI (3.7 g, 22.3 mmol, 6.0 M, 3.6 eq.) was added slowly to control the evolution of nitrogen. After 5.5 h stirring at rt the layers were separated and the aqueous layer was extracted with EtOAc (3 x). The combined organic layers were washed with aqueous $Na_2S_2O_3$ (25 %, 3 x), aqueous HCl (1N, 3 x) and brine (3 x), then dried over $MgSO_4$, concentrated under reduced pressure and purified by column chromatography (cyclohexane: EtOAc 1:1, R_f = 0.5) to give a pale yellow solid (0.59 g, 2.5 mmol, 49 %). ^{1}H-NMR (400 MHz, $(CD_3)_2CO$) δ = 8.62 (br s, 2H), 6.73 (d, J = 2.1 Hz, 2H), 6.34 (t, J = 2.1 Hz, 1H) ppm. ^{13}C-NMR (75 MHz, $(CD_3)_2CO$) δ = 160.0, 116.8, 103.3, 94.2 ppm. The physical and spectroscopic data were in agreement with those described in the literature.[7]

3.5 Synthesis of 5-hydroxy-7-iodo-3-nonyl-4-methylcoumarin (**17**)

16 (0.47 g, 2.0 mmol, 1.0 eq.) and **9** (0.52 g, 2.0 mmol, 1.0 eq.) were dissolved in $CHCl_3$ (6.5 mL) and SSA (4.0 g, 19.3 mmol H^+, 9.6 eq.) was then added to the clear red solution. The reaction mixture was refluxed for 20 h. After completion, hot ethanol was added and SSA filtered off. The filtrate was concentrated under reduced pressure and purified by column chromatography (cyclohexane: EtOAc 5:1, R_f = 0.5) to give a yellow solid (0.044 g, 0.1 mmol, 5.1 %). ^{1}H-NMR (400 MHz, $(CD_3)_2SO$) δ = 7.16 (d, J = 1.7 Hz, 1H), 7.10 (d, J = 1.7 Hz, 1H), 3.01 – 2.98 (m, 2H), 2.04 (s, 3H), 1.52 – 1.46 (m, 2H), 1.42 - 1.36 (m, 2H), 1.31 - 1.23 (m, 10H), 0.85 (m, 3H) ppm. ^{13}C-NMR (75 MHz, $(CD_3)_2CO$) δ = 161.0, 156.5, 155.1, 152.2, 121.4, 121.2, 118.1, 109.7, 95.0, 32.6, 32.2, 30.8, 30.3, 30.1, 30.1, 29.8, 23.3, 14.4, 12.9 ppm. HRMS (ESI+): m/z = 429.0920 $[M+H]^+$, calc.: 429.0927.

3.6 Synthesis of myxocoumarin B (**7**):

17 (61.0 mg, 0.14 mmol, 1.0 eq.), CuI (5.0 mg, 0.02 mmol, 0.2 eq.), $NaNO_2$ (13.0 mg, 0.15 mmol, 1.1 eq.), 18-crown-6 (38.0 mg, 0.14 mmol, 1.0 eq.) and N,N'-diethylethylenediamine (9.0 µL, 0.06 mmol, 0.4 eq.) were dissolved in DMF (1.0 mL) under argon atmosphere. The mixture was stirred for 26 h at 100 °C. EtOAc was then added and the solution washed with water (5x). After concentration under

reduced pressure the crude product was afforded as a dark brown solid (95 mg). The desired product **7** was detected as trace component in the raw extract by EI-MS analysis (EI-MS (+): m/z = 347.2 [M]$^{+\cdot}$, calc.: 347.2), but not detectable by ^{1}H NMR.
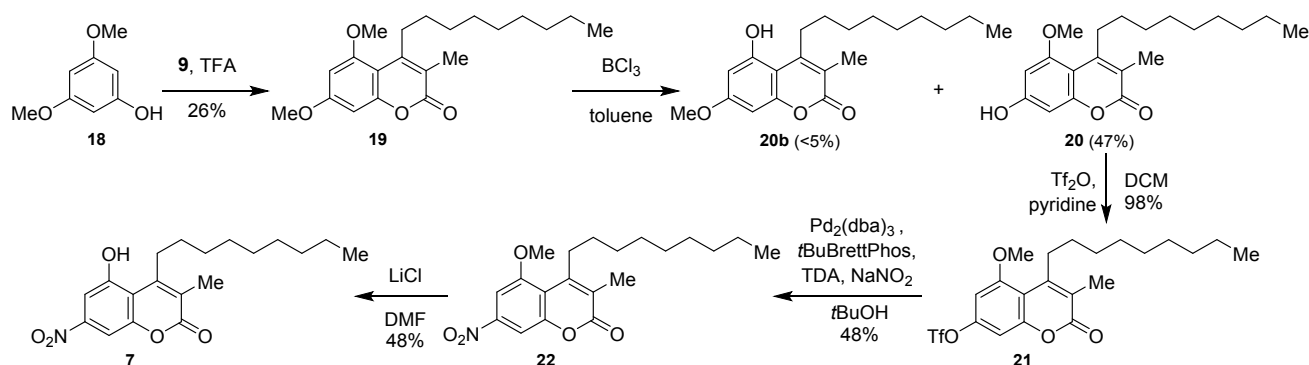
Scheme S4. Synthesis of myxocoumarin B (**7**).

3.7 Synthesis of 5,7-dimethoxy-2-methyl-3-nonylcoumarin (**19**):

3,5-Dimethoxyphenol (**18**, 0.8 g, 5.3 mmol, 1.0 eq.) and **9** (1.4 g, 5.3 mmol, 1.0 eq.) were dissolved in TFA (2.5 mL, 32.7 mmol, 6.2 eq.) and microwave-irradiated for 30 min at 100 °C. The dark red reaction mixture was poured into stirred ice-cold H$_2$O (50 mL). The formed precipitate was dissolved by adding EtOAc (50 mL). The organic layer was separated, the aqueous phase extracted with EtOAc (2 x). The combined organic layers were washed with brine, dried over MgSO$_4$ and the solvent evaporated under reduced pressure. Purification of the raw product by column chromatography (cyclohexane: EtOAc 4:1, R$_f$ = 0.4) afforded a white solid (0.48 mg, 1.4 mmol, 26 %). ^{1}H-NMR (300 MHz, (CD$_3$)$_2$SO) δ = 6.52 (d, J = 2.5 Hz, 1H), 6.47 (d, J = 2.5 Hz, 1H), 3.85 (s, 3H), 3.82 (s, 3H), 2.88 (m, 2H), 2.02 (s, 3H), 1.46 - 1.34 (m, 4H), 1.30 - 1.20 (m, 10H), 0.85 (m, 3H) ppm. ^{13}C-NMR (75 MHz, (CD$_3$)$_2$SO) δ = 161.4, 160.9, 157.9, 154.8, 151.7, 116.5, 103.6, 95.8, 93.4, 56.2, 55.7, 31.4, 31.3, 29.5, 28.9, 28.8, 28.7, 28.4, 22.1, 13.9, 12.1 ppm. HRMS (+): m/z = 347.2218 [M+H]$^+$, calc.: 347.2217.

3.8 Synthesis of 7-hydroxy-5-methoxy-2-methyl-3-nonylcoumarin (**20**):

An oven dried glass pressure tube was flushed with argon and **19** (0.65 g, 1.9 mmol, 1.0 eq.) dissolved in 4 mL toluene. After addition of BCl$_3$ in toluene (1M, 3.9 mL, 3.9 mmol, 2.1 eq.) the pressure tube was sealed with a Teflon screw cap and the reaction mixture stirred at 110 °C for 18 h. The solution was cooled to rt and H$_2$O (10.0 mL) was added carefully. After neutralization with 10% aqueous NaHCO$_3$ (10.0 mL) the solution was extracted with EtOAc (3 x). The combined organic layers were washed with brine, dried over MgSO$_4$ and the solvent was evaporated under reduced pressure. Purification of the raw product by column chromatography (cyclohexane: EtOAc 2:1, R$_f$ (**20**) = 0.4, R$_f$

(**20b**) = 0.5) afforded a white solid (0.30 g, 0.9 mmol, 47 % of isomer **20**; <5% of isomer **20b**). Isomer **20**: ^{1}H-NMR (300 MHz, (CD$_3$)$_2$SO) δ= 10.37 (s, 1H), 6.37 (d, *J* = 2.3 Hz, 1H), 6.30 (d, *J* = 2.3 Hz, 1H), 3.83 (s, 3H), 2.91 (m, 2H), 2.02 (s, 3H), 1.47 – 1.37 (m, 2H), 1.35 - 1.22 (m, 10H), 0.85 (m, 3H) ppm. ^{13}C-NMR (126 MHz, (CD$_3$)$_2$SO) δ= 161.1, 160.1, 158.2, 154.9, 152.1, 115.5, 102.5, 96.3, 95.3, 56.1, 31.5, 31.3, 29.6, 29.0, 28.9, 28.7, 28.5, 22.1, 14.0, 12.1 ppm. HRMS (+): m/z = 333.2060 [M+H]$^+$, calc.: 333.2060. Isomer **20b**: ^{1}H-NMR (400 MHz, (CD$_3$)$_2$SO) δ= 10.62 (s, 1H), 6.40 (d, *J* = 2.6 Hz, 1H), 6.33 (d, *J* = 2.6 Hz, 1H), 3.76 (s, 3H), 2.99 (m, 2H), 2.02 (s, 3H), 1.55 - 1.45 (m, 2H), 1.44 - 1.35 (m, 2H), 1.33 - 1.21 (m, 10H), 0.85 (m, 3H) ppm. ^{13}C-NMR (101 MHz, (CD$_3$)$_2$SO) δ= 161.2, 161.0, 156.6, 155.0, 152.5, 115.6, 102.8, 98.5, 92.6, 55.4, 31.3, 30.9, 29.5, 29.0, 28.8, 28.7, 28.6, 22.1, 13.9, 12.1 ppm. HRMS (+): m/z = 333.2060 [M+H]$^+$, calc.: 333.2060.
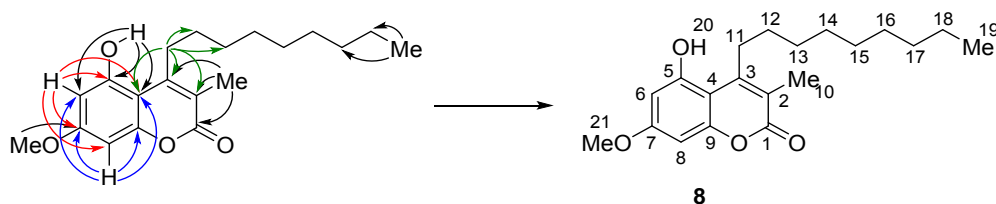
Scheme S5. Selected crucial HMBC interactions of regioisomer **20**.

Table S1. ^{1}H- and ^{13}C-NMR data of isomer **20** recorded in $(CD_3)_2SO$.

Position	δ_c [ppm], type	δ_H [ppm], (J in Hz)	Selected HMBC
1	161.2, C		
2	115.6, C		
3	152.5, C		
4	102.8, C		
5	156.6, C		
6	98.5, CH	6.33, d (2.6)	4, 5, 7, 8
7	161.0, C		
8	92.6, CH	6.40, d (2.6)	4, 6, 7, 9
9	155.0, C		
10	12.1, CH$_3$	2.02, s	1, 2, 3
11	30.9, CH$_2$	2.99, t	2, 3, 4, 12, 13
12	31.3[1], CH$_2$	1.55 - 1.45, m	
13	29.5[1], CH$_2$	1.44 - 1.35, m	
14	29.0[1], CH$_2$	1.33 - 1.21, m	
15	28.8[1], CH$_2$	1.33 - 1.21, m	
16	28.7[1], CH$_2$	1.33 - 1.21, m	
17	28.6[1], CH$_2$	1.33 - 1.21, m	
18	22.1[1], CH$_2$	1.33 - 1.21, m	
19	13.9, CH$_3$	0.85, t	17, 18
20		10.62, s	4, 5, 6
21	55.4, CH$_3$	3.76, s	7

[1] assignment could be interchanged.

3.9 Synthesis of 5-methoxy-2-methyl-3-nonyl-7-trifluoromethanesulfonylcoumarin (**21**):

To a suspension of **20** (191.0 mg, 0.6 mmol, 1.0 eq.) and pyridine (93.0 µL, 91.0 mg, 1.2 mmol, 2.0 eq.) in DCM (1.5 mL), Tf$_2$O (126.0 µL, 211.0 mg, 1.2 mmol, 1.3 eq.) in DCM (309.0 µL) was added dropwise via syringe at 0°C under argon atmosphere. The reaction mixture was warmed to rt under continuous stirring over 30 min. Afterwards, the reactions mixture was diluted with DCM (30 mL), washed with 10% aqueous HCl, H$_2$O and brine, dried over MgSO$_4$ and the solvent evaporated under reduced pressure. Purification of the raw product by column chromatography (cyclohexane: EtOAc 7:1, R$_f$ = 0.5) afforded a slightly yellow solid (263.0 mg, 0.57 mmol, 98 %). ^{1}H-NMR (300 MHz, $(CD_3)_2SO$) δ= 7.21 (d, J = 2.5 Hz, 1H), 7.13 (d, J = 2.5 Hz, 1H), 3.95 (s, 3H), 2.94 (m, 2H), 2.10 (s, 3H), 1.53 – 1.37 (m, 2H) ,1.35 - 1.20 (m, 10H), 0.84 (m, 3H) ppm. ^{13}C-NMR (126 MHz, $(CD_3)_2SO$) δ= 160.0, 158.2, 153.5, 150.4, 149.7, 121.4, 118.2 (q, CF$_3$), 110.0, 102.8, 101.7, 57.2, 31.5, 31.3, 29.5, 29.0, 28.8, 28.7, 28.3, 22.1, 14.0, 12.6 ppm. HRMS (+): m/z = 465.1554 [M+H]$^+$, calc.: 465.1553.

3.10 Synthesis of 5-methoxy-2-methyl-7-nitro-3-nonylcoumarin (**22**):

An oven dried glass pressure tube was flushed with argon and charged with **21** (56.0 mg, 120.0 µmol, 1.0 eq.), Pd$_2$(dba)$_3$ (0.55 mg, 0.5 mol%), *t*BuBrettPhos (0.70 mg, 1.2 mol%), TDA (2.0 mg, 5.0 mol%) and NaNO$_2$ (17.0 mg, 240.0 µmol, 2.0 eq.). After addition of *t*BuOH (0.5 mL) the pressure tube was sealed with a Teflon screw cap and heated to 130 °C for 24 h. The dark red reaction mixture was cooled to rt, diluted with EtOAc (10 mL) and washed with H$_2$O. The solvent was removed under reduced pressure and the obtained raw product that was purified by column chromatography (cyclohexane: EtOAc 7:1, R$_f$ = 0.6) to give a yellow solid (19.0 mg, 54.0 µmol, 48 %). ^{1}H-NMR (500 MHz, (CD$_3$)$_2$SO) δ= 7.78 (d, *J* = 2.3 Hz, 1H), 7.67 (d, *J* = 2.3 Hz, 1H), 4.03 (s, 3H), 2.98 (m, 2H), 2.14 (s, 3H), 1.51 - 1.38 (m, 4H), 1.37 - 1.19 (m, 10H), 0.85 (m, 3H) ppm. ^{13}C-NMR (126 MHz, (CD$_3$)$_2$SO) δ= 159.9, 157.5, 152.9, 150.0, 147.7, 124.1, 114.8, 104.8, 101.8, 57.1, 31.5, 31.3, 29.5, 29.0, 29.8, 28.7, 28.3, 22.1, 14.0, 13.0 ppm. HRMS (+): m/z = 362.1962 [M+H]$^+$, calc.: 362.1962.

3.11 Synthesis of Myxocoumarin B (**7**):

A glass pressure tube was charged with **22** (8.5 mg, 23.5 µmol, 1.0 equiv.) and LiCl (6.0 mg, 141.0 µmol, 6.0 eq.). After addition of DMF (0.5 mL) the tube was sealed with a Teflon screw cap and heated to 155 °C for 18 h. The dark solution was then diluted with EtOAc (10 mL), washed with H$_2$O, and brine. The organic layer was dried over MgSO$_4$ and the solvent removed under reduced pressure. Purification of the raw product by column chromatography (cyclohexane: EtOAc 4:1, R$_f$ = 0.5) afforded a yellow solid (3.9 mg, 11.2 µmol, 48 %). ^{1}H-NMR (500 MHz, CD$_3$OD) δ= 7.52 (d, *J* = 2.4 Hz, 1H), 7.48 (d, *J* = 2.4 Hz, 1H), 3.10 (m, 2H), 2.17 (s, 3H), 1.62 - 1.56 (m, 2H), 1.50 - 1.45 (m, 2H), 1.40 - 1.28 (m, 10H), 0.89 (m, 3H) ppm. ^{13}C-NMR (75 MHz, CD$_3$OD) δ= 162.7, 157.9, 155.0, 153.1, 149.2, 124.3, 115.2, 106.5, 104.0, 33.1, 32.5, 31.1, 30.7, 30.4, 30.4, 30.1, 23.7, 14.4, 13.0 ppm. HRMS (+): m/z = 348.1805 [M+H]$^+$, calc.: 348.1805. The spectroscopic data were in agreement with those described in the literature.[8]
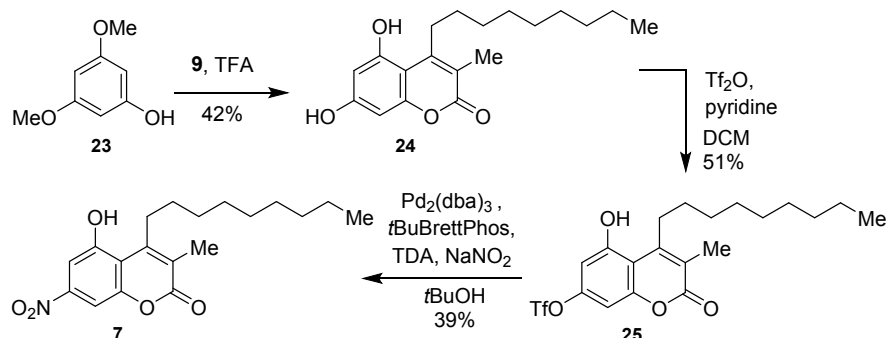
Scheme S6. Synthesis of myxocoumarin B (**7**).

3.12 Synthesis of 5,7-dihydroxy-3-nonyl-4-methylcoumarin (**24**):

Phloroglucinol (0.13 g, 1.0 mmol, 1.0 eq.), **9** (0.24 g, 1.0 mmol, 1.0 eq.) and TFA (0.46 mL, 6.0 mmol, 6.2 eq.) were microwave-irradiated for 75 min at 110 °C. After cooling, the reaction mixture was gradually poured into stirred ice-cold H_2O (20.0 mL). Filtration of the formed precipitate and purification by column chromatography (cyclohexane: EtOAc 2:1, R_f = 0.3) afforded a light yellow solid (0.14 mg, 0.4 mmol, 42 %). ^{1}H-NMR (400 MHz, $(CD_3)_2CO$) δ= 9.41 (s, 1H), 9.04 (s, 1H), 6.37 (d, J = 2.4 Hz, 1H), 6.26 (d, J = 2.4 Hz, 1H), 3.07 (m, 2H), 2.08 (s, 3H), 1.65 - 1.57 (m, 2H), 1.49 - 1.42 (m, 2H), 1.38 - 1.26 (m, 10H), 0.87 (m, 3H) ppm. ^{13}C-NMR (75 MHz, $(CD_3)_2CO$) δ= 162.3, 160.5, 157.4, 156.6, 153.3, 116.6, 103.4, 100.5, 95.9, 32.6, 32.2, 30.9, 30.3, 30.2, 30.1, 29.9, 23.3, 14.4, 12.5 ppm. HRMS (ESI+): m/z = 319.1902 [M+H]$^+$, calc.: 319.1909.

### 3.13 Synthesis of 5-hydroxy-2-methyl-3-nonyl-7-trifluoromethanesulfonylcoumarin (**25**):

To a suspension of **24** (117.0 mg, 0.37 mmol, 1.0 eq.) and pyridine (88.8 µL, 87.0 mg, 1.10 mmol, 3.0 eq.) in DCM (1.2 mL), Tf_2O (73.9 µL, 124.0 mg, 0.44 mmol, 1.2 eq.) in DCM (0.8 mL) was added portion-wise over 45 min via syringe at 0 °C under argon atmosphere. The reaction mixture was stirred at 0 °C for 3 h. Afterwards, the reaction mixture was diluted with DCM, washed with 10% aqueous HCl (2 ×), H_2O (2 ×) and brine (1 ×), dried over $MgSO_4$ and the solvent evaporated under reduced pressure. Purification of the raw product by column chromatography (cyclohexane: acetone 2:1, R_f = 0.6) afforded a white solid (85.0 mg, 0.19 mmol, 51 %). ^{1}H-NMR (400 MHz, $(CD_3)_2SO$) δ= 11.50 (s, 3H), 7.02 (d, J = 2.6 Hz, 1H), 6.78 (d, J = 2.7 Hz, 1H), 2.99 (m, 2H), 2.06 (s, 3H), 1.55 - 1.44 (m, 2H), 1.44 - 1.34 (m, 2H), 1.34 - 1.15 (m, 10H), 0.84 (m, 3H) ppm. ^{13}C-NMR (101 MHz, $(CD_3)_2SO$) δ= 160.2, 157.1, 154.0, 151.1, 149.0, 120.3, 118.2 (q, CF_3), 109.0, 104.2, 100.9, 31.3, 31.0, 29.5, 29.0, 28.8, 28.7, 28.5, 22.1, 14.0, 12.4 ppm. HRMS (+): m/z = 451.1393 [M+H]$^+$, calc.: 451.1397.
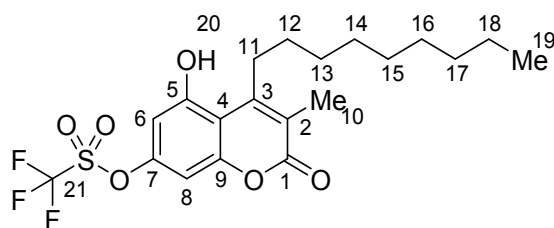
Table S2. ^{1}H- and ^{13}C-NMR data of compound **24** recorded in $(CD_3)_2SO$.

Position	δ_c [ppm], type	δ_H [ppm], (J in Hz)	HMBC
1	160.2, C		
2	120.3, C		
3	151.1, C		
4	109.0, C		
5	157.1, C		
6	104.2, CH	6.78, d (2.7)	4, 5, 8, 9
7	154.1, C		
8	100.9, CH	7.02, d (2.6)	4, 6, 7, 9
9	149.1, C		
10	12.4, CH_3	2.06, s	1, 2, 3, 4
11	31.0, CH_2	2.99, m	2, 3, 4
12	29.5[1], CH_2	1.55 - 1.44, m	
13	29.0[1], CH_2	1.44 - 1.34, m	
14	28.8[1], CH_2	1.34 - 1.15, m	
15	28.7[1], CH_2	1.34 - 1.15, m	
16	28.5[1], CH_2	1.34 - 1.15, m	
17	31.3[1], CH_2	1.34 - 1.15, m	
18	22.1[1], CH_2	1.34 - 1.15, m	
19	14.0, CH_3	0.84, m	17, 18
20		10.50, s	4, 5, 6, 7
21	118.2, C		

[1] assignment could be interchanged.

3.14 Synthesis of myxocoumarin B (**7**):

An oven dried glass pressure tube was flushed with argon and charged with **25** (100.0 mg, 222.0 µmol, 1.0 equiv.), $Pd_2(dba)_3$ (5.1 mg, 2.5 mol%), *t*BuBrettPhos (6.5 mg, 6.0 mol%), TDA (3.6 mg, 5.0 mol%) and $NaNO_2$ (30.6 mg, 444.0 µmol, 2.0 equiv.). After addition of *t*BuOH (600.0 µL) the pressure tube was sealed with a Teflon screw cap and heated to 130°C for 24 h. The dark red reaction mixture was cooled to room temperature, diluted with EtOAc (20 mL) and washed with H_2O (20 mL). The solvent was removed under reduced pressure and the obtained raw product was purified by column

chromatography (cyclohexane: acetone 3:1, R_f = 0.4) to give a yellow solid (30.0 mg, 86.4 µmol, 39%). The spectroscopic data were identical to those described in 2.11.

5.10.2. Strong Antibiotic Activity of the Myxocoumarin Natural Product Family In Vivo and In Vitro

The following manuscript was highlighted in Chapter 3.1.2. It has been obtained by personal communication from the last authors.

Strong Antibiotic Activity of the Myxocoumarin Natural Product Family *in vitro* and *in vivo*

Kalina Kusserow,[a] Gesa Hertrampf,[b] Sandra Vojnovic,[c] Aleksandar Pavic,[c] Jonas I. Müller,[b] Jasmina Nikodinovic-Runic,[c] and Tobias A. M. Gulder*[a,b]

Abstract. *The novel nitro-coumarin natural products myxocoumarin A and B were recently described from Stigmatella aurantiaca MYX-030. While myxocoumarin A possesses exceptional anti-fungal properties against agrochemically relevant pathogenic fungi, the biological function of myxocoumarin B remained elusive. Within this work, we investigated the antibiotic potential of myxocoumarin B against a range of clinically relevant bacterial pathogens. A focused library of structural analogs was synthesized to explore initial structure-activity relationships and to identify equipotent myxocoumarin derivatives devoid of the nitro group to prevent its potentially deleterious effects in vivo. The cytotoxicity of the myxocoumarins as well as their potential to cure bacterial infections in vivo was established using a zebrafish model system, overall revealing the exceptional antibiotic potential of this natural product family.*

Myxobacteria are highly talented producers of complex, biomedically interesting specialized metabolites from most diverse natural product classes. Prominent examples include epothilone A (**1**) and analogs as anti-cancer chemotherapeutics, the antifungal soraphen A1α (**2**), or the antibacterial cystobactamids, such as **3**. These organisms have thus proven to be a promising resource for the discovery of new small molecules with potent biological functions, particularly for applications with increasing demand due to emerging resistance against currently known agents, both in the agrochemical and medical sectors. We have recently described the discovery of two natural products from *Stigmatella aurantiaca* MYX-030, myxocoumarin A (**4**) and B (**5**), both of which being equipped with a long alkyl side chain and a rare aromatic nitro group. Myxocoumarin A (**4**) displayed potent inhibitory effects against a range of agrochemically relevant pathogenic fungi, while **5** could not biologically assessed due to the low production titers and the loss of the viable producing strain. To allow for antifungal evaluation of **5**, a concise total synthesis of this compound was developed, revealing a complete lack of the anticipated antifungal properties. To shed light on the

[a] K. Kusserow, Prof. Dr. T.A.M. Gulder
     Department of Chemistry and Center for Integrated Protein Science Munich (CIPSM)
     Technical University of Munich
     Lichtenbergstraße 11, 85748 Garching, Germany.
     E-mail: tobias.gulder@ch.tum.de
[b] G. Hertrampf, J.I. Müller, Prof. Dr. Tobias A. M. Gulder
     Chair of Technical Biochemistry
     Technical University of Dresden
     Bergstraße 66, 1069 Dresden, Germany.
     E-mail: tobias.gulder@tu-dresden.de
[c] Dr. S. Vojnovic, Dr. A. Pavic, Dr. J. Nikodinovic-Runic
     Institute of Molecular Genetics and Genetic Engineering
     University of Belgrade
     Vojvode Stepe 444a, 11000 Belgrade, Serbia.
     Email:jasmina.nikodinovic@imgge.bg.ac.rs

potential natural function of myxocoumarin B (**5**), we thus set out to more broadly screen the biological properties of myxocoumarin-type molecular scaffolds within this work.
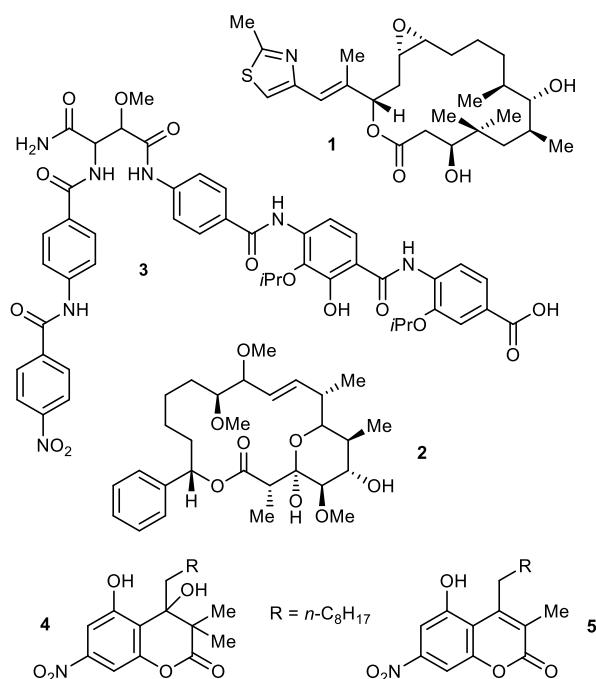
Figure 1. Chemical structures of the myxobacterial natural products epothilone A (**1**), sorphen A1α (**2**), cystobactamid (**3**) and the myxocoumarins A (**4**) and B (**5**).

Initial screening of synthetic **5** against *Candida albicans*, *Enterococcus faecalis* and *Staphylococcus aureus* using classical disk-diffusion assays revealed a strong activity of **5** against the latter, comparable to the employed standard kanamycin. Owing to these promising preliminary results, a closer inspection of the antibiotic potential of the myxocoumarins was targeted. Given the straightforward and flexible synthetic access developed for **5**, the preparation of a focused compound library to give first insights into structure-activity relationships across the myxocoumarin core was conducted. Of particular interest were variations at the prototypical myxocoumarin alkyl side chain to assess its role in granting antibacterial activity. Furthermore, the preparation of analogs without the nitro substituent was of high interest, as antibacterial activity might be a result of the development of non-specific toxic nitroso side-products *in vivo*, a potential inherent metabolic reactivity of the myxocoumarins not desirable for a biomedical application as antibiotic. In addition, the synthesis of myxocoumarin derivatives lacking the nitro function is significantly simplified, giving very fast access to the target molecules.

The method of choice for the synthesis of myxocoumarin analogs was the condensation of β-keto esters with diverse alkyl substitution with phenol building blocks in a TFA-catalyzed Pechmann condensation promoted by microwave irradiation. Ethyl 2-methyl-3-oxobutanoate (**6a**) was deprotonated with *n*-BuLi/DIPA and selectively alkylated with iodoalkanes **7b-l** to deliver the desired b-keto esters **6b-l** (Scheme 1). The analogs bearing linear side chains from C_4 to C_{11} (**6b-6i**) and C_{13} (**6j**) were obtained in yields ranging from 43%-62%. The terminally branched **6k** and the tridecafluoro derivative **6l** gave lower yields of 38% and 23%, respectively. The β-keto esters were subsequently condensed with resorcinol (**7**) and phloroglucinol (**8**) to give the corresponding mono- (**10a-l**) and dihydroxy (**11a-j**) myxocoumarin analogs (for yields, see Table 1).
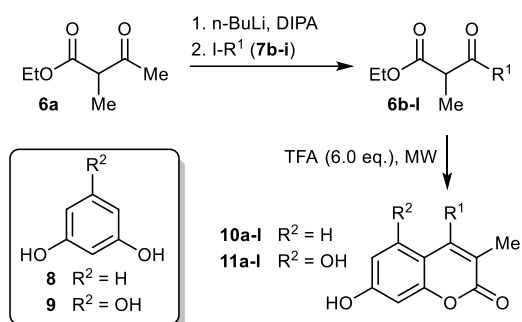
Scheme 1. Synthesis of hydroxy-substituted myxocoumarin analogs **10a-l** and **11a-j** by Pechmann condensation with β-keto esters **6a-l** with different side-chains R^1.

Table 1. Substitution pattern and yields of mycoxoumarin analogs **10** and **11**.

Compound	R^1	yield [%] of **10** (R^2 = H)	yield [%] of **11** (R^2 = OH)
a	C_1	69	100
b	n-C_4	42	30
c	n-C_5	42	33
d	n-C_6	26	27
e	n-C_7	36	32
f	n-C_8	35	25
g	n-C_9	33	42
h	n-C_{10}	30	25
i	n-C_{11}	30	26
j	n-C_{13}	25	28
k	iso-C_6	37	-
l	n-C_{13} (F_{13})	16	-

To further increase the structural diversity of this focused myxocoumarin library beyond hydroxyl analogs of **5**, a small set of *O*-methylated (**12**-**14**) and *O*-acetylated (**15**-**18**) derivatives was prepared (Figure 2), either bearing a methyl substituent at position R^1 or an *n*-C$_9$ alkyl chain as in the original myxocoumarin scaffold. While compounds **12** and **15**-**18** were obtained by either *O*-methylation or *O*-acetylation using MeI or Ac$_2$O, respectively, **13** and **14** were generated by Pechmann condensation of 3,5-dimethoxyphenol with either **6a** or **6g**. Furthermore, the *O*-acetylated derivative **19** was prepared by *O*-acetylation of myxocoumarin B (**5**). In addition, four nitro myxocoumarin derivatives (**19**-**22**), a dimethylamino- (**23**), amino- (**24**), chloro- (**25**) and iodo- (**26**) analog was accessed by Pechmann condensation of the correspondingly functionalized phenols with **6g** (see ESI for experimental details on the synthesis of **12**-**26**).
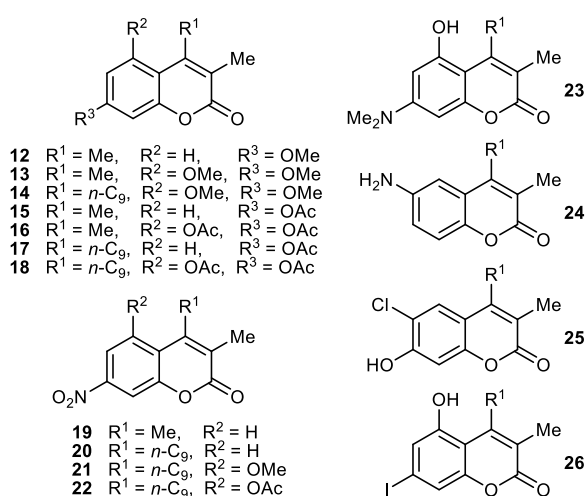
Figure 2. *O*-methylated- (**12**-**14**) and *O*-acetylated- (**15**-**18**) hydroxy myxocoumarin analogs, further nitro myxocoumarins (**19**-**22**) and dimethylamino- (**23**), amino- (**24**), chloro- (**25**) and iodo- (**26**) substituted myxocoumarin analogs (for **23**-**26**, R1 = *n*-C$_9$).

Having this myxocoumarin library composed of above 38 structural analogs in hands, we set out to evaluate their antimicrobial potential. All compounds were inactive against the opportunistic pathogenic yeast *C. albicans*, the gram-negative bacterium *Pseudomonas aeruginosa* as well as the gram-positive *Micrococcus luteus* and *Listeria monocytogenes* at the maximum tested concentrations of 250 µg/mL. However, strong antibacterial potential against the gram-positive bacteria *Bacillus subtilis* NCTC5398 and *S. aureus* NCTC6571 was observed for a number of analogs (Table 2). The natural product **5** exhibited very strong antibacterial activity against these test strains, with MIC values as low as 0.3 µg/mL combined with low LC$_{50}$ values in a zebra fish model (119.6 µg/mL). For the mono-hydroxylated **10** and dihydroxylated **11** compound series, a clear structure-activity relationship was obvious, with the activity correlating with the length of the alkyl side chain. Looking at the activity of analogs **10** against *S. aureus* NCTC6571, strong effects were only observed for **10e-g** with C$_7$ to C$_9$ alkyl

substitution, with lowest MICs for the natural C_9 substituent. Inhibition of *B. subtilis* follows a similar trend but activity extends to C_{10} and to a smaller extent to C_{11} substitution. The dihydroxylated series generally has a broader actvitiy profile in terms of alkyl chain length, already starting with significant activity from C_4 to C_9 substitution. Alkyl chain lengths beyond the natural C_9 substituent lead to a fast drop in antibacterial activity for both **10** and **11**. When correlating these activity relationships with toxicity in the zebra fish model, it becomes evident that longer side chains also lead to drastically increased LC_{50} values and thus less toxicity. Therefore, compounds **10f** (C_8), **10g** (C_9) as well as **11e-11g** (C_7-C_9) have to overall most promising activity profile.

Among all other tested compound **18-26**, only the *O*-methylated **14** and *O*-acetylated analogs **17** and **18** as well as the chlorinated congener **25**, bearing the natural C_9 alkyl substitution, showed antibacterial effects. In addition, the antibacterial activity of the *O*-acetylated derivative **22** of myxocoumarin B (**5**) was twice as high, albeit accompanied with an approx. 5-fold increase in toxicity in the zebra fish model. Most importantly, the antibacterial potential of all active myxocoumarin analogs was also retained in *S. aureus* MRSA, showing the high potential of these compounds to combat this clinically relevant, highly resistant pathogenic bacterium.

Table 2. Antibacterial activity profile of myxocoumarin B (**5**) and its structural analogs **10-26** against *B. subtilis* NCTC5398, *S. aureus* NCTC6571, *S. aureus* MRSA compared to toxicity in a zebra fish embryos. NTCT=National Collection of Type Cultures (NCTC, Culture Collection of Public Health, Salisbury, UK).

Compound	*B. subtilis* NCTC5398 [µg/mL]	*S. aureus* NCTC6571 [µg/mL]	*S. aureus* MRSA [µg/mL]	*Zebrafish* LC_{50} [µg/mL]
5	8	0.3	0.6	119.6
10a	>250	>250	>250	8.9
10b	31.2	62.5	62.5	2.1
10c	200	200	200	2.5
10d	200	200	200	1.5
10e	2	2	2	2.7
10f	15.6	7.8	7.8	21.5
10g	2	3.9	7.8	>151.2
10h	7.8	> 250	250	30.5
10i	62.5	> 250	>250	>82.6
10j	> 250	> 250	>250	>89.6
10k	15.6	> 250	>250	5.2
10l	> 250	>250	>250	>268.1
11a	125	125	62.5	14.7
11b	15.6	15.6	15.6	9.0
11c	7.8	7.8	7.8	5.2
11d	7.8	4	2	4
11e	7.8	2.5	4	24.3
11f	4	15.6	7.8	>152.2
11g	31.2	7.8	31.2	>159.2
11h	> 250	250	250	>158.2
11i	> 250	>250	>250	>173.2
11j	> 250	>250	>250	>187.3
12	>250	>250	>250	12.7
13	>250	>250	>250	1.3
14	62.5	>250	>250	>166.2
15	250	>250	>250	18.4
16	125	>250	>250	11.3
17	15.6	31.2	15.6	118.9
18	31.2	31.2	62.5	180.2
19	> 250	> 250	> 250	25.7
20	> 250	> 250	> 250	>165.7
21	> 250	> 250	> 250	>180.7
22	0.3	0.15	0.15	27.8
23	> 250	>250	>250	>172.7
24	>250	>250	> 250	21.5
25	62.5	> 250	250	67.6
26	125	250	> 250	>168.4

To further explore the antibacterial potential of the myxocoumarins that showed the best selectivity profiles, myxocoumarin B (**5**), its *O*-acetyl analog **22** and the most potent dihydroxylated congener **11e** (C_7 alkyl chain) were evaluated against a panel of *S. aureus* strains, including clinical isolates (Table 3). The strains were collected from veterinary specimens (dog urine, ear swab and mouth swab) and showed resistance to one or more commonly used antibiotics in veterinary practice. *Enterococcus faecium*, as another Gram-positive opportunistic pathogen, was also included in the assessment. To our delight, all compounds showed pronounced antibacterial effects against all tested strains, with **22** being the most active antibacterial across all evaluated organisms (Table 3).

Table 3. Antibiotic activity profile of **5**, **22** and **11e** against a selection of *S. aureus* strains, including clinical isolates (* strains isolated and identified from the clinical specimens delivered to veterinary Laboratory 'VetLab', Belgrade, Serbia including dog urine, mouth and ear swab).

Compound	*S. aureus* ATCC9144 [µg/mL]	*S. aureus* ATCC25923 [µg/mL]	*S. aureus* MRSA [µg/mL]	*Staphylococcus* sp.* 80103770 [µg/mL]	*Staphylococcus* sp* 80100861 [µg/mL]	*Staphylococcus* sp * 80100865 [µg/mL]	*Enterococcus faecium* ATCC6057
5	0.3	12.5	0.6	0.6	0.3	0.3	2
22	0.15	1	0.15	0.3	0.15	0.15	0.6
11e	2.5	12.5	4	7.8	2.5	5	2.5

The likelihood of resistance development against **5**, **22** and **11e** was assessed via multistep resistance selection of *S. aureus* ATCC9144 by propagating cultures with subinhibitory concentrations of the respective individual compound for 20 rounds, followed by one round of growth without selective pressure. Over the course of this treatment, *S. aureus* developed a 5-fold increase in MIC against **5**, a 4-fold increase against **22** and only a 2-fold increase for **11e**. Therefore, high antibiotic potential was retained for all compounds. This indicates a low likelihood of *S. aureus* for developing rapid resistance to the tested myxocoumarins, especially **11e**.

Based on above resistance development assays and the observation that **5** lost some antibacterial potential upon prolonged storage, **22** and **11e** were selected for evaluation of the antibiotic potential in vivo in a *S. aureus*- zebrafish infection model (Figure 3). The zebrafish infection model is a well recognized platform for studying host-pathogen interactions, as well as for the development of therapeutic strategies REFS.

Analyses of zebrafish embryo survival coupled with bacterial proliferation confirmed that both compounds were more efficient in rescuing zebrafish in comparison to vancomycin, with the effect

being dose dependent (Figure 3 A,B). Importantly, 2xMIC of **22** completely eliminated the infection. This was reflected in the efficiency of the reduction of the bacterial burden (Figure 3C).
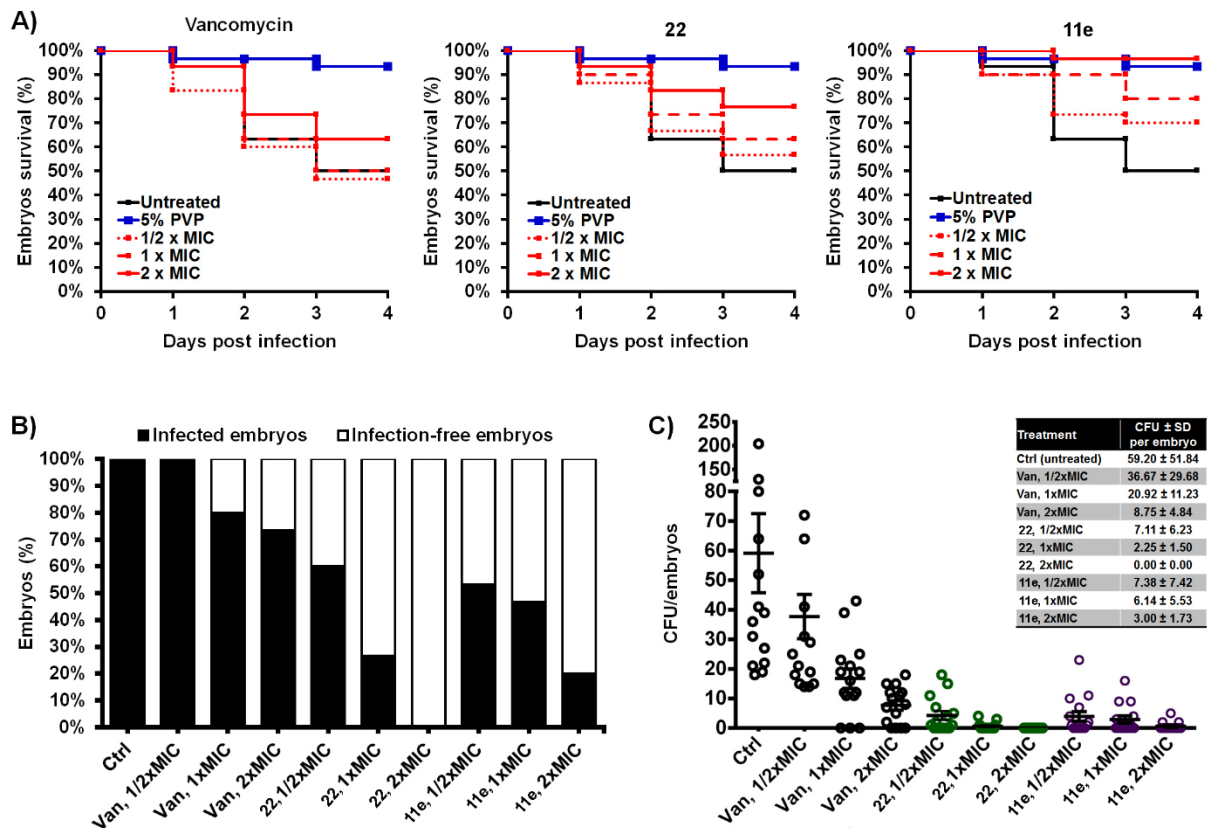
Figure 3. Myxocoumarin derivatives **22** and **11e** rescued zebrafish embryos of *S. aureus* infection (A-B) and significantly decreased the bacterial burden (C). The Kaplan-Meier curves of the infected embryos survival upon different doses of vancomycin (Van) and myxocoumarins **22** and **11e** are shown. Embryos were monitored daily for survival. Data are compilations of two independent experiments using two replicates (n = 20 embryos/replicates) for each group. Bacterial burden was determined at 4 dpi by plating of the crushed embryos for colony forming units (CFUs). Data are compilations of two independent experiments using ten embryos for each group. Each dot represents an individual fish (square – untreated embryos, circle – treated embryos). The mean CFUs ± SEM are shown.

References

(1) Rogers, K., Ed. *Medicine and Healers through History*; Britannica Educated Publishing: New York, 2011.

(2) Cragg, G. M.; Newman, D. J. Natural Products: A Continuing Source of Novel Drug Leads. *Biochim. Biophys. Acta* **2013**, *1830*, 3670 – 3695.

(3) Gould, K. Antibiotics: from prehistory to the present day. *J. Antimicrob. Chemother.* **2016**, *71*, 572 – 575.

(4) Katz, L.; Baltz, R. H. Natural product discovery: past, present, and future. *J. Ind. Microbiol. Biotechnol.* **2016**, *43*, 155 – 176.

(5) Dewick, P. M. *Medicinal Natural Products: A Biosynthetic Approach*; Wiley: Chichester, 2002.

(6) Schäfer, B. *Naturstoffe der chemischen Industrie*; Spektrum Akademischer Verlag: München, 2007.

(7) Newman, D. J.; Cragg, G. M. Natural Products as Sources of New Drugs from 1981 to 2014. *J. Nat. Prod.* **2016**, *79*, 629 – 661.

(8) Walsh, C.; Wencewicz, T. A. *Antibiotics: challenges, mechanisms, opportunities*; ASM Press: Washington, D.C., 2016; pp 23 – 28.

(9) *WHO Model List of Essential Medicines*; World Health Organisation, 2017; p 21.

(10) Estevez, A. M.; Estevez, R. J. A Short Overview on the Medicinal Chemistry of (-)-Shikimic Acid. *Mini-Rev. Med. Chem.* **2012**, *12*, 1443 – 1454.

(11) *WHO Model List of Essential Medicines*; World Health Organisation, 2017.

(12) Caffrey, P.; Lynch, S.; Flood, E.; Finnan, S.; Oliynyk, M. Amphotericin biosynthisis in Streptomyces nodosus: deductions from analysis of polyketide synthase and late genes. *Chem. Biol.* **2001**, *8*, 713 – 723.

(13) *Antimicrobial resistance: global report on surveillance*; World Health Organisation, 2014.

References

(14) Projan, S. J. Why is big Pharma getting out of antibacterial drug discovery? *Curr. Opin. Microbiol.* **2003**, *6*, 427 – 30.

(15) Katz, M. L.; Mueller, L. V.; Polyakov, M.; Weinstock, S. F. Where have all the antibiotic patents gone? *Nat. Biotechnol.* **2006**, *24*, 1529 – 1531.

(16) Silver, L. L. Challenges of Antibacterial Discovery. *Clin. Microbiol. Rev.* **2011**, *24*, 71 – 109.

(17) Baltz, R. H. Marcel Faber Roundtable: is our antibiotic pipeline unproductive because of starvation, constipation or lack of inspiration? *J. Ind. Microbiol. Biotechnol.* **2006**, *33*, 507 – 513.

(18) Patterson, T. F.; Kirkpatrick, W. R.; White, M.; Hiemenz, J. W.; Wingard, J. R.; Dupont, B.; Rinaldi, M. G.; Stevens, D. A.; Graybill, J. R. Invasive aspergillosis. Disease spectrum, treatment practices, and outcomes. I3 Aspergillus Study Group. *Medicine* **2000**, *79*, 250 – 260.

(19) Baddley, J. W.; Strout, T. P.; Salzman, D.; Pappas, P. G. Invasive mold infections in allogeneic bone marrow transplant recipients. *Clin. Infect. Dis.* **2001**, *32*, 1319 – 1324.

(20) Marr, K. A.; Carter, R. A.; Crippa, F.; Wald, A.; Corey, L. Epidemiology and outcome of mould infections in hematopoietic stem cell transplant recipients. *Clin. Infect. Dis.* **2002**, *34*, 909 –917.

(21) Pappas, P. G.; Rex, J. H.; Lee, J.; Hamill, R. J.; Larsen, R. A.; Powderly, W.; Kauffman, C. A.; Hyslop, J. E., N. abd Mangino; Chapman, S.; Horowitz, H. W.; Edwards, J. E.; Dismukes, W. E. A prospective observational study of candidemia: epidemiology, therapy, and influences on mortality in hospitalized adult and pediatric patients. *Clin. Infect. Dis.* **2003**, *37*, 634 – 643.

(22) Hajjeh, R. A. *et al.* Incidence of bloodstream infections due to Candida species and in vitro susceptibilities of isolates collected from 1998 to 2000 in a population-based active surveillance program. *J. Clin. Microbiol.* **2004**, *42*, 1519 –1527.

(23) Pfaller, M. A.; Diekema, D. J. Rare and emerging opportunistic fungal pathogens: concern for resistance beyond Candida albicans and Aspergillus fumigatus. *J. Clin. Microbiol.* **2004**, *42*, 4419 –4431.

(24) Pfaller, M. A.; Pappas, P. G.; Wingard, J. R. Invasive Fungal Pathogens: Current Epidemiological Trends. *Clin. Infect. Dis.* **2006**, *43*, S3 – S14.

(25) Loeffler, J.; Stevens, D. A. Antifungal Drug Resistance. *Clin. Infect. Dis.* **2003**, *36*, S31 – S41.

(26) De Clercq, E.; Li, G. Approved Antiviral Drugs over the Past 50 Years. *Clin. Microbiol. Rev.* **2016**, *29*, 695 – 747.

(27) Milroy, D.; Featherstone, J. Antiviral market overview. *Nat. Rev. Drug Discov.* **2002**, *1*, 11 – 12.

(28) World Health Organisation, Antimicrobial resistance. 2018; `https://www.who.int/en/news-room/fact-sheets/detail/antimicrobial-resistance`, visited on 07.04.2019.

(29) World Health Organisation, Global action plan on antimicrobial resistance. 2019; `https://www.who.int/antimicrobial-resistance/global-action-plan/en/` `(accessed26.04.2019)`, visited on 26.04.2019.

(30) Global Antibiotic Research and Development Partnership, Global Antibiotic Research and Development Partnership. 2019; `https://www.gardp.org/(accessed26.04.2019)`, visited on 26.04.2019.

(31) Infectious Diseases Society of America, The 10 x '20 Initiative: Pursuing a Global Commitment to Develop 10 New Antibacterial Drugs by 2020. *Clin. Infect. Dis.* **2010**, *50*, 1081 – 1083.

(32) Vartoukian, S. R.; Palmer, R. M.; Wade, W. G. Strategies for culture of 'unculturable' bacteria. *FEMS Microbiol. Lett.* **2010**, *309*, 1 – 7.

(33) Hug, L. A. *et al.* A new view of the tree of life. *Nat. Microbiol.* **2016**, *1*, 16048.

(34) Bentley, S. D.; Chater, K. F.; Cerdeño Tárraga, A. M.; Challis, G. L.; Thomson, N. R.; et al., Complete genome sequence of the model actinomycete Streptomyces coelicolor A3(2). *Nature* **2002**, *417*, 141 – 147.

(35) Ikeda, H.; Ishikawa., J.; Huanamoto, A.; Shinose, M.; Kikuchi, H.; Shiba, T.; Sakaki, Y.; Hattori, M.; Ōmura, S. Complete genome sequence and comparative analysis of the industrial microorganism Streptomyces avermitilis. *Nat. Biotechnol.* **2003**, *21*, 526 – 531.

(36) Genilloud, O. Actinomycetes: still a source of novel antibiotics. *Nat. Prod. Rep.* **2017**, *34*, 1203 – 1232.

(37) Hug, J. J.; Bader, C. D.; Remškar, M.; Cirnski, K.; Müller, R. Concepts and Methods to Access Novel Antibiotics from Actinomycetes. *Antibiotics* **2018**, *7*, 797 – 9315.

(38) Reichenbach, H. Myxobacteria, producers of novel bioactive substances. *J. Ind. Microbiol. Biotechnol.* **2001**, *27*, 149 – 156.

(39) Weissman, K. J.; Müller, R. Myxobacterial secondary metabolites: bioactivities and modes-of-action. *Nat. Prod. Rep.* **2010**, *27*, 1267 – 1295.

References

(40) Gerth, K.; Pradella, S.; Perlova, O.; Beyer, S.; Müller, R. Myxobacteria: proficient producers of novel natural products with various biological activities—past and future biotechnological aspects with the focus on the genus Sorangium. *J. Biotechnol.* **2003**, *106*, 233 – 253.

(41) McCormick, M. H.; Stark, W. M.; Pittenger, G. E.; Pittenger, R. C.; McGuire, J. M. Vancomycin, a new antibiotic. *Antibiot. Annu.* **1955-56**, 606 – 611.

(42) Lechevalier, M. P.; Prauser, H.; Labeda, D. P.; Juan, J.-S. Natural product discovery: past, present, and future. *Int. J. Sys. Bacteriol.* **1986**, *36*, 29 – 37.

(43) Nicolaou, K. C.; Boddy, C. N. C.; Bräse, S.; Winssinger, N. Chemistry, Biology, and Medicine of the Glycopeptide Antibiotics. *Angew. Chem. Int. Ed.* **1999**, *38*, 2096 –2152.

(44) Williams, D. H.; Bardsley, B. The Vancomycin Group of Antibiotics and the Fight against Resistant Bacteria. *Angew. Chem. Int. Ed.* **1999**, *38*, 1172 – 1193.

(45) Williamson, M. P.; Williams, D. H. Structure revision of the antibiotic vancomycin. The use of nuclear overhauser effect difference spectroscopy. *J. Am. Chem. Soc.* **1981**, *103*, 6580 – 6585.

(46) Harris, C. M.; Kopecka, H.; Harris, T. M. Vancomycin: structure and transformation to CDP-1. *J. Am. Chem. Soc.* **1983**, *105*, 6915 – 6922.

(47) O'Connell, K. M. G.; Hodgkinson, J. T.; Sore, H. F.; Welch, M.; Salmond, G. P. C.; Spring, D. R. Combating Multidrug-Resistant Bacteria: Current Strategies for the Discovery of Novel Antibacterials. *Angew. Chem. Int. Ed.* **2013**, *52*, 10706 –10733.

(48) Grace, Y.; Thaker, M. N.; Koteva, K.; Wright, G. Glycopeptide antibiotics biosynthesis. *J. Antibiot.* **2014**, *67*, 31 – 41.

(49) *WHO Model List of Essential Medicines*; World Health Organisation, 2017; p 8.

(50) Leclercq, R.; Derlot, E.; Duval, J.; Courvalin, P. Plasmid-Mediated Resistance to Vancomycin and Teicoplanin in Enterococcus Faecium. *N. Engl. J. Med.* **1988**, *319*, 157 – 161.

(51) Courvalin, P. Vancomycin Resistance in Gram-Positive Cocci. *Clin. Infect. Dis.* **2006**, *42*, S25 – S34.

(52) Kahne, D.; Leimkuhler, C.; Lu, W.; Walsh, C. Glycopeptide and Lipoglycopeptide Antibiotics. *Chem. Rev.* **2005**, *105*, 425 – 448.

(53) Perichon, B.; Courvalin, P. VanA-type vancomycin-resistant Staphylococcus aureus. *Antimicrob. Agents Chemother.* **2009**, *53*, 4580 – 4587.

(54) Bugg, T. D. H.; Wright, G. D.; Dutka-Malen, S.; Arthur, M.; Courvalin, P.; Walsh, C. T. Molecular basis for vancomycin resistance in Enterococcus faecium BM4147: biosynthesis of a depsipeptide peptidoglycan precursor by vancomycin resistance proteins VanH and VanA. *Biochemistry* **1991**, *30*, 10408 – 10415.

(55) McComas, C. C.; Crowley, B. M.; Boger, D. L. Partitioning the Loss in Vancomycin Binding Affinity for d-Ala-d-Lac into Lost H-Bond and Repulsive Lone Pair Contributions. *J. Am. Chem. Soc.* **2003**, *125*, 9314 – 9315.

(56) Crowley, B. M.; Boger, D. L. Total Synthesis and Evaluation of [φ[CH$_2$NH]Tpg^4]Vancomycin Aglycon: Reengineering Vancomycin for Dual D-Ala-D-Ala and D-Ala-D-Lac Binding. *J. Am. Chem. Soc.* **2006**, *128*, 2885 – 2892.

(57) James, R. C.; Pierce, J. G.; Okano, A.; Xie, J.; Boger, D. L. Redesign of Glycopeptide Antibiotics: Back to the Future. *ACS Chem. Biol.* **2012**, *7*, 797 – 9315.

(58) Xie, J.; Pierce, J. G.; James, R. C.; Okano, A.; Boger, D. L. A Redesigned Vancomycin Engineered for Dual D-Ala-D-Ala and D-Ala-D-Lac Binding Exhibits Potent Antimicrobial Activity Against Vancomycin-Resistant Bacteria. *J. Am. Chem. Soc.* **2011**, *133*, 13946 –13949.

(59) Xie, J.; Okano, A.; Pierce, J. G.; James, R. C.; Stamm, S.; Crane, C. M.; Boger, D. L. Total Synthesis of [φ[C(=S)NH]Tpg^4]Vancomycin Aglycon, [φ[C(=NH)NH]Tpg^4]Vancomycin Aglycon, and Related Key Compounds: Reengineering Vancomycin for Dual D-Ala-D-Ala and D-Ala-D-Lac Binding. *J. Am. Chem. Soc.* **2012**, *134*, 1284 –1297.

(60) Butler, M. S.; Hansford, K. A.; Blaskovich, M. T.; Halai, R.; Cooper, M. A. Glycopeptide antibiotics: Back to the future. *J. Antibiot.* **2014**, *67*, 631 – 644.

(61) Li, J. W.-H.; Vederas, J. C. Drug Discovery and Natural Products: End of and Era or an Endless Frontier. *Science* **2009**, *325*, 161 – 165.

(62) Kodadek, T. The rise, fall and reinvention of combinatorial chemistry. *Chem. Commun.* **2011**, *47*, 9757 – 9763.

(63) Nett, M.; Ikeda, H.; Moore, B. S. Genomic basis for natural product biosynthetic diversity in the actinomycetes. *Nat. Prod. Rep.* **2009**, *26*, 1362 – 1384.

(64) Bachmann, B. O.; Van Lanen, S. G.; Baltz, R. H. Microbial genome mining for accelerated natural products discovery: is a renaissance in the making? *J. Ind. Microbiol. Biotechnol.* **2014**, *41*, 175 – 184.

(65) Zhu, H.; Sandiford, S. K.; van Wezel, G. P. Triggers and cues that activate antibiotic production by actinomycetes. *J. Ind. Microbiol. Biotechnol.* **2014**, *41*, 371 – 386.

References

(66) Yoon, V.; Nodwell, J. R. Activating secondary metabolism with stress and chemicals. *J. Ind. Microbiol. Biotechnol.* **2014**, *41*, 415 – 424.

(67) Rutledge, P. J.; Challis, G. L. Discovery of microbial natural products by activation of silent biosynthetic gene clusters. *Nat. Rev. Microbiol.* **2015**, *13*, 509 – 523.

(68) Baltz, R. H. Genetic manipulation of secondary metabolite biosynthesis for improved production in Streptomyces and other actinomycetes. *J. Ind. Microbiol. Biotechnol.* **2016**, *43*, 343 – 370.

(69) Katz, M.; Hover, B. M.; F., B. S. Culture-independent discovery of natural products from soil metagenomes. *J. Ind. Microbiol. Biotechnol.* **2016**, *43*, 129 – 41.

(70) Milshteyn, A.; Schneider, J. S.; Brady, S. F. Mining the metabiome: identifying novel natural products from microbial communities. *Chem. Biol.* **2014**, *21*, 1211 – 1223.

(71) Medema, M. H.; Fischbach, M. A. Computational approaches to natural product discovery. *Nat. Chem. Biol.* **2015**, *9*, 639 – 648.

(72) Medema, M. H.; Zhao, H. Synthetic biology and bioinformatics. *Nat. Prod. Rep.* **2016**, *33*, 913 – 914.

(73) Weber, T.; Blin, K.; Duddela, S.; Krug, D.; Kim, H. U.; Bruccoleri, R.; Lee, S. Y.; Fischbach, M. A.; Müller, R.; Wohlleben, W.; R., B.; Takano, E.; Medema, M. H. antiSMASH 3.0 - a comprehensive resource for the genome mining of biosynthetic gene clusters. *Nucleic Acids Res.* **2015**, *43*, W237 – 243.

(74) Blin, K.; Wolf, T.; Chevrette, M. G.; et al., antiSMASH 4.0 - improvements in chemistry prediction and gene cluster boundary identification. *Nucleic Acids Res.* **2017**, *45*, W36 – W41.

(75) Zhang, W.; Tang, Y. Combinatorial Biosynthesis of Natural Products. *J. Med. Chem.* **2008**, *51*, 2629 – 2633.

(76) Sun, H.; Liu, Z.; Zhao, H.; Ang, E. L. Recent advances in combinatorial biosynthesis for drug discovery. *Drug Des. Devel. Ther.* **2015**, *9*, 823 – 833.

(77) Kim, E.; Moore, B. S.; J., Y. Y. Reinvigorating natural product combinatorial biosynthesis with synthetic biology. *Nat. Chem. Biol.* **2015**, *11*, 649 – 659.

(78) Yim, G.; Thaker, M. N.; Koteva, K.; Wright, G. Glycopeptide antibiotic biosynthesis. *J. Antibiot.* **2014**, *67*, 31 – 41.

(79) Singh, S. B.; Jayasuriya, H.; Hazuda, D. L.; Felock, P.; Homnick, C. F.; Sardana, M.; Patane, M. A. Selective and controlled hydrolysis of chloropeptin I. HIV-1 integrase activity of fragments. *Tetrahedron Lett.* **1998**, *39*, 8769 – 8770.

(80) Kanekoa, I.; Kamoshida, K.; Takahashib, S. Complestatin, a potent anti-complement substance produced by Streptomyces lavendulae I. Fermentation, isolation and biological characterization. *J. Antibiot.* **1989**, *42*, 236 – 241.

(81) Seto, H.; Fujioka, T.; Furihata, K.; Kanekoa, I.; Takahashib, S. Structure of complestatin, a very strong inhibitor of protease activity of complement in the human complement system. *Tetrahedron Lett.* **1989**, *30*, 4987 – 4990.

(82) Chiu, H. T.; Hubbard, B. K.; Shah, A. N.; Eide, J.; Fredenburg, R. A.; Walsh, C. T.; Khosla, C. Molecular cloning and sequence analysis of the complestatin biosynthetic gene cluster. *Proc. Natl. Acad. Sci. U.S.A.* **2001**, *98*, 8548 – 8553.

(83) Momota, K.; Kaneko, I.; Kimura, S.; Mitamura, K.; Shimada, K. Inhibition of human immunodeficiency virus type-1-induced syncytium formation and cytopathicity by complestatin. *Biochem. Biophys. Res. Commun.* **1991**, *179*, 243 – 250.

(84) Kwon, Y. J.; Kim, H. J.; Kim, W. G. Complestatin Exerts Antibacterial Activity by the Inhibition of Fatty Acid Synthesis. *Biol. Pharm. Bull.* **2015**, *38*, 715 – 721.

(85) Yoo, I. D.; Yun, B.; Ryoo, I. J.; Lee, S. Y.; Shin, M. H.; Oh, S. Complestatin antagonizes the AMPA/kainate-induced neurotoxicity in cultured chick telencephalic neurons. *Neurochem. Res.* **2002**, *27*, 337 – 343.

(86) Naruse, N.; Tenmyo, O.; Kobaru, S.; Hatori, M.; Tomita, K.; Hamagishi, Y.; Oki, T. New antiviral antibiotics, kistamicins A and B. I. Taxonomy, production, isolation, physico-chemical properties and biological activities. *J. Antibiotic.* **1993**, *46*, 1804 – 1811.

(87) Naruse, N.; Oka, M.; Oki, T. New antiviral antibiotics, kistamicins A and B. II. Structure determination. *J. Antibiotic.* **1993**, *46*, 1812 – 1818.

(88) Okano, A.; Isley, N. A.; Boger, D. L. Total Syntheses of Vancomycin-Related Glycopeptide Antibiotics and Key Analogues. *Chem. Rev.* **2017**, *117*, 11952 – 11933.

(89) Marahiel, M. A.; Stachelhaus, T.; Mootz, H. D. Modular Peptide Synthetases Involved in Nonribosomal Peptide Synthesis. *Chem. Rev.* **1997**, *97*, 2651 – 2674.

(90) Sieber, S. A.; Marahiel, M. A. Molecular Mechanisms Underlying Nonribosomal Peptide Synthesis: Approaches to New Antibiotics. *Chem. Rev.* **2005**, *105*, 715 – 738.

(91) Fischbach, M. A.; Wash, C. T. Assembly-Line Enzymology for Polyketide and Nonribosomal Peptide Antibiotics: Logic, Machinery, and Mechanisms. *Chem. Rev.* **2006**, *106*, 3468 – 3496.

(92) Peschke, M.; Brieke, C.; Goode, R. J. A.; Schittenhelm, R. B.; Cryle, M. J. Chlorinated Glycopeptide Antibiotic Peptide Precursors Improve Cytochrome P450-Catalyzed Cyclization Cascade Efficiency. *Biochemistry* **2017**, *56*, 1239 – 1247.

References

(93) Kittilä, T.; Kittel, C.; Tailhades, J.; Butz, D.; Schoppet, M.; Büttner, A.; Goode, R. J. A.; Schittenhelm, R. B.; van Pee, K.-H.; Süssmuth, R. D.; Wohlleben, W.; Cryle, M. J.; Stegmann, E. Halogenation of glycopeptide antibiotics occurs at the amino acid level during non-ribosomal peptide synthesis. *Chem. Sci.* **2017**, *8*, 5992 – 6004.

(94) Park, O. K.; Choi, H. Y.; Kim, G. W.; Kim, W. G. Generation of New Complestatin Analogues by Heterologous Expression of the Complestatin Biosynthetic Gene Cluster from Streptomyces chartreusis AN1542. *Chembiochem.* **2016**, *17*, 1725 – 1731.

(95) Mollo, A.; von Krusenstiern, A. N.; Bulos, J. A.; Ulrich, V.; Åkerfeldt, K. S.; Cryle, M. J.; Charkoudian, L. K. P450 monooxygenase ComJ catalyses side chain phenolic cross-coupling during complestatin biosynthesis. *RSC Adv.* **2017**, *7*, 35376 – 35384.

(96) Haslinger, K.; Peschke, M.; Brieke, C.; Maximowitsch, E.; Cryle, M. J. X-domain of peptide synthetases recruits oxygenases crucial for glycopeptide biosynthesis. *Nature* **2015**, *521*, 105 – 109.

(97) Richarz, R. Untersuchung oxidativer Funktionalisierungsreaktionen in der Biosynthese mikrobieller Peptidnaturstoffe. Ph.D. thesis, Technical University Munich, 2018.

(98) Hubbard, B. K.; Thomas, M. G.; Walsh, C. T. Biosynthesis of L-*p*-hydroxyphenylglycine, a non-proteinogenic amino acid constituent of peptide antibiotics. *Chem. Biol.* **2000**, *7*, 931 – 942.

(99) Choroba, O. W.; Williams, D. H.; Spencer, J. B. Biosynthesis of the Vancomycin Group of Antibiotics: Involvement of an Unusual Dioxygenase in the Pathway to (S)-4-Hydroxyphenylglycine. *J. Am. Chem. Soc.* **2000**, *122*, 5389 –5390.

(100) Chen, H.; Tseng, C. C.; Hubbard, B. K.; Walsh, C. T. Glycopeptide antibiotic biosynthesis: Enzymatic assembly of the dedicated amino acid monomer (S)-3,5-dihydroxyphenylglycine. *Proc. Natl. Acad. Sci. U.S.A.* **2001**, *98*, 14901 – 14906.

(101) Pfeifer, V.; Nicholson, J., G. J. Ries; Recktenwald, J.; Schefer, A. B.; Shawky, R. M.; Schröder, J.; Wohlleben, W.; S., P. A polyketide synthase in glycopeptide biosynthesis: the biosynthesis of the non-proteinogenic amino acid (S)-3,5-dihydroxyphenylglycine. *J. Biol. Chem.* **2001**, *276*, 38370 – 38377.

(102) Widboom, P. F.; Fielding, E. N.; Liu, Y.; Bruner, S. D. Structural basis for cofactor-independent dioxygenation in vancomycin biosynthesis. *Nature* **2007**, *447*, 342 – 345.

(103) Zerbe, K.; Pylypenko, O.; Vitali, F.; Zhang, W.; Rouset, S.; Heck, M.; Vrijbloed, J. W.; Bischoff, D.; Bister, B.; Süssmuth, R. D.; Pelzer, S.; Wohlleben, W.;

Robinson, J. A.; Schlichting, I. Crystal Structure of OxyB, a Cytochrome P450 Implicated in an Oxidative Phenol Coupling Reaction during Vancomycin Biosynthesis. *J. Biol. Chem.* **2002**, *277*, 47476 – 47485.

(104) Pelzer, S.; Süssmuth, R.; Heckmann, D.; Recktenwald, J.; Huber, P.; Jung, G.; Wohlleben, W. Identification and analysis of the balhimycin biosynthetic gene cluster and its use for manipulating glycopeptide biosynthesis in Amycolatopsis mediterranei DSM5908. *Antimicrob. Agents Chemother.* **1999**, *43*, 1565 – 1573.

(105) Li, T. L.; Huang, F.; Haydock, S. F.; Mironenko, T.; Leadlay, P. F.; Spencer, J. B. Biosynthetic gene cluster of the glycopeptide antibiotic teicoplanin: characterization of two glycosyltransferases and the key acyltransferase. *Chem. Biol.* **2004**, *11*, 107 – 119.

(106) Aldemir, H.; Richarz, R.; Gulder, T. A. The biocatalytic repertoire of natural biaryl formation. *Angew. Chem. Int. Ed.* **2014**, *53*, 8286 – 8293.

(107) Süssmuth, R. D.; Pelzer, S.; Nicholson, G.; Walk, T.; Wohlleben, W.; Jung, G. New Advances in the Biosynthesis of Glycopeptide Antibiotics of the Vancomycin Type from Amycolatopsis mediterranei. *Angew. Chem. Int. Ed.* **1999**, *38*, 1976 – 1979.

(108) Bischoff, D.; Pelzer, S.; Höltzel, A.; Nicholson, G. J.; Stockert, S.; Wohlleben, W.; Jung, G.; Süssmuth, R. D. The Biosynthesis of Vancomycin - Type Glycopeptide Antibiotics - New Insights into the Cyclization Steps. *Angew. Chem. Int. Ed.* **2001**, *40*, 1693 – 1696.

(109) Bischoff, D.; Pelzer, S.; Bister, B.; Nicholson, G. J.; Stockert, S.; Schirle, M.; Wohlleben, W.; Jung, G.; Süssmuth, R. D. The Biosynthesis of Vancomycin - Type Glycopeptide Antibiotics - The Order of the Cyclization Steps. *Angew. Chem. Int. Ed.* **2001**, *40*, 4688 – 4691.

(110) Zerbe, K.; Woithe, K.; Li, D. B.; Vitali, F.; Bigler, L.; Robinson, J. A. An oxidative phenol coupling reaction catalyzed by oxyB, a cytochrome P450 from the vancomycin-producing microorganism. *Angew. Chem. Int. Ed.* **2004**, *43*, 6709 – 6713.

(111) Bischoff, D.; Bister, B.; Bertazzo, M.; Pfeifer, V.; Stegmann, E.; Nicholson, G. J.; Keller, S.; Pelzer, S.; Wohlleben, W.; Süssmuth, R. D. The Biosynthesis of Vancomycin-Type Glycopeptide Antibiotics - A Model for Oxidative Side-Chain Cross-Linking by Oxygenases Coupled to the Action of Peptide Synthetases. *ChemBioChem* **2005**, *6*, 262 – 272.

(112) Woithe, K.; Geib, N.; Zerbe, K.; Li, D. B.; Heck, M.; Fournier-Rousset, S.; Meyer, O.; Vitali, F.; Matoba, N.; Abou-Hadeed, K.; Robinson, J. A. Oxidative Phenol Coupling Reactions Catalyzed by OxyB: A Cytochrome P450 from the Vancomycin Producing Organism. Implications for Vancomycin Biosynthesis. *J. Am. Chem. Soc.* **2007**, *129*, 6887 – 6895.

References

(113) Peschke, P.; Haslinger, K.; Brieke, C.; Reinstein, J.; Cryle, M. J. Regulation of the P450 Oxygenation Cascade Involved in Glycopeptide Antibiotic Biosynthesis. *J. Am. Chem. Soc.* **2016**, *138*, 6746 –6753.

(114) Brieke, C.; Peschke, M.; Haslinger, K.; Cryle, M. J. Sequential In Vitro Cyclization by Cytochrome P450 Enzymes of Glycopeptide Antibiotic Precursors Bearing the X-Domain from Nonribosomal Peptide Biosynthesis. *Angew. Chem. Int. Ed. Engl.* **2015**, *54*, 15715 –15719.

(115) Aldemir, H. Studien zur chemo-enzymatischen Totalsynthese komplexer Peptide mit Biaryl-Strukturelementen. Ph.D. thesis, Technical University Munich, 2015.

(116) Haslinger, K.; Maximowitsch, E.; Brieke, C.; Koch, A.; Cryle, M. J. Cytochrome P450 OxyB$_{tei}$ Catalyzes the First Phenolic Coupling Step in Teicoplanin Biosynthesis. *ChemBioChem* **2014**, *15*, 2719 – 2728.

(117) Peschke, P.; Brieke, C.; Cryle, M. J. F-O-G Ring Formation in Glycopeptide Antibiotic Biosynthesis is Catalysed by OxyE. *Sci. Rep.* **2016**, *35584*.

(118) Forneris, C. C.; Ozturk, S.; Gibson, M. I.; Sorensen, E. J.; Seyedsayamdost, M. R. *In Vitro* Reconstitution of OxyA Enzymatic Activity Clarifies Late Steps in Vancomycin Biosynthesis. *ACS Chem. Biol.* **2017**, *12*, 2248 – 2253.

(119) Brieke, C.; Tarnawski, M.; Greule, A.; Cryle, M. J. Investigating Cytochrome P450 specificity during glycopeptide antibiotic biosynthesis through a homologue hybridization approach. *J. Inorg. Biochem.* **2018**, *185*, 43 – 51.

(120) Li, D. B.; Robinson, J. A. An improved solid-phase methodology for the synthesis of putative hexa- and heptapeptide intermediates in vancomycin biosynthesis. *Org. Biomol. Chem.* **2005**, *3*, 1233 – 1239.

(121) Freund, E.; Robinson, J. A. Solid-phase synthesis of a putative heptapeptide intermediate in vancomycin biosynthesis. *Chem. Commun.* **1999**, 2509 – 2510.

(122) Brieke, C.; Cryle, M. J. A Facile Fmoc Solid Phase Synthesis Strategy To Access Epimerization-Prone Biosynthetic Intermediates of Glycopeptide Antibiotics. *Org. Lett.* **2014**, *16*, 2454 – 2457.

(123) Brieke, C.; Kratzig, V.; Haslinger, K.; Winkler, A.; Cryle, M. J. Rapid access to gylcopeptide antibiotic precursor peptides coupled with cytochrome P450-mediated catalysis: towards biomimetic synthesis of glycopeptide antibiotics. *Org. Biomol. Chem* **2015**, *13*, 2012 – 2021.

(124) Nakano, M. M.; Corbell, N.; Besson, J.; Zuber, P. Isolation and characterization of sfp: a gene that functions in the production of the lipopeptide biosurfactant, surfactin, in Bacillus subtilis. *Mol. Gen. Genet.* **1992**, *232*, 313 – 321.

(125) J., B.; Sonnenschein, E. C.; Vickery, C. R.; Noel, J. P.; Burkart, M. D. The phosphopantetheinyl transferases: catalysis of a post-translational modification crucial for life. *Nat. Prod. Rep.* **2014**, *31*, 61 – 108.

(126) Weckbecker, A.; Hummel, W. G. In *Microbial Enzymes and Biotransformations*; Barredo, J. L., Ed.; Humana Press: Totowa, NJ, 2005; pp 225 - 238.

(127) Geib, N.; Weber, T.; Wörtz, T.; Zerbe, K.; Wohlleben, W.; Robinson, J. A. Genome mining in Amycolatopsis balhimycina for ferredoxins capable of supporting cytochrome P450 enzymes involved in glycopeptide antibiotic biosynthesis. *FEMS Microbiol. Lett.* **2010**, *306*, 45 – 53.

(128) Smith, G. G.; Sivakua, T. Mechanism of the racemization of amino acids. Kinetics of racemization of arylglycines. *J. Org. Chem.* **1983**, *48*, 627 – 634.

(129) Dettner, F.; Hänchen, A.; Schols, D.; Toti, L.; Nusser, A.; Süssmuth, R. D. Total Synthesis of the Antiviral Peptide Antibiotic Feglymycin. *Angew. Chem., Int. Ed.* **2009**, *48*, 1856 – 1861.

(130) Beugelmans, R.; González Zamora, E.; Roussi, G. The First Synthesis of 16+15-Membered Bicyclic Polypeptide Model of A-O-C-B-O-D Rings of Kistamicin. *Tetrahedron Lett.* **1997**, *47*, 81889 – 8192.

(131) Beugelmans, R.; Roussi, G.; González Zamora, E.; Carbonnelle, A.-C. Synthetic Studies Towards Western and Eastern Macropolypeptide Subunits of Kistamicin. *Tetrahedron* **1999**, *55*, 5089 – 5112.

(132) Nazari, B.; Forneris, C. C.; Gibson, M. I.; Moon, K.; Schramma, K. R.; Seyedsayamdost, M. R. Nonomuraea sp. ATCC 55076 harbours the largest actinomycete chromosome to date and the kistamicin biosynthetic gene cluster. *Med Chem Commun.* **2017**, *8*, 780 – 788.

(133) Forneris, C. C.; Ozturk, S.; Sorensen, E. J.; Seyedsayamdost, M. R. Installation of multiple aryl ether crosslinks onto non-native substrate peptides by the vancomycin OxyB. *Tetrahedron* **2018**, *74*, 3231 – 3237.

(134) Garcia, R. O.; Krug, D.; Müller, R. Discovering Natural Products from Myxobacteria with Emphasis on Rare Producer Strains in Combination with Improved Analytical Methods. *Methods. Enzymol.* **2009**, *458*, 59 – 91.

(135) Herrmann, J.; Abou Fayadab, A.; Müller, R. Natural products from myxobacteria: novel metabolites and bioactivities. *Nat. Prod. Rep.* **2017**, *34*, 135 – 160.

(136) Gerth, K.; Irschik, H.; Reichenbach, H.; Trowitzsch, W. Myxothiazol, an antibiotic from Myxococcus fulvus (myxobacterales). I. Cultivation, isolation, physico-chemical and biological properties. *J. Antibiot.* **1980**, *33*, 1474 – 1479.

References

(137) Kunze, B.; Höfle, G.; Reichenbach, H. The aurachins, new quinoline antibiotics from myxobacteria: production, physico-chemical and biological properties. *J. Antibiot.* **1987**, *40*, 258 – 265.

(138) Gulder, T. A. M.; Neff, S.; Schütz,; Winkler, T.; Gees, R.; Böhlendorf, B. The myxocoumarins A and B from Stigmatella aurantiaca strain MYX-030. *Beilstein J. Org. Chem.* **2013**, *9*, 2579 – 2585.

(139) Heide, L. The aminocoumarins: biosynthesis and biology. *Nat. Prod. Rep.* **2009**, *26*, 1241 – 1250.

(140) Silakowski, B.; Kunze, B.; Nordsiek, G.; Blöcker, H.; Höfle, G.; Müller, R. The myxochelin iron transport regulon of the myxobacterium Stigmatella aurantiaca Sg a15. *Eur. J. Biochem.* **2000**, *267*, 6476 – 6485.

(141) Höfle, G.; H., I. Isolation and Biosynthesis of Aurachin P and 5-Nitroresorcinol from Stigmatella erecta. *J. Nat. Prod.* **2008**, *71*, 1946 – 1948.

(142) v. Pechmann, H. Neue Bildungsweise der Cumarine. Synthese des Daphnetins. I. *Berichte der deutschen chemischen Gesellschaft* **1884**, *17*, 929 – 936.

(143) v. Pechmann, H. Studien über Cumarine. I. Über das Verhalten der Amidophenole gegen Acetessigester. *Berichte der deutschen chemischen Gesellschaft* **1899**, *32*, 3681 – 3690.

(144) Sethna, S. M.; Shah, N. M. The Chemistry of Coumarins. *Chem. Rev.* **1945**, *36*, 1 – 62.

(145) Woods, L. L.; Sapp, J. A New One-Step Synthesis of Substituted Coumarins. *J. Org. Chem.* **1962**, *27*, 3703 – 3705.

(146) Katkevičs, M.; Kontijevskis, A.; Mutule, I.; Sūna, E. Microwave-promoted automated synthesis of a coumarin library. *Chem. Heterocycl. Compd.* **2007**, *43*, 151 – 159.

(147) Reddy, B. M.; Thirupathi, B.; Patil, M. K. One-Pot Synthesis of Substituted Coumarins Catalyzed by Silica Gel Supported Sulfuric Acid Under Solvent-Free Conditions. *TOCATJ* **2009**, *2*, 33 – 39.

(148) Amoozadeh, A.; Ahmadzadeh, M.; Kolvari, E. Easy Access to Coumarin Derivatives Using Alumina Sulfuric Acid as an Efficient and Reusable Catalyst under Solvent-Free Conditions. *J. Chem.* **2013**, Article ID 767825.

(149) Opanasenko, M.; Shamzhy, M.; Čejka, J. Solid Acid Catalysts for Coumarin Synthesis by the Pechmann Reaction: MOFs versus Zeolites. *Chem. Cat. Chem.* **2013**, *5*, 1024 – 1031.

(150) Woodruff, E. H. 4-Methylcoumarin. *Org. Synth.* **1944**, *24*, 69.

(151) Valizadeha, H.; Shockravi, A. An efficient procedure for the synthesis of coumarin derivatives using TiCl4 as catalyst under solvent-free conditions. *Tetrahedron Lett.* **2005**, *46*, 3501 – 3503.

(152) Prajapati, D.; Gohain, M. Iodine a Simple, Effective and Inexpensive Catalyst for the Synthesis of Substituted Coumarins. *Catal. Lett.* **2007**, *119*, 59 – 63.

(153) Robertson, A.; Waters, R. B.; Jones, E. T. Hydroxy-carbonyl Compounds. Part VII. Coumarins and 1:4-Benzopyrones derived from m-Cresol. *J. Chem. Soc.* **1932**, 1681 – 1688.

(154) Ahmad, S. Z.; Desai, R. D. Heterocyclic compounds Part III. The synthesis of cyclopenteno- (1': 2': 2: 3)-chromones, and a discussion on the mechanism of the pechmann and the simonis reactions. *Proc. Indian Acad. Sci.* **1937**, *6*, 6 – 11.

(155) Daru, J.; Stirling, A. Mechanism of the Pechmann Reaction: A Theoretical Study. *J. Org. Chem.* **2011**, *76*, 8749 – 8755.

(156) Tyndall, S.; Wong, K. F.; VanAlstine-Parris, M. A. Insight into the Mechanism of the Pechmann Condensation Reaction Using NMR. *J. Org. Chem.* **2015**, *80*, 8951 – 895.

(157) Pornsatitworakul, S.; Boekfa, B.; Maihom, T.; Treesukol, P.; Namuangruk, S.; Jarussophon, S.; Jarussophon, N.; Limtrakul, J. The coumarin synthesis: a combined experimental and theoretical study. *Monatsh. Chem.* **2017**, *148*, 1245 –1250.

(158) Bahekara, S. S.; Shinde, D. B. Samarium(III)-Catalyzed One-Pot Construction of Coumarins. *Tetrahedron Lett.* **2005**, *45*, 7999 – 8001.

(159) Manhas, M. S.; Ganguly, S. N.; Mukherjee, S.; Jain, A. K.; Bose, A. K. Microwave initiated reactions: Pechmann coumarin synthesis, Biginelli reaction, and acylation. *Tetrahedron Lett.* **2006**, *47*, 2423 –2425.

(160) Afri, M.; Gottlieb, H. E.; Frimer, A. A. Superoxide organic chemistry within the liposomal bilayer, part II: a correlation between location and chemistry. *Free Radical Biol. Med.* **2002**, *32*, 605 – 618.

(161) Müller, J. I.; Kusserow, K.; Hertrampf, G.; Pavic, A.; Nikodinovic-Runic, J.; Gulder, T. A. M. Synthesis and initial biological evaluation of myxocoumarin B. *Org. Biomol. Chem.* **2019**, *17*, 1966 – 1969.

(162) Saito, S.; Koizumi, Y. Copper-catalyzed coupling of aryl halides and nitrite salts: a mild Ullmann-type synthesis of aromatic nitro compounds. *Tetrahedron Lett.* **2005**, *46*, 4715 – 4717.

(163) Fors, B. P.; Buchwald, S. L. Pd-Catalyzed Conversion of Aryl Chlorides, Triflates, and Nonaflates to Nitroaromatics. *J. Am. Chem. Soc.* **2009**, *131*, 12898 – 12899.

References

(164) Kusserow, K.; Gulder, T. A. M. Complete Genome Sequence of Actinomadura Parvosata Subsp. Kistnae, A Rich Source of Novel Natural Product (Bio-)Chemistry. *J. Genomics* **2017**, *5*, 75 – 76.

(165) Doroghazi, J. R.; Metcalf, W. W. Comparative genomics of actinomycetes with a focus on natural product biosynthetic genes. *BMC Genomics* **2013**, *14*, 611 – 624.

(166) Aziz, R. K.; Bartels, D.; Best, A. A.; DeJongh, M.; Diszet, T.; et. al., The RAST Server: Rapid Annotations using Subsystems Technology. *BMC Genomics* **2008**, *9*, 75 – 90.

(167) Kearse, M.; Moir, M.; Wilson, A.; Stones-Havas, S.; Cheung, M.; Sturrock, S.; Buxton, S.; Cooper, A.; Markowitz, S.; Duran, C.; Thierer, T.; Ashton, B.; Meintjes, P.; Drummond, A. Geneious Basic: an integrated and extendable desktop software platform for the organization and analysis of sequence data. *Bioinformatics* **2012**, *28*, 1647 – 1649.

(168) Bachmann, B. O.; Ravel, J. Methods for in silico prediction of microbial polyketide and nonribosomal peptide biosynthetic pathways from DNA sequence data. *Methods Enzymol.* **2009**, *458*, 181 – 217.

(169) Felnagle, E. A.; Barkei, J. J.; Park, H.; Podevels, A. M.; McMahon, M. D.; Drott, D. W.; Thomas, M. G. MbtH-Like Proteins as Integral Components of Bacterial Nonribosomal Peptide Synthetases. *Biochemistry* **2010**, *49*, 8815 – 8817.

(170) Zhang, W.; Heemstra, J. R. J.; Walsh, C. T.; Imker, H. J. Activation of the pacidamycin PacL adenylation domain by MbtH-like proteins. *Biochemistry* **2010**, *49*, 9946 – 9947.

(171) Boll, B.; Taubitz, T.; Heide, L. Role of MbtH-like proteins in the adenylation of tyrosine during aminocoumarin and vancomycin biosynthesis. *J. Biol. Chem.* **2011**, *286*, 36281 – 36290.

(172) Davidsen, J. M.; Bartley, D. M.; Townsen, C. A. Non-ribosomal Propeptide Precursor in Nocardicin A Biosynthesis Predicted from Adenylation Domain Specificity Dependent on the MbtH Family Protein NocI. *J. Am. Chem. Soc.* **2018**, *135*, 1749 – 1759.

(173) Schomer, R. A.; Thomas, M. G. Characterization of the Functional Variance in MbtH-like Protein Interactions with a Nonribosomal Peptide Synthetase. *Biochemistry* **2017**, *56*, 5380 – 5390.

(174) Mori, S.; Garzan, A.; Tsodikov, O. V.; Garneau-Tsodikova, S. Deciphering Nature's Intricate Way of N,S-Dimethylating l-Cysteine: Sequential Action of Two Bifunctional Adenylation Domains. *Biochemistry* **2017**, *56*, 6087 – 6097.

(175) Mori, S.; Pang, A. H.; Lundy, T. A.; Garzan, A.; Tsodikov, O. V.; Garneau-Tsodikova, S. Structural basis for backbone N-methylation by an interrupted adenylation domain. *Nat. Chem. Biol.* **2018**, *14*, 428 – 430.

(176) Mori, S.; Green, K. D.; Choi, R.; Buchko, G. W.; Fried, M. G.; Garneau-Tsodikova, S. Using MbtH-Like Proteins to Alter the Substrate Profile of a Nonribosomal Peptide Adenylation Enzyme. *ChemBioChem* **2018**, *19*, 2186 – 2194.

(177) Imker, H. J.; Walsh, C. T.; Wuest, W. M. SylC Catalyzes Ureido-Bond Formation During Biosynthesis of the Proteasome Inhibitor Syringolin A. *J. Am. Chem. Soc.* **2009**, *131*, 18263 – 18265.

(178) Ramel, C.; Tobler, M.; Meyer, M.; Bigler, L.; Ebert, M. O.; Schellenberg, B.; Dudler, R. Biosynthesis of the proteasome inhibitor syringolin A: the ureido group joining two amino acids originates from bicarbonate. *BMC Biochem.* **2009**, *10*.

(179) Dudler, R. The role of bacterial phytotoxins in inhibiting the eukaryotic proteasome. *Trends Microbiol.* **2014**, *22*, 28 – 35.

(180) Zhang, W.; Ostash, B.; Walsh, C. T. Identification of the biosynthetic gene cluster for the pacidamycin group of peptidyl nucleoside antibiotics. *Proc. Natl. Acad. Sci. U.S.A.* **2010**, *107*, 16828 – 16833.

(181) Walsh, C. T.; Zhang, W. Chemical logic and enzymatic machinery for biological assembly of peptidyl nucleoside antibiotics. *ACS Chem. Biol.* **2011**, *6*, 1000 – 1007.

(182) Rouhiainen, L.; Jokela, J.; Fewer, D. P.; Urmann, M.; Sivonen, K. Two Alternative Starter Modules for the Non-Ribosomal Biosynthesis of Specific Anabaenopeptin Variants in *Anabaena* (Cyanobacteria). *ACS Chem. Biol.* **2010**, *17*, 265 – 273.

(183) Kaysser, L.; Tang, X.; Wemakor, E.; Sedding, K.; Hennig, S.; Siebenberg, S.; Gust, B. Identification of a Napsamycin Biosynthesis Gene Clusterby Genome Mining. *ChemBioChem* **2011**, *12*, 477 – 487.

(184) Merrifield, R. B. Solid Phase Peptide Synthesis. I. The Synthesis of a Tetrapeptide. *J. Am. Chem. Soc.* **1963**, *85*, 2149 –2154.

(185) Amblard, M.; Fehrentz, J. A.; Martinez, J.; Subra, G. Methods and protocols of modern solid phase Peptide synthesis. *Mol. Biotechnol.* **2006**, *33*, 239 – 254.

(186) Harre, M.; Nickisch, K.; Tilstam, U. An efficient method for activation and recycling of trityl resins. *React. Funct. Polym.* **1999**, *41*, 111 – 114.

(187) Barlos, K.; Gatos, G.; Kallitsis, I.; Papaioannou, D.; Sotiriou, P. Anwendung von 4-Polystyryltriphenylmethylchlorid zur Synthese von Peptiden und Aminoäure-Derivaten. *Liebigs Ann. Chem.* **1988**, 1079 – 1081.

(188) Bolton, R.; De la Mare, P. B. D.; Suzuki, H. Electrophilic chlorination by sulfuryl chloride. *Recl. Trav. Chim. Pays-Bas* **1966**, *85*, 1206 – 1210.

References

(189) Weist, S.; Kittel, C.; Bischoff, D.; Bister, B.; Pfeifer, V.; Nicholson, G. J.; Wohlleben, W.; Süssmuth, R. D. Mutasynthesis of Glycopeptide Antibiotics: Variations of Vancomycin's AB-Ring Amino Acid 3,5-Dihydroxyphenylglycine. *J. Am. Chem. Soc.* **2004**, *126*, 5942 – 5943.

(190) Li, G.; Patel, D.; Hruby, V. J. An efficient procedure for the demethylation of aryl-methyl ethers in optically pure unusual amino acids. *Tetrahedron Lett.* **1993**, *34*, 5393 – 5396.

(191) Baker, S. R.; Goldsworthy, J.; Harden, R. C.; Salhoff, C. R.; Schoepp, D. D. Enzymatic Resolution and Pharmacological Activity of the Enantiomers of 3,5-Dihydroxyphenylglycine, a Metabotropic Glutamate Receptor Agonist. *Bioorganic. Med. Chem. Lett.* **1995**, *5*, 223 – 228.

(192) Milzarek, T. M. Total Synthesis of a Complestatin Precursor using combined Liquid and Solid Phase Peptide Synthesis. M.Sc. thesis, Technical University Munich, 2018.

(193) Li, X.; Kawakami, T.; Aimoto, S. Direct preparation of peptide thioesters using an Fmoc solid-phase method. *Tetrahedron Lett.* **1998**, *39*, 8669 – 8672.

(194) Zheng, J.-S.; Tang, S.; Qi, Y.-K.; Wang, Z.-W.; Liu, L. Chemical synthesis of proteins using peptide hydrazides as thioester surrogates. *Nat. Protoc.* **2013**, *8*, 2483 – 2495.

(195) Willcott, M. R. MestRe Nova. *J. Am. Chem. Soc.* **2009**, *131*, 13180 – 13180.

(196) Owczarzy, R.; Tataurov, A. V.; Wu, Y.; Manthey, J. A.; McQuisten, K. A.; Almabrazi, H. G.; Pedersen, K. F.; Lin, Y.; Garretson, J.; McEntaggart, N. O.; Sailor, C. A.; Dawson, R. B.; Peek, A. S. IDT SciTools: a suite for analysis and design of nucleic acid oligomers. *Nucleic Acids Res.* **2008**, *36*, W163 – 169.

(197) Miller, J. H. *Experiments in Molecular Genetics*; Cold Spring Harbor Laboratory: Cold Spring Harbor, NY, 1972.

(198) Hanahan, D. Studies on transformation of Escherichia coli with plasmids. *J. Mol. Biol.* **1983**, *166*, 557 – 580.

(199) Shirling, E. B.; Gottlieb, D. Methods for Characterization of Streptomyces Species. *Int. J. Syst. Bacteriol.* **1966**, *16*, 313 – 340.

(200) Thermo Scientific, GeneRuler™1 kb plus DNA Ladder. 2019; `https://www.fishersci.co.uk/shop/products/15283753/15283753`, visited on 05.06.2019.

(201) Thermo Scientific, Pierce™Unstained Protein Molecular Weight Marker. 2019; `https://www.thermofisher.com/order/catalog/product/26610`, visited on 05.06.2019.

(202) Becker, D.; Kazmaier, U. Synthesis of Simplified Halogenated Chondramide Derivatives with Strong Cytostatic Properties. *Eur. J. Org. Chem.* **2015**, 2591 – 2602.

206

(203) Stoller, S.; Sicoli, G.; Baranova, T. Y.; Bennati, M.; Diederichsen, U. TOPP: A Novel Nitroxide-Labeled Amino Acid for EPR Distance Measurements. *Angew. Chem. Int. Ed.* **2011**, *50*, 9743 – 9746.

(204) Garcia, M. J.; Azerad, R. Production of ring-substituted D-phenylglycines by microbial or enzymatic hydrolysis/deracemisation of the corresponding DL-hydantoins. *Tetrahedron: Asymmetry* **1997**, *8*, 85 – 92.

(205) Van Linn, M. L.; Cook, J. M. Mechanistic Studies on the Cis to Trans Epimerization of Trisubstituted 1,2,3,4-Tetrahydro-β-carbolines. *J. Org. Chem.* **2010**, *75*, 3587 – 3599.

(206) Miyazaki, A.; Tsuda, Y.; Fukushima, S.; Yokoi, T.; Vántus, T.; Bökönyi, G.; Szabó, E.; Horváth, G., A. Kéri; Okada, Y. Synthesis of Somatostatin Analogues Containing C-Terminal Adamantane and Their Antiproliferative Properties. *J. Med. Chem.* **2008**, *51*, 5121 – 5124.

List of Abbreviations

ATP	adenosine triphosphate
A	adenylation domain
AA	amino acid
ADP	adenosine diphosphate
Alloc	alloxycarbonyl
ACN	acetonitrile
APS	ammonium persulfate
BGC	biosynthetic gene cluster
BNMRZ	Bayrisches NMR Zentrum
C	condensation domain
Cbz	carboxybenzyl
CDS	coding DNA sequence
CoA	coenzyme A
COMU	(1-cyano-2-ethoxy-2-oxoethylidenaminooxy)dimethylamino-morpholino-carbenium hexafluorophosphate
CYP	cytochrome P450 enzyme
2-CTC	2-chlorotrityl chloride
DBU	1,8-diazabicyclo[5.4.0]undec-7-ene
DCM	dichloromethane
DIC	*N,N'*-diisopropylcarbodiimide
DIPA	diisopropylamine
DIPEA	diisopropylethylamine
DMF	dimethylformamide
DMSO	dimethylsulfoxide
(g)DNA	(genomic) deoxyribonucleic acid
dNTP	desoxyribonucleoside triphosphate
Dpg	4-dihydroxyphenylglycine
E	epimerization domain
EDCl	1-ethyl-3-(3-dimethylaminopropyl)carbodiimide
EDTA	ethylenediaminetetraacetic acid
EMBL	European Molecular Biology Laboratory
EtOAc	ethyl acetate
FAD	flavine adenine dinnucleotide
Fed	ferredoxin
Fmoc(-Cl)	fluorenylmethyloxycarbonyl (chloride)

Fmoc-OSu	fluorenylmethyloxycarbonyl *N*-hydroxysuccinimide ester
Gdh	glucose dehydrogenase
GFM	glucose fish meal
GPA	glycopeptide antibiotic
HATU	hexafluorophosphate azabenzotriazole tetramethyl uronium
HBTU	2-(1 *H*-benzotriazol-1-yl)-1,1,3,3-tetramethyluronium hexafluorophosphate
HI(V)	human immunodeficiency (virus)
HmaS	4-hydroxymandelate synthase
Hmo	4-hydroxymandelate oxidase
HOAt	1-hydroxy-7-azabenzotriazole
HOBt	*N*-hydroxybenzotriazole
HPLC	high-performance liquid chromatography
Hbf	4-hydroxyphenyl benzoylformate
Hpg	4-hydroxyphenylglycine
HpgT	4-hydroxyphenylglycine transferase
(HR-)ESI-MS	(high-resolution) electrospray ionization mass spectrometry
HTS	high-throughput screen
IPTG	isopropyl β-D-1-thiogalactopyranoside
LB	Luria Bertani
(LC-)MS	(liquid chromatography) mass spectrometry
LPPS	liquid phase peptide synthesis
M	methylation domain
MDR	multidrug-resistant
MeOH	methanol
MIC	minimum inhibitory concentration
MPAA	4-mercaptophenylacetic acid
MPLC	medium pressure liquid chromatography
MRSA	methicillin-resistant *Staphylococcus aureus*
MW	microwave
NAD(P)H	nicotinamide adenine dinucleotide (phosphate)
*n*BuLi	*n*buthyllithium
NMM	*N*-methylmorpholine
NMP	*N*-methyl-2-pyrrolidone
NMR	nuclear magnetic resonance spectroscopy
NRPS	nonribosomal peptide synthetase
NTA	nitrilotriacetic acid
OPCR	oxidative phenol coupling reaction
ORF	open reading frame
PCP	peptidyl carrier protein domain
PCR	polymerase chain reaction
Pd$_2$(dba)$_3$	tris(dibenzylideneacetone)dipalladium(0)
PD	prephenate dehydrogenase
PG	protecting group
PKS	polyketide synthase
ppant	phosphopantetheine moeity

PyBOP	benzotriazol-1-yl-oxytripyrrolidinophosphonium hexafluorophosphate
Red	reductase
(r)RNA	(ribosomal) ribonucleic acid
RT	room temperature
SAR	structure-activity relationship
SDS(-PAGE)	sodium dodecyl sulfate(–polyacrylamide gel electrophoresis)
Sfp	surfactin-phosphapantetheinyltransferase
SOC	super optimal broth
SPPS	solid phase peptide synthesis
SSA	silica sulfuric acid
TAE	Tris acetate EDTA
TBTU	2-(1H-benzotriazole-1-yl)-1,1,3,3-tetramethylaminium tetrafluoroborate
tBuBrettPhos	2-(di-$t$butylphosphino)-2',4',6'-triisopropyl-3,6-dimethoxy-1,1'-biphenyl
TDA	tris-(dioxa-3,6-heptyl)-amine
TE	thioesterase domain
TEMED	N,N,N',N'-tetramethylethylene-1,2-diamine
TFA	trifluororacetic acid
THF	tetrahydrofuran
TIPS	triisopropyl silane
TLC	thin layer chromatography
TMS	tetramethylsilane
TMS-Cl	trimethylsilyl chloride
Tris	tris-(hydroxymethyl)-aminomethane
tR	retention time
(t)RNA	(transfer) ribonucleic acid
Trp	tryptophane
Tyr	tyrosine
UV	ultraviolet
VRE	vancomycin-resistant enterococci
WHO	World Health Organization
X	X domain
XDR	extensively drug-resistant